ENRICHMENT AND PROTEOMIC ANALYSIS OF PLACENTA-SPECIFIC EXTRACELLULAR VESICLES TOWARDS NON-INVASIVE DIAGNOSIS OF PREECLAMPSIA

by

Quang Nghia Pham

Master of Engineering (MEng.)

A thesis submitted for the degree of

Doctor of Philosophy

(Biomaterials engineering and nanomedicine; IPHD)

Clinical and health sciences



University of South Australia

September 2022

Contents

Contents ..... **ii**
List of Figures ..... **v**
List of Tables ..... **vii**
Glossary ..... **viii**
Summary ..... **x**
Declaration ..... **xiv**
Acknowledgements ..... **xv**
1 Introduction **2**
1.1 Hypotheses and research aims of thesis 4
1.2 Thesis structure 5
1.3 Thesis outcomes 6
1.4 References 8
2 Literature review **12**
2.1 Extracellular vesicles: classification, biogenesis, and molecular composition 12
2.1.1 Classification and Biogenesis of EVs 12
2.1.2 Molecular composition of EVs 14
2.1.3 Physiological and pathological relevance of EVs 16
2.2 Cellular heterogeneity of the human placenta 17
2.3 Placenta-derived EVs 19
2.4 Current EV isolation/enrichment techniques 21
2.4.1 Bulk isolation of EVs 21
2.4.2 Affinity isolation of EVs 22
2.4.3 Microfluidic-based isolation of EVs 23
2.4.4 Enrichment of placental EVs from biological fluids 24
2.5 Preeclampsia and its current diagnostic limitations 25
2.6 EVs and their pathological links to preeclampsia 26
2.7 Search for preeclampsia biomarkers 32
2.8 References 34
3 Magnetic enrichment of immuno-specific extracellular vesicles for mass spectrometry using biofilm-derived iron oxide nanowires **55**
3.1 Publication details 55
3.2 Statement of authorship 55
3.3 Abstract 56
3.4 Introduction 56
3.5 Materials 60
3.5.1 Preparation of iron oxide NWs 60

3.5.2 Preparation of poly(methacryloyloxyethyl phosphate)$_3$-*block*-poly(acrylamide)$_{20}$ RAFT Polymer (RAFT-3MAPC2-20AAM) 60
3.5.3 Conjugation of Antibody to NWs and Dynabeads 60
3.5.4 Characterisation of iron oxide NWs 61
3.5.5 Cell culture and pre-enrichment of total EVs 62
3.5.6 Enrichment of PLAP+ve EVs by NWs and Dynabead 62
3.5.7 Nanoparticle tracking analysis 63
3.5.8 Quantification of PLAP and CD63 proteins from enriched EVs 63
3.5.9 Proteomic analysis 63
3.6 Results and discussion 65
3.6.1 Characterisation of iron oxide NWs 65
3.6.2 PLAP+ve EV enrichment performance 68
3.6.3 Proteomic analyses of PLAP+ve EVs enriched from BeWo cells 72
3.7 Conclusion 73
3.8 Supplementary figures 74
3.9 References 82
3.10 Appendix A 89
4 Immunomagnetic enrichment of human placental extracellular vesicles from unprocessed plasma with magnetic nanowires 93
4.1 Abstract 93
4.2 Introduction 93
4.3 Methods 96
4.3.1 Collection of plasma sample 96
4.3.2 Preparation of iron-oxide NWs 97
4.3.3 Synthesis of RAFT copolymers 97
4.3.4 Surface functionalisation of iron oxide NWs with RAFT copolymers 98
4.3.5 Preparation of PLAP antibody-functionalised iron oxide NWs 99
4.3.6 Preparation of antibody-functionalised Dynabeads 99
4.3.7 Nanowire characterisation 99
4.3.8 Cell culture for recovery studies 100
4.3.9 Preparation of PLAP+ve EV-spiked plasma 100
4.3.10 Dot blot assay 100
4.3.11 Direct immuno-enrichment of PLAP+ve EVs in plasma 101
4.3.12. Nanoparticle tracking analyses of immuno-enriched EVs 101
4.3.13. Protein biomarker quantification with ELISA 101
4.4 Results and discussion 102
4.4.1 Characterisation of iron oxide nanowires coated with mixed RAFT polymers 104
4.4.2 Binding performance in plasma 108
4.4.3 EV capture capability of iron oxide nanowire 110
4.4.4 Enrichment and quantification of PLAP+ve EV associated proteins in pregnancy plasma samples 113
4.5 Conclusion 116

4.6 References 118
5 Proteomic profiling of two placental extracellular vesicle subtypes sequentially enriched from maternal plasma after preeclampsia diagnosis 126
5.1 Abstract 126
5.2 Introduction 126
5.3 Methods 129
5.3.1 Plasma sample collection 129
5.3.2 Preparation of iron oxide NWs for the immuno-enrichment of EVs 129
5.3.3 Cell culture for the model EV enrichment study 130
5.3.4 Enrichment of total plasma EVs 130
5.3.5 Nanoparticle tracking analysis 130
5.3.6 Preparation of placental EV-spiked plasma for model study 131
5.3.7 Sequential enrichment of immuno-specific placental EVs from plasma 131
5.3.8 Quantification of PLAP and HLA-G proteins 132
5.3.9 Liquid chromatography tandem mass spectrometry 132
5.3.10 Label-free quantification of differentially expressed proteins 133
5.3.11 Statistics 133
5.4 Results and discussion 134
5.4.1 Enrichment and analysis of spiked plasma-derived placental EVs 134
5.4.2 Sequential enrichment of placental EVs from spiked plasma (containing PLAP+ve and HLA-G+ve EVs) 138
5.4.3 Sequential enrichment of PLAP+ve and HLA-G+ve EVs from a preeclamptic plasma sample 140
5.4.4 Placenta associated proteins enriched from NW-PLAP and NW-HLA-G preeclamptic plasma EVs 144
5.4.5 Comparative proteomic analyses of two-step enrichment and direct enrichment 149
5.5 Conclusion 154
5.6 References 156
6 Discussion of the research findings and future research recommendations 164
6.1 References 170

List of Figures

Figure 2-1 Biogenesis and secretion of various EV subtypes. 13
Figure 2-2 Molecular compositions of EVs. 15
Figure 2-3 Cellular structure of the placenta. 19
Figure 3-1 Surface modification of iron oxide NWs and enrichment of PLAP+ve EVs. 59
Figure 3-2 SEM images of (A) NW and (B) NW-*p*AAm. 66
Figure 3-3 XPS analyses of NW, NW-*p*AAm, and NW-IgG. 67
Figure 3-4 Optimisation of NW amount and enrichment time. 69
Figure 3-5 Recovery efficiency of PLAP and CD63 proteins. 71
Figure 3-6 Mass spectrometry analysis of BeWo EV proteins. 73
Figure 3-7 3D-printed magnetic separation rack. 74
Figure 3-8 DLS, TEM and magnetic characterisation of NWs. 75
Figure 3-9 SEM and DLS characterisation of Dynabeads. 76
Figure 3-10 NTA analysis of eluted EVs and their purity ratio. 77
Figure 3-11 PLAP and CD63 recovery quantification. 78
Figure 3-12 Proteins identified in 3 replicates of NW-PLAP and Dynabead-PLAP. 79
Figure 3-13 Gene ontology (GO) analyses of BeWo EV proteins. 80
Figure 4-1 Surface coating of NWs and direct EV enrichment procedure. 102
Figure 4-2 SEM, DLS and zeta potential characterisation of NWs. 105
Figure 4-3 FTIR and XPS characterisation of NWs. 107
Figure 4-4 Binding performance of dual and single coated NWs and Dynabead. 110
Figure 4-5 Effect of enrichment conditions on PLAP recovery. 111
Figure 4-6 NTA characterisation of eluted PLAP+ve EVs. 112
Figure 4-7 Protein concentrations of PLAP and CD63 proteins. 114
Figure 4-8 Percent protein recovery for NEP and PP13.. 115
Figure 4-9 Protein concentrations of NEP and PP13 proteins. 116
Figure 5-1 Experimental schematic for sequential immuno-enrichment of placental EV subtypes. 134
Figure 5-2 Enrichment and analysis of spiked plasma-derived placental EVs. 136
Figure 5-3 Cellular component ontology of identified proteins. 137
Figure 5-4 Tissue expression of identified proteins. 138
Figure 5-5 Recovery of PLAP and HLA-G measured by ELISA. 140

Figure 5-6 Mass spectrometry analysis of EVs sequentially enriched from the preeclamptic plasma sample. 142
Figure 5-7 Cellular component of identified proteins. 143
Figure 5-8 Tissue expression of identified proteins..... 144
Figure 5-9 Mass spectrometry analysis of EVs directly enriched from the preeclamptic plasma samples. 150
Figure 5-10 Comparison of contaminants between two-step and direct EV enrichment. 152
Figure 5-11 Comparative proteomic analyses of two-step and direct EV enrichment. 154

List of Tables

Table 2-1 Classification of EVs' biogenesis and mechanism of release 14
Table 2-2 Differentially expressed EV-derived proteins, miRNAs, and lipids in preeclampsia. 29
Table 3-1 Summary of XPS elemental and components 68
Table 3-2 Batch-to-batch validation of antibody conjugation to NWs 81
Table 4-1 Summary of XPS elemental composition and components 108
Table 5-1 Proteins (28) enriched by UC + NW-PLAP and identified as placenta and preeclampsia associated 146
Table 5-2 Proteins (28) enriched by UC + NW-HLA-G and identified as placenta and preeclampsia associated 148
Table 5-3 Proteins (15) directly enriched by NW-PLAP and identified as placenta and preeclampsia associated 150
Table 5-4 Proteins (9) directly enriched by NW-HLA-G and identified as placenta and preeclampsia associated 151

Glossary

AAM	Acrylamide
ATR-FTIR	Attenuated total reflectance Fourier-transform infrared spectroscopy
BCA assay	Bicinchoninic acid assay
BSA	Bovine serum albumin
DAVID	Database for annotation, visualization and integrated discovery
DLS	Dynamic light scattering
DPBS	Dulbecco's phosphate-buffered saline
EDC-HCl	1-Ethyl-3-(3-dimethylaminopropyl)carbodiimide hydrochloride
ELISA	Enzyme-linked immunosorbent assay
EOPE	Early onset preeclampsia
ESCRT	Endosomal sorting complexes required for transport
EV	Extracellular vesicle
EVTB	Extravillous trophoblast
FasL	Fas ligand
FBS	Fetal bovine serum
FE-SEM	Field emission scanning electron microscope
FDR	False discovery rate
GO	Gene ontology
HCD	Higher energy collision dissociation
HLA-G	Human leukocyte antigen G
IgG	Immunoglobulin G
ILV	Intraluminal vesicle
ISEV	International Society for Extracellular Vesicles
LC-MS/MS	Liquid chromatography-tandem mass spectrometry
LFQ	Label-free quantification
LOPE	Late onset preeclampsia
MAPC2	Methacryloyloxyethyl phosphate
MEM α	Minimum Essential Medium α
MES	2-(N-morpholino)ethanesulfonic acid
MHC Class I	histocompatibility class I
MISEV	Minimal Information for Studies of Extracellular Vesicles
MVB	Multivesicular body
MWCO	Molecular weight cut-offs
NEP	Neprilysin

NHS	N-hydroxysuccinimide
NK cell	Natural killer cell
NTA	Nanoparticle tracking analysis
NW	Nanowire
PE	Preeclampsia
PEO	Ethylene oxide
PEG	Polyethylene glycol
PHA	Phytohemagglutinin
PLAP	Placental alkaline phosphatase
PlGF	Placenta growth factor
PP13	Placental protein 13
PZP	Pregnancy zone protein
RAFT	Reversible addition-fragmentation chain transfer
RPMI	Roswell Park Memorial Institute media
SCTB	Syncytiotrophoblast
SEC	Size exclusion chromatography
sFlt-1	Soluble Fms-like tyrosine kinase-1
STBEV	Syncytiotrophoblast-derived EV
STBM	SCTB-derived microvesicle
TEM	Transmission electron microscope
TF	Transferrin
VCTB	Villous cytotrophoblast
VEGF	Vascular endothelial growth factor
XPS	X-ray photoelectron spectroscopy
UC	Ultracentrifugation

Summary

Preeclampsia is a pregnancy complication clinically characterised by high blood pressure and/or multi-organ dysfunction. Despite tremendous efforts to identify preeclampsia biomarkers, the heterogeneous nature of the disease as well as its elusive underlying causes (possibly involving both maternal and placental/fetal factors) have hampered the development of effective early prediction and diagnostic approaches. Due to their central role in mediating intercellular communication and several biological processes key to pregnancy, extracellular vesicles (EVs) have emerged as a promising source of biomarkers for many pathological conditions including preeclampsia. These nano- to micron-sized vesicles are naturally released by cells, including placental cells, and are known to carry various biomolecules (e.g. proteins and RNAs). Therefore, enrichment of EVs and profiling of their molecular cargoes using contemporary omics technologies (e.g. proteomics and transcriptomics) are strong potential to provide a better and more comprehensive understanding of the molecular mechanisms underpinning placental dysfunctions including preeclampsia, and consequently to facilitate prediction, diagnosis and prevention.

Towards addressing this need, this PhD thesis aimed to develop a method to efficiently enrich placenta-specific EV of specific cellular origins (EV subtype) and to develop and validate downstream proteomics towards profiling protein pathways potentially associated to preeclampsia. Magnetic iron oxide nanowires (NWs) were employed for the first time for the immuno-affinity enrichment of placental EVs derived from trophoblast cells in the maternal plasma. Experimentally, the surface of the magnetic NWs was modified using polymer specifically synthesised using reversible addition fragmentation chain transfer (RAFT) polymerisation to improve the biointerfacial properties and enable conjugation with anti-placental alkaline phosphatase (PLAP) and anti-human leukocyte antigen-G (HLA-G). These two antibodies were selected to specifically target PLAP and HLA-G proteins displayed on the membranes of EVs derived from syncytiotrophoblasts (SCTBs) and extravillous trophoblasts (EVTBs) placental cells, respectively.

This PhD project was initiated by establishing a novel magnetic immuno-enrichment protocol for PLAP+ve EVs using iron oxide NWs and investigating the compatibility of this protocol with downstream mass spectrometry analysis of the enriched EV proteins. The NWs were extracted and purified from the biofilms of zetaproteobacteria

Mariprofundus ferrooxydans provided by SA Water (South Australia) through an environmentally friendly process, yielding a cost-effective and highly scalable approach to obtain magnetic nanomaterials with extremely high surface area. The NWs were surface initially modified with a single poly(methacryloyloxyethyl phosphate)$_3$-*block*-poly(acrylamide)$_{20}$ RAFT polymer (RAFT-3MAPC2-20AAm) and further conjugated with anti-PLAP antibodies. After optimising the protocol, we demonstrated in model studies the utility of these NWs for the enrichment of PLAP+ve EVs from the total EVs of BeWo cells (trophoblast-like model cells), which were pre-enriched from cell culture media using ultracentrifugation. The enrichment performance of the NWs was demonstrated to be comparable with the current gold standard immune-magnetic beads, Dynabead in terms of recovery of PLAP protein, high particle-to-protein ratio and low non-specific binding of non-target EVs. Building on this efficient EV enrichment protocol, we then optimised an analytical pathway for downstream liquid chromatography-tandem mass spectrometry (LC-MS/MS) analysis. The pathway was validated using the BeWo cell-EV model, yielding a high number of identified proteins with excellent reproducibility.

In the second part of the project, we endeavoured to adapt the developed protocol to enable direct enrichment of PLAP+ve EVs from plasma samples of preeclamptic pregnancies. Instead of using the previous single RAFT polymer and towards improving the biointerfacial properties of the magnetic NWs, we modified the surface of NWs with two RAFT polymers, namely poly(methacryloyloxyethyl phosphate)$_5$-*block*-poly(acrylamide)$_{15}$-*block*-poly(ethylene oxide)$_3$ **(**RAFT-5MAPC2-15AAM-3PEO) and poly(methacryloyloxyethyl phosphate)$_5$-*block*-poly(acrylamide)$_{70}$ (RAFT-5MAPC2-70AAM). We demonstrated that this dual polymer coating improved the performance of the NWs in the complex condition of plasma compared to the single polymer coating used initially. This mixed polymer coating also outperformed the surface chemistry pre-defined for gold-standard Dynabeads. Specifically, the dual polymer coating improved the enrichment of PLAP+ve EVs from plasma 1.7 fold based on PLAP recovery compared to Dynabeads (normalised to the same amount of magnetic materials). We further demonstrated the feasibility of direct EV enrichment using the NWs in two preeclamptic plasma samples and a matched healthy control. In this study, we demonstrated not only the enrichment of specific target PLAP+ve EVs but also the feasibility of quantifying Neprilysin and Placental Protein 13, two proteins known

reported to associate with PLAP+ve EVs and to have pathological links with preeclampsia.

In the last part of the project, we explored the potential of the magnetic NWs for the specific enrichment of two placental EV subtypes, PLAP+ve and HLA-G+ve EVs. We first tested immune-enrichment using NW-PLAP and NW-HLA-G in combination with a standard EV pre-enrichment step, ultracentrifugation, aimed at obtaining the total EV of the plasma sample. Using an EV-spiked plasma model, we first demonstrated that the magnetic NWs could enrich PLAP+ve EVs from the total EVs pre-enriched from ultracentrifuged plasma. This yielded highly pure placenta-specific EVs for LC-MS/MS analysis and high numbers of placenta-relevant proteins were identified with excellent reproducibility. We then, for the first time, successfully employed the NW system for the sequential enrichment of PLAP+ve and HLA-G+ve EVs from a single plasma sample (500 µL). This approach yielded similar EV enrichment efficiency as compared to separate/parallel enrichment for these two EV subtypes. A key aspect of this novel approach is that it could be beneficial when investigating biobanked plasma samples where only limited volumes are available, which was our original motivation for testing this approach. Next, we applied this sequential approach to enrich the two placental PLAP+ve and HLA-G+ve EV subtypes in a representative plasma sample from a pregnancy with clinically confirmed preeclampsia. This demonstrated the recovery of placental cell-specific EV proteins (i.e. SCTB- and EVTB-specific) identified by LC-MS/MS, many of which were found to associate with preeclampsia when cross-referenced with previous publications. Given the potential of the dual polymers coated NWs for direct enrichment of plasma-derived placental EVs, we also compare the protein profiles of the two placental EV subtypes sequentially enriched by the standard two-step (with total EV pre-enrichment) and direct enrichment methods. Despite showing increasing binding of non-specific plasma proteins, direct enrichment still yielded recovery of placenta-specific and preeclampsia-associated proteins. Although further optimisations and investigations are warranted in a larger sample scale, direct enrichment of placental EV subtypes from maternal plasma is a promising tool for mass spectrometry-based profiling of EV proteins considering the small sample volume required (100 µL) and short EV enrichment process (1.5 h).

Looking forward, the magnetic NWs and methodologies developed and validated during this PhD project for the enrichment of placenta-specific EVs from maternal plasma and

downstream mass spectrometry analysis have significant potential to advance the understanding of preeclampsia and other placental insufficiency complications of pregnancy and, as a result, to support the development of much needed risk-stratification strategies for these common conditions.

Declaration

This thesis presents work carried out by myself and does not incorporate without acknowledgement any material previously submitted for a degree or diploma in any university; to the best of my knowledge it does not contain any materials previously published or written by another person except where due reference is made in the text; and all substantive contributions by others to the work presented, including jointly authored publications, are clearly acknowledged.



Quang Nghia Pham
September 2022

Acknowledgements

First and foremost I would like to express my deep gratitude to my principal supervisor, Professor Benjamin Thierry, for his invaluable guidance and constant support throughout my PhD journey from inception to completion. I also would like to thank my co-supervisor, Dr Marnie Winter, for her patience and generous time in helping me develop experimental plans for my PhD project.

I would like to thank my REPL, Dr Zlatko Kopecki, for his constant help in preparing relevant documents as well as the extension of my PhD course. I am also grateful to all members of the Bionanoengineering group (Future Industries Institute, University of South Australia) for their help and motivations, especially Dr Duy Tran for his valuable advice and encouragement, Dr Valentina Milanova for her guidance on developing chemical surface modification, Mr Edward Cheah for his help fabricating the magnetic separation rack for my experiment, and Mr Luke Bredberge for sharing difficulties I experience during my PhD.

I place on record, my sincere thanks to Professor Peter Hoffmann, Dr Mark R. Condina and Dr Clifford Young (Clinical and Health Sciences, University of South Australia) for providing me with access to the mass spectrometry facilities, developing the methodology for proteomics, and interpreting proteomic data.

I take this opportunity to express gratitude to Professor Dusan Losic, Dr Tran Thanh Tung and Mr Trong Tuan Anh Tran (School of Chemical Engineering and Advanced Materials, The University of Adelaide) for providing me with iron oxide nanowires and opportunities to characterise nanowires with Fourier-transform infrared spectroscopy. I also would like to acknowledge Dr Nguyen T. H. Pham (School of Chemistry, The University of Sydney) for providing me with the polymers for surface modification of nanowires as well as staff and patients at the Women's and Children's Hospital (Adelaide) and Clinpath Laboratories for providing plasma samples.

I would like to sincerely thank Professor Claire Roberts (Flinders University), who was my mentor as part of the Healthy Development Adelaide Research Training Program during my candidature. Her invaluable guidance on career development and academic research has not only expanded my knowledge but also shaped my career path.

Getting through my dissertation required more than academic support, thus I would like to express my gratitude to the technical team at Future Industries Institute for providing technical training and assistance, especially Dr Nobuyuki Kawashima, Dr Patrick Sherman, Dr John Denman, Dr Christopher Bassell and Dr Alex-Anthony Cavallaro. I would also like to show gratitude to the Australian National Fabrication Facility (South Australia Node) for giving me a chance to learn and have hands-on experience in microfabrication of microfluidics in the clean room.

I also place on record, my sense of gratitude and honour to receive the financial aid from the Research Training Program (RTP) scholarships funded by the Australian Government and from the PhD Excellence Award funded by the Healthy Development Adelaide and Channel 7 Children's Research Foundation, which constantly support me to make this work possible.

Finally, I would like to express my very profound gratitude to my parents, my younger sister as well as my friends for their constant encouragement, which did help motivate me throughout my years of doing PhD and living in Australia regardless of the distance, without which this accomplishment would not have been realised.

Thank you!

Chapter 1

Introduction

1 Introduction

Preeclampsia is one of the most common placental disorders, occurring in approximately 8% of pregnant women[1,2]. Critically, it is a leading cause of maternal and fetal morbidity and mortality globally.[1,2] The significant incidence of preeclampsia together with its long-term consequences has driven research aimed at investigating its molecular causes as well as novel diagnostic and therapeutic approaches. Despite this intense research effort, the precise molecular mechanisms of preeclampsia and more generally placental dysfunction still remains ill-defined. Therefore, improving the molecular understanding of the disease would assist in the development of better diagnostic approaches and, potentially, treatments. This demand leads to the search for predictive biomarkers (e.g. proteins and RNAs) for preeclampsia, which either freely circulate in the maternal plasma or associate with extracellular vesicles (EVs). While plasma-derived biomarkers circulating in maternal blood have been actively investigated for the prediction of preeclampsia, current methods for detecting these biomarkers have several limitations. One major challenge is that some biomarkers may be present in low concentrations in plasma, which can hinder accurate detection.[3,4] In addition, interference from background noise and other contaminants in plasma samples can further complicate detection.[5] Moreover, there can be variability in biomarker levels both between individuals and within an individual over time, making it difficult to establish consistent diagnostic thresholds.[6,7] These limitations must be addressed in order to develop accurate and reliable diagnostic tools for the detection of plasma-derived biomarkers. In this regards, EV-derived markers are promising alternatives since they are better protected from degradation by extracellular enzymes and likely offer a more targeted insight into placental/maternal cellular metabolisms and dysfunctions due to their specific biological biogenesis.

Secreted by many cell types under both physiological and pathological conditions, EVs are membrane-bound cargos capable of carrying signalling molecules. EVs are now known to play important roles in intercellular communication. The placenta produces a diverse pool of EVs due to its cellular heterogeneity.[3] These placental EVs serve as signal carriers that maintain the communication between the fetus and mother as well as regulate many immunological mechanisms in pregnancy by interacting with immune cells and endothelial cells.[4] Therefore, abnormal EV secretion could signify pathological changes in the placenta including in preeclampsia. In fact, EVs can act as molecular harbingers of alterations in molecular communication at the fetal-maternal interface.[5] These changes

can result in elevated proinflammatory effects or apoptosis of trophoblastic cells, cumulatively contributing to placental dysfunction in conditions such as preeclampsia.[2] Therefore, investigating changes in the number of placental EVs together with changes in their biological cargos could help to elucidate the molecular differences between normal and preeclamptic pregnancies. More broadly, placental EVs may provide novel and non-invasive insights into the health of the placenta and hence pregnancy.

The enrichment of EVs from body fluids is an essential step to analyse their molecular content. In many cases, EVs are enriched based on their physicochemical properties (i.e. density and size) using ultracentrifugation and size exclusion chromatography.[8] Alternatively, EVs can be enriched according to the surface proteins on their lipid membrane using immunoaffinity approaches. These methods usually involve the conjugation of antibodies onto magnetic materials to immunologically enrich specific subtypes of EVs. Immuno-magnetic enrichment therefore produces isolates of EVs with low contamination rates in a rapid and efficient manner,[9-12] thus offering a suitable approach e.g. proteomic and transcriptomic analyses of EVs. Among different magnetic materials investigated for immuno-magnetic EV enrichment, iron oxide nanowires (NWs) stand out as a promising candidate having a high surface area for efficient capture of target EVs and strong magnetic strength for efficient magnetic recovery.[13] However, the production of previously reported magnetic NWs for the enrichment of EVs is low-throughput and often requires complex synthesis route, which hampers their routine use. Towards an efficient, simple, cost-effective and scalable method for EV subtype immuno-enrichment, herein we present a novel approach using magnetic NWs obtained from bacterial biofilm. These naturally occurring NWs are coated with polymers designed to enable antibody conjugation and improve target EV recovery. This novel EV enrichment approach is shown in this thesis to be compatible with multiple downstream analysis methods including proteomics with mass spectrometry.

As noted above, placental EVs likely offer specific important non-invasive insights into placental health. Due to the complexity of plasma, the enrichment of placental EVs from maternal blood is challenging as they generally are present in low abundance (~0.5−20% of the total plasma EVs),[14,15] and their identification is confounded by the dominance of several high abundant proteins such as albumin and immunoglobulins.[16] For this reason, plasma samples are usually pre-processed, for example, by ultracentrifugation or size exclusion chromatography, from which placental EVs are eventually subsequently

immuno-enriched.[17-19] Such two-step enrichment process may result in the loss of low abundant EVs, especially in the case where the sample source is limited. In addition, the time and resource intensive nature of plasma pre-processing methods has been a limiting factor in the development and translation of cell-type specific EV diagnostics. Therefore, a direct yet efficient immuno-enrichment method with minimal sample preparation is desirable to simplify the enrichment process of placental EVs. For this reason, we explored the potential of magnetic NWs for single-step immuno-enrichment of placental EVs from maternal plasma.

Proteomic profiling of EV-specific placental cells is a promising approach to understand the dysfunction mechanisms underlying preeclampsia and towards early prediction of this placental dysfunction. While proteomic profiling of pregnancy-associated EVs compared between preeclampsia and normal pregnancy has been performed on plasma,[16,20,21] umbilical cord blood[22] and placental villous explants,[23] most of these studies analyse the protein profiles of the total EVs with an exception for EVs from placental explants which were established from the villous tissues of the syncytiotrophoblast. Although the enrichments of EVs specific to placental cells including syncytiotrophoblast (EVs expressing Placental Alkaline Phosphatase (PLAP) on their membrane, PLAP+ve EVs) and extravillous trophoblast (EVs expressing Human Leukocyte Antigen-G, HLA-G+ve EVs) have been reported previously,[19,24-26] quantitative proteomic profiling of these two immuno-specific placental EVs has not been demonstrated. This PhD research project for the first time reports the proteomic comparison of two immuno-specific placental EVs, PLAP+ve and HLA-G+ve EVs sequentially enriched from a single plasma source of third-trimester preeclamptic pregnancies.

1.1 Hypotheses and research aims of thesis

The overarching objective of this research project was to develop an efficient enrichment methodology for placental EVs from maternal plasma and to apply this method for downstream proteomics, therefore enabling the investigation of placental EV protein profiles. For this purpose, the three main research hypotheses and aims of this PhD thesis were:

1) Hypothesis: Immuno-magnetic enrichment of placental EVs using iron oxide NWs will facilitate a selective and efficient capture of placental EVs, thereby allowing for effective mass spectrometry analysis of EV proteins.

Aim: Develop and implement a novel immuno-magnetic enrichment for placental EVs for downstream mass spectrometry analysis of EV proteins using iron oxide NWs extracted from natural bacterial biofilms.

2) Hypothesis: Single-step direct enrichment of placental EVs from maternal plasma using iron oxide NWs will provide a rapid and efficient method for EV subtype protein quantification.

   Aims: Investigate the potential bacteria-derived NWs for the single-step direct enrichment of PLAP+ve EVs from maternal plasma for placental EV specific protein quantification.

3) Hypothesis: Sequential enrichment of two placental EV subtypes will provide a non-invasive means of gaining insights into the molecular mechanisms underlying both the placenta and preeclampsia.

   Aim: Investigate the potential of bacteria-derived NWs for the enrichment and proteomic analysis of two key placental EV subtypes in maternal plasma.

1.2 Thesis structure

This thesis is entitled 'Enrichment and proteomic analysis of placenta-specific extracellular vesicles towards non-invasive diagnosis of preeclampsia' The thesis is composed of 6 chapters presented in the format of a 'thesis with publications': Chapter 1: Introduction; Chapter 2: Literature review; Chapter 3-5: Results chapters, which are self-contained with their own introduction, methods, results/discussion and conclusion; Chapter 6: Conclusion and perspective.

Chapter 1 is an introduction to the thesis, specifying the overall research aims and outlining the thesis structure as well as the thesis outcomes.

Chapter 2 reviews the relevant literature regarding EVs, preeclampsia, enrichment of placental EVs and their pathological link to preeclampsia.

Chapter 3 is entitled "Magnetic enrichment of immuno-specific extracellular vesicles for mass spectrometry using biofilm-derived iron oxide nanowires". In this study, we reported an optimised protocol for immuno-magnetic enrichment of specific EV subtypes and their subsequent processing with liquid chromatography-tandem mass spectrometry.

Chapter 4 is entitled “Immunomagnetic enrichment of human placental extracellular vesicles from unprocessed plasma with magnetic nanowires”. In this chapter, we report a direct immuno-enrichment method for PLAP+ve EVs from maternal plasma using naturally occurring bacterial biofilm-derived iron oxide NWs and demonstrate the quantification of proteins associated with PLAP+ve EVs relevant to preeclampsia.

Chapter 5 is entitled “Proteomic profiling of two placental extracellular vesicle subtypes sequentially enriched from maternal plasma after preeclampsia diagnosis”. This chapter reports the proteomic profiling of two placenta-specific EV subtypes derived from syncytiotrophoblast (PLAP+ve EVs) and extravillous trophoblast (HLA-G+ve EVs) sequentially enriched from a single plasma source of a preeclamptic patient.

Chapter 6 discusses the overall outcomes of this PhD project and outlines possible future work.

1.3 Thesis outcomes

The results chapters of this PhD project are anticipated to be published as three first author research papers. The details and status of these outcomes are as follow:

1) Quang Nghia Pham, Marnie Winter, Valentina Milanova, Clifford Young, Mark R. Condina, Peter Hoffmann, Nguyen T. H. Pham, Tran Thanh Tung, Dusan Losic, Benjamin Thierry. Magnetic Enrichment of Immuno-Specific Extracellular Vesicles for Mass Spectrometry Using Biofilm-Derived Iron Oxide Nanowires. *Nanoscale*, 2023, 15, 1236-1247

2) Quang Nghia Pham, Marnie Winter, Valentina Milanova, Clifford Young, Mark R. Condina, Peter Hoffmann, Nguyen T. H. Pham, Tran Thanh Tung, Dusan Losic, Benjamin Thierry. Direct Enrichment of Placental Extracellular Vesicles: A Rapid and Improved Tool for Preeclampsia Diagnosis? *In preparation*.

3) Quang Nghia Pham, Marnie Winter, Valentina Milanova, Clifford Young, Mark R. Condina, Peter Hoffmann, Nguyen T. H. Pham, Tran Thanh Tung, Dusan Losic, Benjamin Thierry. Proteomic Profiling of Two Placental Extracellular Vesicle Subtypes Sequentially Enriched from Plasma after Preeclampsia Diagnosis. *In preparation*.

In addition, this research was presented at the following conferences:

1) 12th International Nanomedicine Conference, Sydney, Australia, 2022, poster presentation titled: *Magnetic Enrichment of Immuno-Specific Extracellular Vesicles for Mass Spectrometry Using Biofilm-Derived Iron Oxide Nanowires.*

2) Selected for an oral presentation at Australian and New Zealand Society for Extracellular Vesicles (ANZSEV) 2022, Gold Coast, Australia 2022. Presentation titled: *Immunomagnetic enrichment and proteomics of placental extracellular vesicles subtypes: Towards non-invasive insights into placental health and disease.*

3) Invited presentation: ANZPRA mini symposium – Into the future: New Technologies and Techniques in Placenta Research. *Title: Bioengineering in pregnancy: From liquid biopsy to organs-on-chips* (presented by supervisor Dr Marnie Winter, detailing my PhD research).

1.4 References

1 Palmer, K. R. & Tong, S. Accurately Predicting the Risk of Serious Maternal Morbidity in Preterm Preeclampsia: Can It Be Done? *Hypertension* **71**, 569-571, doi:10.1161/HYPERTENSIONAHA.117.10442 (2018).

2 Karrar, S. A. & Hong, P. L. in *StatPearls* (2022).

3 Kim, K. *et al.* Clinically accurate diagnosis of Alzheimer's disease via multiplexed sensing of core biomarkers in human plasma. *Nat Commun* **11**, 119, doi:10.1038/s41467-019-13901-z (2020).

4 Qian, W. J., Jacobs, J. M., Liu, T., Camp, D. G., 2nd & Smith, R. D. Advances and challenges in liquid chromatography-mass spectrometry-based proteomics profiling for clinical applications. *Mol Cell Proteomics* **5**, 1727-1744, doi:10.1074/mcp.M600162-MCP200 (2006).

5 Ray, S. *et al.* Proteomic technologies for the identification of disease biomarkers in serum: advances and challenges ahead. *Proteomics* **11**, 2139-2161, doi:10.1002/pmic.201000460 (2011).

6 Thyagarajan, B. *et al.* Analytical and biological variability in biomarker measurement in the Hispanic Community Health Study/Study of Latinos. *Clin Chim Acta* **463**, 129-137, doi:10.1016/j.cca.2016.10.019 (2016).

7 Newman, L. A. *et al.* Importance of between and within Subject Variability in Extracellular Vesicle Abundance and Cargo when Performing Biomarker Analyses. *Cells* **10**, doi:10.3390/cells10030485 (2021).

8 Brennan, K. *et al.* A comparison of methods for the isolation and separation of extracellular vesicles from protein and lipid particles in human serum. *Sci Rep* **10**, 1039, doi:10.1038/s41598-020-57497-7 (2020).

9 Singh, K. *et al.* Separation of distinct exosome subpopulations: isolation and characterization approaches and their associated challenges. *Analyst* **146**, 3731-3749, doi:10.1039/d1an00024a (2021).

10 Rosi, N. L. & Mirkin, C. A. Nanostructures in biodiagnostics. *Chem Rev* **105**, 1547-1562, doi:10.1021/cr030067f (2005).

11 Gudbergsson, J. M., Johnsen, K. B., Skov, M. N. & Duroux, M. Systematic review of factors influencing extracellular vesicle yield from cell cultures. *Cytotechnology* **68**, 579-592, doi:10.1007/s10616-015-9913-6 (2016).

12 Yang, D. *et al.* Progress, opportunity, and perspective on exosome isolation - efforts for efficient exosome-based theranostics. *Theranostics* **10**, 3684-3707, doi:10.7150/thno.41580 (2020).

13 Takahashi, H., Baba, Y. & Yasui, T. Oxide nanowire microfluidics addressing previously-unattainable analytical methods for biomolecules towards liquid biopsy. *Chem Commun (Camb)* **57**, 13234-13245, doi:10.1039/d1cc05096f (2021).

14 Sadovsky, Y. *et al.* Placental small extracellular vesicles: Current questions and investigative opportunities. *Placenta* **102**, 34-38, doi:10.1016/j.placenta.2020.03.002 (2020).

15 Tannetta, D., Collett, G., Vatish, M., Redman, C. & Sargent, I. Syncytiotrophoblast extracellular vesicles - Circulating biopsies reflecting placental health. *Placenta* **52**, 134-138, doi:10.1016/j.placenta.2016.11.008 (2017).

16 Tan, K. H. *et al.* Plasma biomarker discovery in preeclampsia using a novel differential isolation technology for circulating extracellular vesicles. *Am J Obstet Gynecol* **211**, 380 e381-313, doi:10.1016/j.ajog.2014.03.038 (2014).

17 Nogueras-Ortiz, C. J. *et al.* Astrocyte- and Neuron-Derived Extracellular Vesicles from Alzheimer's Disease Patients Effect Complement-Mediated Neurotoxicity. *Cells* **9**, doi:10.3390/cells9071618 (2020).

18 Sharma, P., Diergaarde, B., Ferrone, S., Kirkwood, J. M. & Whiteside, T. L. Melanoma cell-derived exosomes in plasma of melanoma patients suppress functions of immune effector cells. *Sci Rep* **10**, 92, doi:10.1038/s41598-019-56542-4 (2020).

19 Menon, R. *et al.* Protein Profile Changes in Circulating Placental Extracellular Vesicles in Term and Preterm Births: A Longitudinal Study. *Endocrinology* **161**, doi:10.1210/endocr/bqaa009 (2020).

20 McElrath, T. F. *et al.* Late first trimester circulating microparticle proteins predict the risk of preeclampsia < 35 weeks and suggest phenotypic differences among affected cases. *Sci Rep* **10**, 17353, doi:10.1038/s41598-020-74078-w (2020).

21 Navajas, R. *et al.* Quantitative proteomic analysis of serum-purified exosomes identifies putative pre-eclampsia-associated biomarkers. *Clin Proteomics* **19**, 5, doi:10.1186/s12014-022-09342-4 (2022).

22 Jia, R. *et al.* Comparative Proteomic Profile of the Human Umbilical Cord Blood Exosomes between Normal and Preeclampsia Pregnancies with High-Resolution Mass Spectrometry. *Cell Physiol Biochem* **36**, 2299-2306, doi:10.1159/000430193 (2015).

23 Baig, S. *et al.* Proteomic analysis of human placental syncytiotrophoblast microvesicles in preeclampsia. *Clin Proteomics* **11**, 40, doi:10.1186/1559-0275-11-40 (2014).

24 Sabapatha, A., Gercel-Taylor, C. & Taylor, D. D. Specific isolation of placenta-derived exosomes from the circulation of pregnant women and their immunoregulatory consequences. *Am J Reprod Immunol* **56**, 345-355, doi:10.1111/j.1600-0897.2006.00435.x (2006).

25 Lai, A., Elfeky, O., Rice, G. E. & Salomon, C. Optimized Specific Isolation of Placenta-Derived Exosomes from Maternal Circulation. *Methods Mol Biol* **1710**, 131-138, doi:10.1007/978-1-4939-7498-6_10 (2018).

26 Fitzgerald, W., Gomez-Lopez, N., Erez, O., Romero, R. & Margolis, L. Extracellular vesicles generated by placental tissues ex vivo: A transport system for immune mediators and growth factors. *Am J Reprod Immunol* **80**, e12860, doi:10.1111/aji.12860 (2018).

Chapter 2

Literature Review

2 Literature review

2.1 Extracellular vesicles: classification, biogenesis, and molecular composition

The presence of extracellular vesicles (EVs) was first reported in bovine serum in the mid-1970s.[1] Since then, research on EVs has been continuously expanding, focusing not only on the biological and functional roles of EVs but also on their therapeutic and diagnostic applications.[2-7] EVs are a heterogenous group of phospholipid bilayer membrane-enclosed particles generated from cells through different mechanisms. They can be enriched from a wide range of physiological fluids including culture media of mammalian and prokaryotic cells, blood plasma, saliva, amniotic fluid, urine, etc.[8-11] EVs carry various biomolecules (nucleic acids, proteins, lipids and different metabolites) that generally reflect the origin and phenotypic status of their parental cells and are also involved in intercellular communication amongst cells and tissues.[12-15] EVs are increasingly recognised for their key roles in regulating normal physiological cellular functions and predicting the pathological development of several diseases.[13,16-18]

2.1.1 Classification and Biogenesis of EVs

The classification of EVs has been continuously revised and updated by the International Society for Extracellular Vesicles (ISEV). Although size-based classification slightly varies among studies, EVs can be generally categorised into small (< 200 nm) and large EVs (> 200 nm) according to Minimal Information for Studies of Extracellular Vesicles (MISEV) 2018.[19] These two EV categories can be further classified into exomeres, exosomes, ectosomes or shedding microvesicles, migrasomes and apoptotic bodies (Figure 2-1 and Table 2-1).[20-23] Besides size, EVs can also be categorised based on a defined range of density (low, middle or high) or their specific proteins (CD9+ve, CD63+ve, CD81+ve, etc.).[24] The mechanism underlying biogenesis and secretion of each EV subtype is complex and is being continuously studied and updated.[23]

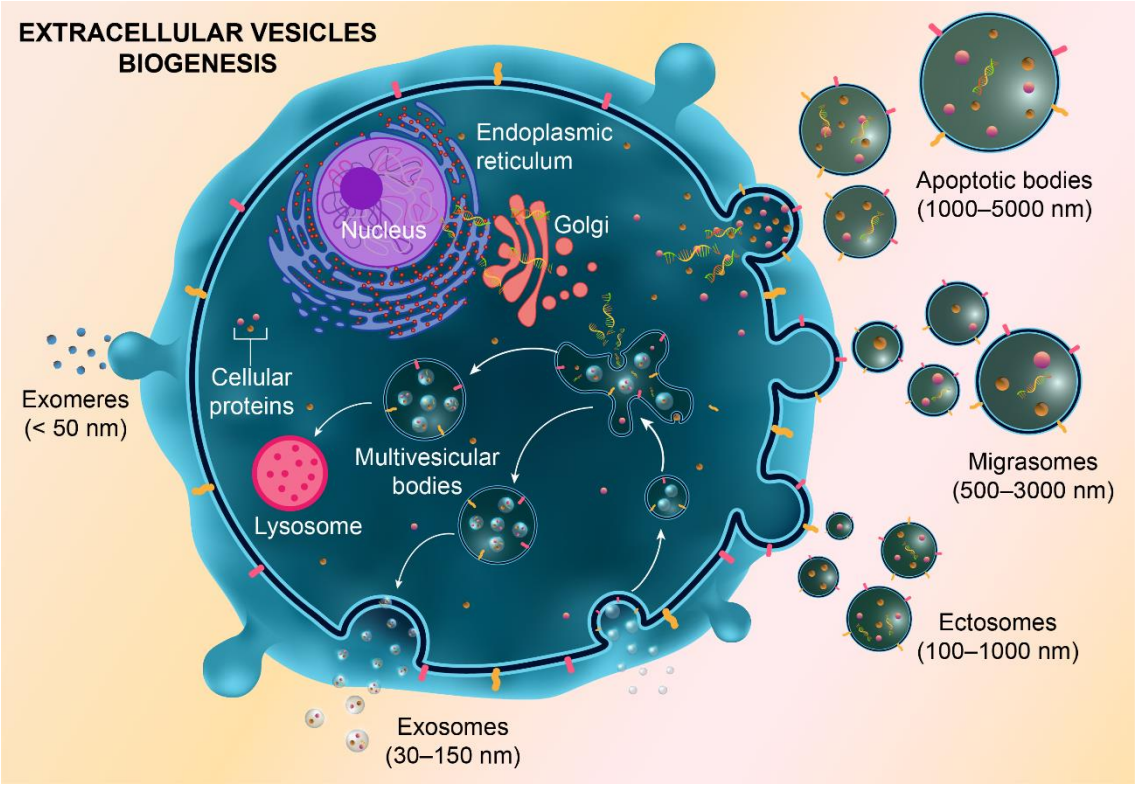

Figure 2-1 Biogenesis and secretion of various EV subtypes.
Figure was created using Adobe Illustrator v27.4.

Among the different EV subtypes, exosomes have received the greatest interest and are the most commonly studied. Exosomes are formed through the endosomal pathway which initiates with the invagination of the plasma membrane (endocytosis) to form early endosomes containing membrane proteins and/or soluble molecules in the extracellular space. These early endosomes then mature and fuse with the pre-existing early endosomes to form late endosomes or multivesicular bodies (MVBs), the invagination of which results in the formation of intraluminal vesicles (ILVs).[23,25] These MVBs function as specialised endosomes where packaging, recycling and transport of molecules processed by the endoplasmic reticulum or Golgi apparatus and cytosolic molecules in the cellular matrix into intraluminal vesicles take place.[26] MVBs can either combine with lysosomes, resulting in the degradation of the inner contents,[27,28] or combine with the plasma membrane, resulting in the secretion of ILVs (i.e exosomes) into the extracellular space. Although the trafficking mechanisms of MVBs are not fully understood, evidence suggests that these degradation or exocytosis processes involve Rab GTPases, the most abundant protein family of small GTPase.[29,30] Cargo packaging and secretion of ILVs are mainly regulated by the endosomal sorting complexes required for transport (ESCRT) machinery.[31,32]

Table 2-1 Classification of EVs' biogenesis and mechanism of release

EV types	Size (nm)	Biogenesis	Mechanism of release / Characteristics
Exomere	< 50	Unknown	First enriched from Argonaute 1-3 and amyloid precursor proteins with distinct functions.[33]
Exosome	30–150	Endosomal pathway; Fusion of MVBs	Cargo sorting is mainly ESCRT-dependant but has recently been reported to be also ESCRT-independent
Ectosomes (Shedding microvesicles)	100–1000	Outward budding of the plasma membrane	Budding requires the disassembly of the actin cytoskeleton and actomyosin-based membrane abscission, induced by the increase of cytosolic Ca^{2+}, activation of enzymes degrading cytoskeleton components and externalisation of phosphatidylserines.[34-36] Once discharged, ectosomes can release their cargo or endocytosed by target cells to induce phenotypic changes.[37]
Migrasome	500–3000	Possibly by the disintegration of retraction fibres (migracytosis)	Generation may involve proteins regulating the interactions between cells and the extracellular matrix.[38]
Apoptotic body	1000–5000	Disassembly of apoptotic cells	Formation of apoptotic bodies is important in the clearance of cell debris and the protection of healthy cells from cytotoxic substances and degrading enzymes.[39-41] Contents released from apoptotic bodies can also be delivered to healthy recipient cells to regulate intercellular communication.[42]

2.1.2 Molecular composition of EVs

Owing to their bilipid membrane, EVs function as natural delivery cargoes which not only encapsulate and transport a diverse range of biological molecules but also protect these molecules from the degradation by extracellular enzymes (proteases, nucleases).[43-45] In general, EVs contain membrane and cytoplasmic proteins, lipid raft complexes,

nucleic acids (DNA, RNA, mRNA), metabolites and enzymes (Figure 2-2). The loading composition of EVs is determined by cell type, mode of biogenesis, and physiological/pathological conditions of parental cells, which suggests that EVs of different subtypes carry vesicle-specific in addition to shared molecules.[43]

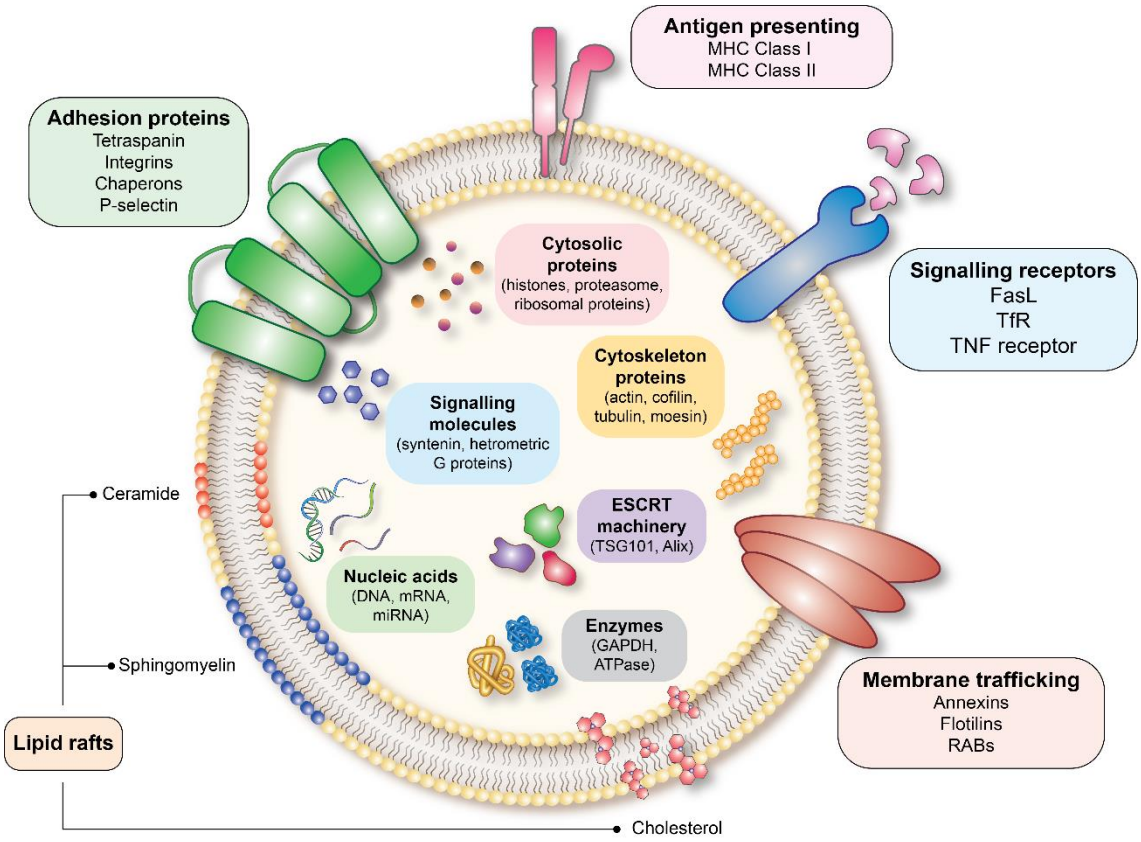

Figure 2-2 Molecular compositions of EVs.
Figure was created using Adobe Illustrator v27.4.

The protein composition of EVs has been comprehensively studied, identifying various proteins with different functions as well as of diagnostic and prognostic potentials. Tetraspanins (CD9, CD63, CD81) are membrane proteins widely reported to be enriched in EVs with approximately five copies of any of tetraspanins presenting on one EV and two out of three tetraspanins coexpressed on 30% of EVs.[46,47] Common proteins that are shared among EVs are tetraspanins (CD9, CD63, CD81), signalling receptor proteins (LAMP1, TfR), antigen-presenting molecules (MHC Class I and II), ESCRT proteins (TSG101, Alix), heat shock chaperones (Hsc70, Hsp90), cytoskeleton proteins (actin, tubulin, etc.), and metabolic enzymes.[43,48,49] While exosomes are mostly enriched with ESCRT proteins, shedding microvesicles are enriched with abundant membrane proteins and post-translationally modified proteins (glycoproteins and phosphoproteins). Apoptotic bodies tend to carry high amounts of proteins associated with subcellular

fragments such as nucleus (histones), mitochondria, Golgi apparatus and endoplasmic reticulum (Grp94).[49,50] It is noted that different EV proteomic profiles have been reported among studies due to different techniques used for EV isolation and characterisation.[51] In addition, a set of protein markers rather than a single marker is usually used to determine enriched EV types. However, it is important to note that a consensus of specific protein markers which definitively identifies EV subtypes is not currently established.[43,50]

A diverse range of nucleic acids is carried by EVs. Various types of DNA with different distributions are found to associate with almost all types of EVs, including genomic and mitochondrial DNA.[52,53] As well as DNA, RNA molecules are also carried by EVs with many coding and non-coding variants (sncRNAs, mRNAs, rRNAs, lncRNAs and miRNA).[54,55] Presenting in ng/mL concentrations, most EV-derived RNA exist as fragments predominantly in the size range of 20–200 nucleotides, however, larger RNA can also be carried and are generally enclosed in EVs or bound to protein complexes associated with EVs.[46,56] Approximately 50% of plasma-derived circulating RNA is carried by EVs.[57] Of the various RNA types that can be found in EVs, miRNAs have been the most widely studied due to their ability to modulate gene expression post-transcriptionally and their promise as disease biomarkers.[58,59] miRNAs have been shown to be functional when carried by EVs in both *in vitro* and *in vivo* disease models.[60-63]

Emerging later than proteins and RNAs, the lipid composition of EVs has been recently uncovered with hundreds of lipid molecules discovered so far.[46] Among them, EV-derived lipids mainly originate from the lipid-based formations (cholesterol, sphingomyelin and phosphatidylserine) constructing the membranes of EVs.[64-67] In addition to these lipid raft components, EVs are capable of transporting other bioactive lipids (eicosanoids, fatty acids), possibly inducing changes in the immunity and metabolism of the target cells.[64,66,67] EV lipid compositions are characteristic from the cell they are derived from.[68] Moreover, despite sharing lipid content with the parent cell, EVs also encapsulate unique lipid derivatives which possibly facilitate EV membrane properties (fluidity, curvature) and allow EV trafficking in the donor and recipient cell.[43,69]

2.1.3 Physiological and pathological relevance of EVs

The physiological and pathological functions of EVs result from their diverse composition and capacity to mediate intercellular communication throughout the body.

Different biological effects induced by EVs have been reported in various bodily fluids. For example in blood, the largest EV population produced by platelets (~25% of total blood EVs) enhances the procoagulant activity, thus playing an important role in haemostasis.[70,71] EVs enriched from human cerebrospinal fluid have been reported to control synaptic-plasticity activity, myelination, and neuroprotective inflammation.[72,73] In urine, EVs function to remove senescent cellular proteins and lipids, regulate trafficking of AQP2 protein to control the water permeability of nephrons in kidneys, and participate in the host defence system as immune effectors in the urinary tract.[74-76] EVs have been also demonstrated to promote vascular repair and tissue regeneration, enhance mineralisation in bone formation, and mediate pro-inflammation in the innate immune system.[1,77,78]

Advances in proteomics, transcriptomics and metabolomics/lipidomics have discovered several EV-derived protein, RNA, and lipid biomarker candidates for cancer, cardiovascular disease, neurodegenerative diseases, autoimmune disorders and pregnancy complications.[79] The discovery of these markers not only provides insights into the mechanisms of the pathological conditions but also assists in the development of prediction strategies and potentially therapeutic treatments of the diseases. Compared to healthy controls, most pathological conditions coincide with abnormal changes in the number of EVs and/or dysregulations of selective EV-derived protein, RNA, or lipid molecules.[80-84] EVs are increasingly considered promising for non-invasive diagnosis due to their presence in almost all body fluids, their diverse biological cargoes protected by the lipid bilayers and ability to reflect the state-specific conditions of the parent cells, leading to the rapid growth of the EV biomarker field.[85-87] Until recently there were no FDA-approved EV-based assays. In 2019 Bio-Techne obtained FDA approval for their ExoDx Prostate IntelliScore (EPI) urine-based liquid biopsy assay. Complementing the prostate-specific antigen (PSA) blood test, the current prostate cancer screening standard, EPI measures the expression levels of three exosome-derived RNA targets (PCA3, ERG, SPDEF) to provide a risk score prediction for high-grade prostate cancer demonstrating the potential of EV derived biomarkers in disease detection.[88,89]

2.2 Cellular heterogeneity of the human placenta

Successful pregnancy involves a complex coordinated series of events starting from fertilisation and implantation of the blastocyst to formation of the embryo, fetus and

placenta. The placenta plays a key role in establishing the fetomaternal interface and maintaining fetal homeostasis during pregnancy.[90] Single-cell transcriptomic studies of placental parenchyma biopsies revealed that the human placenta is highly heterogeneous and can be divided into eight major groups having both maternal and fetal origins. Specifically, the maternal decidual cells, maternal uterine dendritic cells, maternal/fetal lymphocytes, maternal/fetal erythrocyte cells, fetal vascular smooth muscle cells, fetal stromal cells, fetal macrophage-like cells, and fetal trophoblastic cells.[91] These cells interact, regulate the immunological homeostasis of the placenta, and maintain maternal-fetal tolerance to support the development of a healthy placenta. Trophoblastic cells are one of the fundamental placental cells responsible for the formation of the placenta/maternal interface and can be divided into three lineages including villous cytotrophoblast (VCTB), syncytiotrophoblast (SCTB), and extravillous trophoblast (EVTB) (Figure 2-3).[92] Placental alkaline phosphatase (PLAP) and human leukocyte antigen G (HLA-G) are specifically expressed by SCTB and EVTB, respectively.[93,94] Differentiation and invasion of trophoblast cells is an essential step for the successful development of human pregnancy. In the early phase of their growth, the outer layer of the human blastocyst grows and gives rise to the first trophoblast lineage, the early mononuclear VCTBs.[95] After implantation, VCTBs expand and differentiate into a multinucleated SCTB layer, which directly contacts the maternal blood for nutrient transport and gas exchange. VCTBs can also differentiate into invasive EVTBs, which penetrate the maternal decidua and maternal circulatory immune system to remodel the uterine spiral arteries.[96,97] Sufficient migration and invasion of EVTBs are important processes in placentation, which is one of the prerequisites contributing to the development of a healthy pregnancy. Abnormalities can occur during placentation, which leads to defective placental structures and eventually pathological pregnancies. Many studies have demonstrated that inadequate invasion of EVTB plays a key role in the pathogenesis of early onset preeclampsia, which leads to poor remodelling of the maternal spiral artery, reducing blood flow into the placenta (placenta hypoxia and placental ischemia), damaged placental structure and release of pro-inflammatory and anti-angiogenic factors.[98-101] The complex mixture of cell types in the placenta, its coordinated development, and the immune modulation necessary for a viable pregnancy have been reported to associate with EV signalling.[102-105] Therefore, further investigating placental EVs are likely to provide important new insights into placental dysfunctions including preeclampsia.

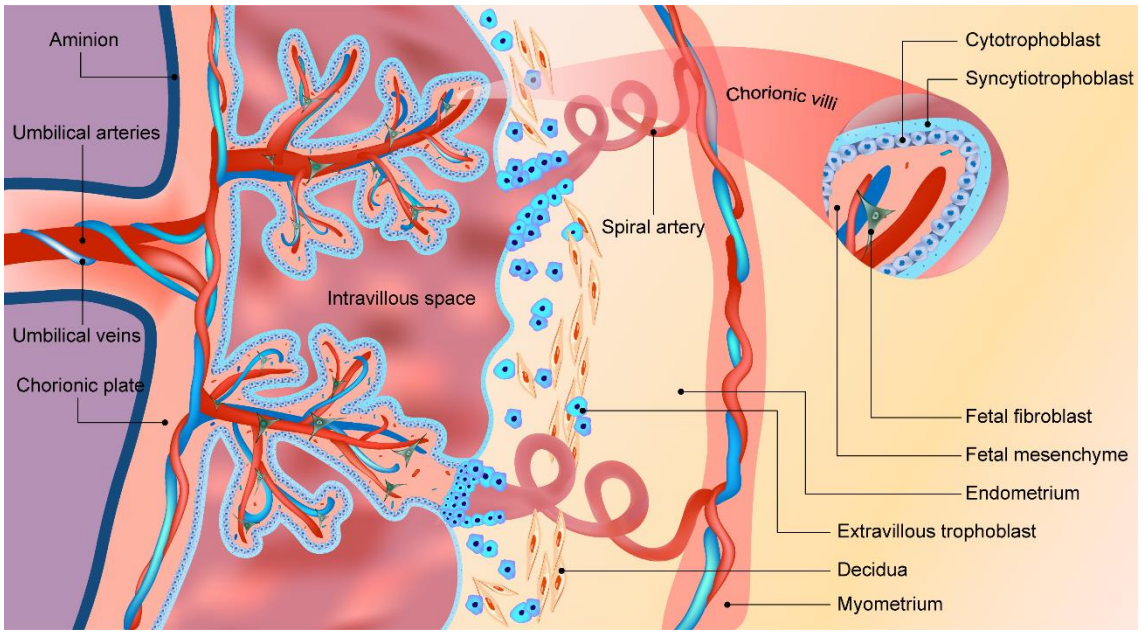

Figure 2-3 Cellular structure of the placenta.
Figure was created using Adobe Illustrator v27.4.

2.3 Placenta-derived EVs

During pregnancy, the placenta releases a wide range of EVs into the maternal circulation. Roughly 0.5−20% of EVs found in the maternal circulation express placental-specific PLAP.[106] The number of placental EVs, as well as total EVs, in plasma is higher for pregnant women compared to non-pregnant ones and progressively increases with increasing gestational age.[107,108 109] In addition to plasma and serum of pregnant women where placental EVs are mostly enriched, they can also be isolated from the placental perfusate or explant,[110,111] umbilical cord blood,[112] amniotic fluid[113] and trophoblast cell lines.[93,114,115] Similar to EVs derived from other tissues, placental EVs carry a wide range of biomolecules, some of which are specifically associated with pregnancy and the placenta such as placental alkaline phosphatase (PLAP),[93] human leukocyte antigen G (HLA-G),[116] syncytin-1,[108] placenta growth factor (PlGF)[117] and pregnancy zone protein (PZP).[52]

As the main cellular component of the placenta, trophoblast cells have been shown to secrete a broad range of EVs during pregnancy.[118] The majority of placental EVs in maternal blood are released from SCTBs that primarily express PLAP, making this protein a surrogate marker for pregnancy, particularly syncytiotrophoblast-derived EVs (STBEVs). Using scattering and fluorescence modes of nanoparticle tracking analysis (NTA), PLAP was found to be expressed more on microvesicles than exosomes isolated

from placental perfusates, possibly due to differences in their size and biogenesis mechanisms.[119] In early pregnancy, 1 mL of maternal plasma was estimated to contain 1–2 × 10^{11} exosomes, 10–20% of which are PLAP+ve EVs.[106,107] Presence of PLAP+ve exosomes have been detected as early as 6 weeks of gestation in maternal plasma.[107]

Along with SCTBs, EVTBs are another source of trophoblast-derived EVs in maternal blood.[120] In pregnancy, EVTB are known to specifically express HLA-G which is one of the major types of histocompatibility class I (MHC Class I).[94] Using flow cytometry, plasma-derived HLA-G+ve EVs were detected in the third trimester[121] as well as throughout pregnancy with decreasing concentrations towards term, though still significantly higher than that of non-pregnant controls.[122] Exosomes isolated from the culture supernatants of first trimester villous explants were also found to contain soluble HLA-G (HLA-G5 isoform), whereas little or no HLA-G was detected from exosomes of term villous explants.[123]

Considered an essential means of feto-maternal communication, placental EVs play an important role in modulating the maternal immune system during pregnancy.[124] For instance, placental EVs have anti-inflammatory effects on maternal immune cells preventing rejection of the fetus.[125] It has been demonstrated that STBEVs can reduce the responsiveness and proliferation of T cells to phytohemagglutinin (PHA) induced by the sequestration of transferrin (TF), Fas ligand (FasL)-associated EVs and loss of CD3-zeta.[126] Indeed, STBEVs carrying FasL and TRAIL were reported to mediate the apoptosis of activated lymphocytes to maintain the immune privilege of the fetus.[127] Surface proteins of STBEVs like MHC class I chain-related proteins A and B and UL-16-binding protein were reported to downregulate the expression of surface NKG2D, thereby reducing the cytotoxic activity of natural killer (NK) cells.[128,129] In contrast to the immuno-suppressive effect, STBEVs can also induce monocytes and peripheral blood mononuclear cells to release various pro-inflammatory cytokines.[130] This counterintuitive effect suggests that placental EVs may cope with the suppression of T and NK cells to strengthen the maternal immune system.[129] Nevertheless, the immune-suppressive functions of STBEVs are found to be more prominent than their pro-inflammatory effects, contributing to the establishment of fetal immune tolerance in pregnancy.[90] In summary, EVs are released from the placenta into the maternal circulation and have a wide range of functions including regulating the immunologic responses to pregnancy.

2.4 Current EV isolation/enrichment techniques

Isolation is the first and an important step for most EV studies and analyses. Various isolation methods for EVs have been developed so far, utilising their physical characteristics (size, density, negatively charged membrane) and biochemical content (membrane proteins and lipids). It is important to note that a consensus procedure for EV isolation has not been yet established, which can contribute to discrepancies in results reported among EV studies.[131] In general, EV isolation techniques can be classified into three major groups, including high-throughput bulk methods, affinity isolation and microfluidic approaches.

2.4.1 Bulk isolation of EVs

Bulk isolation mostly relies on differences in size and density to fractionate EV subtypes. A typical example of this approach is ultracentrifugation (UC), which isolates EVs based on their sedimentation rate and is still to date the gold standard and reliable method of EV enrichment used in both laboratory and clinical settings.[132,133] Differential centrifugation usually precedes ultracentrifugation to first separate EVs from contaminants like cells and cellular debris at low speeds (< 2000 × *g*) and then pellet EV subtypes at higher speeds (~10 000–12 000 × *g* for microvesicles and ~100 000–120 000 × *g* for exosomes).[134,135] As protein aggregates tend to be co-enriched with EVs during UC, a density gradient medium (e.g. sucrose, iodixanol, etc.) can be combined with UC (density gradient UC) to separate EVs into layers of similar densities, thus improving the purity of enriched EVs in terms of protein contamination.[136,137] However, particles with similar densities to target EVs can still be co-isolated, for example lipoproteins.[138] Apart from being time-intensive (~5–6 h) and possibly inducing EV aggregates, multiple centrifugal purification steps associated with UC-based methods can result in sample loss, which possibly affects the criterion of sufficient EV enrichment required for certain downstream analyses (e.g mass spectrometry).[133]

Popular size-based bulk isolation methods of EVs include ultrafiltration and size exclusion chromatography (SEC). Ultrafiltration uses filters of different pore sizes and molecular weight cut-offs (MWCO) to sequentially concentrate target EV subtypes of different sizes (e.g 100 kDa MWCO for exosome isolation).[137] This method greatly shortens the isolation time compared to UC, but can suffer from filter clogging and co-isolation of proteins and particles with comparable sizes to target vesicles.[139-141] SEC

isolates EVs by utilising gravity to pass the biological fluids through a column manually packed with a porous gel polymer matrix (e.g Sephadex, Sepharose) or commercialised pre-packed columns (e.g qEV of iZON).[142] Larger particles elute first while small ones diffuse through the pores thus eluting later. Although EVs enriched by SEC are of high purity and integrity size compared to UC-based and ultrafiltration methods, the enrichment throughput and yield are often lower.[9] Nevertheless, the use of SEC for selective enrichment of EV subtypes especially exosomes has increased since 2019 besides UC and density gradient UC according to ISEV.[143]

Along with density and size-dependent methods, polymer-based precipitation is another approach commonly used to isolate EVs in bulk. The method uses hydrophilic polymers (e.g polyethylene glycol, PEG) to decrease the solubility of EVs and precipitate them at low centrifugal forces.[137] Due to its simplicity and high scalability, the precipitation method has been widely applied to quickly isolate EVs as seen by the use of many commercial kits such as ExoQuick (System Biosciences), Total Exosome Isolation Reagent (Invitrogen), miRCURY (Qiagen) and Exosome Purification Kit (Norgen Biotek).[144] Despite its high EV yield, the method was reported to induce large EV aggregates and co-precipitate protein complexes along with EVs, which in some cases limits downstream analysis including omics assays.[145]

2.4.2 Affinity isolation of EVs

In contrast to size- and density-based enrichment methods, affinity-based approaches isolate EVs by targeting their membrane components. Utilising antigen-antibody interaction, immunoaffinity separates EVs based on ubiquitous or specific proteins displayed on their membranes, allowing the enrichment of particular EV sub-populations with reduced contamination rates of co-purified proteins or protein-RNA complexes.[146] For example, ubiquitous tetraspanins (CD63, CD81, CD9) have been extensively used to enrich EVs. Several specific EV markers, used individually or in combination, have been used for the enrichment of different EV subsets, for example hepatocellular carcinoma-derived EVs (EpCAM, ASGPR1, CD147),[147] EVs of endothelial cells or endothelial progenitor cells (CD105 or CD34),[148] platelet-derived EVs (CD61 or CD41)[149,150] and blast-derived EVs from acute myeloid leukaemia (CD34).[149] Immunoaffinity enrichment is usually adopted by immobilising antibodies or aptamers to a solid support, for example magnetic micron-sized beads or nanoparticles, from which EVs are captured and optionally eluted for subsequent characterisations. Although immunoaffinity provides

specificity for the enrichment of immuno-specific EV subsets, the method can be expensive due to the need for antibodies and magnetic beads and require long incubation time.

Other emerging affinity-based isolation methods take advantage of lipid components constructing the membrane of EVs. One of this approach is to use TiO_2, which has a high affinity to the hydrophilic phosphate groups of the amphiphilic phospholipids exposing on the outer membrane of EVs.[151] Another example is the use of Tim4 protein, which strongly binds to the phosphatidylserine, one of the main constituents of the EV membrane.[152] Both approaches were demonstrated to improve the EV enrichment yield with reduced non-specific adsorption of plasma proteins compared to UC and precipitation method.

2.4.3 Microfluidic-based isolation of EVs

Microfluidics has gradually emerged in the field of EVs in the past few years with many demonstrations of EV enrichment platforms based on size, density and immunoaffinity capture. Among them, microfluidic-based immuno-capture is the most popular approach which enriches EVs through antibodies immobilised on the surface of the microchannels or by the use of antibody-conjugated magnetic micron-sized beads.[153] This approach has been employed for many microfluidic devices with various mixing structures (herringbone grooves, Y-shape microposts)[154,155] designed to increase the probability of bindings between EVs and capture antibodies.

Size-, density- and charge-based approaches were also reported for microfluidic enrichment of EVs, which were achieved by employing integrated nanoporous membranes (for pressure-driven filtration),[156] dialysis membranes (for electrophoresis-driven separation),[157] arrays of nanowire-on-micropillar structures (for size-based trapping),[158] embedded ZnO/Al_2O_3 core-shell nanowires (for electrostatic collection),[159] an acoustic standing field (size-, density- and compressibility-based sorting)[160] or a viscoelastic sheath fluid (e.g diluted polyoxyethylene for size-based sorting).[161] Microfluidic devices can enrich EVs rapidly and efficiently due to their miniaturised scale, but their uses can be limited due to complicated manufacturing processes and scale up, or when high sample throughput is required.[162,163]

2.4.4 Enrichment of placental EVs from biological fluids

Enriching and quantifying placental EVs from plasma presents several biological and technical challenges. A primary challenge is that placental EVs in maternal plasma make up only a minority of the total EV population, which complicates their enrichment and quantification.[164] Additionally, the co-isolation of EVs with plasma proteins and lipoproteins can result in contamination and false-positive results.[165] Another significant challenge is the composition variability of placental EVs, which can vary depending on factors such as gestational age, maternal or placental health status, and fetal growth.[166] This variability makes it challenging to establish consistent and reproducible results across different samples and studies.[167] Furthermore, pre-analytical variables such as sample collection, processing, and storage can significantly impact the yield and quality of EVs, leading to variability in results.[168] Therefore, developing standardized and reproducible protocols for EV enrichment and identification of specific markers for these vesicles is crucial to overcome these challenges and obtain reliable results.

Despite the variety of EV enrichment techniques available, UC-based methods are the most commonly employed method in recent studies for the isolation of total placental EVs or size-specific placental EV subtypes (i.e microvesicles and exosomes) from different biological sources[117,169-172]. Combinations of EV isolation techniques rather than individual ones are reported to improve the purity of size-specific EV isolation,[173] some of which were also applied widely in the research of placental EVs.

Along with size-specific EVs, the presence of pregnancy-specific EV markers has been exploited for studies on cell-specific placental EVs. In general, enrichment of immuno-specific placental EVs from biological fluids is challenging due to the complex composition of the biological fluids and the low abundance nature of target placental subtypes. As a popular source for placental EVs, maternal blood (and hence plasma) contains abundant plasma proteins as well as non-placental EVs released from different blood cells and other tissues, which altogether outnumbers STBEVs (100:1).[174] This probably explains the use of combined techniques reported for the isolation of immuno-specific placental EVs. Indeed, the use of centrifugation combined with affinity capture was recommended for the isolation of cell-specific EVs and their subsequent -omics research, providing a more accurate molecular profiling of EV content to understand the biological functions of EVs.[175]

An early attempt of enriching PLAP+ve exosomes from 2.5 mL of plasma obtained from pregnant women was achieved using SEC and UC to collect total exosomes, from which PLAP+ve exosomes were subsequently separated by anti-PLAP conjugated agarose microbeads.[176] A similar approach of combining differential UC and immunoaffinity enrichment of plasma-derived immuno-specific placental EVs was also recently reported to enrich PLAP+ve and HLA-G+ve EVs.[177,178]

The selection of capture antibodies for immunoaffinity capture is one of the key factors contributing to efficient isolation of EVs. In terms of placenta EVs, two different clones of anti-PLAP were reported, H17E2 and 8B6, and successfully used to enrich PLAP+ve EVs.[177] The selection of antibody clones for the isolation of HLA-G+ve EVs may be more difficult due to not only the diversity of HLA-G isoforms (seven including membrane-bound HLA-G1, 2, 3, 4 and soluble HLA-G5, 6, 7) but also the lack of evidence confirming the type HLA-G isoforms presenting on EV membranes. Nevertheless, different anti-HLA-G clones (e.g. MEM-G/9, MEM-G/1, 4H84) have been reported to detect HLA-G+ve EVs in pregnancy using flow cytometry.[122,179] Anti-PLAP (8B6) and anti-HLA-G (87G) conjugated to magnetic nanoparticles were used previously to capture immuno-specific placental EVs from total EVs isolated from placental villous and amnion explants using the commercialised ExoQuick TC kit.[180]

2.5 Preeclampsia and its current diagnostic limitations

Although the underlying aetiology of preeclampsia remains poorly defined, the disease is characterised as a multisystem disorder which results from maternal and fetal/placental factors. Preeclampsia is broadly classified into early onset (EOPE, <34 weeks) and late onset (LOPE, >34 weeks) based on the time clinical symptoms are first observed.[181] Importantly, EOPE and LOPE have different clinical manifestations, maternal and fetal outcomes as well as associated complications.[182] EOPE closely reflects placental disorders and results from the impaired invasion of extravillous trophoblast (EVTB) and arterial modelling and is associated with severe perinatal mortality and morbidity.[183] In contrast, LOPE arises after normal placentation through maternal factors and accounts for 75-80% of all preeclampsia cases with lower rates of severe complications.[184] In terms of placental factors, preeclampsia is generally characterised by the abnormal development of the uteroplacental circulation and the impaired remodelling of the spiral artery in early pregnancy leading to placental ischemia or reduced nutrient delivery to the intervillous

space. Preeclampsia can also be linked with maternal vascular dysfunction and metabolic abnormalities such as obesity and diabetes.[185]

Currently, the only definitive treatment for preeclampsia is delivery of the placenta, however, the prematurity risks associated with early delivery must be weighed against the risks to the mother. Moreover, it is now well understood that preeclampsia has significant long-term effects with increased risks of cardiovascular disease and diabetes in both mothers and offsprings.[186] While drugs are being investigated to treat preeclampsia, these typically only alleviate the symptoms and do not stop disease progression. Therefore, improving the understanding of the molecular basis of preeclampsia and identifying reliable "first trimester biomarkers" would likely lead to improvement in antenatal care for both mothers and their babies as well as potentially aid in developing better treatments.

2.6 EVs and their pathological links to preeclampsia

The biological consequences and pathological roles of EVs, particularly exosomes, make them an attractive source of biomarkers for the mechanistic investigation and prediction of preeclampsia. Several studies have demonstrated biological effects of EVs in preeclampsia observing increasing number of EVs secreted in the maternal blood, abnormal functions of EVs as well as dysregulated expression of EV-derived protein and nucleic acids. In comparison to normal pregnancies, the number of total EVs in preeclamptic pregnancies was shown to increase significantly (~2–2.4 fold difference, second to third trimester).[108,187] Research on plasma-derived EVs also suggested that the majority of elevated total EVs in preeclampsia are released from the endothelial cells,[188] which experience dysfunction causing the clinical disease symptoms of preeclampsia.

In contrast to the increasing trend of total EVs associated with preeclampsia observed in many studies, changes in the number of STBEVs in preeclampsia compared to normal pregnancy are not consistently reported. In one study, SCTB-derived microvesicles (STBMs) were isolated from the perfusion media of placenta obtained from caesarean section, and PLAP+ve STBMs were stained for flow cytometry using fluorescence-tagged NDOG2 antibody, which is a SCTB-specific antibody recognising PLAP. Using flow cytometry, the number of these PLAP+ve STBMs was lower in preeclampsia compared to normal controls.[189] In another study using syncytin-1 instead of PLAP as the specific marker for STBEVs, a similar decrease in the number of syncytitin-1+ve EVs in

the preeclamptic plasma relative to healthy controls of third trimester pregnancy was also observed using fluorescence NTA, which is possibly due to the reduction of placental EVs and/or downregulated expression of placental markers on EVs.[108] In contrast to the decreasing trend of PLAP+EVs, an increase of plasma-derived placental EVs was reported for preeclamptic patients compared to normal pregnancy using flow cytometry, which was observed for both PLAP+ve EVs and PLAP+ve/AV+ve (Annexin V) EVs with 3.95 fold increase.[190]

Changes in STBEV number, however may not necessarily reflect similar changes in PLAP content of EVs, especially regarding their subtypes. Using ELISA, exosomal PLAP content in preeclamptic plasma was shown to either increase with advanced gestation (11–34 weeks)[187] or increase in EOPE (vs ≤ 33 weeks controls) and decrease in LOPE (vs ≥ 34 weeks controls).[191] A different result was obtained via western blot, in which there was a decrease in PLAP content of STBMs of preeclampsia subjects compared to normal controls.[189] The disparities in STBEV number and their PLAP content reported suggest that several factors such as enrichment/detection method, used antibodies, target EV subtypes and gestation age may largely affect the final results.

While the intravascular inflammation induced by placental EVs is regulated moderately in normal pregnancy, this effect is exaggerated in preeclampsia.[51] EVs isolated from preeclamptic plasma were shown to activate and reduce the migration of THP-1 monocytes as well as induce the expression of pro-inflammatory TNF-α cytokines.[130] The excessive inflammation effect of STBEVs in preeclampsia was also reported to stimulate platelet activation and thus increased consumption of platelets for blood coagulation, which possibly explains the low blood platelet count (thrombocytopenia) commonly observed in preeclamptic patients.[126,192] In addition to exaggerated inflammation, EVs from preeclamptic pregnancies were found to be involved in the imbalance of angiogenesis and endothelial dysfunction associated with preeclampsia. Exosomes isolated from preeclamptic plasma were reported to carry anti-angiogenic factors soluble Fms-like tyrosine kinase-1 (sFlt-1) and soluble endoglin (sEng) to the endothelial cells, which impairs vascular development.[193] The level of endothelial nitric oxide synthases (eNOS), an enzyme catalysing the production of vasodilator nitric oxide (NO) in pregnancy, carried by STBEVs was found to be reduced in preeclampsia compared to healthy controls, leading to reduced bioavailability of NO and thereby affecting the vascular function.[194]

In addition to the elevated quantity of EVs, dysregulation of proteins and miRNAs in placental EVs was reported in preeclampsia. Although many plasma proteins secreted by the placenta have been discovered and tested for preeclampsia diagnosis, the predictive ability of these markers is limited and mostly restricted to the third trimester of pregnancy. Since the placenta releases EVs into the maternal circulation in the first trimester, proteins and RNA carried by placenta EVs may be useful for early diagnosis of pregnancy complications. Indeed, many proteins, miRNAs and lipid molecules have been reported to be either upregulated or downregulated in preeclamptic pregnancies (Table 2-2). In preeclamptic pregnancies, there is an increase in the concentrations of anti-angiogenic factors, including sFlt-1. Elevated levels of sFlt-1 reduce the concentrations of angiogenic factors, such as vascular endothelial growth factor (VEGF) and PlGF, which hampers the formation of new blood vessels as well as the fenestration of endothelial cells.[195] A sFlt-1/PlGF ratio ≤ 38 highly rules out the development of preeclampsia in the next week with a negative predictive value of 99.3% in women suspected with preeclampsia between 24 and 36 weeks of pregnancy.[196] Pregnant women diagnosed with a ratio greater than 38 are at risk of developing preeclampsia over the next 4 weeks with a positive predictive value of 36.7%, suggesting that they should be more closely monitored as preeclampsia can progress quickly and suddenly.

Table 2-2 Differentially expressed EV-derived proteins, miRNAs, and lipids in preeclampsia.

Target	EV type[1]	EV source	Enrichment method	Gestational age (weeks')	Profiling method	Year
GAPDH ↑ HSPB1 ↑ HSPA5 ↑[2]	STBM	Placental villous explant (n = 3)	Differential UC	Third trimester (36.09 ± 0.95)	LC-MS/MS[197] (Agilent 6538 Q-TOF, intensity normalised by Mascot)	2014
HRG ↑ TTR ↓ FGB ↓ FGG ↓[2]	Exosome	Umbilical cord blood (n = 10)	Differential UC	At delivery (34.3 ± 4.6)	LC-MS/MS[198] (Thermo Fisher Q-Exactive Orbitrap, median normalisation)	2015
PP13 ↓(*)	STBEV[2]	Placental perfusate (n = 20)	Differential UC	At delivery (32.4–35.6)	WB[199] (intensity normalised to total EV protein)	2018
sEng ↑ sFlt-1 ↑	Exosome	Plasma (1 mL, n = 10)	ExoQuick kit	Third trimester (36.71 ± 0.7)	WB and ELISA[193]	2018
NEP ↑(*)	STBEV[2]	Placental perfusate (n = 5)	Differential UC	Third trimester (34.8 ± 1.5)	WB[110] (intensity normalised to total EV protein)	2019
SIGLEC6 ↑	STBEV[2]	Placental perfusate (n = 11)	Centrifugation	At delivery (34 ± 3.7)	WB[200] (normalisation by same loading protein mass)	2020
Syncytin-1 ↓	Mostly exosome	Plasma (250 µL, n = 21)	SEC + UF + UC	Third trimester (31.3 ± 4.4)	WB[108]	2020

APOE ↑ AMBP ↑ TF ↑ ITIH4 ↑ PZP ↓ FCN2 ↓[2]	Exosome	Serum (500 µL, n = 35)	Centrifugation + SEC	Late second, early third trimester (25–34) and at delivery	LC-MS/MS[201] (AB SCIEX 5600 Triple TOF, intensity normalised by Mascot search engine)	2022
miR-486-1-5p ↑ miR-486-2-5p ↑	Exosome	Plasma (1 mL, n = 13)	Centrifugation + Density gradient UC	Across gestation (12 ± 0.1, 23 ± 0.1, 33 ± 0.11)	RNA sequencing[187] (Illumina NextSeq 500, count normalisation by DESeq2 R package)	2017
miR-155 ↑	Exosome	Serum (200 µL, n = 10)	Centrifugation + PEG precipitation	Third trimester (38.3 ± 2.15)	RT-qPCR[202] (expression normalised to miR-39)	2018
miR-223-3p ↑ miR-490-3p ↑ miR-126-3p ↑ miR-190a-5p ↑ miR-23a-3p ↑ miR-324-3p ↑	Exosome	Plasma (n = 30)	miRCURY kit (Qiagen)	EOPE (37 ± 1.9)	RNA sequencing[203] (NanoString nCounter SPRINT Profiler, input RNA normalised to total miRNA count)	2019
miR-297 ↑ miR-202-3p ↑ miR-375 ↓ miR-488-3p ↓				LOPE (32.4 ± 2.19)		
miR-224-5p ↑ miR-532-5p ↑	Exosome	Plasma (2 mL, n = 20)	DGU	Third trimester (28–32)	RT-qPCR[204]	2020

miR-222-3p ↑ miR-153-3p ↓ miR-325 ↓ miR-342-3p ↓ miR-653-5p ↓					(expression normalised to 1) miR-191-5p, miR-339-5p, miR, 221-3p, miR-324-5p, 2) Housekeeping genes and 3) miR-21-5p)	
PS ↑ PI ↓ PA ↓ GM3 ↓	STBM	Placental villous explant (n = 6)	Centrifugation + UC	At delivery (31.82 ± 3.24)	LC-MS/MS[205] (Applied Biosystem 3200 QTRAP, intensity normalised to total lipid levels)	2013

[1]EV type defined by cited publications.

[2]Targets listed are cross-referenced to sets of proteins with consistent expression patterns throughout quantitative proteomic analyses of placenta (18 proteins) and serum/plasma (29 proteins) samples compared between preeclampsia and healthy controls (2004–2020).[201]

(*) indicates PLAP associated.

↑ and ↓ denote upregulation and downregulation.

Notes: **AMBP**: Alpha-1-microglobulin; **APOE**: Apolipoprotein E; **FCN2**: Ficolin-2; **FGG** and **FGB**: Fibrinogen α and β chain; **Flt-1**: Fms-like tyrosine kinase-1 (or vascular endothelial growth factor receptor-1); **GAPDH**: Glyceraldehyde 3-phosphate dehydrogenase; **HRG**: Histidine-rich glycoprotein; **HSPB1**: Heat schock factor-binding protein 1; **HSPA5**: Heat shock 70-kDa protein 5; **ITIH4**: Inter-alpha-trypsin inhibitor heavy chain 4; **NEP** (*MME*): Neprilysin (or CD10); **PA**: Phosphatidic acid; **PI**: Phosphatidylinositol; **PP13** (*LGALS13*): Placental protein 13 (or Galectin-13); **PS**: Phosphatidylserine; **PZP**: Pregnancy zone protein; **sEng**: soluble Endoglin (or CD105); **SIGLEC6**: Sialic acid-binding Ig-like lectin 6**; STBEV**: Syncytiotrophoblast-derived EVs (including microvesices and exosomes); **STBM**: Syncytiotrophoblast microvesicles; **Syncytin-1** (*ERVW-1*) or enverin; **TF**: Serotransferrin; **TTR**: Transthyretin (or TBPA)); **UC**: Ultracentrifugation; **UF**: Ultrafiltration; **WB**: Western blot

2.7 Search for preeclampsia biomarkers

Due to the heterogenous nature of preeclampsia, omics approaches particularly proteomics and transcriptomics have been utilised to study the molecular differences between preeclampsia and healthy pregnancy, and towards discovering new biomarkers for preeclampsia. Proteomics can identify dysregulated proteins in preeclamptic pregnancies compared to healthy ones and assist the establishment of pathway analysis of proteins involved in cellular functions to gain insights into the molecular mechanism of the disease, ultimately aiding in the improvements of preeclampsia diagnosis and, eventually, therapy. The search for candidate biomarkers usually focuses on plasma. The results vary greatly among studies and most of the proteomic data were built on third-trimester maternal samples with only a few reports for first- and second trimesters.[206,207] In addition, plasma-derived biomarkers associated with placental dysfunctions are generally present at low concentrations and their identification is confounded by the dominance of high abundance proteins such as albumin and immunoglobulins, which interfere and reduce the sensitivity of proteomics.[208] This issue makes EVs a promising alternative for proteomic approaches. Protein profiling of STBEVs from placental explants was established in previous studies using mass spectrometry to elucidate the pathophysiological relevance of EVs to preeclampsia.[197] However, only a few proteomic profiling analyses of plasma-derived EVs compared between preeclampsia and normal pregnancy have been published to date.[198,201] Isolating placental EVs from early pregnancy plasma will enrich biomarker signals and as a result likely provide a powerful means to reveal novel markers that are otherwise undetectable by conventional proteomic analysis of maternal plasma.

Similarly, transcriptomics also provides a powerful approach to understand the molecular mechanisms and signalling pathways associated with preeclampsia, and thereby discovering new biomarkers. Several dysregulated RNA molecules were identified in preeclampsia when analysing the transcriptome of maternal plasma,[209,210] decidua[211,212] and the umbilical cord.[213] However, many of these markers are not found in detectable concentrations in the early first trimester.[187] The possibility to significantly enrich preeclampsia-associated RNA carried and protected by EVs, the high abundance of circulating miRNA associated with EVs (~60%), and the ability of EV-derived RNAs to reflect the physiological and pathological conditions of the source cells have significant potential to enable more specific transcriptomics and therefore to achieve higher

predictive value.[55] A pioneer of this approach is Salomon et al. (2017), who isolated total exosomes from the plasma of preeclamptic pregnancies, sequenced the vesicular RNA cargo, and identified that miR-486-1-5p and miR-486-2-5p were upregulated in preeclampsia regardless of gestational age.[187] Another similar work was carried out by Devor et al. (2020), which examined the expression of exosomal microRNA in preeclamptic plasma at each trimester of pregnancy. Eight different miRNAs were reported to be differentially regulated in preeclamptic pregnancies with four of them being dysregulated in the first trimester.[214] These two studies demonstrate the promise of EVs for the early prediction of preeclampsia.

In summary, investigating placental EVs with omics approaches holds considerable promise to improve our understanding of the molecular mechanism of the disease and identify new candidate biomarkers, which may enable better prediction strategies and ultimately, improve antenatal monitoring and outcomes.

2.8 References

1 Yarana, C. *et al.* Extracellular vesicle-mediated macrophage activation: An insight into the mechanism of thioredoxin-mediated immune activation. *Redox Biol* **26**, 101237, doi:10.1016/j.redox.2019.101237 (2019).

2 Srivastava, A. *et al.* Progress in extracellular vesicle biology and their application in cancer medicine. *Wiley Interdiscip Rev Nanomed Nanobiotechnol* **12**, e1621, doi:10.1002/wnan.1621 (2020).

3 Ibrahim, A., Ibrahim, A. & Parimon, T. Diagnostic and Therapeutic Applications of Extracellular Vesicles in Interstitial Lung Diseases. *Diagnostics (Basel)* **11**, doi:10.3390/diagnostics11010087 (2021).

4 Ipinmoroti, A. O. & Matthews, Q. L. Extracellular Vesicles: Roles in Human Viral Infections, Immune-Diagnostic, and Therapeutic Applications. *Pathogens* **9**, doi:10.3390/pathogens9121056 (2020).

5 Kato, T., Vykoukal, J. V., Fahrmann, J. F. & Hanash, S. Extracellular Vesicles in Lung Cancer: Prospects for Diagnostic and Therapeutic Applications. *Cancers (Basel)* **13**, doi:10.3390/cancers13184604 (2021).

6 Stremersch, S., De Smedt, S. C. & Raemdonck, K. Therapeutic and diagnostic applications of extracellular vesicles. *J Control Release* **244**, 167-183, doi:10.1016/j.jconrel.2016.07.054 (2016).

7 Zhao, Y. *et al.* Trends in the biological functions and medical applications of extracellular vesicles and analogues. *Acta Pharm Sin B* **11**, 2114-2135, doi:10.1016/j.apsb.2021.03.012 (2021).

8 Brennan, K. *et al.* A comparison of methods for the isolation and separation of extracellular vesicles from protein and lipid particles in human serum. *Sci Rep* **10**, 1039, doi:10.1038/s41598-020-57497-7 (2020).

9 Guerreiro, E. M. *et al.* Efficient extracellular vesicle isolation by combining cell media modifications, ultrafiltration, and size-exclusion chromatography. *PLoS One* **13**, e0204276, doi:10.1371/journal.pone.0204276 (2018).

10 Thomas, S. C., Kim, J. W., Pauletti, G. M., Hassett, D. J. & Kotagiri, N. Exosomes: Biological Pharmaceutical Nanovectors for Theranostics. *Front Bioeng Biotechnol* **9**, 808614, doi:10.3389/fbioe.2021.808614 (2021).

11 Yanez-Mo, M. *et al.* Biological properties of extracellular vesicles and their physiological functions. *J Extracell Vesicles* **4**, 27066, doi:10.3402/jev.v4.27066 (2015).

12 Gangoda, L., Boukouris, S., Liem, M., Kalra, H. & Mathivanan, S. Extracellular vesicles including exosomes are mediators of signal transduction: are they protective or pathogenic? *Proteomics* **15**, 260-271, doi:10.1002/pmic.201400234 (2015).

13 Iraci, N., Leonardi, T., Gessler, F., Vega, B. & Pluchino, S. Focus on Extracellular Vesicles: Physiological Role and Signalling Properties of Extracellular Membrane Vesicles. *Int J Mol Sci* **17**, 171, doi:10.3390/ijms17020171 (2016).

14 Anand, S., Samuel, M., Kumar, S. & Mathivanan, S. Ticket to a bubble ride: Cargo sorting into exosomes and extracellular vesicles. *Biochim Biophys Acta Proteins Proteom* **1867**, 140203, doi:10.1016/j.bbapap.2019.02.005 (2019).

15 Maas, S. L. N., Breakefield, X. O. & Weaver, A. M. Extracellular Vesicles: Unique Intercellular Delivery Vehicles. *Trends Cell Biol* **27**, 172-188, doi:10.1016/j.tcb.2016.11.003 (2017).

16 Yates, A. G. *et al.* In sickness and in health: The functional role of extracellular vesicles in physiology and pathology in vivo: Part II: Pathology: Part II: Pathology. *J Extracell Vesicles* **11**, e12190, doi:10.1002/jev2.12190 (2022).

17 Stahl, P. D. & Raposo, G. Extracellular Vesicles: Exosomes and Microvesicles, Integrators of Homeostasis. *Physiology (Bethesda)* **34**, 169-177, doi:10.1152/physiol.00045.2018 (2019).

18 Ramis, J. M. Extracellular Vesicles in Cell Biology and Medicine. *Sci Rep* **10**, 8667, doi:10.1038/s41598-020-65826-z (2020).

19 Thery, C. *et al.* Minimal information for studies of extracellular vesicles 2018 (MISEV2018): a position statement of the International Society for Extracellular Vesicles and update of the MISEV2014 guidelines. *J Extracell Vesicles* **7**, 1535750, doi:10.1080/20013078.2018.1535750 (2018).

20 Bebelman, M. P., Smit, M. J., Pegtel, D. M. & Baglio, S. R. Biogenesis and function of extracellular vesicles in cancer. *Pharmacol Ther* **188**, 1-11, doi:10.1016/j.pharmthera.2018.02.013 (2018).

21 Zha, Q. B., Yao, Y. F., Ren, Z. J., Li, X. J. & Tang, J. H. Extracellular vesicles: An overview of biogenesis, function, and role in breast cancer. *Tumour Biol* **39**, 1010428317691182, doi:10.1177/1010428317691182 (2017).

22 Zijlstra, A. & Di Vizio, D. Size matters in nanoscale communication. *Nat Cell Biol* **20**, 228-230, doi:10.1038/s41556-018-0049-8 (2018).

23 Wang, W. *et al.* Biogenesis and function of extracellular vesicles in pathophysiological processes of skeletal muscle atrophy. *Biochem Pharmacol* **198**, 114954, doi:10.1016/j.bcp.2022.114954 (2022).

24 Bazzan, E. *et al.* Critical Review of the Evolution of Extracellular Vesicles' Knowledge: From 1946 to Today. *Int J Mol Sci* **22**, doi:10.3390/ijms22126417 (2021).

25 Zhang, Y., Liu, Y., Liu, H. & Tang, W. H. Exosomes: biogenesis, biologic function and clinical potential. *Cell Biosci* **9**, 19, doi:10.1186/s13578-019-0282-2 (2019).

26 Kowal, J., Tkach, M. & Thery, C. Biogenesis and secretion of exosomes. *Curr Opin Cell Biol* **29**, 116-125, doi:10.1016/j.ceb.2014.05.004 (2014).

27 Kalluri, R. & LeBleu, V. S. The biology, function, and biomedical applications of exosomes. *Science* **367**, doi:10.1126/science.aau6977 (2020).

28 van Niel, G., D'Angelo, G. & Raposo, G. Shedding light on the cell biology of extracellular vesicles. *Nat Rev Mol Cell Biol* **19**, 213-228, doi:10.1038/nrm.2017.125 (2018).

29 Blanc, L. & Vidal, M. New insights into the function of Rab GTPases in the context of exosomal secretion. *Small GTPases* **9**, 95-106, doi:10.1080/21541248.2016.1264352 (2018).

30 Jin, H. *et al.* Rab GTPases: Central Coordinators of Membrane Trafficking in Cancer. *Front Cell Dev Biol* **9**, 648384, doi:10.3389/fcell.2021.648384 (2021).

31 Mashouri, L. *et al.* Exosomes: composition, biogenesis, and mechanisms in cancer metastasis and drug resistance. *Mol Cancer* **18**, 75, doi:10.1186/s12943-019-0991-5 (2019).

32 Pegtel, D. M. & Gould, S. J. Exosomes. *Annu Rev Biochem* **88**, 487-514, doi:10.1146/annurev-biochem-013118-111902 (2019).

33 Zhang, Q. *et al.* Transfer of Functional Cargo in Exomeres. *Cell Rep* **27**, 940-954 e946, doi:10.1016/j.celrep.2019.01.009 (2019).

34 Muralidharan-Chari, V., Clancy, J. W., Sedgwick, A. & D'Souza-Schorey, C. Microvesicles: mediators of extracellular communication during cancer progression. *J Cell Sci* **123**, 1603-1611, doi:10.1242/jcs.064386 (2010).

35 Meldolesi, J. Exosomes and Ectosomes in Intercellular Communication. *Curr Biol* **28**, R435-R444, doi:10.1016/j.cub.2018.01.059 (2018).

36 Pang, A. *et al.* Shear-induced integrin signaling in platelet phosphatidylserine exposure, microvesicle release, and coagulation. *Blood* **132**, 533-543, doi:10.1182/blood-2017-05-785253 (2018).

37 Cocucci, E. & Meldolesi, J. Ectosomes and exosomes: shedding the confusion between extracellular vesicles. *Trends Cell Biol* **25**, 364-372, doi:10.1016/j.tcb.2015.01.004 (2015).

38 Ma, L. *et al.* Discovery of the migrasome, an organelle mediating release of cytoplasmic contents during cell migration. *Cell Res* **25**, 24-38, doi:10.1038/cr.2014.135 (2015).

39 Li, M., Liao, L. & Tian, W. Extracellular Vesicles Derived From Apoptotic Cells: An Essential Link Between Death and Regeneration. *Front Cell Dev Biol* **8**, 573511, doi:10.3389/fcell.2020.573511 (2020).

40 Liu, D. *et al.* Circulating apoptotic bodies maintain mesenchymal stem cell homeostasis and ameliorate osteopenia via transferring multiple cellular factors. *Cell Res* **28**, 918-933, doi:10.1038/s41422-018-0070-2 (2018).

41 Kakarla, R., Hur, J., Kim, Y. J., Kim, J. & Chwae, Y. J. Apoptotic cell-derived exosomes: messages from dying cells. *Exp Mol Med* **52**, 1-6, doi:10.1038/s12276-019-0362-8 (2020).

42 Akers, J. C., Gonda, D., Kim, R., Carter, B. S. & Chen, C. C. Biogenesis of extracellular vesicles (EV): exosomes, microvesicles, retrovirus-like vesicles, and apoptotic bodies. *J Neurooncol* **113**, 1-11, doi:10.1007/s11060-013-1084-8 (2013).

43 Abels, E. R. & Breakefield, X. O. Introduction to Extracellular Vesicles: Biogenesis, RNA Cargo Selection, Content, Release, and Uptake. *Cell Mol Neurobiol* **36**, 301-312, doi:10.1007/s10571-016-0366-z (2016).

44 Shurtleff, M. J. *et al.* Broad role for YBX1 in defining the small noncoding RNA composition of exosomes. *Proc Natl Acad Sci U S A* **114**, E8987-E8995, doi:10.1073/pnas.1712108114 (2017).

45 Pua, H. H. *et al.* Increased Hematopoietic Extracellular RNAs and Vesicles in the Lung during Allergic Airway Responses. *Cell Rep* **26**, 933-944 e934, doi:10.1016/j.celrep.2019.01.002 (2019).

46 Veziroglu, E. M. & Mias, G. I. Characterizing Extracellular Vesicles and Their Diverse RNA Contents. *Front Genet* **11**, 700, doi:10.3389/fgene.2020.00700 (2020).

47 Tian, Y. *et al.* Protein Profiling and Sizing of Extracellular Vesicles from Colorectal Cancer Patients via Flow Cytometry. *ACS Nano* **12**, 671-680, doi:10.1021/acsnano.7b07782 (2018).

48 Tauro, B. J. *et al.* Comparison of ultracentrifugation, density gradient separation, and immunoaffinity capture methods for isolating human colon cancer cell line LIM1863-derived exosomes. *Methods* **56**, 293-304, doi:10.1016/j.ymeth.2012.01.002 (2012).

49 Doyle, L. M. & Wang, M. Z. Overview of Extracellular Vesicles, Their Origin, Composition, Purpose, and Methods for Exosome Isolation and Analysis. *Cells* **8**, doi:10.3390/cells8070727 (2019).

50 Zaborowski, M. P., Balaj, L., Breakefield, X. O. & Lai, C. P. Extracellular Vesicles: Composition, Biological Relevance, and Methods of Study. *Bioscience* **65**, 783-797, doi:10.1093/biosci/biv084 (2015).

51 Veerman, R. E. *et al.* Molecular evaluation of five different isolation methods for extracellular vesicles reveals different clinical applicability and subcellular origin. *J Extracell Vesicles* **10**, e12128, doi:10.1002/jev2.12128 (2021).

52 Burkova, E. E., Sedykh, S. E. & Nevinsky, G. A. Human Placenta Exosomes: Biogenesis, Isolation, Composition, and Prospects for Use in Diagnostics. *Int J Mol Sci* **22**, doi:10.3390/ijms22042158 (2021).

53 Hur, J. Y. & Lee, K. Y. Characteristics and Clinical Application of Extracellular Vesicle-Derived DNA. *Cancers (Basel)* **13**, doi:10.3390/cancers13153827 (2021).

54 Elzanowska, J., Semira, C. & Costa-Silva, B. DNA in extracellular vesicles: biological and clinical aspects. *Mol Oncol* **15**, 1701-1714, doi:10.1002/1878-0261.12777 (2021).

55 O'Brien, K., Breyne, K., Ughetto, S., Laurent, L. C. & Breakefield, X. O. RNA delivery by extracellular vesicles in mammalian cells and its applications. *Nat Rev Mol Cell Biol* **21**, 585-606, doi:10.1038/s41580-020-0251-y (2020).

56 Zhou, Z. *et al.* Extracellular RNA in a single droplet of human serum reflects physiologic and disease states. *Proc Natl Acad Sci U S A* **116**, 19200-19208, doi:10.1073/pnas.1908252116 (2019).

57 Karimi, N. *et al.* Detailed analysis of the plasma extracellular vesicle proteome after separation from lipoproteins. *Cell Mol Life Sci* **75**, 2873-2886, doi:10.1007/s00018-018-2773-4 (2018).

58 Condrat, C. E. *et al.* miRNAs as Biomarkers in Disease: Latest Findings Regarding Their Role in Diagnosis and Prognosis. *Cells* **9**, doi:10.3390/cells9020276 (2020).

59 Sarkar, J. P. *et al.* Identification of miRNA Biomarkers for Diverse Cancer Types Using Statistical Learning Methods at the Whole-Genome Scale. *Front Genet* **11**, 982, doi:10.3389/fgene.2020.00982 (2020).

60 Liu, C. G., Song, J., Zhang, Y. Q. & Wang, P. C. MicroRNA-193b is a regulator of amyloid precursor protein in the blood and cerebrospinal fluid derived exosomal microRNA-193b is a biomarker of Alzheimer's disease. *Mol Med Rep* **10**, 2395-2400, doi:10.3892/mmr.2014.2484 (2014).

61 Morel, L. *et al.* Neuronal exosomal miRNA-dependent translational regulation of astroglial glutamate transporter GLT1. *J Biol Chem* **288**, 7105-7116, doi:10.1074/jbc.M112.410944 (2013).

62 Zhang, L. *et al.* Microenvironment-induced PTEN loss by exosomal microRNA primes brain metastasis outgrowth. *Nature* **527**, 100-104, doi:10.1038/nature15376 (2015).

63 Chen, C. C. *et al.* Elucidation of Exosome Migration across the Blood-Brain Barrier Model In Vitro. *Cell Mol Bioeng* **9**, 509-529, doi:10.1007/s12195-016-0458-3 (2016).

64 Record, M., Carayon, K., Poirot, M. & Silvente-Poirot, S. Exosomes as new vesicular lipid transporters involved in cell-cell communication and various pathophysiologies. *Biochim Biophys Acta* **1841**, 108-120, doi:10.1016/j.bbalip.2013.10.004 (2014).

65 Skotland, T., Sandvig, K. & Llorente, A. Lipids in exosomes: Current knowledge and the way forward. *Prog Lipid Res* **66**, 30-41, doi:10.1016/j.plipres.2017.03.001 (2017).

66 Flaherty, S. E., 3rd *et al.* A lipase-independent pathway of lipid release and immune modulation by adipocytes. *Science* **363**, 989-993, doi:10.1126/science.aaw2586 (2019).

67 Wang, W. *et al.* The crosstalk: exosomes and lipid metabolism. *Cell Commun Signal* **18**, 119, doi:10.1186/s12964-020-00581-2 (2020).

68 Skotland, T., Hessvik, N. P., Sandvig, K. & Llorente, A. Exosomal lipid composition and the role of ether lipids and phosphoinositides in exosome biology. *J Lipid Res* **60**, 9-18, doi:10.1194/jlr.R084343 (2019).

69 Lydic, T. A. *et al.* Rapid and comprehensive 'shotgun' lipidome profiling of colorectal cancer cell derived exosomes. *Methods* **87**, 83-95, doi:10.1016/j.ymeth.2015.04.014 (2015).

70 Lopez, E. *et al.* Platelet-derived- Extracellular Vesicles Promote Hemostasis and Prevent the Development of Hemorrhagic Shock. *Sci Rep* **9**, 17676, doi:10.1038/s41598-019-53724-y (2019).

71 Arraud, N. *et al.* Extracellular vesicles from blood plasma: determination of their morphology, size, phenotype and concentration. *J Thromb Haemost* **12**, 614-627, doi:10.1111/jth.12554 (2014).

72 An, K. *et al.* Exosomes neutralize synaptic-plasticity-disrupting activity of Abeta assemblies in vivo. *Mol Brain* **6**, 47, doi:10.1186/1756-6606-6-47 (2013).

73 Holm, M. M., Kaiser, J. & Schwab, M. E. Extracellular Vesicles: Multimodal Envoys in Neural Maintenance and Repair. *Trends Neurosci* **41**, 360-372, doi:10.1016/j.tins.2018.03.006 (2018).

74 Kwon, S. H. Extracellular vesicles in renal physiology and clinical applications for renal disease. *Korean J Intern Med* **34**, 470-479, doi:10.3904/kjim.2019.108 (2019).

75 van Balkom, B. W., Pisitkun, T., Verhaar, M. C. & Knepper, M. A. Exosomes and the kidney: prospects for diagnosis and therapy of renal diseases. *Kidney Int* **80**, 1138-1145, doi:10.1038/ki.2011.292 (2011).

76 Pisitkun, T., Shen, R. F. & Knepper, M. A. Identification and proteomic profiling of exosomes in human urine. *Proc Natl Acad Sci U S A* **101**, 13368-13373, doi:10.1073/pnas.0403453101 (2004).

77 Oggero, S., Austin-Williams, S. & Norling, L. V. The Contrasting Role of Extracellular Vesicles in Vascular Inflammation and Tissue Repair. *Front Pharmacol* **10**, 1479, doi:10.3389/fphar.2019.01479 (2019).

78 Yan, H. C. *et al.* The Delivery of Extracellular Vesicles Loaded in Biomaterial Scaffolds for Bone Regeneration. *Front Bioeng Biotechnol* **8**, 1015, doi:10.3389/fbioe.2020.01015 (2020).

79 Mathieu, M., Martin-Jaular, L., Lavieu, G. & Thery, C. Specificities of secretion and uptake of exosomes and other extracellular vesicles for cell-to-cell communication. *Nat Cell Biol* **21**, 9-17, doi:10.1038/s41556-018-0250-9 (2019).

80 Verma, M., Lam, T. K., Hebert, E. & Divi, R. L. Extracellular vesicles: potential applications in cancer diagnosis, prognosis, and epidemiology. *BMC Clin Pathol* **15**, 6, doi:10.1186/s12907-015-0005-5 (2015).

81 Dickhout, A. & Koenen, R. R. Extracellular Vesicles as Biomarkers in Cardiovascular Disease; Chances and Risks. *Front Cardiovasc Med* **5**, 113, doi:10.3389/fcvm.2018.00113 (2018).

82 Yuan, Q., Li, X. D., Zhang, S. M., Wang, H. W. & Wang, Y. L. Extracellular vesicles in neurodegenerative diseases: Insights and new perspectives. *Genes Dis* **8**, 124-132, doi:10.1016/j.gendis.2019.12.001 (2021).

83 Zhang, J., Li, H., Fan, B., Xu, W. & Zhang, X. Extracellular vesicles in normal pregnancy and pregnancy-related diseases. *J Cell Mol Med* **24**, 4377-4388, doi:10.1111/jcmm.15144 (2020).

84 Wu, W. C., Song, S. J., Zhang, Y. & Li, X. Role of Extracellular Vesicles in Autoimmune Pathogenesis. *Front Immunol* **11**, 579043, doi:10.3389/fimmu.2020.579043 (2020).

85 Zhou, B. *et al.* Application of exosomes as liquid biopsy in clinical diagnosis. *Signal Transduct Target Ther* **5**, 144, doi:10.1038/s41392-020-00258-9 (2020).

86 Liu, J. *et al.* Extracellular Vesicles in Liquid Biopsies: Potential for Disease Diagnosis. *Biomed Res Int* **2021**, 6611244, doi:10.1155/2021/6611244 (2021).

87 Yekula, A. *et al.* From laboratory to clinic: Translation of extracellular vesicle based cancer biomarkers. *Methods* **177**, 58-66, doi:10.1016/j.ymeth.2020.02.003 (2020).

88 Margolis, E. *et al.* Predicting high-grade prostate cancer at initial biopsy: clinical performance of the ExoDx (EPI) Prostate Intelliscore test in three independent prospective studies. *Prostate Cancer Prostatic Dis*, doi:10.1038/s41391-021-00456-8 (2021).

89 Kretschmer, A. *et al.* Validation of a CE-IVD, urine exosomal RNA expression assay for risk assessment of prostate cancer prior to biopsy. *Sci Rep* **12**, 4777, doi:10.1038/s41598-022-08608-z (2022).

90 Nair, S. & Salomon, C. Extracellular vesicles and their immunomodulatory functions in pregnancy. *Semin Immunopathol* **40**, 425-437, doi:10.1007/s00281-018-0680-2 (2018).

91 Tsang, J. C. H. *et al.* Integrative single-cell and cell-free plasma RNA transcriptomics elucidates placental cellular dynamics. *Proc Natl Acad Sci U S A* **114**, E7786-E7795, doi:10.1073/pnas.1710470114 (2017).

92 Ortega, M. A. *et al.* The Pivotal Role of the Placenta in Normal and Pathological Pregnancies: A Focus on Preeclampsia, Fetal Growth Restriction, and Maternal Chronic Venous Disease. *Cells* **11**, doi:10.3390/cells11030568 (2022).

93 Awoyemi, T. *et al.* Syncytiotrophoblast Extracellular Vesicles From Late-Onset Preeclampsia Placentae Suppress Pro-Inflammatory Immune Response in THP-1 Macrophages. *Front Immunol* **12**, 676056, doi:10.3389/fimmu.2021.676056 (2021).

94 Goldman-Wohl, D. S., Ariel, I., Greenfield, C., Hanoch, J. & Yagel, S. HLA-G expression in extravillous trophoblasts is an intrinsic property of cell differentiation: a lesson learned from ectopic pregnancies. *Mol Hum Reprod* **6**, 535-540, doi:10.1093/molehr/6.6.535 (2000).

95 Knofler, M. *et al.* Human placenta and trophoblast development: key molecular mechanisms and model systems. *Cell Mol Life Sci* **76**, 3479-3496, doi:10.1007/s00018-019-03104-6 (2019).

96 Tarrade, A. *et al.* Characterization of human villous and extravillous trophoblasts isolated from first trimester placenta. *Lab Invest* **81**, 1199-1211, doi:10.1038/labinvest.3780334 (2001).

97 Lyall, F., Robson, S. C. & Bulmer, J. N. Spiral artery remodeling and trophoblast invasion in preeclampsia and fetal growth restriction: relationship to clinical outcome. *Hypertension* **62**, 1046-1054, doi:10.1161/HYPERTENSIONAHA.113.01892 (2013).

98 Weel, I. C. *et al.* Association between Placental Lesions, Cytokines and Angiogenic Factors in Pregnant Women with Preeclampsia. *PLoS One* **11**, e0157584, doi:10.1371/journal.pone.0157584 (2016).

99 Staff, A. C. *et al.* Failure of physiological transformation and spiral artery atherosis: their roles in preeclampsia. *Am J Obstet Gynecol* **226**, S895-S906, doi:10.1016/j.ajog.2020.09.026 (2022).

100 Albrecht, E. D. & Pepe, G. J. Regulation of Uterine Spiral Artery Remodeling: a Review. *Reprod Sci* **27**, 1932-1942, doi:10.1007/s43032-020-00212-8 (2020).

101 Heazell, A. E. *et al.* IFPA Gabor Than Award Lecture: Recognition of placental failure is key to saving babies' lives. *Placenta* **36 Suppl 1**, S20-28, doi:10.1016/j.placenta.2014.12.017 (2015).

102 Chiarello, D. I. *et al.* Foetoplacental communication via extracellular vesicles in normal pregnancy and preeclampsia. *Mol Aspects Med* **60**, 69-80, doi:10.1016/j.mam.2017.12.002 (2018).

103 Burnett, L. A. & Nowak, R. A. Exosomes mediate embryo and maternal interactions at implantation and during pregnancy. *Front Biosci (Schol Ed)* **8**, 79-96, doi:10.2741/s448 (2016).

104 Tong, M. *et al.* In vivo targets of human placental micro-vesicles vary with exposure time and pregnancy. *Reproduction* **153**, 835-845, doi:10.1530/REP-16-0615 (2017).

105 Nakahara, A. *et al.* Circulating Placental Extracellular Vesicles and Their Potential Roles During Pregnancy. *Ochsner J* **20**, 439-445, doi:10.31486/toj.20.0049 (2020).

106 Sadovsky, Y. *et al.* Placental small extracellular vesicles: Current questions and investigative opportunities. *Placenta* **102**, 34-38, doi:10.1016/j.placenta.2020.03.002 (2020).

107 Sarker, S. *et al.* Placenta-derived exosomes continuously increase in maternal circulation over the first trimester of pregnancy. *J Transl Med* **12**, 204, doi:10.1186/1479-5876-12-204 (2014).

108 Levine, L. *et al.* Syncytiotrophoblast extracellular microvesicle profiles in maternal circulation for noninvasive diagnosis of preeclampsia. *Sci Rep* **10**, 6398, doi:10.1038/s41598-020-62193-7 (2020).

109 Salomon, C. *et al.* A gestational profile of placental exosomes in maternal plasma and their effects on endothelial cell migration. *PLoS One* **9**, e98667, doi:10.1371/journal.pone.0098667 (2014).

110 Gill, M. *et al.* Placental Syncytiotrophoblast-Derived Extracellular Vesicles Carry Active NEP (Neprilysin) and Are Increased in Preeclampsia. *Hypertension* **73**, 1112-1119, doi:10.1161/HYPERTENSIONAHA.119.12707 (2019).

111 Tong, M. & Chamley, L. W. Isolation and Characterization of Extracellular Vesicles from Ex Vivo Cultured Human Placental Explants. *Methods Mol Biol* **1710**, 117-129, doi:10.1007/978-1-4939-7498-6_9 (2018).

112 Pan, H. T. *et al.* Profiling of exosomal microRNAs expression in umbilical cord blood from normal and preeclampsia patients. *BMC Pregnancy Childbirth* **22**, 124, doi:10.1186/s12884-022-04449-w (2022).

113 Dixon, C. L. *et al.* Amniotic Fluid Exosome Proteomic Profile Exhibits Unique Pathways of Term and Preterm Labor. *Endocrinology* **159**, 2229-2240, doi:10.1210/en.2018-00073 (2018).

114 Maduray, K., Moodley, J. & Mackraj, I. The impact of circulating exosomes derived from early and late onset pre-eclamptic pregnancies on inflammatory cytokine secretion by BeWo cells. *Eur J Obstet Gynecol Reprod Biol* **247**, 156-162, doi:10.1016/j.ejogrb.2020.02.032 (2020).

115 Salomon, C. *et al.* Extravillous trophoblast cells-derived exosomes promote vascular smooth muscle cell migration. *Front Pharmacol* **5**, 175, doi:10.3389/fphar.2014.00175 (2014).

116 Konecna, B., Tothova, L. & Repiska, G. Exosomes-Associated DNA-New Marker in Pregnancy Complications? *Int J Mol Sci* **20**, doi:10.3390/ijms20122890 (2019).

117 Tong, M. *et al.* Proteomic characterization of macro-, micro- and nano-extracellular vesicles derived from the same first trimester placenta: relevance for feto-maternal communication. *Hum Reprod* **31**, 687-699, doi:10.1093/humrep/dew004 (2016).

118 Go, Y. Y., Lee, C. M., Ju, W. M., Chae, S. W. & Song, J. J. Extracellular Vesicles (Secretomes) from Human Trophoblasts Promote the Regeneration of Skin Fibroblasts. *Int J Mol Sci* **22**, doi:10.3390/ijms22136959 (2021).

119 Tannetta, D., Collett, G., Vatish, M., Redman, C. & Sargent, I. Syncytiotrophoblast extracellular vesicles - Circulating biopsies reflecting placental health. *Placenta* **52**, 134-138, doi:10.1016/j.placenta.2016.11.008 (2017).

120 Kupper, N. & Huppertz, B. The endogenous exposome of the pregnant mother: Placental extracellular vesicles and their effect on the maternal system. *Mol Aspects Med*, 100955, doi:10.1016/j.mam.2021.100955 (2021).

121 Pap, E. *et al.* T lymphocytes are targets for platelet- and trophoblast-derived microvesicles during pregnancy. *Placenta* **29**, 826-832, doi:10.1016/j.placenta.2008.06.006 (2008).

122 Orozco, A. F. *et al.* Placental release of distinct DNA-associated micro-particles into maternal circulation: reflective of gestation time and preeclampsia. *Placenta* **30**, 891-897, doi:10.1016/j.placenta.2009.06.012 (2009).

123 Kshirsagar, S. K. *et al.* Immunomodulatory molecules are released from the first trimester and term placenta via exosomes. *Placenta* **33**, 982-990, doi:10.1016/j.placenta.2012.10.005 (2012).

124 Tong, M., Abrahams, V. M. & Chamley, L. W. Immunological effects of placental extracellular vesicles. *Immunol Cell Biol*, doi:10.1111/imcb.12049 (2018).

125 Das, M. & Kale, V. Extracellular vesicles: Mediators of embryo-maternal crosstalk during pregnancy and a new weapon to fight against infertility. *Eur J Cell Biol* **99**, 151125, doi:10.1016/j.ejcb.2020.151125 (2020).

126 Tannetta, D., Masliukaite, I., Vatish, M., Redman, C. & Sargent, I. Update of syncytiotrophoblast derived extracellular vesicles in normal pregnancy and preeclampsia. *J Reprod Immunol* **119**, 98-106, doi:10.1016/j.jri.2016.08.008 (2017).

127 Mincheva-Nilsson, L. Immunosuppressive Protein Signatures Carried by Syncytiotrophoblast-Derived Exosomes and Their Role in Human Pregnancy. *Front Immunol* **12**, 717884, doi:10.3389/fimmu.2021.717884 (2021).

128 Siemaszko, J., Marzec-Przyszlak, A. & Bogunia-Kubik, K. NKG2D Natural Killer Cell Receptor-A Short Description and Potential Clinical Applications. *Cells* **10**, doi:10.3390/cells10061420 (2021).

129 Tannetta, D., Dragovic, R., Alyahyaei, Z. & Southcombe, J. Extracellular vesicles and reproduction-promotion of successful pregnancy. *Cell Mol Immunol* **11**, 548-563, doi:10.1038/cmi.2014.42 (2014).

130 Kovacs, A. F. *et al.* The impact of circulating preeclampsia-associated extracellular vesicles on the migratory activity and phenotype of THP-1 monocytic cells. *Sci Rep* **8**, 5426, doi:10.1038/s41598-018-23706-7 (2018).

131 Dong, L. *et al.* Comprehensive evaluation of methods for small extracellular vesicles separation from human plasma, urine and cell culture medium. *J Extracell Vesicles* **10**, e12044, doi:10.1002/jev2.12044 (2020).

132 Royo, F., Thery, C., Falcon-Perez, J. M., Nieuwland, R. & Witwer, K. W. Methods for Separation and Characterization of Extracellular Vesicles: Results of a Worldwide Survey Performed by the ISEV Rigor and Standardization Subcommittee. *Cells* **9**, doi:10.3390/cells9091955 (2020).

133 Burton, J. B., Carruthers, N. J. & Stemmer, P. M. Enriching extracellular vesicles for mass spectrometry. *Mass Spectrom Rev*, doi:10.1002/mas.21738 (2021).

134 Kowal, J. *et al.* Proteomic comparison defines novel markers to characterize heterogeneous populations of extracellular vesicle subtypes. *Proc Natl Acad Sci U S A* **113**, E968-977, doi:10.1073/pnas.1521230113 (2016).

135 Chhoy, P., Brown, C. W., Amante, J. J. & Mercurio, A. M. Protocol for the separation of extracellular vesicles by ultracentrifugation from in vitro cell culture models. *STAR Protoc* **2**, 100303, doi:10.1016/j.xpro.2021.100303 (2021).

136 Zhang, M. *et al.* Methods and Technologies for Exosome Isolation and Characterization. *Small Methods* **2**, 1800021, doi:https://doi.org/10.1002/smtd.201800021 (2018).

137 Chen, J. *et al.* Review on Strategies and Technologies for Exosome Isolation and Purification. *Front Bioeng Biotechnol* **9**, 811971, doi:10.3389/fbioe.2021.811971 (2021).

138 Zhang, X., Borg, E. G. F., Liaci, A. M., Vos, H. R. & Stoorvogel, W. A novel three step protocol to isolate extracellular vesicles from plasma or cell culture medium with both high yield and purity. *J Extracell Vesicles* **9**, 1791450, doi:10.1080/20013078.2020.1791450 (2020).

139 Yu, L. L. *et al.* A Comparison of Traditional and Novel Methods for the Separation of Exosomes from Human Samples. *Biomed Res Int* **2018**, 3634563, doi:10.1155/2018/3634563 (2018).

140 Soda, N., Rehm, B. H. A., Sonar, P., Nguyen, N. T. & Shiddiky, M. J. A. Advanced liquid biopsy technologies for circulating biomarker detection. *J Mater Chem B* **7**, 6670-6704, doi:10.1039/c9tb01490j (2019).

141 Alvarez, M. L., Khosroheidari, M., Kanchi Ravi, R. & DiStefano, J. K. Comparison of protein, microRNA, and mRNA yields using different methods of urinary exosome isolation for the discovery of kidney disease biomarkers. *Kidney Int* **82**, 1024-1032, doi:10.1038/ki.2012.256 (2012).

142 Monguio-Tortajada, M., Galvez-Monton, C., Bayes-Genis, A., Roura, S. & Borras, F. E. Extracellular vesicle isolation methods: rising impact of size-exclusion chromatography. *Cell Mol Life Sci* **76**, 2369-2382, doi:10.1007/s00018-019-03071-y (2019).

143 Sidhom, K., Obi, P. O. & Saleem, A. A Review of Exosomal Isolation Methods: Is Size Exclusion Chromatography the Best Option? *Int J Mol Sci* **21**, doi:10.3390/ijms21186466 (2020).

144 Li, P., Kaslan, M., Lee, S. H., Yao, J. & Gao, Z. Progress in Exosome Isolation Techniques. *Theranostics* **7**, 789-804, doi:10.7150/thno.18133 (2017).

145 Zarovni, N. *et al.* Integrated isolation and quantitative analysis of exosome shuttled proteins and nucleic acids using immunocapture approaches. *Methods* **87**, 46-58, doi:10.1016/j.ymeth.2015.05.028 (2015).

146 Zhao, Z., Wijerathne, H., Godwin, A. K. & Soper, S. A. Isolation and analysis methods of extracellular vesicles (EVs). *Extracell Vesicles Circ Nucl Acids* **2**, 80-103, doi:10.20517/evcna.2021.07 (2021).

147 Sun, N. *et al.* Purification of HCC-specific extracellular vesicles on nanosubstrates for early HCC detection by digital scoring. *Nat Commun* **11**, 4489, doi:10.1038/s41467-020-18311-0 (2020).

148 Chen, Y., Tang, Y., Long, W. & Zhang, C. Stem Cell-Released Microvesicles and Exosomes as Novel Biomarkers and Treatments of Diseases. *Stem Cells Int* **2016**, 2417268, doi:10.1155/2016/2417268 (2016).

149 Hong, C. S., Muller, L., Boyiadzis, M. & Whiteside, T. L. Isolation and characterization of CD34+ blast-derived exosomes in acute myeloid leukemia. *PLoS One* **9**, e103310, doi:10.1371/journal.pone.0103310 (2014).

150 Wang, J. *et al.* Analyses of Endothelial Cells and Endothelial Progenitor Cells Released Microvesicles by Using Microbead and Q-dot Based Nanoparticle Tracking Analysis. *Sci Rep* **6**, 24679, doi:10.1038/srep24679 (2016).

151 Gao, F. *et al.* A novel strategy for facile serum exosome isolation based on specific interactions between phospholipid bilayers and TiO2. *Chem Sci* **10**, 1579-1588, doi:10.1039/c8sc04197k (2019).

152 Nakai, W. *et al.* A novel affinity-based method for the isolation of highly purified extracellular vesicles. *Sci Rep* **6**, 33935, doi:10.1038/srep33935 (2016).

153 Guo, S. C., Tao, S. C. & Dawn, H. Microfluidics-based on-a-chip systems for isolating and analysing extracellular vesicles. *J Extracell Vesicles* **7**, 1508271, doi:10.1080/20013078.2018.1508271 (2018).

154 Zhang, Y. *et al.* A herringbone mixer based microfluidic device HBEXO-chip for purifying tumor-derived exosomes and establishing miRNA signature in pancreatic cancer. *Sensors and Actuators B: Chemical* **332**, 129511 (2021).

155 Zhang, P., He, M. & Zeng, Y. Ultrasensitive microfluidic analysis of circulating exosomes using a nanostructured graphene oxide/polydopamine coating. *Lab Chip* **16**, 3033-3042, doi:10.1039/c6lc00279j (2016).

156 Liang, L. G. *et al.* An integrated double-filtration microfluidic device for isolation, enrichment and quantification of urinary extracellular vesicles for detection of bladder cancer. *Sci Rep* **7**, 46224, doi:10.1038/srep46224 (2017).

157 Cho, S. *et al.* Isolation of extracellular vesicle from blood plasma using electrophoretic migration through porous membrane. *Sensors and Actuators B: Chemical* **233**, 289-297 (2016).

158 Wang, Z. *et al.* Ciliated micropillars for the microfluidic-based isolation of nanoscale lipid vesicles. *Lab Chip* **13**, 2879-2882, doi:10.1039/c3lc41343h (2013).

159 Yasui, T. *et al.* Unveiling massive numbers of cancer-related urinary-microRNA candidates via nanowires. *Sci Adv* **3**, e1701133, doi:10.1126/sciadv.1701133 (2017).

160 Wu, M. *et al.* Isolation of exosomes from whole blood by integrating acoustics and microfluidics. *Proc Natl Acad Sci U S A* **114**, 10584-10589, doi:10.1073/pnas.1709210114 (2017).

161 Liu, C. *et al.* Field-Free Isolation of Exosomes from Extracellular Vesicles by Microfluidic Viscoelastic Flows. *ACS Nano* **11**, 6968-6976, doi:10.1021/acsnano.7b02277 (2017).

162 Raju, D., Bathini, S., Badilescu, S., Ghosh, A. & Packirisamy, M. Microfluidic Platforms for the Isolation and Detection of Exosomes: A Brief Review. *Micromachines* **13**, 730 (2022).

163 Reategui, E. *et al.* Engineered nanointerfaces for microfluidic isolation and molecular profiling of tumor-specific extracellular vesicles. *Nat Commun* **9**, 175, doi:10.1038/s41467-017-02261-1 (2018).

164 Foley, H. B. *et al.* Extracellular vesicle-enriched miRNA profiles across pregnancy in the MADRES cohort. *PLoS One* **16**, e0251259, doi:10.1371/journal.pone.0251259 (2021).

165 Karttunen, J., Heiskanen, M., Lipponen, A., Poulsen, D. & Pitkanen, A. Extracellular Vesicles as Diagnostics and Therapeutics for Structural Epilepsies. *Int J Mol Sci* **20**, doi:10.3390/ijms20061259 (2019).

166 Ortega, M. A. *et al.* Unfolding the role of placental-derived Extracellular Vesicles in Pregnancy: From homeostasis to pathophysiology. *Front Cell Dev Biol* **10**, 1060850, doi:10.3389/fcell.2022.1060850 (2022).

167 Menon, R. & Shahin, H. Extracellular vesicles in spontaneous preterm birth. *Am J Reprod Immunol* **85**, e13353, doi:10.1111/aji.13353 (2021).

168 Yin, P., Lehmann, R. & Xu, G. Effects of pre-analytical processes on blood samples used in metabolomics studies. *Anal Bioanal Chem* **407**, 4879-4892, doi:10.1007/s00216-015-8565-x (2015).

169 Martire, S. *et al.* A First Phenotypic and Functional Characterization of Placental Extracellular Vesicles from Women with Multiple Sclerosis. *Int J Mol Sci* **22**, doi:10.3390/ijms22062875 (2021).

170 Ayala-Ramirez, P. *et al.* Assessment of Placental Extracellular Vesicles-Associated Fas Ligand and TNF-Related Apoptosis-Inducing Ligand in Pregnancies Complicated by Early and Late Onset Preeclampsia. *Front Physiol* **12**, 708824, doi:10.3389/fphys.2021.708824 (2021).

171 Nair, S. *et al.* Human placental exosomes in gestational diabetes mellitus carry a specific set of miRNAs associated with skeletal muscle insulin sensitivity. *Clin Sci (Lond)* **132**, 2451-2467, doi:10.1042/CS20180487 (2018).

172 Bai, K. *et al.* Human placental exosomes induce maternal systemic immune tolerance by reprogramming circulating monocytes. *J Nanobiotechnology* **20**, 86, doi:10.1186/s12951-022-01283-2 (2022).

173 Stam, J., Bartel, S., Bischoff, R. & Wolters, J. C. Isolation of extracellular vesicles with combined enrichment methods. *J Chromatogr B Analyt Technol Biomed Life Sci* **1169**, 122604, doi:10.1016/j.jchromb.2021.122604 (2021).

174 Cooke, W. R., Jones, G. D., Redman, C. W. G. & Vatish, M. Syncytiotrophoblast Derived Extracellular Vesicles in Relation to Preeclampsia. *Maternal-Fetal Medicine* **3**, 151-160, doi:10.1097/fm9.0000000000000093 (2021).

175 Morgan, T. K. Cell- and size-specific analysis of placental extracellular vesicles in maternal plasma and pre-eclampsia. *Transl Res* **201**, 40-48, doi:10.1016/j.trsl.2018.08.004 (2018).

176 Sabapatha, A., Gercel-Taylor, C. & Taylor, D. D. Specific isolation of placenta-derived exosomes from the circulation of pregnant women and their immunoregulatory consequences. *Am J Reprod Immunol* **56**, 345-355, doi:10.1111/j.1600-0897.2006.00435.x (2006).

177 Menon, R. *et al.* Protein Profile Changes in Circulating Placental Extracellular Vesicles in Term and Preterm Births: A Longitudinal Study. *Endocrinology* **161**, 1-19, doi:10.1210/endocr/bqaa009 (2020).

178 Lai, A., Elfeky, O., Rice, G. E. & Salomon, C. Optimized Specific Isolation of Placenta-Derived Exosomes from Maternal Circulation. *Methods Mol Biol* **1710**, 131-138, doi:10.1007/978-1-4939-7498-6_10 (2018).

179 Cho, K., Kook, H., Kang, S. & Lee, J. Study of immune-tolerized cell lines and extracellular vesicles inductive environment promoting continuous expression and secretion of HLA-G from semiallograft immune tolerance during pregnancy. *J Extracell Vesicles* **9**, 1795364, doi:10.1080/20013078.2020.1795364 (2020).

180 Fitzgerald, W., Gomez-Lopez, N., Erez, O., Romero, R. & Margolis, L. Extracellular vesicles generated by placental tissues ex vivo: A transport system for immune mediators and growth factors. *Am J Reprod Immunol* **80**, e12860, doi:10.1111/aji.12860 (2018).

181 Weitzner, O., Yagur, Y., Weissbach, T., Man El, G. & Biron-Shental, T. Preeclampsia: risk factors and neonatal outcomes associated with early- versus late-onset diseases. *J Matern Fetal Neonatal Med* **33**, 780-784, doi:10.1080/14767058.2018.1500551 (2020).

182 Tong, J., Niu, Y., Chen, Z. J. & Zhang, C. Comparison of the transcriptional profile in the decidua of early-onset and late-onset pre-eclampsia. *J Obstet Gynaecol Res* **46**, 1055-1066, doi:10.1111/jog.14257 (2020).

183 Sheridan, M. A. *et al.* Early onset preeclampsia in a model for human placental trophoblast. *Proc Natl Acad Sci U S A* **116**, 4336-4345, doi:10.1073/pnas.1816150116 (2019).

184 E., G., Akurati, L. & Radhika, K. Early onset and late onset preeclampsia-maternal and perinatal outcomes in a rural teritiary health center. *2018* **7**, 4, doi:10.18203/2320-1770.ijrcog20182333 (2018).

185 Gupte, S. & Wagh, G. Preeclampsia-eclampsia. *J Obstet Gynaecol India* **64**, 4-13, doi:10.1007/s13224-014-0502-y (2014).

186 Nguyen, T. P. H., Patrick, C. J., Parry, L. J. & Familari, M. Using proteomics to advance the search for potential biomarkers for preeclampsia: A systematic review and meta-analysis. *PLoS One* **14**, e0214671, doi:10.1371/journal.pone.0214671 (2019).

187 Salomon, C. *et al.* Placental Exosomes as Early Biomarker of Preeclampsia: Potential Role of Exosomal MicroRNAs Across Gestation. *J Clin Endocrinol Metab* **102**, 3182-3194, doi:10.1210/jc.2017-00672 (2017).

188 Wang, Z., Zhao, G., Zeng, M., Feng, W. & Liu, J. Overview of extracellular vesicles in the pathogenesis of preeclampsiadagger. *Biol Reprod* **105**, 32-39, doi:10.1093/biolre/ioab060 (2021).

189 Tannetta, D. S., Dragovic, R. A., Gardiner, C., Redman, C. W. & Sargent, I. L. Characterisation of syncytiotrophoblast vesicles in normal pregnancy and pre-eclampsia: expression of Flt-1 and endoglin. *PLoS One* **8**, e56754, doi:10.1371/journal.pone.0056754 (2013).

190 Chen, Y. *et al.* Association of placenta-derived extracellular vesicles with pre-eclampsia and associated hypercoagulability: a clinical observational study. *BJOG* **128**, 1037-1046, doi:10.1111/1471-0528.16552 (2021).

191 Pillay, P., Maharaj, N., Moodley, J. & Mackraj, I. Placental exosomes and pre-eclampsia: Maternal circulating levels in normal pregnancies and, early and late onset pre-eclamptic pregnancies. *Placenta* **46**, 18-25, doi:10.1016/j.placenta.2016.08.078 (2016).

192 Thalor, N. *et al.* A correlation between platelet indices and preeclampsia. *Hematol Transfus Cell Ther* **41**, 129-133, doi:10.1016/j.htct.2018.08.008 (2019).

193 Chang, X. *et al.* Exosomes From Women With Preeclampsia Induced Vascular Dysfunction by Delivering sFlt (Soluble Fms-Like Tyrosine Kinase)-1 and sEng (Soluble Endoglin) to Endothelial Cells. *Hypertension* **72**, 1381-1390, doi:10.1161/HYPERTENSIONAHA.118.11706 (2018).

194 Motta-Mejia, C. *et al.* Placental Vesicles Carry Active Endothelial Nitric Oxide Synthase and Their Activity is Reduced in Preeclampsia. *Hypertension* **70**, 372-381, doi:10.1161/HYPERTENSIONAHA.117.09321 (2017).

195 Hagmann, H., Thadhani, R., Benzing, T., Karumanchi, S. A. & Stepan, H. The promise of angiogenic markers for the early diagnosis and prediction of preeclampsia. *Clin Chem* **58**, 837-845, doi:10.1373/clinchem.2011.169094 (2012).

196 Zeisler, H. *et al.* Predictive Value of the sFlt-1:PlGF Ratio in Women with Suspected Preeclampsia. *N Engl J Med* **374**, 13-22, doi:10.1056/NEJMoa1414838 (2016).

197 Baig, S. *et al.* Proteomic analysis of human placental syncytiotrophoblast microvesicles in preeclampsia. *Clin Proteomics* **11**, 40, doi:10.1186/1559-0275-11-40 (2014).

198 Jia, R. *et al.* Comparative Proteomic Profile of the Human Umbilical Cord Blood Exosomes between Normal and Preeclampsia Pregnancies with High-Resolution Mass Spectrometry. *Cell Physiol Biochem* **36**, 2299-2306, doi:10.1159/000430193 (2015).

199 Sammar, M. *et al.* Reduced placental protein 13 (PP13) in placental derived syncytiotrophoblast extracellular vesicles in preeclampsia - A novel tool to study the impaired cargo transmission of the placenta to the maternal organs. *Placenta* **66**, 17-25, doi:10.1016/j.placenta.2018.04.013 (2018).

200 Awoyemi, T. *et al.* Glycosylated Siglec-6 expression in syncytiotrophoblast-derived extracellular vesicles from preeclampsia placentas. *Biochem Biophys Res Commun* **533**, 838-844, doi:10.1016/j.bbrc.2020.09.081 (2020).

201 Navajas, R. *et al.* Quantitative proteomic analysis of serum-purified exosomes identifies putative pre-eclampsia-associated biomarkers. *Clin Proteomics* **19**, 5, doi:10.1186/s12014-022-09342-4 (2022).

202 Shen, L. *et al.* Placentaassociated serum exosomal miR155 derived from patients with preeclampsia inhibits eNOS expression in human umbilical vein endothelial cells. *Int J Mol Med* **41**, 1731-1739, doi:10.3892/ijmm.2018.3367 (2018).

203 Pillay, P., Vatish, M., Duarte, R., Moodley, J. & Mackraj, I. Exosomal microRNA profiling in early and late onset preeclamptic pregnant women reflects pathophysiology. *Int J Nanomedicine* **14**, 5637-5657, doi:10.2147/IJN.S208865 (2019).

204 Li, H. *et al.* Unique microRNA Signals in Plasma Exosomes from Pregnancies Complicated by Preeclampsia. *Hypertension* **75**, 762-771, doi:10.1161/HYPERTENSIONAHA.119.14081 (2020).

205 Baig, S. *et al.* Lipidomic analysis of human placental syncytiotrophoblast microvesicles in adverse pregnancy outcomes. *Placenta* **34**, 436-442, doi:10.1016/j.placenta.2013.02.004 (2013).

206 Navajas, R., Corrales, F. & Paradela, A. Quantitative proteomics-based analyses performed on pre-eclampsia samples in the 2004-2020 period: a systematic review. *Clin Proteomics* **18**, 6, doi:10.1186/s12014-021-09313-1 (2021).

207 McElrath, T. F. *et al.* Late first trimester circulating microparticle proteins predict the risk of preeclampsia < 35 weeks and suggest phenotypic differences among affected cases. *Sci Rep* **10**, 17353, doi:10.1038/s41598-020-74078-w (2020).

208 Vykoukal, J. *et al.* Plasma-derived extracellular vesicle proteins as a source of biomarkers for lung adenocarcinoma. *Oncotarget* **8**, 95466-95480, doi:10.18632/oncotarget.20748 (2017).

209 Rasmussen, M. *et al.* RNA profiles reveal signatures of future health and disease in pregnancy. *Nature* **601**, 422-427, doi:10.1038/s41586-021-04249-w (2022).

210 Yadama, A. P. *et al.* Early-pregnancy transcriptome signatures of preeclampsia: from peripheral blood to placenta. *Sci Rep* **10**, 17029, doi:10.1038/s41598-020-74100-1 (2020).

211 Tong, J. *et al.* Transcriptomic Profiling in Human Decidua of Severe Preeclampsia Detected by RNA Sequencing. *J Cell Biochem* **119**, 607-615, doi:10.1002/jcb.26221 (2018).

212 Liu, J. L., Zhang, W. Q. & Huang, M. Y. Transcriptional signature of the decidua in preeclampsia. *Proc Natl Acad Sci U S A* **115**, E5434-E5436, doi:10.1073/pnas.1802234115 (2018).

213 Cao, M. *et al.* Differential circular RNA expression profiles in umbilical cord blood exosomes from preeclampsia patients. *BMC Pregnancy Childbirth* **21**, 303, doi:10.1186/s12884-021-03777-7 (2021).

214 Devor, E., Santillan, D., Scroggins, S., Warrier, A. & Santillan, M. Trimester-specific plasma exosome microRNA expression profiles in preeclampsia. *J Matern Fetal Neonatal Med* **33**, 3116-3124, doi:10.1080/14767058.2019.1569614 (2020).

Chapter 3

Magnetic Enrichment of Immuno-Specific Extracellular Vesicles for Mass Spectrometry Using Biofilm-Derived Iron Oxide Nanowires

3 Magnetic enrichment of immuno-specific extracellular vesicles for mass spectrometry using biofilm-derived iron oxide nanowires

3.1 Publication details

This chapter was published as a paper in Nanoscale. The manuscript was submitted on 11 Oct 2022, accepted on 14 Dec 2022 and first published on 19 Dec 2022 (doi.org/10.1039/D2NR05619D, *Nanoscale*, 2023,15, 1236-1247).

Magnetic enrichment of immuno-specific extracellular vesicles for mass spectrometry using biofilm-derived iron oxide nanowires

Quang Nghia Pham,[a] Marnie Winter,[*a] Valentina Milanova,[a] Clifford Young,[b] Mark R. Condina,[a] Peter Hoffmann,[b] Nguyen T. H. Pham,[c] Tran Thanh Tung,[d] Dusan Losic,[d] Benjamin Thierry[*a]

[a]Future Industries Institute, University of South Australia, Mawson Lakes Campus, Mawson Lakes, Adelaide, South Australia 5095, Australia. E-mail: marnie.winter@unisa.edu.au, benjamin.thierry@unisa.edu.au

[b]Clinical and Health Sciences, University of South Australia, City West Campus, Adelaide, South Australia 5000, Australia

[c]School of Chemistry, The University of Sydney, Sydney, New South Wales 2006, Australia

[d]School of Chemical Engineering and Advanced Materials, The University of Adelaide, Adelaide, South Australia 5005, Australia

[*]Corresponding authors

3.2 Statement of authorship

This paper reports on original research I conducted during the period of my Higher Degree by Research candidature and is not subject to any obligations or contractual agreements with a third party that would constrain its inclusion in this thesis I am the primary author of this paper.

A statement of authorship describing details of each author's contribution to this publication is provided in Appendix A, page 89.

3.3 Abstract

Immuno-specific enrichment of extracellular vesicles (EVs) can provide important information into cellular pathways underpinning various pathologies and for non-invasive diagnostics, including mass spectrometry-based analyses. Herein, we report an optimised protocol for immuno-magnetic enrichment of specific EV subtypes and their subsequent processing with liquid chromatography-tandem mass spectrometry (LC-MS/MS). Specifically, we conjugated placental alkaline phosphatase (PLAP) antibodies to magnetic iron oxide nanowires (NWs) derived from bacterial biofilms and demonstrated the utility of this approach by enriching placenta-specific EVs (containing PLAP) from cell culture media. We demonstrate efficient PLAP+ve EV enrichment for both NW-PLAP and Dynabeads™-PLAP, with high PLAP protein recovery (83.7 ± 8.9% and 83.2 ± 5.9%, respectively), high particle-to-protein ratio (7.5 ± 0.7 × 109 and 7.1 ± 1.2 × 109, respectively), and low non-specific binding of non-target EVs (7 ± 3.2% and 5.4 ± 2.2%, respectively). Furthermore, our optimized EV enrichment and processing approach identified 2518 and 2545 protein groups with LC-MS/MS for NW-PLAP and Dynabead™-PLAP, respectively, with excellent reproducibility (Pearson correlation 0.986 and 0.988). These findings demonstrate that naturally occurring iron oxide NWs have comparable performance to current gold standard immune-magnetic beads. The optimized immuno-specific EV enrichment for LC-MS/MS method provides a low-cost and highly-scalable yet efficient, high-throughput approach for quality EV proteomic studies.

3.4 Introduction

Extracellular vesicles (EVs) are a collective group of lipid bilayer-enclosed particles present in most biological fluids such as blood, amniotic fluid, urine, cerebrospinal fluid and cell culture media.[1-3] EVs are important in many biological processes including intercellular communication, signal transduction, immune response and maintenance of cellular homeostasis.[4,5] EVs have been increasingly recognized as a promising source of biomarkers since the biomolecule cargo including DNA, mRNA, proteins, lipids and microRNA, often reflect the physiological and pathological conditions of the parent cells.[6] Moreover, biomolecules are better protected from enzymatic degradation while

being transported within EVs as compared to free proteins and RNAs.[7-9] Given that EVs can be non-invasively obtained through blood serum and plasma, analyses of EV number and molecular content have already provided important insights for the understanding and diagnosis of diseases.[10-14]

According to the Minimal Information for Studies of Extracellular Vesicles 2018 (MISEV2018), EVs can be classified as small (<200 nm) and large EVs (>200 nm).[15] Ultracentrifugation and size exclusion chromatography are the most popular approaches used to enrich EVs based on their physicochemical properties, namely density and size.[16] Importantly, EVs display specific proteins which relate to their biogenesis and cell of origin. These proteins can be exploited for immuno-specific enrichment of EV subtypes.[17,18] To this end, affinity ligands such as antibodies and aptamers are typically immobilized on a solid support allowing for selective enrichment.[19] The most common immunoaffinity approach is based on magnetic materials conjugated with antibodies to bind specific EV proteins followed by separation under a magnetic field. Immuno-magnetic methods produce high-purity isolates of immuno-specific EVs with low contamination rates in a rapid and efficient manner.[20-23] Immunoaffinity EV enrichment can also be achieved with microfluidic devices.[24] However, microfluidic approaches typically suffer from low throughput which limits their use for applications that require a large amount of EVs for downstream analyses including biomarker discovery, particularly when low-abundant EV subtypes are the target.[25,26] Immuno-magnetic isolation therefore currently offers the best approach for the enrichment of EV subtypes and has been shown to be compatible with proteomic approaches such as liquid chromatography-tandem mass spectrometry analysis (LC-MS/MS).[27]

Many types of magnetic materials have been investigated for immuno-magnetic EV enrichment. These materials are typically selected based on their responsiveness to magnetic fields and high surface area for binding. Iron oxide-based particles are the most common and a range of sizes have been used including micron-sized magnetic beads[25] (e.g. Dynabead)[28] and nanoparticles.[29] The availability of commercially available beads such as Dynabead and automated technologies have made their use more widespread and standardized, with well-established protocols available for many applications.[30]

Importantly, a necessary trade-off should be established with respect to the dimension of the magnetic materials used for EV enrichment. On one hand, high surface area such as

in the case of magnetic nanoparticles enables high EV capture yield. On the other hand, larger materials such as in the case of magnetic microbeads afford better magnetic recovery of the EVs and their biological cargo. Magnetic nanowires (NWs) offer an excellent compromise balancing the requirements of high surface area (for efficient capture of target EVs) and strong magnetic strength (for efficient magnetic recovery).[31] Several magnetic NWs have shown utility in a range of bioanalytical applications, including the enrichment of cells, proteins, RNA, DNA and EVs.[32-34] For example, magnetic poly pyrrole NWs (electrochemically prepared from an anodised aluminium oxide (AAO) template by embedding iron oxide magnetic nanoparticles) allowed rapid enrichment of EVs with relatively high yield and purity when conjugated to a cocktail of EV specific antibodies (anti-CD9, anti-CD63 and anti-CD81), with a threefold increase in the yield compared to commercially available methods such as ExoQuick™ and Invitrogen Total Exosome Isolation Kit.[35] The same approach could also be used to achieve rapid and high yield capture of cell-free DNA and circulating tumour cells while minimizing DNA loss and damage.[36] The *in vitro* cellular uptake and internalization of magnetic nickel NWs has also been shown to be a fast and cost-effective approach for non-specific EV enrichment from cell culture.[34] While these studies convincingly outline the potential of magnetic NWs, the reliance on complex, expensive and inherently low-throughput synthesis routes such as templating hampers the routine use of magnetic NWs for EV enrichment. A simple, cost-effective and scalable method to prepare magnetic NWs for immunomagnetic enrichment of EVs and other relevant biomolecules is extremely desirable.

Towards addressing this challenge, we report here an immuno-magnetic enrichment method for specific EV subtypes and their subsequent analysis with mass spectrometry. We benchmarked the enrichment performance of naturally produced iron oxide NWs with commercially available Dynabead and perform mass spectrometry on enriched EVs. The magnetic NWs are extracted and purified from biofilms of zetaproteobacteria *Mariprofundus ferrooxydans* through an environmentally friendly process.[37] These NWs have previously been shown to have a large surface to volume ratio, respond rapidly to magnetic fields, and have been explored as magnetically targeted drug carriers.[37] For bioconjugation with antibodies and improved colloidal stability, we modified the NWs with reversible addition-fragmentation chain transfer (RAFT)s diblock copolymers (*p*AAm) with high binding affinities to iron oxide (Figure. 3-1A). As a proof of concept,

we demonstrated the immuno-specific enrichment of EVs based on the expression of placental alkaline phosphatase (PLAP) (Figure 3-1B). PLAP is expressed in the human placenta mainly by syncytiotrophoblasts and is known to be present in maternal blood with levels increasing over gestation.[38,39] Syncytiotrophoblasts derived EVs are anticipated to provide a non-invasive window into placental (and hence fetal) health.[40] However, compared to maternal EVs, PLAP+ve EVs represent only a portion of total EVs in the maternal circulation (up to ~20% in early pregnancy),[41] meaning that efficient immuno-enrichment is required in order to fully understand the relevance of these vesicles or harness their diagnostic utility. The magnetic NWs conjugated with anti-PLAP antibodies efficiently enriched PLAP+ve EVs produced by the trophoblast-like chorionic carcinoma BeWo cell line used as a model, similar to that afforded by the current commercial gold standard Dynabead. In addition, we also designed and optimized a protocol for LC-MS/MS analysis of the enriched PLAP+ve EVs.

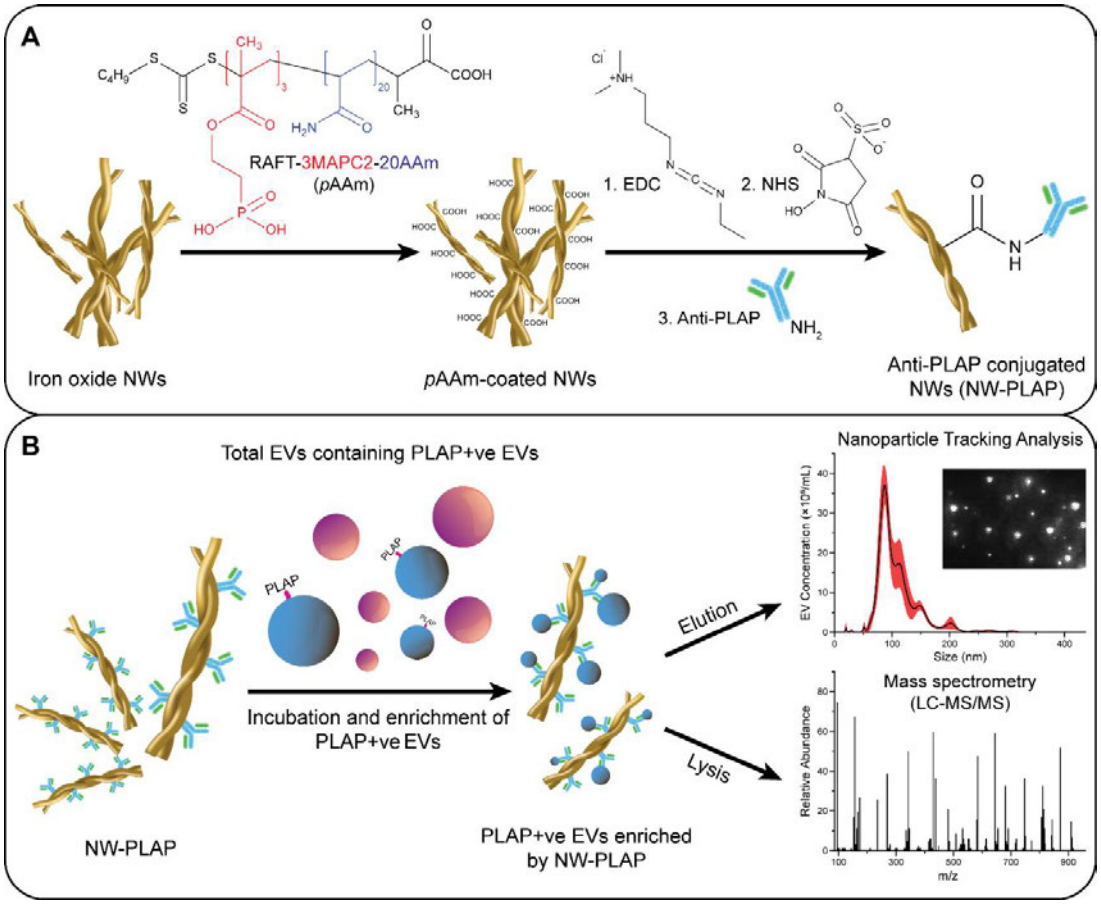

Figure 3-1 Surface modification of iron oxide NWs and enrichment of PLAP+ve EVs.
(A) Schematic of biofunctionalization route of the NWs with diblock RAFT copolymers (poly(methacryloyloxyethyl phosphate)$_3$-*block*-poly(acrylamide)$_{20}$, referred to as *p*AAm) and anti-PLAP antibodies. (B) Enrichment procedure of PLAP+ve EVs for downstream analyses with nanoparticle tracking analysis and mass spectrometry (LC-MS/MS).

3.5 Materials

1-Ethyl-3-(3-dimethylaminopropyl)carbodiimide hydrochloride (EDC-HCl), N-hydroxysuccinimide (NHS), 4-morpholineethanesulfonic acid monohydrate (MES monohydrate), ethanolamine, bovine serum albumin (BSA) were purchased from Sigma Aldrich. Anti-PLAP antibody (8B6) was purchased from Life Technologies Pty Ltd.

3.5.1 Preparation of iron oxide NWs

Bacteria-derived NWs were extracted and purified as described previously.[37,42] Briefly, bacteria biofilm waste provided by SA Water (South Australia) was resuspended in milli-Q water and purified through repeated washing and centrifuge cycles to remove organic and inorganic impurities. The purified NWs extracted from the biofilms were annealed at 600 °C to change their crystal phase and increase their magnetic properties. After thermal annealing, the NWs were washed again with milli-Q water, dried at 70 °C and stored at room temperature until use.

3.5.2 Preparation of poly(methacryloyloxyethyl phosphate)$_3$-*block*-poly(acrylamide)$_{20}$ RAFT Polymer (RAFT-3MAPC2-20AAM)

RAFT-3MAPC2-20AAM diblock polymers, referred to as *p*AAm, were synthesised based on a previously published procedure with small modifications.[43] Briefly, the RAFT diblock polymer consisted of RAFT-COOH agent (2-(((butylthio)carbonothioyl)-thio)-propanoic acid), anchoring (methacryloyloxy)ethyl phosphonate groups (n = 3 monomers) and a block of stabilising polyacrylamide polymer (n = 20 monomers).

3.5.3 Conjugation of Antibody to NWs and Dynabeads

The NWs were first coated with the *p*AAm diblock polymers. NWs (10 mg) and *p*AAm (50 mg) were first resuspended in milli-Q water and sonicated. The pH of *p*AAm solution was adjusted to 4 using 0.1 M sodium hydroxide and added dropwise to the NW suspension while being sonicated on ice. The mixture was left to react under continuous mixing (300 rpm) on an orbital shaker for 18 h at room temperature. After that, the pH of the mixture was sequentially adjusted to pH 5 and then 6 using 0.1 M sodium hydroxide with ice-cold sonication in between. *p*AAm-coated NWs (NW-*p*AAm) were washed with milli-Q water three times to remove salts and unreacted copolymers and finally resuspended in milli-Q water to the desired concentration of 10 mg/mL. Carbodiimide coupling reaction was carried out to covalently conjugate antibodies to the NW-*p*AAm through the terminal carboxylic acid functional groups. Briefly, NW-*p*AAm (1 mg),

EDC-HCl (76 mg/mL) and NHS (11.5 mg/mL) were mixed in milli-Q water (mixture pH 5.7) for 5 min at room temperature. The activated NWs were then subsequently washed once with milli-Q water and phosphate buffer saline (1 × PBS pH 7.4, 10010023, Life Technologies) and immediately added to PBS buffer containing the antibodies (40 µg). The conjugation reaction was carried out under continuous mixing (800 rpm) for 2 h at room temperature using a ThermoMixer (Eppendorf). The resulting antibody-conjugated NWs were washed three times with PBS buffer to remove non-reacted antibodies, further reacted with 50 mM ethanolamine to quench non-reacted activated carboxylic acid groups and blocked with 0.5% BSA. The antibody-conjugated NWs were finally resuspended in PBS buffer, stored at 4 °C and used within two weeks of conjugation. The conjugation efficiency of antibodies to NWs was determined by:

$$\frac{\text{Input antibody} - \text{Unconjugated antibody}}{\text{Input antibody}} \times 100$$

Dynabeads M-270 carboxylic acid (14305D, Invitrogen) were used as the reference gold standard. The beads were activated and conjugated to antibodies according to the manual. Briefly, Dynabead (3 mg) were washed with 25 mM MES buffer and reacted with EDC-HCl (50 mg/mL) and NHS (50 mg/mL) with shaking for 30 min at room temperature. Activated beads were subsequently washed with 25 mM MES buffer and PBS buffer and reacted with antibodies (120 µg) for 2 h at room temperature. Antibody-conjugated Dynabead were washed twice with PBS buffer, quenched with 50 mM ethanolamine, and blocked with 0.5% BSA. The beads were resuspended in PBS buffer, stored at 4 °C and used within two weeks of conjugation.

3.5.4 Characterisation of iron oxide NWs

The morphology of the NWs was analysed by field emission scanning electron microscope (FE-SEM, Carl Zeiss Microscopy Merlin) and transmission electron microscope (TEM, Tecnai G2 operated at 120 kV and equipped with an EDAX X-ray detector). The relative evolution of the NW sizes upon biofunctionalization was monitored by measuring changes in the scattering profile with dynamic light scattering (DLS, Zetasizer Nano ZS90, Malvern). The elemental composition was measured using X-ray photoelectron spectroscopy (XPS, Kratos AXIS Ultra DLD) for NWs casted onto silicon wafer substrates as described previously.[44] XPS survey scans (0–1200 eV) were performed with a pass energy of 160 eV and a step size of 0.5 eV. High-resolution spectra

of C 1s, O 1s and N 1s were scanned with the pass energy of 20 eV and step size of 0.1 eV. XPS spectra were analyzed using the CasaXPS software (v2.3.18). The binding energy of the survey and high-resolution scan was referenced to that of C 1s CC/CH peak at 284.8 eV. The magnetic property of these iron oxide NWs derived from biofilms was evaluated by a vibrating sample magnetometer (VSM) using a magnetic field of ± 20 kOe.

3.5.5 Cell culture and pre-enrichment of total EVs

BeWo choriocarcinoma cells (trophoblast-like cell line) were cultured at 37 °C in a humidified incubator with 5% CO_2 in Roswell Park Memorial Institute media (RPMI 1640, Gibco) supplemented with 10% fetal bovine serum (FBS, Gibco) and penicillin/streptomycin (10 000 U/mL, Gibco). Once 80–90% confluency was reached, the culture media was removed, and the cells were washed twice with 1 × Dulbecco's phosphate-buffered saline (DPBS, Gibco). The cells were then continuously cultured in the FBS-free medium for an additional 48 h. Culture media was collected and total EVs were pre-enriched based on a previously published protocol.[45] First, the media containing EVs (22 mL) was centrifuged for 20 min and 2000 × *g* for 20 min at 4 °C (5699-R rotor, Rotanta 460 R, Hettich) to remove dead cells and debris. The supernatant was then centrifuged at 10 000 × *g* for 30 min at 4 °C to pellet large EVs and then ultracentrifuged at 120 000 × *g* for 70 min at 4 °C (70 Ti rotor, Optima L-80 XP, Beckman Coulter) to pellet small EVs. Pellets of small and large EVs were washed twice with PBS buffer, combined together, resuspended in PBS buffer and stored at −80 °C for two weeks.

3.5.6 Enrichment of PLAP+ve EVs by NWs and Dynabead

Pre-enriched BeWo EVs were incubated with comparable amounts of anti-PLAP antibody conjugated magnetic NWs or Dynabead (NW-PLAP or Dynabead-PLAP) overnight at 4 °C with shaking (800 rpm) to promote attachment of EVs. EV-captured NWs and Dynabead were separated using 0.5 T neodymium magnets (3489, Aussie Magnet) fixed into a 3D-printed magnetic separation rack (Figure 3-7, Section 3.5), and the supernatants were collected for the quantification of PLAP proteins. EV-captured NWs and Dynabead were washed three times with 500 μL of PBS buffer. EVs were either released from the magnetic NWs/Dynabead for nanoparticle tracking analysis (NTA) or lysed directly to extract the protein cargo. After applying the magnet, the lysates were collected and stored at −80 °C for ELISA and mass spectrometry analysis.

3.5.7 Nanoparticle tracking analysis

The concentration and size of EVs were characterized by NTA (Nanosight NS300, Malvern). EVs enriched by NWs and Dynabead were eluted using 0.1 M Glycine-HCl pH 2.8 with an incubation of 30 min at room temperature. After magnetic removal of NWs and Dynabead, the supernatant containing eluted EVs was collected and neutralized by the addition of 1 M Tris pH 8. EVs were diluted in ultrapure water to obtain approximately 50 particles per frame for optimal counting. All measurements were performed in triplicate and each sample was analyzed five times with the same camera settings (shutter speed: 30.15 ms, camera level: 15, capture duration: 60 s).

3.5.8 Quantification of PLAP and CD63 proteins from enriched EVs

After incubating pre-enriched EVs with NW-PLAP or Dynabead-PLAP, the captured EVs were lysed with 1 × RIPA buffer (Merck Millipore, 0.5 M Tris-HCl pH 7.4, 1.5 M NaCl, 2.5% deoxycholic acid, 10% NP-40, 10 mM EDTA) containing 1 × cOmplete™ Mini EDTA-free Protease Inhibitor Cocktail (Roche) for 20 min at 4 °C. As a control, pre-enriched EVs were directly lysed without isolation. Lysates were quantified for PLAP and CD63 proteins using a human PLAP ELISA kit (MBS289869, MyBiosource) and a human CD63 ELISA kit (EH95RBX5, Thermo Fisher Scientific). The recovery of PLAP protein was calculated by dividing the amount of PLAP or CD63 proteins extracted by that of the pre-enriched sample.

3.5.9 Proteomic analysis

Sodium dodecyl sulfate polyacrylamide gel electrophoresis (SDS-PAGE) of extracted EV proteins followed by in-gel digestion of proteins were used to process the samples for mass spectrometry analyses. EV-captured NWs and Dynabead were resuspended in 1 × RIPA buffer containing 1× protease inhibitor as described above, and the lysates were collected after removing the NWs and Dynabead with a magnet. Prior to in-gel digestion, the total protein concentration was quantified by bicinchoninic acid (BCA) assay (Pierce™ BCA Protein Assay Kit, Thermo Fisher Scientific). EV protein extracts were mixed with 4X NuPAGE™ LDS sample buffer (Invitrogen) and heated at 70 °C for 10 min prior to running on NuPAGE™ 4–12% Bis-Tris gels (Invitrogen) for 5 min to ensure the complete removal of remnant NWs and Dynabead. Areas of gel containing proteins were then excised in reference to a prestained protein ladder, with those areas subsequently cut into smaller pieces prior to performing an in-gel digestion method

adapted from the gel-aided sample preparation (GASP) protocol.[46] Briefly, gel pieces were dehydrated with acetonitrile and dried at room temperature. Protein-containing gel pieces were then reduced with 10 mM dithiothreitol (Sigma) in 100 mM ammonium bicarbonate at 56 °C for 45 min, dehydrated again with acetonitrile, and then alkylated with 55 mM 2-chloroacetamide (Sigma) in 100 mM ammonium bicarbonate in the dark at room temperature for 30 min. After removing the liquid, gel pieces were rehydrated with 5 mM ammonium bicarbonate and dehydrated again in acetonitrile prior to re-hydration with enzymatic digestion (Trypsin/Lys-C mix, Promega) in 5 mM ammonium bicarbonate overnight at 37 °C. Peptides were sequentially extracted from the gel using 1% formic acid (40 µL), 50% acetonitrile in 1% formic acid (50 µL), and acetonitrile alone (100 µL) followed by sonication of 15 min in between before supernatants were collected. Peptide-containing extracts were vacuum-dried and resuspended in 0.1% formic acid prior to liquid chromatography-tandem mass spectrometry (LC-MS/MS) analysis.

LC–MS/MS analyses were conducted on an EASY-nLC 1200 system (Thermo Scientific) coupled to an Orbitrap Exploris 480 mass spectrometer (Thermo Scientific). Five microlitres of the peptide sample were loaded onto a 50 °C heated C18 fused silica column (75 µm × 25 cm) at a flow rate of 600 nL/min. The column was packed with 1.9 µm ReproSil-Pur 120 C18-AQ particles (Dr. Maisch) and possessed a pulled tip. Peptide chromatography was performed over a 70 min linear gradient (3–20% acetonitrile in 0.1% formic acid) with a flow rate of 300 nL min^{-1}. Two compensation voltages (–50 and –70 V) were alternately applied from a FAIMS Pro interface (Thermo Scientific) to regulate the entry of ionized peptides into the mass spectrometer. MS scans (*m/z* 300 to 1500) were acquired at resolution 60000 (*m/z* 200) in positive ion mode (2 kV spray voltage). MS/MS scans were measured at resolution 15000 after multiply charged peptide precursors (minimum intensity 10000) were sequentially fragmented with higher energy collision dissociation (HCD) at 27.5% normalized collision energy. A dynamic exclusion period of 40 s was specified, and cycle times were restricted to 1.5 s.

The raw LC-MS/MS data files were subjected to label-free quantification (LFQ) using Maxquant (v1.6.2.6) with peptide spectra searched against the human UniProt database (downloaded on 4/2021) using the integrated Andromeda search engine.[47] For the identification of peptides, the digestion enzyme was set to Trypsin/P with a maximum of two missed cleavages, a fixed modification of cysteine carbamidomethylation, and

variable modifications of protein N-terminal acetylation and methionine oxidation. Mass tolerances of 20 ppm and 0.1 Da were used for precursor ions and fragment ions, respectively. The false discovery rate (FDR) was 1% for both peptides and proteins. LFQ data were processed with Perseus (v1.6.2.1) to determine correlations between the sample triplicates. Protein groups identified by LC-MS/MS were compared with the Vesiclepedia database and Functional Enrichment analysis tool (FunRich v3.1.3). A Venn diagram was generated by InteractiVenn tool, and gene ontology (GO) analyses were performed using the database for annotation, visualization and integrated discovery (DAVID, v6.8).[48]

3.6 Results and discussion

3.6.1 Characterisation of iron oxide NWs

The morphologies of the pristine iron oxide NWs and NW-*p*AAm are presented in Figure 3-2. SEM analysis revealed that the bacteria-derived NWs used in this study appeared as helical-like structures comprising of twisted NWs (Figure 3-2A). These NWs varied in size, ranging approximately 460–950 nm with a polydispersity of 0.62 as estimated by DLS (Figure 3-8A, Section 3.5). The average diameter of a single NW was 66.7 ± 16.7 nm as measured by SEM. TEM image showed the dimensions and morphology of iron oxide NWs (50–80 nm) which are consistent with SEM images (Figure 3-8B, Section 3.5). Their polycrystalline structures with lattice refractions are corresponding to a mixture of magnetite and hematite (Figure 3-8C, Section 3.5). The magnetic property studied by the measurements of magnetic hysteresis revealed that the iron oxide NWs exhibited a ferromagnetic behaviour (Figure 3-8D, Section 3.5). NWs coated with the diblock copolymers showed similar wire-like structures (Figure 3-2B) with increased size distribution as seen by the increased scattering in the DLS measurements (688 ± 22 nm for NWs and 1110 ± 26 nm for NW-*p*AAm) (Figure 3-8A, Section 3.5). Note that diameters from the DLS measurements should only be considered coarse approximations considering the non-spherical nature of the NWs.[49] After the conjugation of antibodies, the approximated hydrodynamic size of NW-IgG increased to 1154 ± 19.5 nm with a polydispersity of 0.44 (Figure 3-8A, Section 3.5). Dynabead were also imaged with SEM to confirm their homogeneous spherical morphologies. A mean size of 2.7 µm and a polydispersity of 0.093 were measured by DLS (Figure 3-9, Section 3.5).

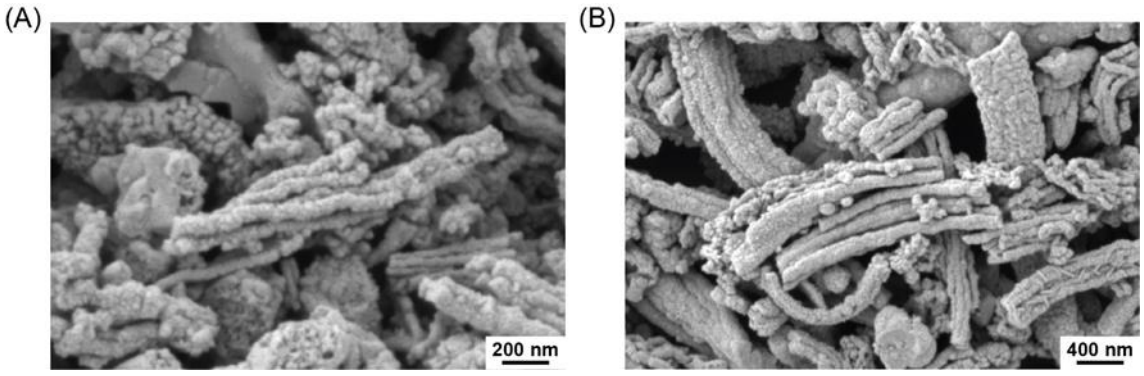

Figure 3-2 SEM images of (A) NW and (B) NW-*p*AAm.

To further confirm the successful functionalization of the NWs with carboxylic acid groups and conjugation with antibodies, chemical analyses with XPS were performed for NWs, NW-*p*AAm and NW-IgG (Figure 3-3). As shown in Figure 3-3A, elemental survey scans contained peaks attributed to Fe 2p at 711.7 eV (Fe $2p_{3/2}$) and 725.1 eV (Fe $2p_{1/2}$) in all three samples, which are the characteristics of Fe (III) of α-Fe_2O_3.[50,51] A peak at the lower binding energy of approximately 708 eV corresponding to Fe (II) was not observed. These features were in accordance with previous results conducted by X-ray diffraction (XRD) and Fourier-transform infrared (FTIR) analyses of iron oxide NW-derived from *M. ferrooxydans*.[42] Quantification of the elemental composition of the three samples (Table 3-1) showed increases in the intensities of carbon (C 1s at 284.8 eV), oxygen (O 1s at 530 eV), and nitrogen (N 1s at 399.4 eV), which indicate successful coating of the NWs with the copolymers and further conjugation with antibodies. Specifically, compared to the NWs, both NW-*p*AAm and NW-IgG showed significant increases in elemental carbon contents (39.51% for NW-*p*AAm and 47.79% for NW-IgG vs. 30.67% for NW), which was mainly attributed to increased hydrocarbon indicated by the CC/CH component at 284.8 eV in the high-resolution scans (Figure 3-3B). The increases in the intensity of CN (285.6 eV) and changes in the intensity of the CO (286.3 eV), C=O (288.1 eV), and O-C=O (289 eV) components can also be attributed to the presence of the copolymer on the surface of the NWs. Deconvolution of the O 1s high-resolution spectra in Figure 3-3C shows the presence of the expected Fe-O component at approximately 529.7 eV in all three samples. After coating and antibody conjugation, the intensities of the O=C component (531.6 eV) increased, which is in agreement with the changes observed in the C 1s spectra. While nitrogen was not detected in the pristine NWs (Figure 3-3D), N 1s high-resolution spectra showed a prominent peak attributed to CN at approximately 399.8 eV for both NW-*p*AAm and NW-IgG. As expected, the N%

substantially increased after conjugation with antibodies (3.34% for NW vs. 8.13% for NW-IgG). Using 1 mg of NWs and 40 µg of antibodies, the conjugation efficiency was determined to be 89%. As the NWs used in this study are heterogeneous in size and shape, the batch-to-batch variation of the surface modification and antibody conjugation was also examined. As shown in Table 3-2, minimal variations in the XPS elemental composition percentages were observed after *p*AAm coating and antibody conjugation for two independent NW batches, demonstrating the reproducibility of the modification and conjugation processes.

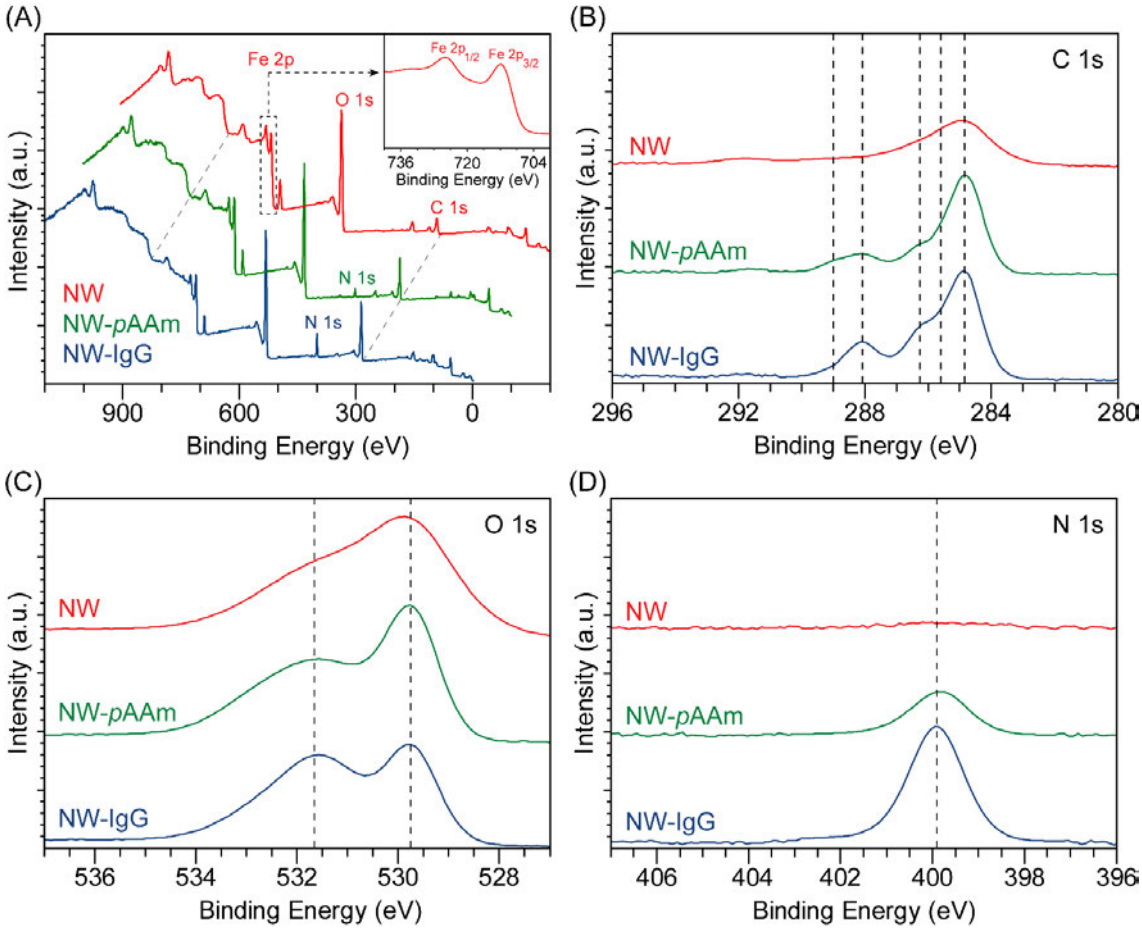

Figure 3-3 XPS analyses of NW, NW-*p*AAm, and NW-IgG.
(A) Survey scan spectra with inset displaying Fe 2p peak. (B) High-resolution spectra of C 1s. Dashed lines indicate major peaks of CC/CH (284.8 eV), CN (285.6 eV), CO (286.3 eV), C=O (288.1 eV), and O-C=O (289 eV). (C) High-resolution spectra of O 1s. Dashed lines indicate major peaks attributed to Fe-O (529.7 eV) and O=C (531.6 eV). (D) High-resolution spectra of N 1s. Dashed line indicates CN (399.8 eV).

Table 3-1 Summary of XPS elemental and components

NW samples	XPS elemental composition (%)			C 1s components (%)					O 1s components (%)	
	C	N	O	CC/CH	CN	CO	C=O	O-C=O	Fe-O	O=C
NW	30.67	-	69.33	53.82	-	28.94	10.56	6.68	56.49	43.51
NW-*p*AAM	39.51	3.34	57.15	64.26	3.83	17.04	11.25	3.62	34.21	65.79
NW-IgG	47.79	8.13	44.09	61.12	9.8	11.34	15.34	2.4	25.78	72.42

"-" indicates below the detection limit.

3.6.2 PLAP+ve EV enrichment performance

To assess the EV capture performance of the iron oxide NWs and Dynabead, EVs enriched from the culture media of the BeWo cell line were used as model. BeWo EVs contain PLAP on their lipid bilayer membranes, with PLAP+ve EVs accounting for approximately 28.8% of the total EVs as quantified by fluorescent nanoparticle tracking analysis (NTA),[52] making BeWo a good model for testing the enrichment of immuno-specific EVs. Due to the comparatively low number of EVs in cell culture media, an ultracentrifugation step was first used to concentrate total BeWo EVs (defined as the "pre-enriched" sample). Specific amounts of NW-PLAP and Dynabead-PLAP were then added to 250 µL of the pre-enriched BeWo EVs containing 44.5 µg/mL of proteins. The magnetic NWs are readily collected using an external magnetic field, in agreement with a previous report.[37]

We used NTA to characterize the size distribution and concentration of the PLAP+ve EVs enriched by both NW-PLAP and Dynabead-PLAP. Specifically, EVs were eluted by Glycine-HCl prior to NTA analysis as it is not possible to enumerate bound EVs with NTA. For all other EV analysis methods reported, EVs were lysed directly after immuno-magnetic enrichment without elution. Although elution efficiency was not specifically examined, the size distribution of the eluted EVs was 62–245 nm with the mean/mode size of 147.2 ± 2.6/108.7 ± 14.5 nm and 132.4 ± 10.6/113.8 ± 13.2 nm in the case of the NWs and Dynabead ($p > 0.05$), respectively (Figure 3-10A-C, Section 3.5). This data indicates that enriched PLAP+ve EVs include both small and large EVs.

We then further investigated the EV capture efficiency for the magnetic NWs by varying the amount of NW-PLAP used (0.02, 0.05, 0.1, 1 and 2 mg) and the enrichment time (10, 30, 60, 120 and 240 min). EVs captured on the NW-PLAP were lysed and the amount of PLAP protein in the lysate was referenced to the amount in the pre-enriched EVs solution. As the amount of NW-PLAP increased from 0.02 to 1 mg, the PLAP recovery plateaued at approximately 80% from 0.5 mg of NW-PLAP (Figure 3-4A). We therefore selected

0.5 mg of NW-PLAP per sample for subsequent optimization experiments. As shown in Figure 3-4B, the recovery of PLAP increased from 35% to 82% as the time increased from 10 min to 240 min. The optimal enrichment time was 60 min (83.7 ± 5.7%), with prolonged incubations leading to no further improvement in PLAP recovery. The optimized sample processing method was therefore, selected to include a 60 min incubation for the recovery of PLAP+ve EVs in a 250-µL sample (corresponding to 44.5 µg/mL of proteins) with 0.5 mg of NW-PLAP.

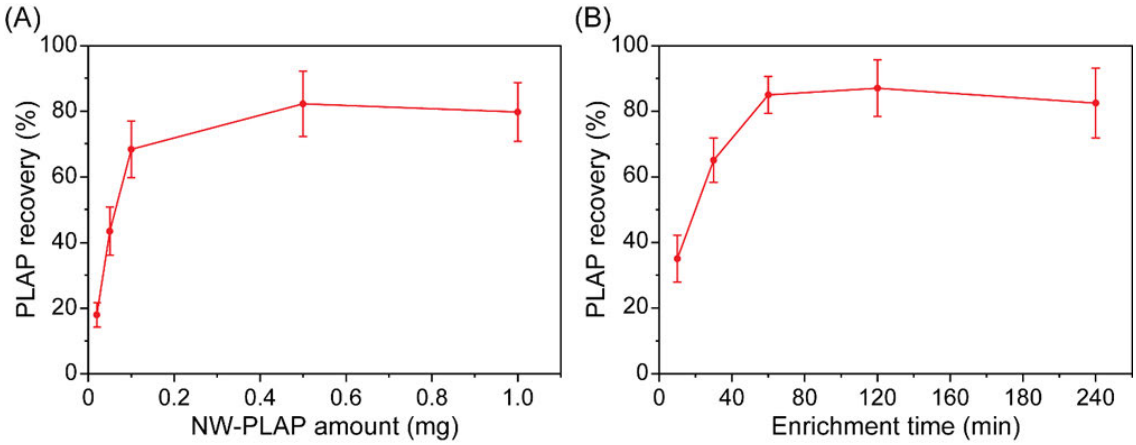

Figure 3-4 Optimisation of NW amount and enrichment time.
Effect of (A) the amount of NW-PLAP (0.02, 0.05, 0.1, 0.5 and 1 mg) and (B) enrichment time (10, 30, 60, 120 and 240 min) on the recovery of PLAP proteins from model BeWo EV samples. Data are presented as means ± standard deviation (SD) (n = 3).

Having determined the optimum recovery conditions for the anti-PLAP conjugated NWs, we then benchmarked their performance against the broadly used commercially available Dynabead. Performance comparisons were performed using the same weight of NWs and Dynabead (1 mg). The amount of soluble protein co-enriched with EVs was first determined by measuring the particle to protein ratios described previously as a measure of EV purity.[53] Using NTA to quantify the number of eluted EVs after immuno-magnetic enrichment and BCA assay to quantify the total protein concentrations in the lysates, the particle to protein ratio for the NWs ($2.84 \pm 1.12 \times 10^{10}$) was found to be comparable to that of the Dynabead ($2.53 \pm 1.1 \times 10^{10}$) ($p > 0.05$) (Figure 3-10D, Section 3.5). Both ratios were in the range expected of a pure EV preparation ($> 2 \times 10^{10}$)[54] and comparable to purity ratios previously reported for immuno-magnetic EV enrichment from cell culture media[25] and plasma,[55] confirming that both magnetic NWs and Dynabead can be used to enrich EVs with high purity.

We then evaluated the specificity of the NW-PLAP and Dynabead-PLAP in terms of non-specific EV-binding. PLAP+ve EVs were recovered from the pre-enriched total BeWo EVs (prepared as described above) using the same weight of NWs and Dynabead (1 mg) conjugated with either anti-PLAP or irrelevant IgG antibodies as a negative control. Samples including the pre-enrich, EVs captured by the NW-PLAP and Dynabead-PLAP (bound), and the supernatants (unbound) collected after the immuno-enrichment were quantified for PLAP and CD63 proteins. The total measured PLAP proteins (sum of bound and unbound PLAP) in these samples were similar to that of the pre-enriched sample, indicating that there was minimal loss of PLAP (less than 12%) during the whole enrichment process (Figure 3-5A and B). PLAP+ve EVs were enriched with high efficiency by both the anti-PLAP conjugated NWs and Dynabead, as 83.7 ± 8.9% and 83.2 ± 5.9% of the PLAP proteins were recovered respectively from the pre-enriched sample (Figure 3-5A and Figure 3-11A, Section 3.5). These enrichments were significantly higher than the negative controls ($p < 0.0001$), which were 15.3 ± 5% and 12.4 ± 3.5% for the NWs and Dynabead conjugated with an irrelevant antibody, respectively (Figure 3-5A). This data confirms that the enrichment of the PLAP+ve EVs with both NW-PLAP and Dynabead-PLAP is predominantly specific and mediated by the conjugated anti-PLAP antibodies. The PLAP+ve EV recovery performance can also be assessed using the ratio of bound PLAP protein (i.e. lysed from NW-PLAP / Dynabead-PLAP) relative to the total bound and unbound (supernatant) PLAP protein. Enrichments of 87.2 ± 4.57% and 90.4 ± 4.54% were obtained for anti-PLAP conjugated NWs and Dynabead, respectively (Figure 3-11B, Section 3.5). These recovery efficiencies are comparable to that reported by Menon et al. (95%) using the same clone of anti-PLAP (8B6) conjugated to protein-A agarose beads.[56] It is noteworthy that in our study the irrelevant antibody controls captured non-specifically smaller amounts of PLAP proteins (17.1 ± 5.27% and 14.1 ± 2.3% for NWs and Dynabead, respectively) (Figure 3-11B, Section 3.5), compared to 30% reported by Menon et al. in plasma samples.

As a measure of the total EV population, we quantified the CD63 protein, a canonical marker expressed by most EV subtypes including both microvesicles and exosomes.[52,57] As approximately 30% of all EVs from BeWo cells are expected to express PLAP, CD63 recovery yields of 37.7% and 34.8% for the NW-PLAP and Dynabead-PLAP were obtained respectively, which further confirmed successful enrichment of the subpopulation of PLAP+ve EVs (Figure 3-5B and Figure 3-11C, Section 3.5). The NWs

and Dynabead conjugated with the irrelevant antibody controls yielded very low amounts of CD63 protein recovery with 7 ± 3.2% for NWs and 5.4 ± 2.2% for Dynabead (Figure 3-5B), confirming that non-specific binding of EVs onto both NWs and Dynabead is low. The significant reduction in the ratios of CD63 to PLAP proteins also observed for both NW-PLAP and Dynabead-PLAP from the pre-enriched sample further demonstrates that PLAP+ve EVs were specifically enriched with low contamination from non-target PLAP-ve EVs (Figure 3-11D, Section 3.5). The purity of the target EV subtype (i.e. PLAP+ve EVs) and the purity of their protein/RNA molecular cargo are important to obtain reliable proteomic/transcriptomic data.[58] Specifically, both target EV recovery yield and purity are important for insightful proteomic analyses with LC-MS.[59]

While this data does not establish a significant performance improvement for the iron oxide NWs compared to Dynabeads™, several advantages should be noted. First, NWs are extracted from bacterial biofilm. The magnetic NWs are obtained in large quantities (up to kgs) through an environmentally friendly process that does not require the use of harsh chemicals and conditions. Second, the valorisation of this biowaste of the drinking water industry is also directly aligned with the concept of circular economy. Finally, the magnetic NWs provide cost-effective and scalable high surface area magnetic materials for immuno-enrichment, with likely opportunity for further increase in performance, for example via improvement of the biointerfacial properties.

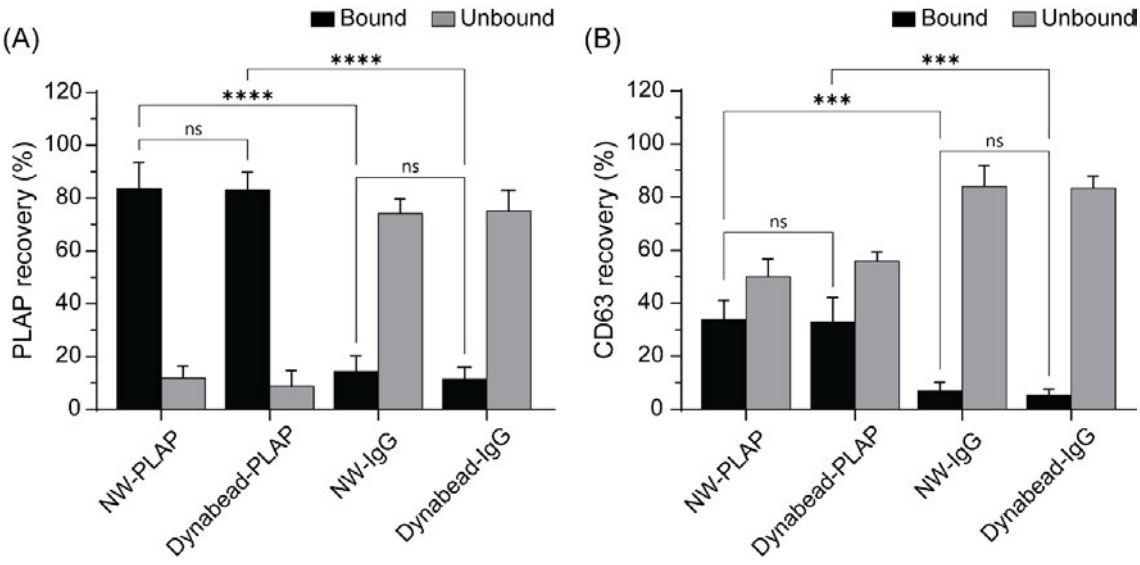

Figure 3-5 Recovery efficiency of PLAP and CD63 proteins.
Recovery of (A) PLAP and (B) CD63 proteins extracted from EVs captured by NWs and Dynabead conjugated with either anti-PLAP or an irrelevant IgG (bound) and the corresponding supernatants (unbound). Data are presented as means + SD (n = 3, one-way ANOVA with Tukey's post-test, ns = not significant, ***p < 0.001, and ****p < 0.0001).

3.6.3 Proteomic analyses of PLAP+ve EVs enriched from BeWo cells

After demonstrating the potential of using iron oxide magnetic NWs to enrich PLAP+ve EVs, we further performed comparative proteomic analyses for the model EVs enriched from the culture media of BeWo cells by LC-MS/MS. As shown in Figure 3-12 (Section 3.5), ultracentrifugation followed by immuno-magnetic enrichment of EVs using the same weight of NW-PLAP and Dynabead-PLAP (1 mg) identified a total of 2822 and 2732 protein groups (in triplicate), respectively, 80.5% and 83.9% of which were enriched in all three replicates of NW-PLAP and Dynabead-PLAP, respectively. The number of proteins identified from EVs enriched from BeWo cell culture media was comparable to other previous reports using other approaches. For example, polyethylene glycol (PEG)-based exosome isolation from HeLa cell culture media identified 6299 proteins, 3254 (51.6%) of which were enriched in all three replicates.[60]

Using label-free quantification, we selected 2518 (89%) and 2545 (93%) protein groups that were identified in at least two out of three replicates for NW-PLAP and Dynabead-PLAP, respectively, for subsequent analyses. Cross-reference against the Vesiclepedia database showed that 95% of the selected protein sets could be identified as EV proteins (Figure 3-6A). As shown in Table 3-3, LC-MS/MS analyses also confirmed the presence of PLAP as well as several other markers commonly associated with EVs including transmembrane proteins (tetraspanins CD9, CD63, CD81) and several cytosolic membrane-associated proteins (TSG101, HSPA8, PDCD6IP, *etc.*). Pairwise intensity correlation of identified protein groups showed strong Pearson correlation coefficients for three replicates of either Dynabead-PLAP or NW-PLAP (0.987) as well as between their replicates (0.961), demonstrating not only the reproducibility of the EV enrichment methods but also the comparable enrichment performance of the NWs derived from biofilms of zetaproteobacteria *Mariprofundus ferrooxydans* to that of Dynabead, a commercial gold-standard (Figure 3-6B).

Detailed information about the cellular components of enriched proteins was further acquired by analyzing gene ontology (GO, DAVID Bioinformatics Resources).[48] As shown in Figure 3-13A (Section 3.5), GO analysis demonstrated that the extracellular exosome category was the most highly enriched in the NW-PLAP sample, while this category ranked second for samples enriched with Dynabead-PLAP after the cytosol category. Specifically, among the identified protein groups enriched by Dynabead-PLAP and NW-PLAP, 36% and 37.8% were respectively found to be located in the extracellular

exosome category (GO:0070062) while the majority of proteins were categorized into the cytoplasm (GO:0005737), cytosol (GO:0005829), and nucleus (GO:0005634) categories (Figure 3-13B, Section 3.5). This result is attributed to the fact that PLAP proteins were demonstrated to be detected in microvesicles (100–1000 nm) and exosomes (50–200 nm) isolated by ultracentrifugation at 10,000 × *g* and 100,000 × *g*, respectively.[61,62] Microvesicles have been reported to carry several proteins from the cytoplasm and nucleus.[63] The insights obtained from GO analyses agreed with those obtained from the Vesiclepedia database and NTA result, demonstrating the ability of the magnetic NWs to specifically enrich PLAP+ve EVs.

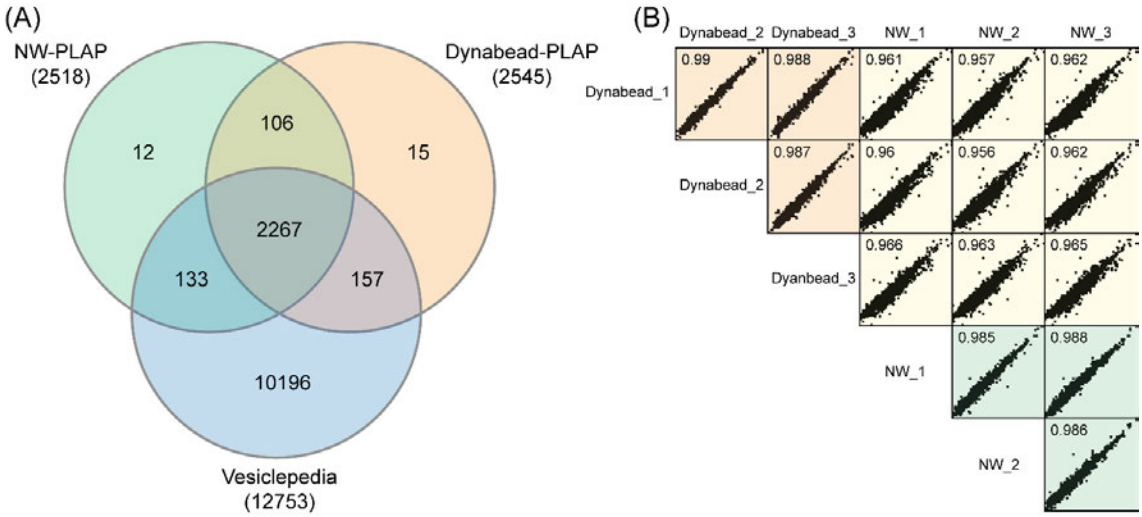

Figure 3-6 Mass spectrometry analysis of BeWo EV proteins.
Comparative proteomic analyses of proteins identified in BeWo EVs enriched with NW-PLAP and Dynabead-PLAP. (A) Overlap of protein groups enriched with that of pre-enriched sample and Vesiclepedia database filtered to include EV proteins. (B) Pairwise correlation of intensities of protein groups enriched within replicates of NW-PLAP and Dynabead™-PLAP as well as between their replicates. Inset numbers indicate Pearson correlations.

3.7 Conclusion

We report an immuno-magnetic enrichment approach for specific EV subtypes and their subsequent processing for high quality mass spectrometry. Specifically, we have demonstrated comparable EV-enrichment yield and purity using biofilm-derived iron oxide NWs to that of Dynabead, using PLAP+ve EVs as a model for a physiologically relevant EV subtype. In addition, low non-specific binding of non-targeted EVs (7% for NW) was achieved. The captured EVs could be readily eluted or directly lysed for downstream analyses. We subsequently optimized an EV mass spectrometry method after immunomagnetic enrichment with both NWs and Dynabead, which consistently yielded a high number of EV proteins. The immuno-specific EVs enrichment for mass

spectrometry approach using naturally occurring iron oxide magnetic NWs or Dynabead provides an efficient method for EV proteomic studies.

3.8 Supplementary figures

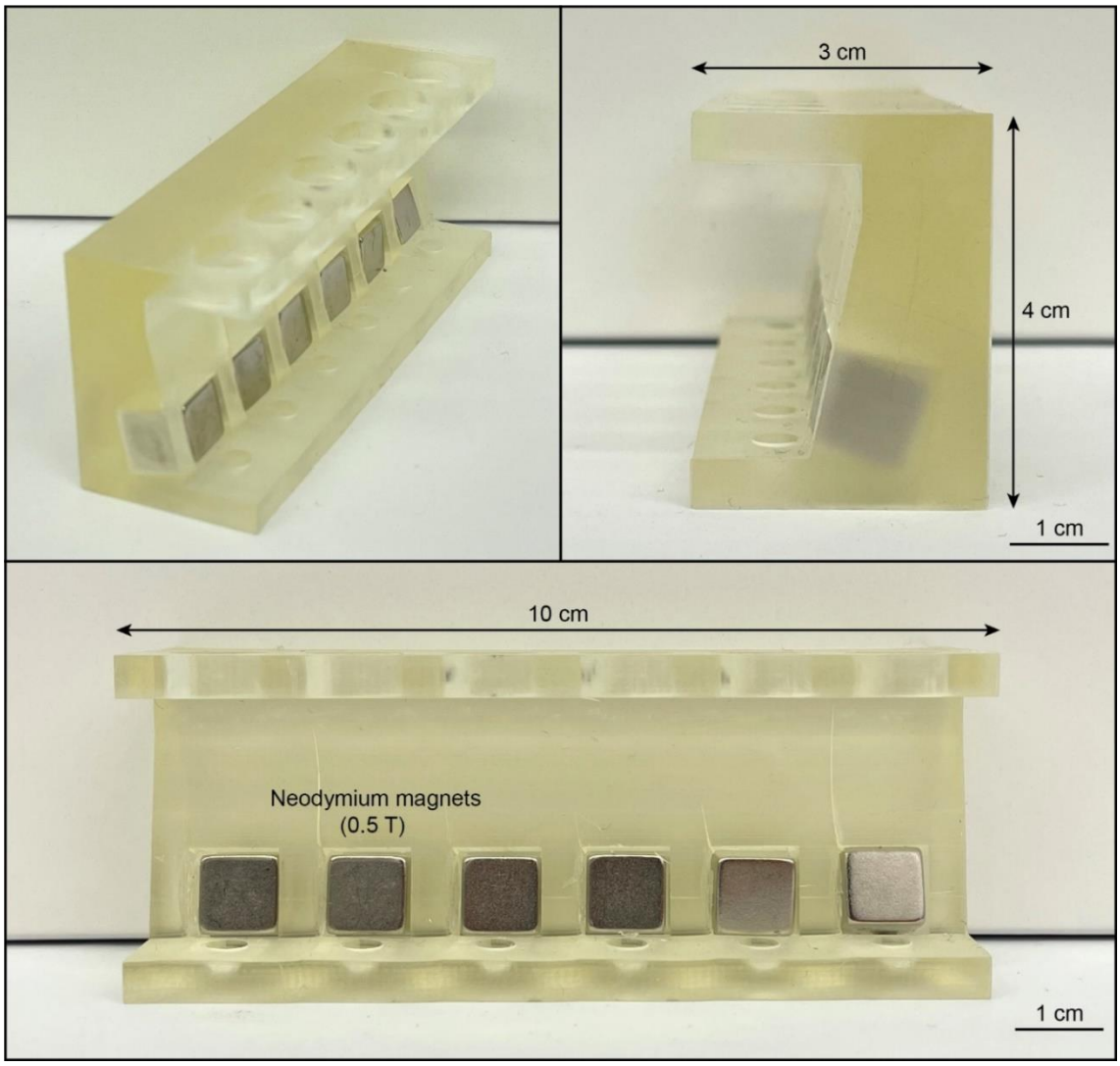

Figure 3-7 3D-printed magnetic separation rack.
Images of the in-house 3D-printed magnetic separation rack used for immuno-magnetic isolation of EVs. The rack was designed to fit 1.5-mL and 2.0-mL Eppendorf tubes and neodymium magnets (Grade N42, 0.5 T, 10 × 10 × 10 mm).

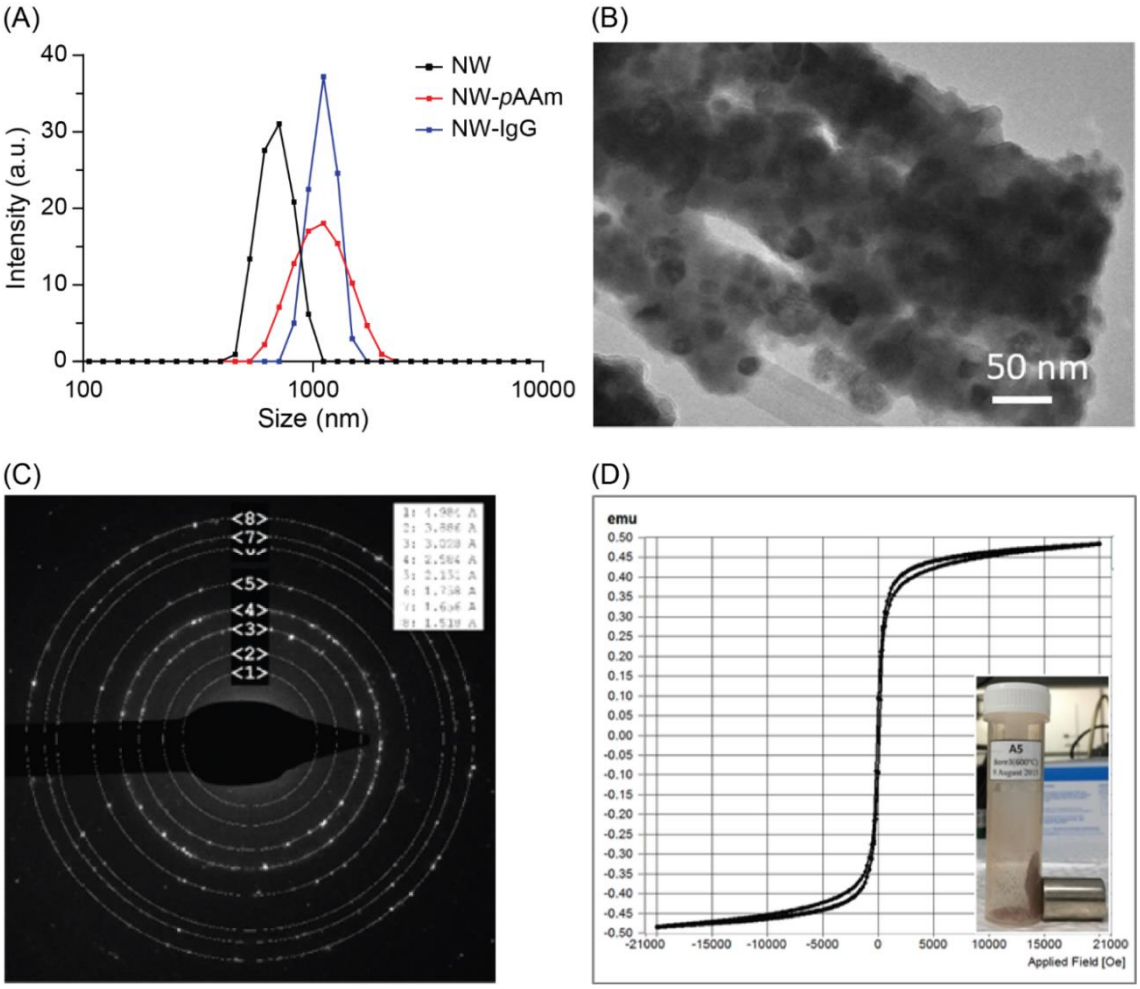

Figure 3-8 DLS, TEM and magnetic characterisation of NWs.
(A) Monitoring of changes in NWs' scattering by dynamic light scattering during the coating procedure. (B) Transmission electron microscope image and (C) diffraction pattern of iron oxide NWs showing wire-like structures with diameters of 50–80 nm and polycrystalline rings with lattice refractions corresponding to a mixture of magnetite and hematite structures. (D) The magnetic hysteresis curves of iron oxide NWs revealing a ferromagnetic behaviour of the material with a photo (inset) demonstrating the magnetic property of iron oxide NWs using a magnet.

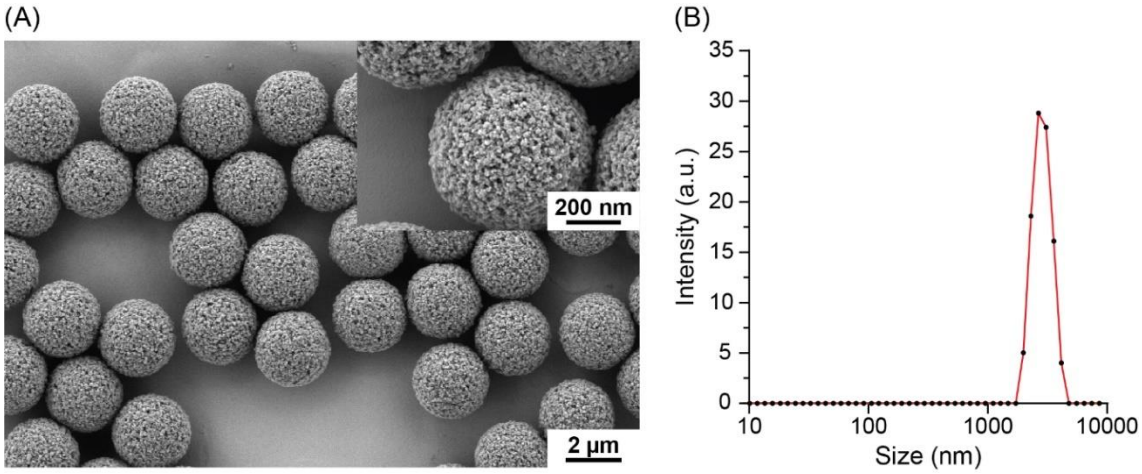

Figure 3-9 SEM and DLS characterisation of Dynabeads.
(A) Scanning electron microscopy images of Dynabeads M-270 carboxylic acid. Inset is the SEM image at a higher magnification. (B) Dynamic light scattering size measurement of Dynabeads.

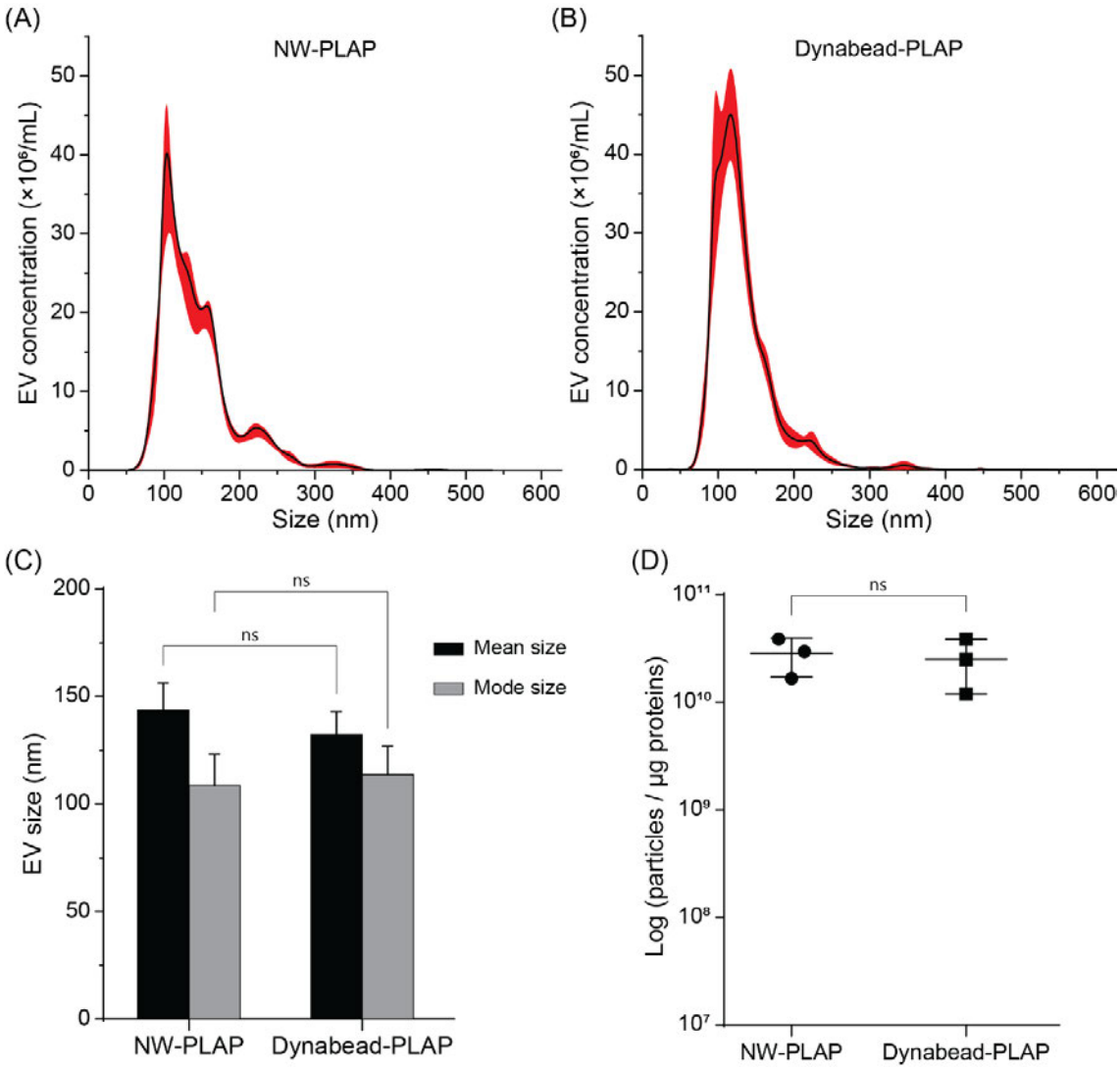

Figure 3-10 NTA analysis of eluted EVs and their purity ratio.
Nanoparticle tracking analysis of eluted EVs enriched by (A) NW-PLAP and (B) Dynabead-PLAP. (C) Mean size and mode size of eluted EVs. (D) The particle to protein ratio of PLAP+ve EVs enriched by NW-PLAP and Dynabead-PLAP. Data are presented as means + SD (n = 3, independent Student's t-test with 95% confidence interval, ns = not significant, $p > 0.05$).

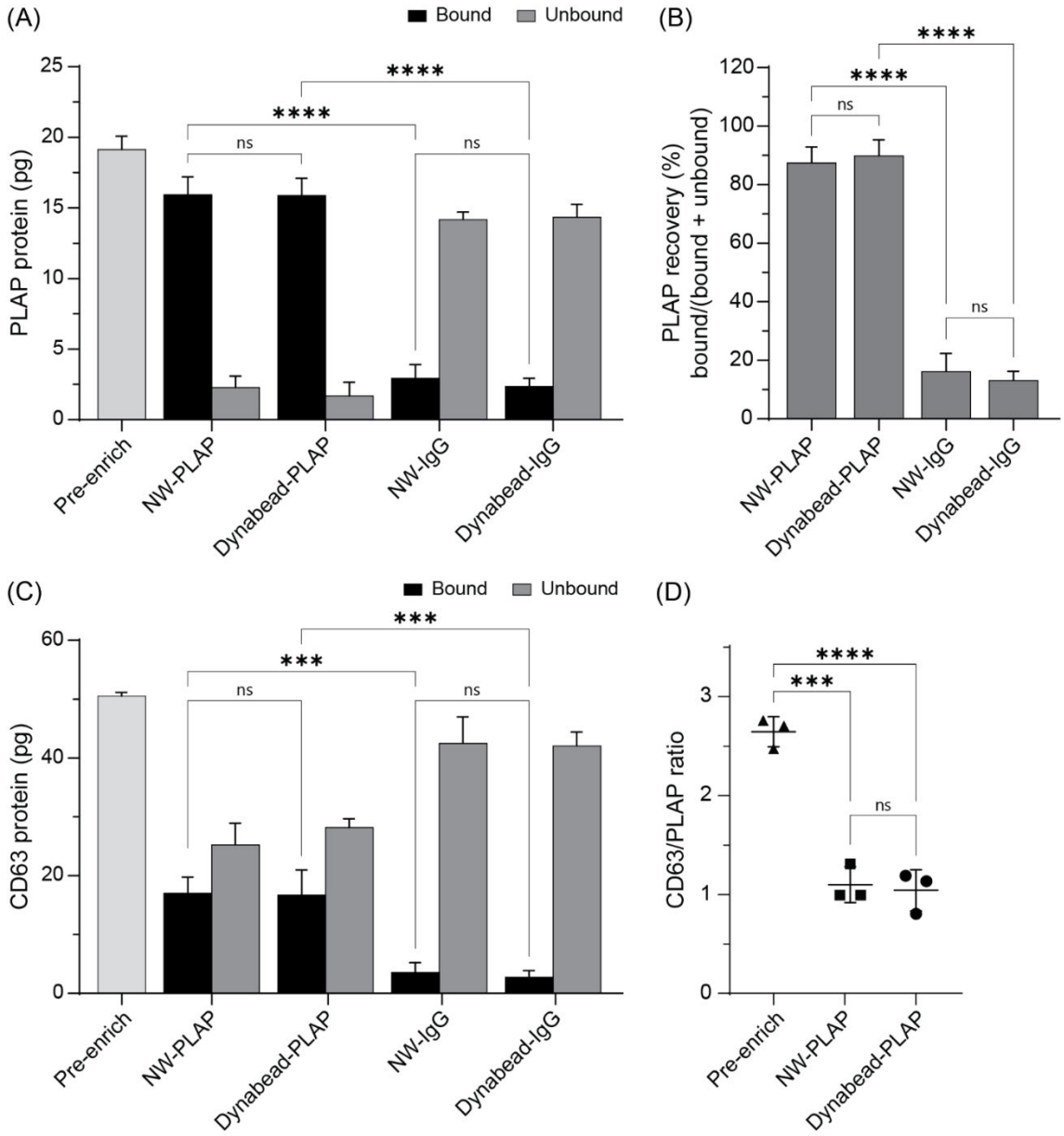

Figure 3-11 PLAP and CD63 recovery quantification.
(A) Quantification of PLAP in the pre-enriched sample (after ultracentrifugation of BeWo cell culture media), EVs captured by NWs and Dynabeads conjugated with either anti-PLAP or irrelevant IgG (bound) and the corresponding supernatants (unbound). (B) PLAP recovery of EVs enriched by NW-PLAP and Dynabead-PLAP presented by the ratio of bound to the total of bound and unbound. (A) Quantification of CD63 in the pre-enriched sample, bound and unbound of NW-PLAP and Dynabead-PLAP. (D) The ratio of CD63 to PLAP (pg/pg) calculated for the pre-enriched sample, NW-PLAP and Dynabead-PLAP. Data are presented as means + SD (n = 3, one-way ANOVA with Tukey's post-test, ns = not significant, ***$p < 0.001$, and ****$p < 0.0001$).

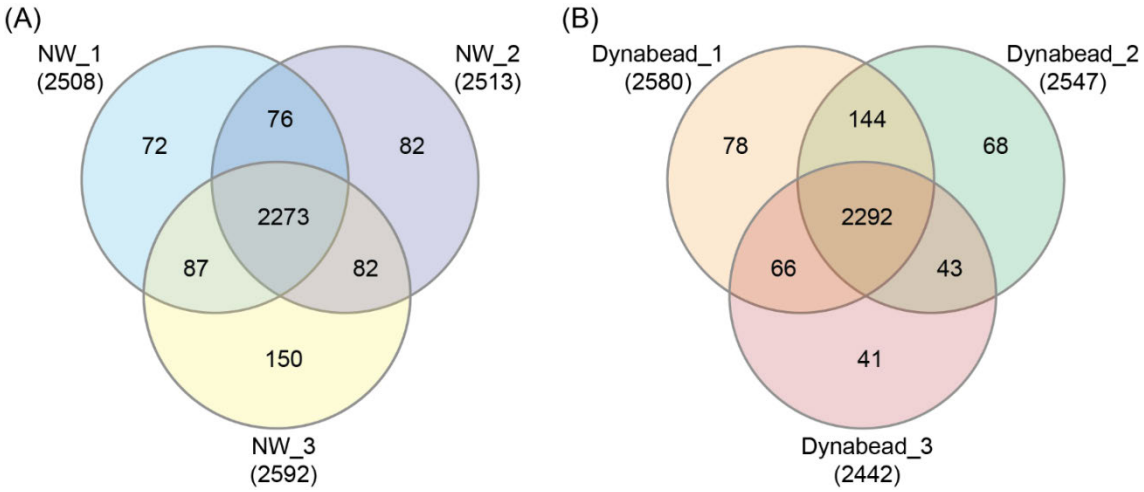

Figure 3-12 Proteins identified in 3 replicates of NW-PLAP and Dynabead-PLAP.
Overlap of protein groups enriched by three replicates of (A) NW-PLAP and (B) Dynabead-PLAP.

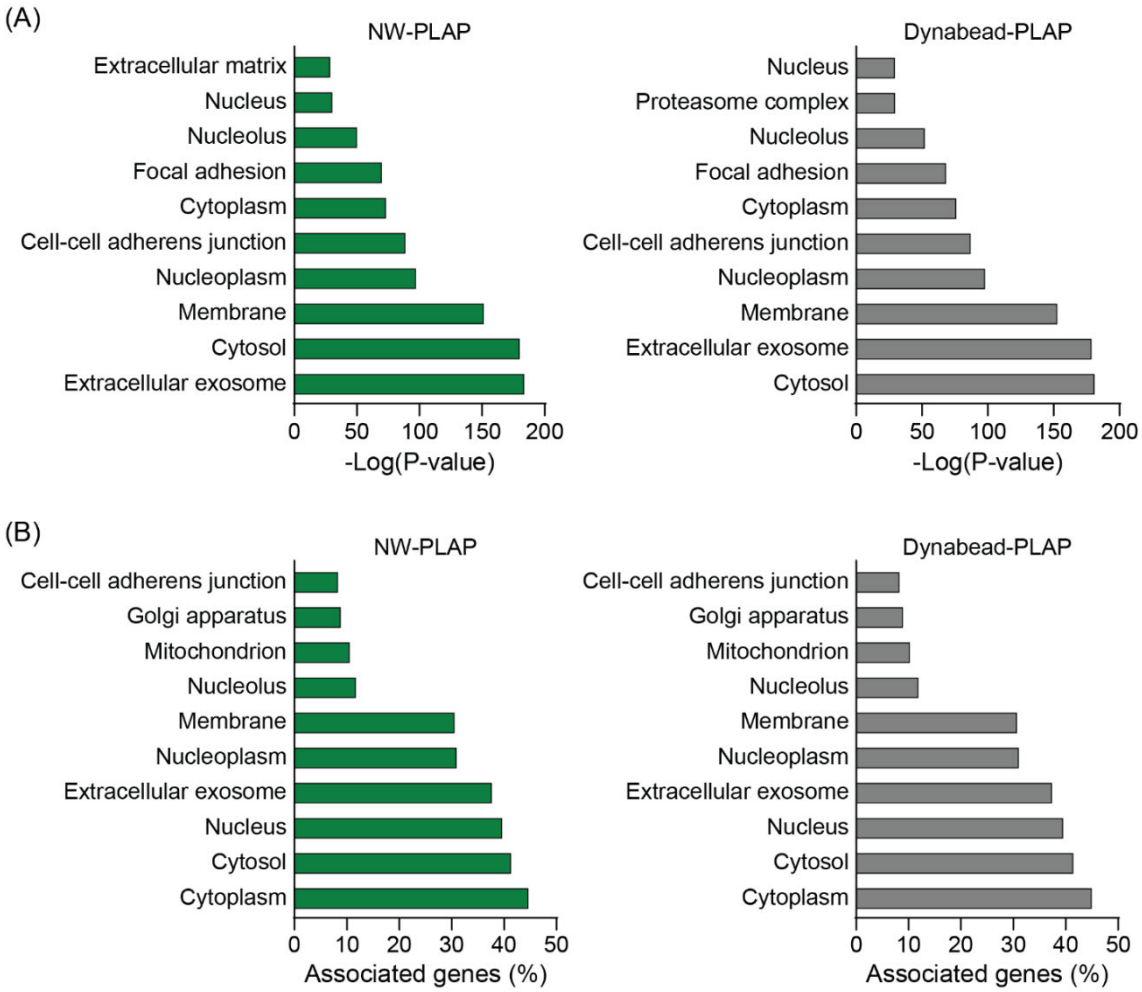

Figure 3-13 Gene ontology (GO) analyses of BeWo EV proteins.
Gene ontology (GO) analyses of the protein groups in BeWo EVs enriched by NW-PLAP and Dynabead-PLAP according to DAVID Bioinformatics Resources. Top 10 GO categories were reported for (A) Cellular component and (B) The percentage of associated genes.

Table 3-2 Batch-to-batch validation of antibody conjugation to NWs

NW samples	XPS elemental composition (%)		
	C	N	O
NW Batch 1 Antibody conjugation 1	47.79	8.13	44.09
NW Batch 1 Antibody conjugation 2	45.80	7.51	46.69
NW Batch 2 Antibody conjugation 1	49.12	7.85	43.03

3.9 References

1 Shao, H. *et al.* New Technologies for Analysis of Extracellular Vesicles. *Chem Rev* **118**, 1917-1950, doi:10.1021/acs.chemrev.7b00534 (2018).

2 Sun, Y. *et al.* Systematic comparison of exosomal proteomes from human saliva and serum for the detection of lung cancer. *Anal Chim Acta* **982**, 84-95, doi:10.1016/j.aca.2017.06.005 (2017).

3 Yuana, Y., Sturk, A. & Nieuwland, R. Extracellular vesicles in physiological and pathological conditions. *Blood Rev* **27**, 31-39, doi:10.1016/j.blre.2012.12.002 (2013).

4 Maas, S. L. N., Breakefield, X. O. & Weaver, A. M. Extracellular Vesicles: Unique Intercellular Delivery Vehicles. *Trends Cell Biol* **27**, 172-188, doi:10.1016/j.tcb.2016.11.003 (2017).

5 Raposo, G. & Stahl, P. D. Extracellular vesicles: a new communication paradigm? *Nat Rev Mol Cell Biol* **20**, 509-510, doi:10.1038/s41580-019-0158-7 (2019).

6 Kadota, T., Fujita, Y., Araya, J., Ochiya, T. & Kuwano, K. Extracellular vesicle-mediated cellular crosstalk in lung repair, remodelling and regeneration. *Eur Respir Rev* **31**, 210106, doi:10.1183/16000617.0106-2021 (2022).

7 O'Brien, K., Breyne, K., Ughetto, S., Laurent, L. C. & Breakefield, X. O. RNA delivery by extracellular vesicles in mammalian cells and its applications. *Nat Rev Mol Cell Biol* **21**, 585-606, doi:10.1038/s41580-020-0251-y (2020).

8 Karasu, E., Eisenhardt, S. U., Harant, J. & Huber-Lang, M. Extracellular Vesicles: Packages Sent With Complement. *Front Immunol* **9**, 721, doi:10.3389/fimmu.2018.00721 (2018).

9 Chen, I. H. *et al.* Phosphoproteins in extracellular vesicles as candidate markers for breast cancer. *Proc Natl Acad Sci U S A* **114**, 3175-3180, doi:10.1073/pnas.1618088114 (2017).

10 Heydari, R., Abdollahpour-Alitappeh, M., Shekari, F. & Meyfour, A. Emerging Role of Extracellular Vesicles in Biomarking the Gastrointestinal Diseases. *Expert Rev Mol Diagn* **21**, 939-962, doi:10.1080/14737159.2021.1954909 (2021).

11 Tian, F. *et al.* Protein analysis of extracellular vesicles to monitor and predict therapeutic response in metastatic breast cancer. *Nat Commun* **12**, 2536, doi:10.1038/s41467-021-22913-7 (2021).

12 Dickhout, A. & Koenen, R. R. Extracellular Vesicles as Biomarkers in Cardiovascular Disease; Chances and Risks. *Front Cardiovasc Med* **5**, 113, doi:10.3389/fcvm.2018.00113 (2018).

13 Margolis, L. & Sadovsky, Y. The biology of extracellular vesicles: The known unknowns. *PLoS Biol* **17**, e3000363, doi:10.1371/journal.pbio.3000363 (2019).

14 Melo, S. A. *et al.* Glypican-1 identifies cancer exosomes and detects early pancreatic cancer. *Nature* **523**, 177-182, doi:10.1038/nature14581 (2015).

15 Thery, C. *et al.* Minimal information for studies of extracellular vesicles 2018 (MISEV2018): a position statement of the International Society for Extracellular Vesicles and update of the MISEV2014 guidelines. *J Extracell Vesicles* **7**, 1535750, doi:10.1080/20013078.2018.1535750 (2018).

16 Brennan, K. *et al.* A comparison of methods for the isolation and separation of extracellular vesicles from protein and lipid particles in human serum. *Sci Rep* **10**, 1039, doi:10.1038/s41598-020-57497-7 (2020).

17 Murphy, D. E. *et al.* Extracellular vesicle-based therapeutics: natural versus engineered targeting and trafficking. *Exp Mol Med* **51**, 1-12, doi:10.1038/s12276-019-0223-5 (2019).

18 Marcoux, G. *et al.* Revealing the diversity of extracellular vesicles using high-dimensional flow cytometry analyses. *Sci Rep* **6**, 35928, doi:10.1038/srep35928 (2016).

19 Liangsupree, T., Multia, E. & Riekkola, M. L. Modern isolation and separation techniques for extracellular vesicles. *J Chromatogr A* **1636**, 461773, doi:10.1016/j.chroma.2020.461773 (2021).

20 Singh, K. *et al.* Separation of distinct exosome subpopulations: isolation and characterization approaches and their associated challenges. *Analyst* **146**, 3731-3749, doi:10.1039/d1an00024a (2021).

21 Rosi, N. L. & Mirkin, C. A. Nanostructures in biodiagnostics. *Chem Rev* **105**, 1547-1562, doi:10.1021/cr030067f (2005).

22 Gudbergsson, J. M., Johnsen, K. B., Skov, M. N. & Duroux, M. Systematic review of factors influencing extracellular vesicle yield from cell cultures. *Cytotechnology* **68**, 579-592, doi:10.1007/s10616-015-9913-6 (2016).

23 Yang, D. *et al.* Progress, opportunity, and perspective on exosome isolation - efforts for efficient exosome-based theranostics. *Theranostics* **10**, 3684-3707, doi:10.7150/thno.41580 (2020).

24 Contreras-Naranjo, J. C., Wu, H. J. & Ugaz, V. M. Microfluidics for exosome isolation and analysis: enabling liquid biopsy for personalized medicine. *Lab Chip* **17**, 3558-3577, doi:10.1039/c7lc00592j (2017).

25 Cai, S. *et al.* Immuno-modified superparamagnetic nanoparticles via host-guest interactions for high-purity capture and mild release of exosomes. *Nanoscale* **10**, 14280-14289, doi:10.1039/c8nr02871k (2018).

26 Reategui, E. *et al.* Engineered nanointerfaces for microfluidic isolation and molecular profiling of tumor-specific extracellular vesicles. *Nat Commun* **9**, 175, doi:10.1038/s41467-017-02261-1 (2018).

27 Rosa-Fernandes, L., Rocha, V. B., Carregari, V. C., Urbani, A. & Palmisano, G. A Perspective on Extracellular Vesicles Proteomics. *Front Chem* **5**, 102, doi:10.3389/fchem.2017.00102 (2017).

28 Hildonen, S., Skarpen, E., Halvorsen, T. G. & Reubsaet, L. Isolation and mass spectrometry analysis of urinary extraexosomal proteins. *Sci Rep* **6**, 36331, doi:10.1038/srep36331 (2016).

29 Farhana, F. Z. *et al.* Isolation and Detection of Exosomes Using Fe2O3 Nanoparticles. *ACS Applied Nano Materials* **4**, 1175-1186, doi:10.1021/acsanm.0c02807 (2021).

30 Pedersen, K. W., Kierulf, B. & Neurauter, A. Specific and Generic Isolation of Extracellular Vesicles with Magnetic Beads. *Methods Mol Biol* **1660**, 65-87, doi:10.1007/978-1-4939-7253-1_7 (2017).

31 Takahashi, H., Baba, Y. & Yasui, T. Oxide nanowire microfluidics addressing previously-unattainable analytical methods for biomolecules towards liquid biopsy. *Chem Commun (Camb)* **57**, 13234-13245, doi:10.1039/d1cc05096f (2021).

32 Hong, W., Lee, S., Chang, H. J., Lee, E. S. & Cho, Y. Multifunctional magnetic nanowires: A novel breakthrough for ultrasensitive detection and isolation of rare cancer cells from non-metastatic early breast cancer

patients using small volumes of blood. *Biomaterials* **106**, 78-86, doi:10.1016/j.biomaterials.2016.08.020 (2016).

33 Nemati, Z. *et al.* Magnetic Isolation of Cancer-Derived Exosomes Using Fe/Au Magnetic Nanowires. *ACS Applied Nano Materials* **3**, 2058-2069, doi:10.1021/acsanm.0c00263 (2020).

34 Nemati, Z. *et al.* Isolation of Cancer-Derived Exosomes Using a Variety of Magnetic Nanostructures: From Fe3O4 Nanoparticles to Ni Nanowires. *Nanomaterials (Basel)* **10**, 1662, doi:10.3390/nano10091662 (2020).

35 Lim, J. *et al.* Direct isolation and characterization of circulating exosomes from biological samples using magnetic nanowires. *J Nanobiotechnology* **17**, 1, doi:10.1186/s12951-018-0433-3 (2019).

36 Lee, H. *et al.* Magnetic Nanowire Networks for Dual-Isolation and Detection of Tumor-Associated Circulating Biomarkers. *Theranostics* **8**, 505-517, doi:10.7150/thno.21967 (2018).

37 Kumeria, T. *et al.* Naturally Derived Iron Oxide Nanowires from Bacteria for Magnetically Triggered Drug Release and Cancer Hyperthermia in 2D and 3D Culture Environments: Bacteria Biofilm to Potent Cancer Therapeutic. *Biomacromolecules* **17**, 2726-2736, doi:10.1021/acs.biomac.6b00786 (2016).

38 Sarker, S. *et al.* Placenta-derived exosomes continuously increase in maternal circulation over the first trimester of pregnancy. *J Transl Med* **12**, 204, doi:10.1186/1479-5876-12-204 (2014).

39 Chaparro, A. *et al.* Gingival Crevicular Placental Alkaline Phosphatase Is an Early Pregnancy Biomarker for Pre-Eclampsia. *Diagnostics (Basel)* **11**, 661, doi:10.3390/diagnostics11040661 (2021).

40 Jin, J. & Menon, R. Placental exosomes: A proxy to understand pregnancy complications. *Am J Reprod Immunol* **79**, e12788, doi:10.1111/aji.12788 (2018).

41 Sadovsky, Y. *et al.* Placental small extracellular vesicles: Current questions and investigative opportunities. *Placenta* **102**, 34-38, doi:10.1016/j.placenta.2020.03.002 (2020).

42 Wang, L. *et al.* Iron Oxide Nanowires from Bacteria Biofilm as an Efficient Visible-Light Magnetic Photocatalyst. *ACS Appl Mater Interfaces* **8**, 20110-20119, doi:10.1021/acsami.6b06486 (2016).

43 Bryce, N. S. *et al.* The composition and end-group functionality of sterically stabilized nanoparticles enhances the effectiveness of co-administered cytotoxins. *Biomater Sci* **1**, 1260-1272, doi:10.1039/c3bm60120j (2013).

44 Thierry, B. & Griesser, H. J. Dense PEG layers for efficient immunotargeting of nanoparticles to cancer cells. *Journal of Materials Chemistry* **22**, 8810-8819, doi:10.1039/C2JM30210A (2012).

45 Thery, C., Amigorena, S., Raposo, G. & Clayton, A. Isolation and characterization of exosomes from cell culture supernatants and biological fluids. *Curr Protoc Cell Biol* **Chapter 3**, Unit 3.22, doi:10.1002/0471143030.cb0322s30 (2006).

46 Fischer, R. & Kessler, B. M. Gel-aided sample preparation (GASP)--a simplified method for gel-assisted proteomic sample generation from protein extracts and intact cells. *Proteomics* **15**, 1224-1229, doi:10.1002/pmic.201400436 (2015).

47 Cox, J. & Mann, M. MaxQuant enables high peptide identification rates, individualized p.p.b.-range mass accuracies and proteome-wide protein quantification. *Nat Biotechnol* **26**, 1367-1372, doi:10.1038/nbt.1511 (2008).

48 Huang da, W., Sherman, B. T. & Lempicki, R. A. Systematic and integrative analysis of large gene lists using DAVID bioinformatics resources. *Nat Protoc* **4**, 44-57, doi:10.1038/nprot.2008.211 (2009).

49 Liu, T. & Xiao, Z. Dynamic light scattering of rigid rods–a universal relationship on the apparent diffusion coefficient as revealed by numerical studies and its use for rod length determination. *Macromolecular Chemistry and Physics* **213**, 1697-1705 (2012).

50 Flak, D. *et al.* In situ ambient pressure XPS observation of surface chemistry and electronic structure of α-Fe2O3 and γ-Fe2O3 nanoparticles. *Applied Surface Science* **455**, 1019-1028, doi:https://doi.org/10.1016/j.apsusc.2018.06.002 (2018).

51 Alduhaish, O. *et al.* Facile Synthesis of Mesoporous alpha-Fe2O3@g-C3N4-NCs for Efficient Bifunctional Electro-catalytic Activity (OER/ORR). *Sci Rep* **9**, 14139, doi:10.1038/s41598-019-50780-2 (2019).

52 Levine, L. *et al.* Syncytiotrophoblast extracellular microvesicle profiles in maternal circulation for noninvasive diagnosis of preeclampsia. *Sci Rep* **10**, 6398, doi:10.1038/s41598-020-62193-7 (2020).

53 Webber, J. & Clayton, A. How pure are your vesicles? *J Extracell Vesicles* **2**, 19861, doi:10.3402/jev.v2i0.19861 (2013).

54 Bellotti, C., Lang, K., Kuplennik, N., Sosnik, A. & Steinfeld, R. High-grade extracellular vesicles preparation by combined size-exclusion and affinity chromatography. *Sci Rep* **11**, 10550, doi:10.1038/s41598-021-90022-y (2021).

55 Chen, S., Shiesh, S. C., Lee, G. B. & Chen, C. Two-step magnetic bead-based (2MBB) techniques for immunocapture of extracellular vesicles and quantification of microRNAs for cardiovascular diseases: A pilot study. *PLoS One* **15**, e0229610, doi:10.1371/journal.pone.0229610 (2020).

56 Menon, R. *et al.* Protein Profile Changes in Circulating Placental Extracellular Vesicles in Term and Preterm Births: A Longitudinal Study. *Endocrinology* **161**, 1-19, doi:10.1210/endocr/bqaa009 (2020).

57 Boriachek, K. *et al.* Avoiding Pre-Isolation Step in Exosome Analysis: Direct Isolation and Sensitive Detection of Exosomes Using Gold-Loaded Nanoporous Ferric Oxide Nanozymes. *Anal Chem* **91**, 3827-3834, doi:10.1021/acs.analchem.8b03619 (2019).

58 Sodar, B. W. *et al.* Best practice of identification and proteomic analysis of extracellular vesicles in human health and disease. *Expert Rev Proteomics* **14**, 1073-1090, doi:10.1080/14789450.2017.1392244 (2017).

59 Tauro, B. J. *et al.* Comparison of ultracentrifugation, density gradient separation, and immunoaffinity capture methods for isolating human colon cancer cell line LIM1863-derived exosomes. *Methods* **56**, 293-304, doi:10.1016/j.ymeth.2012.01.002 (2012).

60 Weng, Y. *et al.* Effective isolation of exosomes with polyethylene glycol from cell culture supernatant for in-depth proteome profiling. *Analyst* **141**, 4640-4646, doi:10.1039/c6an00892e (2016).

61 Gill, M. *et al.* Placental Syncytiotrophoblast-Derived Extracellular Vesicles Carry Active NEP (Neprilysin) and Are Increased in Preeclampsia. *Hypertension* **73**, 1112-1119, doi:10.1161/HYPERTENSIONAHA.119.12707 (2019).

62 Dragovic, R. A. *et al.* Isolation of syncytiotrophoblast microvesicles and exosomes and their characterisation by multicolour flow cytometry and fluorescence Nanoparticle Tracking Analysis. *Methods* **87**, 64-74, doi:10.1016/j.ymeth.2015.03.028 (2015).

63 Lv, Y., Tan, J., Miao, Y. & Zhang, Q. The role of microvesicles and its active molecules in regulating cellular biology. *J Cell Mol Med* **23**, 7894-7904, doi:10.1111/jcmm.14667 (2019).

3.10 Appendix A

University of South Australia

Statement of Authorship

Title of Paper	Magnetic enrichment of immuno-specific extracellular vesicles for mass spectrometry using biofilm-derived iron oxide nanowires
Publication Status	☒ Published ☐ Accepted for Publication ☐ Submitted for Publication ☐ Unpublished and Unsubmitted work written in manuscript style
Publication Details Relevant reference details	Article type: Paper Submitted: 11 Oct 2022 Accepted: 14 Dec 2022 First published: 19 Dec 2022 DOI: https://doi.org/10.1039/D2NR05619D Citation: Nanoscale, 2023,15, 1236-1247
PRINCIPAL AUTHOR	
Name of Principal Author (Candidate)	**Quang Nghia Pham**
Contribution to the Paper Brief description of your work in this publication	Conceptualisation; Methodology; Software; Validation; Formal analysis; Data curation; Writing - original draft and preparation; Writing - review and editing; Visualisation
Overall Percentage (%)	**40%**
Certification	This paper reports on original research I conducted during the period of my Higher Degree by Research candidature and is not subject to any obligations or contractual agreements with a third party that would constrain its inclusion in this thesis. I am the primary author of this paper.
Signature *Signatures will be redacted by the Library at the time of publication*	[redacted] Date: 1-Jun-23
CO-AUTHOR CONTRIBUTIONS	
By signing the Statement of Authorship, each author certifies that: I. the candidate's stated contribution to the publication is accurate (as detailed above); II. permission is granted for the candidate in include the publication in the thesis; and III. the sum of all co-author contribution is equal to 100% less the candidate's stated contribution.	
Name of Co-Author 1	**Marnie Winter**

% Contribution to the Paper	**20%**	
Signature *Signatures will be redacted by the Library at the time of publication*	[redacted]	Date: 1-Jun-23
Name of Co-Author 2	**Valentina Milanova**	
Overall Percentage (%)	**4%**	
Signature *Signatures will be redacted by the Library at the time of publication*	[redacted]	Date: 2-Jun-23
Name of Co-Author 3	**Clifford Young**	
Overall Percentage (%)	**4%**	
Signature *Signatures will be redacted by the Library at the time of publication*	[redacted]	Date: 6-Jun-23
Name of Co-Author 4	**Mark R. Condina**	
Overall Percentage (%)	**4%**	
Signature *Signatures will be redacted by the Library at the time of publication*	[redacted]	Date: 10-Jun-23
Name of Co-Author 5	**Peter Hoffmann**	
Overall Percentage (%)	**3%**	
Signature *Signatures will be redacted by the Library at the time of publication*	[redacted]	Date: 6-Jun-23
Name of Co-Author 6	**Nguyen T. H. Pham**	
Overall Percentage (%)	**3%**	
Signature *Signatures will be redacted by the Library at the time of publication*	[redacted]	Date: 2-Jun-23
Name of Co-Author 7	**Tran Thanh Tung**	
Overall Percentage (%)	**4%**	
Signature *Signatures will be redacted by the Library at the time of publication*	[redacted]	Date: 7-Jun-23
Name of Co-Author 8	**Dusan Losic**	
Overall Percentage (%)	**3%**	

Signature *Signatures will be redacted by the Library at the time of publication*	[redacted]	Date: 7-Jun-23
Name of Co-Author 9	**Benjamin Thierry**	
Overall Percentage (%)	**15%**	
Signature *Signatures will be redacted by the Library at the time of publication*	[redacted]	Date: 1-Jun-23

Chapter 4

Immunomagnetic Enrichment of Human Placental Extracellular Vesicles from Unprocessed Plasma with Magnetic Nanowires

4 Immunomagnetic enrichment of human placental extracellular vesicles from unprocessed plasma with magnetic nanowires

4.1 Abstract

Symptomatic onset of preeclampsia can occur rapidly. Improved biomarkers and rapid diagnostic approaches to "rule-in" disease are necessary to triage care in suspected preeclampsia cases. During pregnancy, extracellular vesicles (EVs) are released from the placenta into the maternal circulation and provide an opportunity for non-invasive diagnostic insights. Syncytiotrophoblast EVs (STBEVs) shed from the placenta are known to carry relevant placental markers (e.g., placental alkaline phosphatase (PLAP) Neprilysin (NEP), Placental Protein 13 (PP13)) and their analysis may improve predictive assay sensitivity/specificity. However, a lack of standardised approaches combined with labour intensive and time-consuming methods has hampered clinical STBEV investigations. Herein, we report a direct plasma immuno-enrichment method for STBEVs, using naturally occurring iron-oxide nanowires (NWs). NW modification with two length reversible-addition-fragmentation-chain-transfer (RAFT) polymers to enhance the sterical stability, increased STBEV recovery compared to Dynabeads in plasma samples. Anti-PLAP conjugated NWs recovered STBEVs within 1.5 hours with minimal sample manipulation and without expensive equipment. Quantifying PP13 and NEP within PLAP+ve STBEVs, demonstrated protein co-localisation and recovery, detecting differences between preeclamptic samples and a gestation matched control. Direct immuno-enrichment of STBEVs with this method, may provide a clinically useful tool for STBEV biomarker studies towards developing a rapid diagnostic tool to triage symptomatic pregnancies.

4.2 Introduction

Preeclampsia is a hypertensive condition that affects 5–8% of all pregnancies.[1] Symptomatic onset of preeclampsia may be difficult to distinguish from other complications and can progress rapidly (within a matter of hours) leading to high blood pressure and organ dysfunction.[2] Undiagnosed and unmanaged, the condition in its most severe form can cause the death of both the mother and the fetus.[3,4] Considering its heterogenous presentation in both onset timing and severity, it is often critical to 'rule in'

or at least ‘rule out’ a preeclampsia diagnosis and establish severity as quickly as possible, as this dictates the immediate optimal management of the pregnancy.[5,6]

Biomarkers to diagnose preeclampsia and stratify the risk of adverse fetal and maternal complications hold great promise to improve care. For example, the ratio of soluble Fms-like tyrosine kinase-1 (sFlt-1) to Placental Growth Factor (PlGF) is validated clinically to rule-out preeclampsia in symptomatic pregnancies, and a result can be returned quickly (within hours) for rapid decision making.[7] While this approach has a very high negative predictive value (i.e. ability to identify symptomatic pregnancies who are not affected), it suffers from a insufficient positive predictive value (i.e. ability to confirm the condition in symptomatic pregnancies or identify asymptomatic women who will be affected).[8] Improved biomarkers and rapid diagnostic approaches to “rule-in” preeclampsia are needed to better triage care in suspected preterm preeclampsia cases, and ensure optimal patient management and pregnancy outcomes.[9]

During pregnancy the placenta sheds extracellular vesicles (EVs) into the maternal blood circulation. Placental EVs are now known to be necessary for a successful pregnancy.[10] The number of placental EVs in maternal blood and their composition change to reflect disease states.[11,12] As a result of their ability to protect their content from enzymatic degradation, EVs are now recognised as a promising target for liquid biopsies of many diseases such as cancer, neurodegenerative diseases and pregnancy complications.[13-15]

EVs derived from syncytiotrophoblasts (STBEVs) are the most studied placental EVs and the most abundant EV types in the maternal circulation in the second half of pregnancy.[16] Most STBEVs display the placental alkaline phosphatase (PLAP) membrane protein and the quantity of both STBEVs and PLAP is known to be altered not only across gestation[17,18] but also in preeclampsia[19] and other pregnancy complications.[20] Roughly 0.5−20% of EVs found in the maternal circulation express PLAP, making their enrichment a promising means to analyse STBEVs and their associated molecular cargo which likely holds diagnostic insights.[21,22] For example, STBEVs are known to carry protein biomarkers which have an altered expression in preeclampsia including PLGF, FLT-1, Neprilysin (NEP), and Placental Protein 13 (PP13).

PP13 represents 7% of total placental protein[23] and is known to be a placental alarmin (or stress sensor).[24] PP13 has shown considerable promise as a first trimester biomarker for preeclampsia with decreased levels identifying preeclampsia with a sensitivity of 62%

and specificity of 84%.[25] PP13 is known to play a role in uterine and vein expansion, and decreased PP13 is one of the earliest known signs of preeclampsia development.[26,27] PP13 expression is also altered in the second and third trimester, and as a late gestation marker has a 77.3% sensitivity and 91.5% specificity for mild preeclampsia detection, and a 88.5% sensitivity and 100% specificity for severe preeclampsia detection.[28] While PP13 is specifically expressed in the placenta, in maternal plasma it is present both in a soluble form and associated with extracellular vesicles.[29] In the maternal circulation it is likely that free PP13 and EV-associated PP13 have different pathophysiological effects (e.g. immune tolerance, inflammation, arterial stiffness).[29] Given this and the co-localisation of proteins within STBEVs being altered in pregnancy complications, the analysis of STBEV-associated PP13 could provide an improved diagnosis or even predictive marker for preeclampsia.[30]

Serum NEP is another protein with known association with preeclampsia. NEP has been shown to be higher in both mild and severe preeclampsia, and is positively correlated with maternal systolic and diastolic blood pressure.[31] Excessive NEP quantity and activity are associated with hypertension, heart failure and amyloid deposition playing an active role in the development of preeclampsia[17] and other conditions such as cardiovascular disease.[32] NEP is expressed in many organs and has been investigated as a biomarker for chronic kidney disease, diabetes and heart failure. NEP is known to be associated with EVs including STBEVs expressing PLAP, and in preeclampsia the placenta releases more NEP with greater activity.[17] NEP-bound STBEVs likely play a role in preeclampsia pathogenesis and could serve as a useful biomarker to establish preeclampsia diagnosis and severity.

Given the complexity of plasma as a biofluid, STBEVs enrichment and analysis is complicated, highly variable and often time-consuming, which limits diagnostic utility. Affinity-based EV isolation methods are required to enrich cell type-specific EVs from plasma, for example STBEVs. Plasma samples are generally pre-processed (e.g. using ultracentrifugation, size exclusion chromatography (SEC)) before immuno-enrichment[33-35] or alternatively enriched with a broad EV marker such as CD63.[36] The quality of pre-processing or pre-enrichment often dictates the success of the subsequent EV immuno-capture[37] and there have been only few reports of direct immune-enrichment from unprocessed plasma samples.[36] This requirement for pre-processing is a limiting factor in the development and translation of cell-type specific EV diagnostics. As outlined by

Tannetta *et al.,* ideally STBEV enrichment for diagnostic purposes should be performed with routine blood handling techniques and minimal samples preparation, towards producing in a timely fashion high yield of undamaged pure STBEVs in a small volume.[38] Therefore, direct immuno-enrichment of EVs from unprocessed maternal plasma is promising towards realising the full potential of placental EVs in preeclampsia diagnosis. However, the presence of large amounts of proteins in unprocessed plasma is a challenge, as it can interfere with the immuno-enrichment process. Specifically, the formation of protein corona and its negative impact on target recognition is now well-established. In addition, as PLAP is present in maternal plasma in high levels as a soluble protein, it may compete with STBEVs if the immuno-enrichment is performed in whole plasma without an EV pre-enrichment step.[22]

Herein, we report on an efficient single-step immuno-enrichment of STBEVs in plasma using bacteria-derived iron oxide NWs. Extracted from the biofilms of zetaproteobacteria *Mariprofundus ferrooxydans* by a simple centrifugation process, these naturally magnetic NWs are promising materials for immuno-magnetic isolation of EVs due to their large surface-to-volume ratio and strong magnetism.[39] The magnetic NWs were surface modified with single or dual block copolymers synthesised by reversible addition fragmentation chain transfer (RAFT) polymerisation, towards improving the biointerfacial properties of the NWs in plasma and introduces functional carboxylic acid groups for antibody conjugation. As a proof of concept, we first demonstrated the immuno-magnetic enrichment of PLAP+ve EVs in plasma samples spiked with cell-derived EVs and compared the performance of the magnetic NWs to that of gold standard Dynabeads. We then explored the diagnostic potential of this approach by quantifying STBEV-associated NEP and PP13 from STBEV enriched from plasma from healthy and preeclamptic pregnancies.

4.3 Methods

4.3.1 Collection of plasma sample

Maternal peripheral blood samples were collected at the Adelaide Women's and Children's Hospital. The study was conducted in accordance with the Declaration of Helsinki, and the protocol was approved by the Women's and Children's Human Research Ethics committee (WCH Application No: WEC/13/WCHN 45) and The University of South Australia Human Research Ethics Committee (0000036112). Written

informed consent was obtained from patients prior to inclusion/sample collection. Three blood samples were used, one from a third-trimester healthy (H) pregnancy (sample taken at 32+5 weeks' gestation, female fetus) and two from preeclamptic (PE) pregnancies (both samples taken at 32+4 weeks' gestation). PE1 carried a male fetus, PE2 carried a female fetus which also had intrauterine growth restriction. Maternal age was between 28-29 years. Blood samples from non-pregnant healthy women were also collected. Peripheral blood (10 mL) was drawn into k3EDTA Vacutainers tubes and transported on ice. Plasma was collected after centrifugation at 1500 × g for 10 min and stored at −80 °C until use. All samples were processed within 6 h after collection.

4.3.2 Preparation of iron-oxide NWs

Biofilm-derived iron oxide NWs were obtained and prepared as previously described.[40] In brief, raw biofilm waste obtained from SA Water was processed by repeated cycles of suspension, vortexing and centrifugation to separate the iron oxide magnetic NWs from the organic and salt impurities. The purified NWs were heated at 600 °C, washed with milli-Q water, air-dried at 70 °C and stored at room temperature until further use.

4.3.3 Synthesis of RAFT copolymers

A short block copolymer with a molecular weight of 2200, poly(methacryloyloxyethyl phosphate)$_5$-*block*-poly(acrylamide)$_{15}$-*block*-poly(ethylene oxide)$_3$ **(**RAFT-5MAPC2-15AAM-3PEO) was prepared by dissolving methoxy triethylene glycol modified 2-{[butylsulfanyl)cabonothioyl]sulfanyl}propanoic acid (1.0 g), acrylamide (2.8 g), 4,4'-azobis(4-cyanovaleric acid) (0.050 g) and dioxane (10 g) in milli-Q water (10 g). The mixture was then purged with nitrogen gas for 15 min followed by polymerisation at 70 °C for 2 h. After air cooling the reaction, (methacryloyloxy)-ethyl]phosphonic acid (2.5 g) and 4,4'-azobis(4-cyanovaleric acid) (0.05 g) was added to the mixture before purging with nitrogen gas for 15 min and heating at 70 °C for 4 h. The obtained polymer was precipitated in acetone, repurified and collected by centrifugation and dried to a constant mass for storage at room temperature until use.

A higher molecular weight (MW) carboxylated block copolymer (MW 6400), poly(methacryloyloxyethyl phosphate)$_5$-*block*-poly(acrylamide)$_{70}$ (RAFT-5MAPC2-70AAM-COOH), was synthesised by dissolving 2-(((butylthio)carbonothioyl)-thio)-propanoic acid (RAFT-COOH, 0.2 g), 4,4′-azobis(4-cyanovaleric acid) (0.012 g), acrylamide (4.17 g), dioxane (7.8 g) in milli-Q water (12.1 g) under magnetic stirring at

70 °C for 4 h in an inert atmosphere. The mixture was then cooled down before adding [2-(methacryloyloxy)-ethyl]phosphonic acid (0.81 g) and 4,4'-azobis(4-cyanovaleric acid) (0.012 g) for further reaction. After purging with nitrogen for 15 min, the mixture was magnetically stirred at 70 °C for 4 h. The polymer was precipitated in acetone, repurified, collected by centrifugation, dried to a constant mass and stored at room temperature until use.

A third carboxylated block copolymer with a molecular weight of 2400, poly(methacryloyloxyethyl phosphate)$_3$-*block*-poly(acrylamide)$_{20}$ (RAFT-3MAPC2-20AAM-COOH) was synthesised via the method described above for the synthesis of RAFT-5MAPC2-70AAM-COOH. The quantities of all materials were adjusted accordingly as well as the reaction times which were reduced to 2.5 and 3 h.

4.3.4 Surface functionalisation of iron oxide NWs with RAFT copolymers

The surface of the iron oxide NWs was modified to introduce carboxylic acid groups *via* coating with RAFT copolymers. Two different coatings were used in this study, namely a dual copolymer and single copolymer coating. For the dual coating, a mixture of RAFT-5MAPC2-15AAM-3PEO and RAFT-5MAPC2-70AAM-COOH block copolymers (molar ratio 7:3) was used. RAFT-5MAPC2-70AAM-COOH allows for attachment of a targeting moiety, while RAFT-5MAPC2-15AAM-3PEO assists in achieving better grafting density onto the surface of the NWs and therefore, an improved colloidal stability of the NWs. Anchoring of the polymers was established by the covalent bonding between the iron oxide NWs and the phosphonic acid groups of the copolymers. In brief, RAFT-5MAPC2-15AAM-3PEO (20 mg) and RAFT-5MAPC2-70AAM (22.8 mg) were dissolved in milli-Q water and the pH was adjusted to 4 using 0.1 M NaOH. The polymer mixture was then added gradually to NWs (10 mg) resuspended in milli-Q water under ice-cold probe sonication for 10 min followed by an overnight end-over-end mixing (HulaMixer, Thermo Fisher Scientific) at room temperature. The pH of the obtained mixture was further adjusted to 5 and then 6 using 0.1 M NaOH with 10 min of ice-cold sonication in between. Polymer-coated NWs (referred to as NW-*p*AAm) were washed with milli-Q water three times to remove impurities and unreacted polymers, resuspended in milli-Q water and stored at room temperature until use. A similar protocol was used for the single copolymer coating with RAFT-3MAPC2-20AAM-COOH.

4.3.5 Preparation of PLAP antibody-functionalised iron oxide NWs

Bioconjugation of the NWs with PLAP antibodies was carried out using the standard carbodiimide coupling chemistry (Figure 1). In brief, NW-*p*AAm (1 mg), 25 µL of EDC-HCl (76 mg/mL) and 25 µL of NHS (11.5 mg/mL) were mixed in milli-Q water and allowed to react for 5 min at room temperature. NWs were sequentially washed once with milli-Q water and once with phosphate buffer saline (1 × PBS pH 7.4, 10010023, Life Technologies) to remove excess EDC and NHS. Activated NWs were added to PBS buffer containing 40 µg of anti-PLAP antibodies followed by an end-over-end mixing (HulaMixer) for 2 h at room temperature. Anti-PLAP conjugated NWs (referred to as NW-PLAP) were washed with PBS buffer three times, quenched with 50 mM ethanolamine and blocked with 0.5% bovine serum albumin (BSA, Sigma). After washing and resuspension in PBS buffer, the antibody-conjugated NWs were kept at 4 °C and used within two weeks of conjugation.

4.3.6 Preparation of antibody-functionalised Dynabeads

Dynabeads M-270 carboxylic acid (14305D, Thermo Fisher Scientific) were conjugated to antibodies according to the manual. Dynabeads (3 mg) were washed with 25 mM MES buffer and activated with EDC-HCl (50 mg/mL) and NHS (50 mg/mL) for 30 min at room temperature. After washing the Dynabeads three times with 25 mM MES buffer, activated Dynabeads were conjugated with 120 µg of anti-PLAP antibodies in PBS buffer for 2 h at room temperature. Anti-PLAP conjugated Dynabeads (referred to as Dynabead-PLAP) were washed twice with PBS buffer, quenched with 50 mM ethanolamine, and blocked with 0.5% BSA. The beads were resuspended in PBS buffer, stored at 4 °C and used within two weeks of conjugation.

4.3.7 Nanowire characterisation

Field emission scanning electron microscope (FE-SEM, Carl Zeiss Microscopy Merlin) was used to characterise the morphology of the NWs. Relative changes in the size of NWs before and after surface modification and antibody conjugation were monitored by dynamic light scattering (DLS, Zetasizer Nano ZS90, Malvern). X-ray photoelectron spectroscopy (XPS, Kratos AXIS Ultra DLD) and attenuated total reflectance Fourier-transform infrared spectroscopy (ATR-FTIR, Nicolet 6700) were used to characterise and evaluate the surface modification and antibody conjugation of NWs. For FTIR, NW samples prepared in solution were left to dry at room temperature. ATR-FTIR spectra of

powder-like NW samples and polymers were measured in the range of 400−4000 cm^{-1} with 30 scans per measurement at 4 cm^{-1} resolution. For XPS, NW samples were casted onto silicon wafer substrates as described previously.[41] XPS survey scans were taken in the range of 0–1200 eV with a pass energy of 160 eV and a step size of 0.5 eV. High-resolution spectra of C 1s and N 1s were scanned with the pass energy of 20 eV and step size of 0.1 eV. XPS spectra were analysed using the CasaXPS software (version 2.3.18) using binding energy of C 1s C-C/C-H peak at 284.8 eV as reference.

4.3.8 Cell culture for recovery studies

BeWo choriocarcinoma cells (a trophoblast-like cell line) were used as a placental EV model. BeWo cells were cultured in Roswell Park Memorial Institute media (RPMI 1640, Gibco), 10% fetal bovine serum (FBS, Gibco) and 10,000 U/mL of penicillin/streptomycin (Gibco) at 37 °C in a 5% CO_2 humidified incubator. Once 90% confluency was reached, the culture media was discarded and the cells were washed twice with 1 × Dulbecco's phosphate-buffered saline (DPBS, Gibco). The cells were then cultured in FBS-free medium for an additional 48 h followed by the collection of the culture media, which was stored at −80 °C until use.

4.3.9 Preparation of PLAP+ve EV-spiked plasma

Total EVs from the culture media of BeWo cells and plasma of non-pregnant women were first collected by differential ultracentrifugation. Cell culture media (80 mL) and plasma (500 µL) were thawed in a 37 °C water bath and sequentially centrifuged at 300 × g for 30 min and 2000 × *g* for 30 min at 4 °C (5699-R rotor, Rotanta 460 R, Hettich) to remove dead cells and debris. The supernatant was then centrifuged at 12,000 × *g* for 30 min and ultracentrifuged at 120,000 × *g* for 70 min at 4 °C (70 Ti rotor, Optima L-80 XP, Beckman Coulter) to pellet large and small EVs, respectively. Pellets of EVs were resuspended in PBS buffer, combined and stored at −80 °C and used within two weeks. Plasma samples containing PLAP+ve EVs were prepared by spiking total BeWo EVs into 500 µL of plasma so that the number of PLAP+ve EVs accounted for 10% of the final total EVs in plasma. This percentage was selected to mimic the proportion of PLAP+ve EVs in the maternal plasma.

4.3.10 Dot blot assay

A dot blot assay was used to assess the stability of the polymeric coatings on the NWs and Dynabeads as well as their binding performance in plasma. NWs and Dynabeads were

first conjugated with anti-mouse IgG (H+L) highly cross-adsorbed antibody produced in goat as described in Section 2.5 and mixed with 1%, 10% and 50% (in PBS buffer) and 100% plasma for 1 h at room temperature under continuous end-over-end mixing (Hula Mixer; Thermofisher Scientific). In parallel, nitrocellulose membranes were spotted with 1 µL of three different concentrations of anti-goat IgG (H+L) antibody produced in mouse (1, 0.1 and 0.01 mg/mL), air-dried for 15 min and blocked with 10% BSA for 20 min at room temperature. The blocked membranes were added to the plasma samples containing anti-mouse IgG conjugated NWs and Dynabead and incubated for 1 h at room temperature on an orbital shaker. After incubation, the membranes were washed in milli-Q water and visualised under a stereo microscope (Nikon SMZ25). Binding of NWs and Dynabead onto the nitrocellulose membranes was quantified by ImageJ (v1.8.0).

4.3.11 Direct immuno-enrichment of PLAP+ve EVs in plasma

Plasma (100 µL) was thawed at room temperature, diluted with PBS buffer to 50% and centrifuged at 2000 × *g* for 30 min at 4 °C to remove cells and debris. The resultant supernatant was mixed with 1 mg of NW-PLAP or Dynabead-PLAP and incubated for 1 h at room temperature. After washing three times with 1 mL of PBS buffer, EVs captured by NWs and Dynabead were either eluted for NTA measurement using 0.1 M Glycine-HCl pH 2.8 or lysed directly for protein quantification by bicinchoninic acid (BCA) assay or enzyme-linked immunosorbent assay (ELISA).

4.3.12. Nanoparticle tracking analyses of immuno-enriched EVs

After immuno-enrichment, captured EVs were eluted using 0.1 M Glycine-HCl with an incubation of 30 min at RT. The supernatant containing eluted EVs was collected and neutralised by the addition of 1 M Tris pH 8. EV samples were diluted in ultrapure water (Thermo Fisher Scientific) and analysed by Nanosight NS300 (Malvern). All measurements were performed in triplicate with 5 recordings of 60 s taken for each measurement under the same camera settings (shutter speed: 30.15 ms, camera level: 15).

4.3.13. Protein biomarker quantification with ELISA

The concentrations of PLAP, NEP and PP13 proteins were quantified using ELISA kits obtained from MyBiosource (MBS289869, MBS2533291 and MBS2703307, respectively). The concentration of CD63 protein was quantified using an ELISA kit obtained from Thermo Fisher (EH95RBX5). The recovery of PLAP was used to evaluate

the EV enrichment efficiencies calculated by the ratio of measured PLAP protein amounts to that present in the original plasma sample.

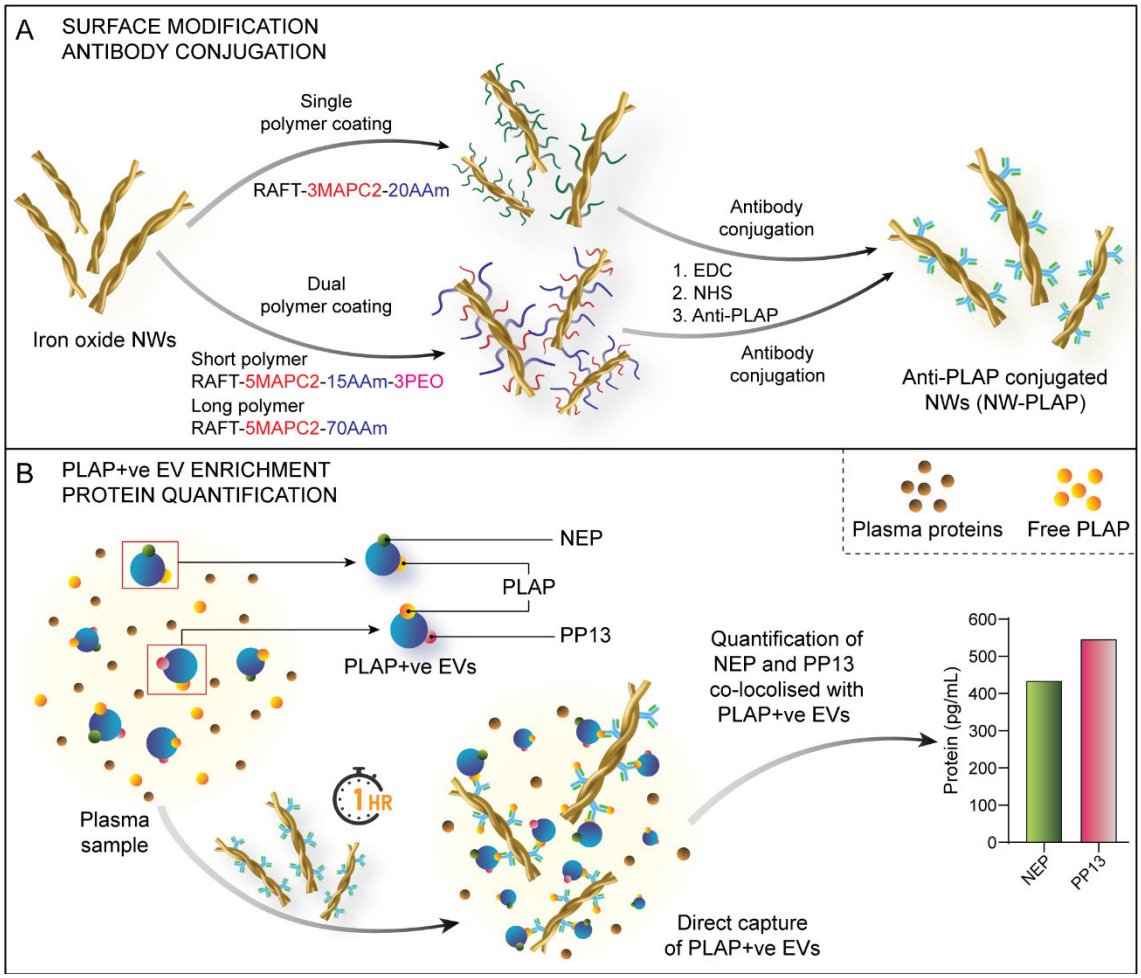

Figure 4-1 Surface coating of NWs and direct EV enrichment procedure.
Schematic diagram for (A) the surface coating of NWs with RAFT polymers and antibody conjugation to NWs and (B) procedure of direct enrichment PLAP+ve EVs.

4.4 Results and discussion

We have previously reported an immuno-magnetic EV enrichment method for cell culture media EV based on magnetic NWs coated with poly(methacryloyloxyethyl phosphate)$_3$-*block*-poly(acrylamide)$_{20}$ RAFT polymer (RAFT-3MAPC2-20AAM, referred to here as "single coating").[42] A dual coating protocol with polyacrylamide-based RAFT copolymers of different molecular weights was shown to efficiently stabilise iron oxide nanoparticles, enabling efficient application as lymphotropic MRI contrast agent.[43] In addition, nanoparticle coating with polymers of different molecular weight was previously shown to improve the binding affinity of the conjugated ligands.[44] Given the added complexities faced in the direct immuno-enrichment of EVs from plasma

compared to enrichment performed after a pre-enrichment step, we first investigated the use of a dual polyacrylamide polymer coating of the magnetic NW (NW-*p*AAm) based on a mixture of short polymers (RAFT-5MAPC2-15AAM-3PEO - length n = 15 AAM units) and long polymers (RAFT-5MAPC2-70AAM - length n = 70 AAM units) with terminal carboxylic groups for conjugation with antibodies via carbodiimide coupling. Specifically, we aimed to investigate if using mixed polymeric layers improves the yield and/or specificity of EV immuno-enrichment.

Surface modification with RAFT polymers of varying lengths can improve colloidal stability by creating a more complex and diverse surface coating. RAFT polymers offer precise control over molecular weight and polydispersity, resulting in a highly controlled and defined coating. Varying the length of the polymer can lead to a more diverse coating that provides better coverage and adhesion to the particle surface. Longer polymers can offer steric stabilisation by extending further away from the particle surface, while shorter polymers can provide improved coverage and adhesion. This combination of polymer lengths can result in enhanced colloidal stability in different media, including aqueous solutions and biological fluids. In Chapter 4, the incorporation of polyacrylamide polymers into both short and long copolymers has been shown to increase the solubility of NWs, thereby improving the overall steric stability of NWs and preventing their aggregation in aqueous-based dispersing phases as well as physiological solutions like plasma. The short and long copolymers are capped with PEO (polyethylene oxide) and carboxylic functional groups, respectively, which further stabilises the NWs and provides surface moieties for antibody conjugation.

Given that the substantially higher protein concentrations in plasma compared to cell culture media likely presents a greater challenge for direct EV immune-enrichment compared to enrichment performed after a pre-enrichment step, we first aimed to investigate an alternative NW coating, with a mixture of short and long chain RAFT-5MAPC2-15AAM-3PEO and RAFT-5MAPC2-70AAM (referred to as "NW-*p*AAm"). Specifically, we aimed to investigate if using mixed polymeric layers improves EV immuno-enrichment by providing greater specificity. To this end, we first investigated the physicochemical properties of the NWs with a dual coating (4.3.1) before testing the binding performance of both single and dual coated NWs in plasma (4.3.2).

4.4.1 Characterisation of iron oxide nanowires coated with mixed RAFT polymers

The morphologies of iron oxide NWs purified from the bacterial biofilms and NW-*p*AAm were characterised by SEM as shown in Figure 4-2A and B respectively. Both pristine NWs and NW-*p*AAm displayed an entangled helical structure consisting of five or more NWs with an average length of approximately 600 nm. Due to the non-spherical structures of the NWs, DLS could only be used to approximate the relative size and evaluate the stability of NWs after coating and antibody conjugation. As shown in Figure 4-2C, the size of the NWs slightly increased after coating with the RAFT copolymers, from 523 ± 19 nm for pristine NWs to 575 ± 23 nm for NW-*p*AAM, in agreement with the size estimated by SEM. After conjugation with monoclonal antibodies (NW-IgG), the size of the NWs further increased to 618 ± 7 nm, demonstrating that the biofunctionalization protocol did not induce drastic aggregation of the highly magnetic NWs. Changes in the zeta potentials of NW-*p*AAM and NW-IgG compared to that of pristine NWs further confirmed successful coating with the RAFT copolymers and conjugation of antibodies (Figure 4-2D). Specifically, while pristine NWs displayed negative charges of approximately –40 ± 2 mV, it decreased to –32 ± 1 mV ($p < 0.01$) upon coating with the polyacrylamide copolymers. The zeta potential greatly reduced to –16 ± 2 nm ($p < 0.0001$) after antibody conjugation.

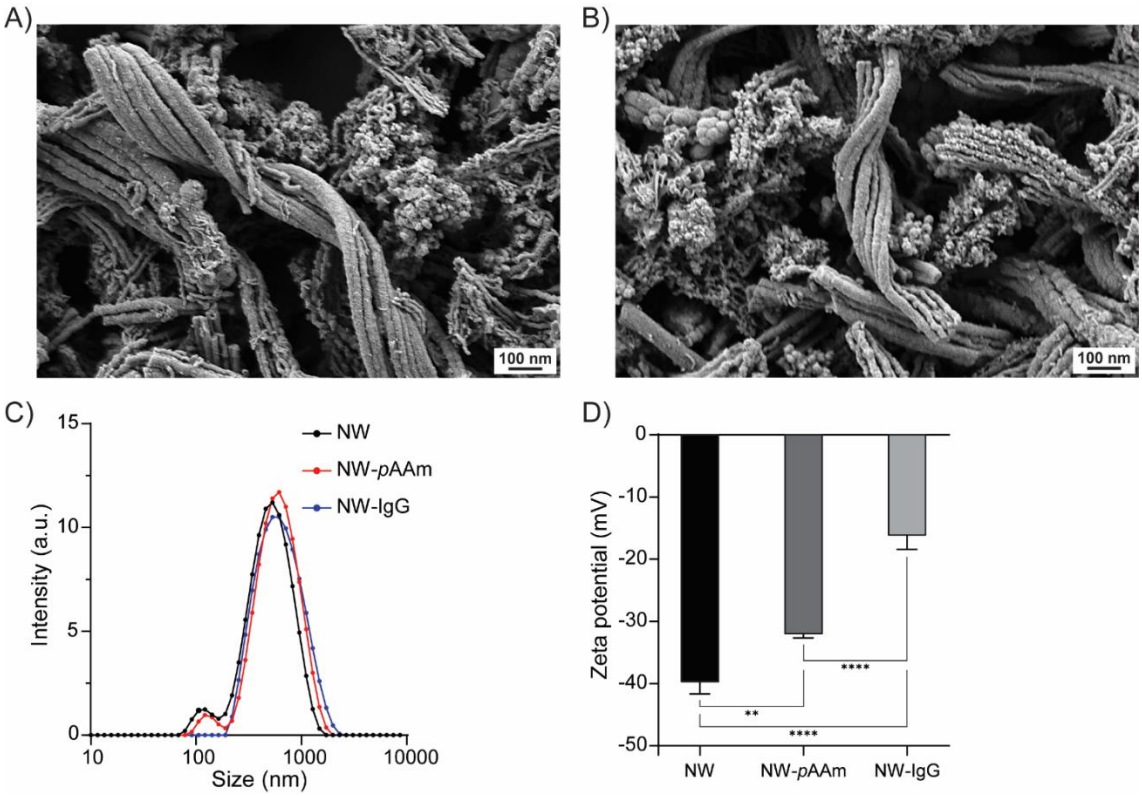

Figure 4-2 SEM, DLS and zeta potential characterisation of NWs.
Scanning electron microscopy images showing the twisted structures of A) NW and B) NW-*p*AAm. C) Dynamic light scattering size measurements for NW, NW-*p*AAm and NW-IgG. D) Zeta potentials for NW, NW-*p*AAm and NW-IgG. Data are presented as means + SD (n = 3, one-way ANOVA with Tukey's post-test, $^{**}p < 0.01$ and $^{****}p < 0.0001$).

The chemical compositions of the NW, NW-*p*AAm and NW-IgG samples were then characterised by FTIR and XPS to confirm the presence of RAFT copolymers and antibodies on the surfaces of NWs. The FTIR spectra of the short and long RAFT copolymers as well as those of the NWs before and after polymer coating and antibody conjugation are shown in Figure 4-3A. In particular, the IR spectra of short (RAFT-5MAPC2-15AAM-3PEO) and long (RAFT-5MAPC2-70AAM) copolymers were similar, displaying major bands at 3360, 3190, 1660, 1454, 1161 and 930 cm^{-1}. The bands at 930 and 1161 cm^{-1} are related to the stretching vibrations of P=O and P–O–C respectively, indicating the presence of phosphate groups in the polymer structure, while the band at 1454 cm^{-1} can be assigned to the vibration of CH_2 scissor of the carbon chain. The presence of amide groups in the two RAFT copolymers was reflected by the prominent band at 1660 cm^{-1} attributed to C=O stretching and the two bands at 3190 and 3360 cm^{-1} associated to N–H stretching. The presence of O–H stretching in the range of 2500–3400 cm^{-1} may also associate with the hydroxyl and carboxyl groups of ethylene

oxide (PEO) monomers and carboxylic acid moieties in the short and long copolymer respectively. These results, along with NMR spectra (data not shown) confirmed the successful syntheses of the two RAFT copolymers. Pristine NWs displayed a band of O–H stretching for hydroxyl groups from 3000–3500 cm^{-1}, which agrees with the negative zeta potential measured for the pristine NWs as mentioned in Figure 4-2D and explains the stable suspension of NWs during polymeric coating. An adsorption band at 524 cm^{-1} and a broad band at 1065 cm^{-1} present in the spectra of NWs, NW-*p*AAm and NW-IgG can be assigned to the vibration of Fe–O bond and C–O stretching, respectively. The presence of bands at 1660, 3190 and 3360 cm^{-1} in the spectra of NW-*p*AAm and NW-IgG indicated the presence of amide groups and thus suggests successful polymer coating and antibody conjugation onto NWs.

The XPS spectra obtained for the NW, NW-*p*AAm and NW-IgG samples were in qualitative agreement with the FTIR spectra. The elemental survey scans and high-resolution spectra of Fe 2p are shown in Figure 4-3B and C respectively for the three samples. Two peaks at 711 eV (Fe $2p_{3/2}$) and 724.5 eV (Fe $2p_{1/2}$) are visible, which correspond to the signature of hematite α-Fe_2O_3. Quantification of the major elemental compositions of the three samples (Table 4-1) showed increases in carbon (C 1s at 284.8 eV) after polymer coating and nitrogen (N 1s 399.8 eV) after antibody conjugation. Specifically, the carbon content for pristine the NWs was 10.6% which increased to 26.5% for NW-*p*AAm and 43.75% for NW-IgG. These changes were mainly due to increases in the carbon proportion of the C–C/C–H (284.8 eV), C–N (285.4 eV) and C=O (288.4 eV) components observed in C 1s spectra deconvolution (Figure 4-3D). Nitrogen was not detected in pristine NW, but increased to 3.7% and 7.6% for NW-*p*AAm and NW-IgG respectively, which was in agreement with the increase of the C–N component (399.8 eV) observed in the high-resolution spectra for N 1s (Figure 4-3E). Deconvolution of O 1s spectra revealed two peaks that can be assigned to Fe–O (529.3 eV) and O=C (531.4 eV) (Figure 4-3F). The increases in the intensities of the O=C component observed for NW-*p*AAm (55.2%) and NW-IgG (63.5%) compared the pristine NW (50.4%) were in agreement with changes observed for the C=O component of C 1s spectra. These results further confirmed that NWs were successfully functionalised with RAFT copolymers and subsequently conjugated with antibodies.

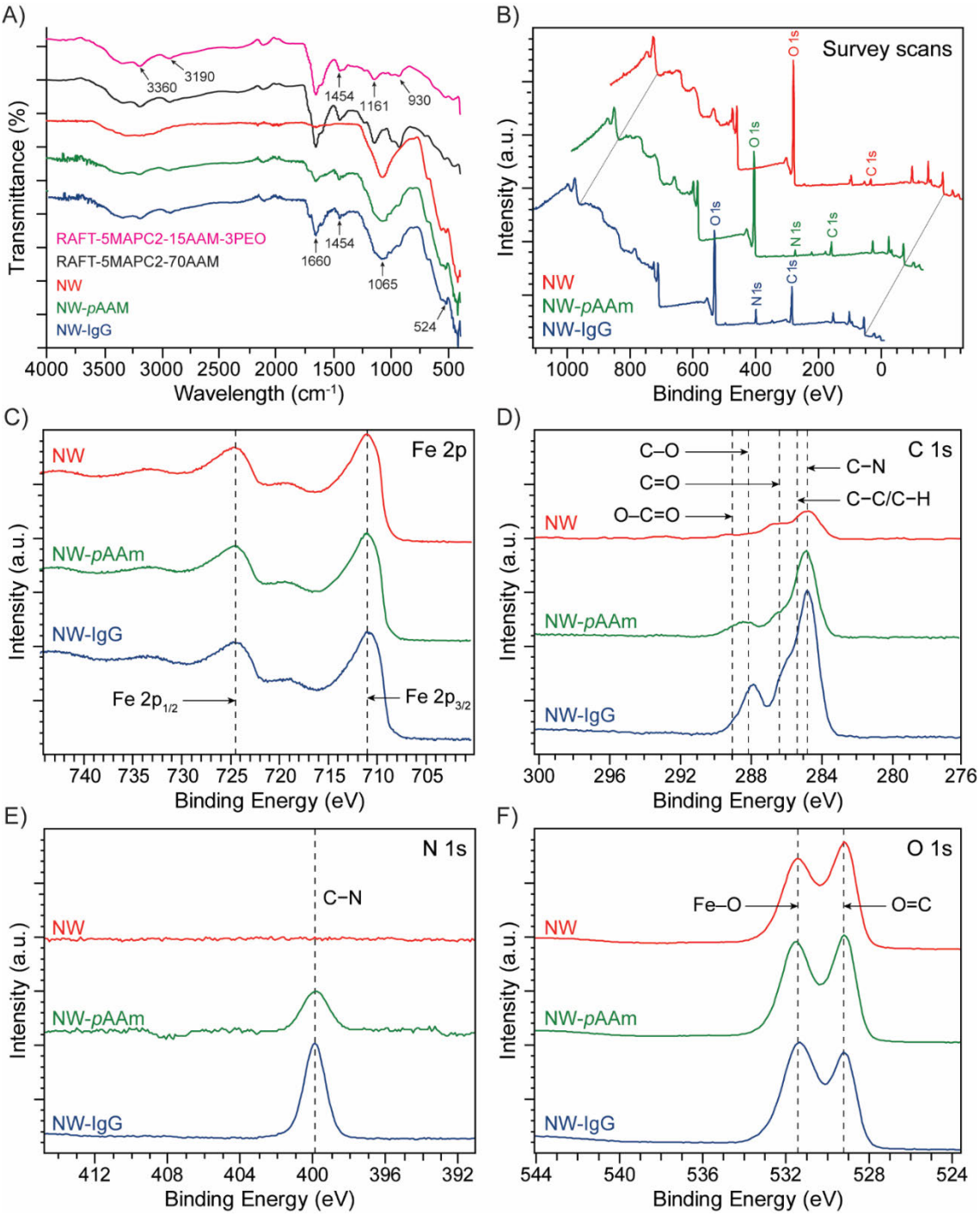

Figure 4-3 FTIR and XPS characterisation of NWs.
(A) FTIR spectra of RAFT-5MAPC2-15AAM-3PEO and RAFT-5MAPC2-70AAM block copolymers, pristine NW, NW-*p*AAm, and NW-IgG. (B) XPS survey scan spectrum of NW, NW-*p*AAm, and NW-IgG. (C) High-resolution spectra for Fe 2p with dashed lines indicating peaks of Fe $2p_{3/2}$ (711 eV) and Fe $2p_{1/2}$ (724.5 eV). (D) High-resolution spectra for C 1s with dashed lines indicating major peaks of C–C/C–H (284.8 eV), C–N (285.4 eV), C–O (286.3 eV), C=O (288.4 eV), and O–C=O (289 eV). (D) High-resolution spectra for N 1s with a dashed line indicating the major peak of C–N (399.8 eV). (D) High-resolution spectra for O 1s with dashed lines indicating the major peaks of Fe–O (529.3 eV) and O=C (531.4 eV).

Table 4-1 Summary of XPS elemental composition and components

Nanowire samples	XPS elemental composition (%)			C 1s components (%)					O 1s component (%)	
	C	N	O	C–C/C–H	C–N	C–O	C=O	O–C=O	Fe–O	O=C
NW	10.64	-	89.36	35.42	-	45.7	8.15	10.73	50.55	50.45
NW-*p*AAm	26.53	3.72	69.75	48.2	12.82	19.4	17.52	2.06	44.81	55.19
NW-Ab	43.75	7.58	48.66	47.04	17.1	15.31	18.03	2.52	36.47	63.53

"-" denoted under the detection limit.

4.4.2 Binding performance in plasma

To assess the binding affinity of the antibody functionalised NWs, a dot blot assay was designed using model antibodies. Specifically, the binding to nitrocellulose membranes spotted with mouse IgG of NWs conjugated with anti-mouse IgG prepared with either the dual or single coating protocol was measured in both PBS and plasma. Anti-mouse conjugated carboxylic acid Dynabeads were used as benchmarked. As shown in Figure 4-4A, concentration-dependant binding in PBS was observed for both NW samples and Dynabeads, with no/minimal binding in the negative nitrocellulose membrane controls spotted with Anti-Mouse IgG (H+L). Quantification of binding intensity (Figure 4-4B) demonstrated that NWs with the dual coating, resulted in significantly higher binding compared to the single coating (132.8 vs 90.5, respectively, P-value = 0.005) and Dynabeads (132.8 vs 76.3, respectively, P-value = 0.008). This demonstrates the importance of the polymeric interface nanoarchitecture even in a non-complex solution such as PBS and suggests that the mixed copolymer coating comprising both long and short polymers improves the availability of the ligand and consequently the binding ability of the NWs compared to the single coating used in our previous study.[42] This result is also in agreement with the previous report by Ishii et al.[44] that the used mixed molecular weight PEG chains to improve target recognition.

Next, we assessed the retention of the binding performance in presence of increasing amounts of plasma proteins. The binding affinities of the NWs and Dynabeads clearly decreased with increasing concentration of plasma proteins with no detectable specific binding in 100% plasma for all magnetic materials. This observation can likely be related to the protein corona effect, which describes the cloaking of nanoparticles by proteins in physiological fluids.[45] Interestingly, the NWs appeared to be more resistant than Dynabeads. However, given that the NWs are smaller than the Dynabeads, and therefore possess greater surface-to-volume ratios, there is a greater number of NWs compared to

Dynabeads for a given weight which was the case here as 1 mg of magnetic materials was used in the dot-blot assay. To account for these differences when investigating binding occurring in the presence of plasma, the binding data was normalised to each samples own PBS positive binding data. As shown in Figure 4-4C, the dual polymer NW-*p*AAm performed well in 1% and 10% plasma with approximately 86% and 77% retention of binding relative to the PBS situation. On the other hand, Dynabeads showed significant decrease in binding ability in 1% plasma and almost no binding in 10% plasma with 35% and 10% binding retention, respectively. Interestingly, while binding in 50% plasma reduced compared to 10% for all samples, the NWs with dual and to a lesser extent single coatings maintained significantly better binding compared to Dynabeads (0.62, 0.45 and 0.26, P-value = 0.007 and 0.024 respectively). Abundant literature describes the formation of protein corona on nanoparticles in protein-rich environment of plasma.[46,47] The importance of nanoparticle surface coatings in modulating their physicochemical properties (surface charge, hydrophobicity *etc.*) and as a result the formation of protein corona is now well established.[48,49] Our observation can therefore be related to the presence of the RAFT polymeric biointerface as polyacrylamide-based nanoparticle coating substantially reduces protein fouling.[50] Interestingly, the dual coating protocol yielded a significantly higher retention of the binding affinity in 50% plasma with ~62% compared with 38% for NWs prepared with the single coating protocol (P-value = 0.073). This again illustrates the importance of the polymeric interface in mitigating the formation of protein corona and the resulting loss of target recognition.

Given the acceptable retention of binding affinity in 50% compared to 10% plasma for NWs prepared with the dual copolymer protocol (65% vs 77%, respectively) and considering the concentration requirements for clinical samples, we selected 50% diluted

plasma to investigate subsequent direct placental PLAP+ve EV enrichment with the dual coated NW-*p*AAm.

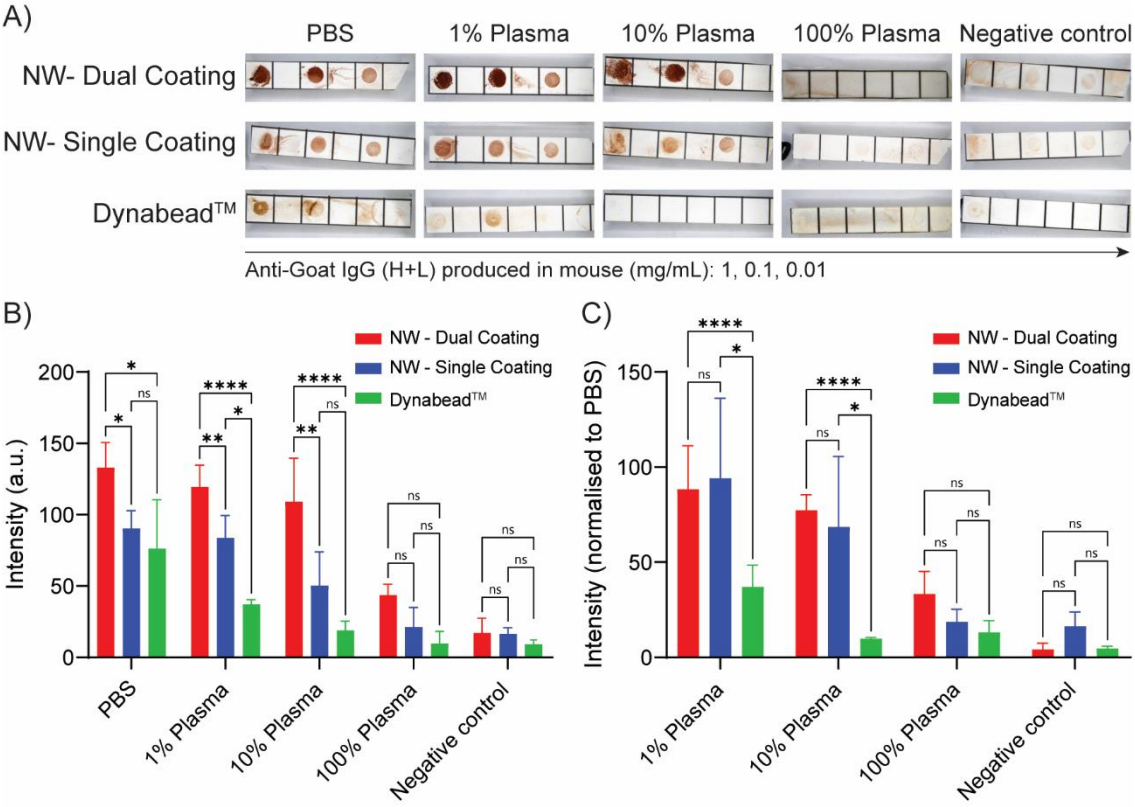

Figure 4-4 Binding performance of dual and single coated NWs and Dynabead.
(A) Representative images of nitrocellulose papers used to compare the binding of NW and Dynabead in dot blot assay (performed in triplicate). Dot blot analyses investigating the binding of A) NW and B) Dynabead in PBS and human plasma (1%, 10%, and 100%). NW and Dynabead were conjugated with Anti-Mouse IgG (H+L) antibodies produced in goat and incubated with nitrocellulose membranes spotted with Anti-Goat IgG (H+L) highly cross-adsorbed antibodies produced in mouse at three different concentrations (1, 0.1, and 0.01 mg/mL). Controls are membranes spotted with Anti-Mouse IgG (H+L). Data are presented as means + SD for 1 mg/mL of Anti-Goat IgG (n = 3, Student's t-tests, ns: non significant ($p > 0.5$), *$p < 0.1$, **$p < 0.01$ and ****$p < 0.0001$).

4.4.3 EV capture capability of iron oxide nanowire

We next investigated the ability of the NW-*p*AAm to enrich PLAP+ve EVs directly from 50% diluted plasma without EV pre-enrichment using an EV-spiking model. To this end, the PLAP+ve EVs enrichment performance of the NW-*p*AAm conjugated with anti-PLAP antibodies (NW-PLAP) was investigated in PBS (BeWo EVs resuspended in PBS) and in 50% plasma spiked with BeWo EVs. Dynabead-PLAP were used as a control to benchmark the enrichment ability of the magnetic NWs. The amounts of PLAP in the EV-enriched fractions using NWs and Dynabeads relative to the amount of PLAP in the starting PBS and 50% spiked plasma were measured using ELISA. The recovery

efficiencies of PLAP extracted from EVs enriched with increasing amounts of NW-PLAP and Dynabead-PLAP (0.02, 0.05, 01, 0.5 and 1 mg) in PBS and 50% spiked plasma are presented in Figure 4-5. As expected, the PLAP recovery efficiency increased with increasing amounts of NW-PLAP and Dynabead-PLAP but plateaued at 0.5 mg with the highest recovery of 85% achieved for the NW-PLAP. However, while there was no significant difference in PLAP recovery between the NW-PLAP and Dynabead-PLAP in PBS (Figure 4-5A), enrichment for EVs spiked in 50% plasma was significantly different between the two magnetic materials (Figure 4-5B). Starting from 0.1 mg ($p < 0.05$), NW-PLAP significantly outperformed Dynabead-PLAP, and this difference was more pronounced at 0.5 and 1 mg ($p < 0.001$). In 50% spiked plasma, the highest recovery of PLAP was approximately 57.6% and 32.3% for the NW-PLAP and Dynabead-PLAP, respectively.

respectively.

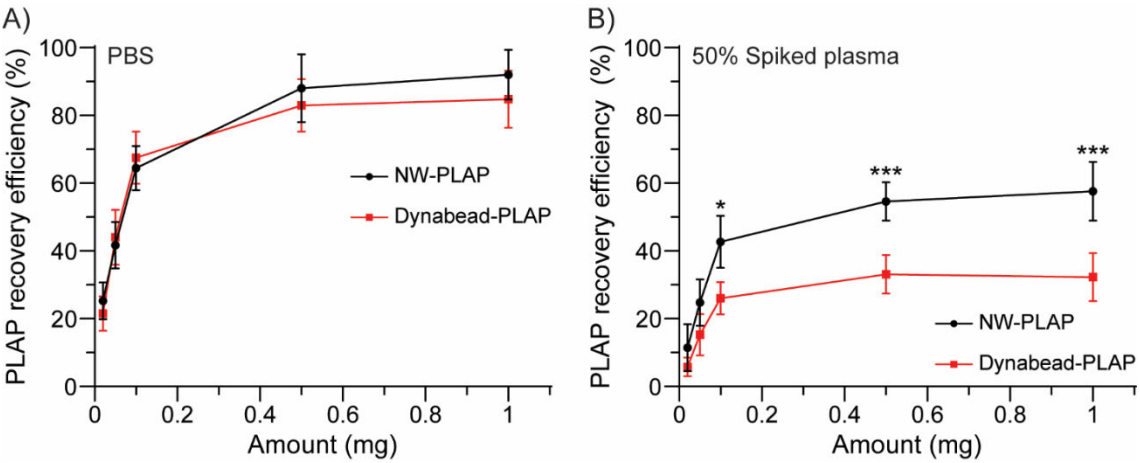

Figure 4-5 Effect of enrichment conditions on PLAP recovery.
PLAP-recovery efficiency using different amounts of NW-PLAP and Dynabead-PLAP (0.02, 0.05, 0.1, 0.5 and 1 mg) for PLAP+ve EVs spiked in A) PBS and B) 50% plasma. Data are presented as means ± SD (n = 3, Student's t-test, *$p < 0.1$ and ***$p < 0.001$).

The improved enrichment of PLAP+ve EVs afforded by the NW-PLAP compared to Dynabead-PLAP in 50% spiked plasma agrees with the model binding performance in the dot blot assay (Figure 4-4C). Although the structural differences between the NWs and Dynabeads may play a role, this data supports the rationale of coating immuno-magnetic materials with hydrophilic RAFT copolymers towards enabling improved specific capture of EVs in protein-rich samples. Dynabeads are very commonly used as solid support in a variety of bio-magnetic separation applications including protein and

cellular enrichment, and their M-270 coating that includes a hydrophilic layer of glycidyl ether with terminal carboxylic acid groups allows straightforward conjugation with ligands.[51] Although the Dynabead coating has been designed to reduce non-specific binding in a wide variety of buffers,[51] our data shows that in 50% plasma, the binding ability of Dynabeads is drastically reduced. Dynamic non-specific adsorption of biomolecules (such as plasma proteins and lipids) onto the magnetic material surface upon exposure to plasma likely cloaks the beads surface, preventing specific binding between the antibody and its target. In contrast, the RAFT copolymers used here to biofunctionalise the iron oxide NWs enabled greater PLAP+ve EV capture even in 50% plasma environment, especially when a mixture of short and long RAFT copolymer chains was used.

Finally, we investigated the feasibility of eluting the PLAP+ve EVs enriched using the NW-PLAP using Glycine-HCl. Eluted EVs were characterised in regard to their size distribution and concentration by NTA. As shown in Figure 4-6, the EVs ranged in size from 55 to 250 nm with a mean/mode size of 132 ± 2/98 ± 2 nm, indicating that both small (< 200 nm) and large (> 200 nm) EVs were enriched, as expected for PLAP+ve EVs. The particle to protein ratio purity ratio was $8.9 \pm 1.7 \times 10^9$, indicating a pure EV enrichment.[52]

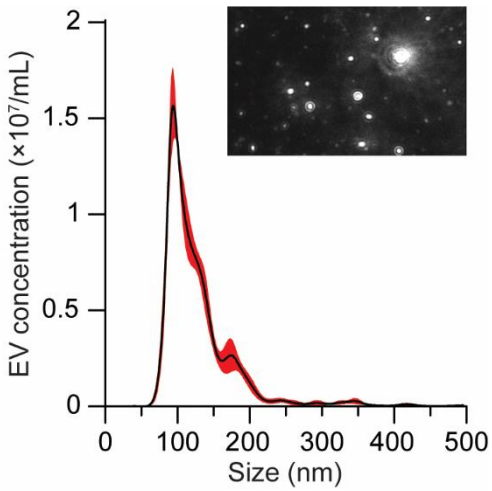

Figure 4-6 NTA characterisation of eluted PLAP+ve EVs.
NTA characterisation of eluted PLAP+ve EVs enriched using the NW-PLAP showing the size and concentration. Inset displays a representative image taken with the NTA apparatus.

4.4.4 Enrichment and quantification of PLAP+ve EV associated proteins in pregnancy plasma samples

It has been previously shown that the levels of PLAP, PP13 and NEP are altered in preeclampsia.[17,53,54] It has also been suggested that protein levels in STBEVs may provide better diagnostic sensitivity/specificity than measuring biomarkers directly in maternal plasma.[30] In order to assess the diagnostic potential of direct STBEV enrichment from unprocessed plasma, we next aimed to demonstrate the feasibility of quantifying STBEV-associated NEP and PP13. To this end, the concentrations of PP13 and NEP as well as CD63 (used as a broad EV marker) were measured by ELISA before and after enrichment of PLAP+ve EVs from diluted plasma samples (50% plasma: PBS) from gestation-matched healthy and preeclamptic pregnancies.

Compared to our simplistic spiking model where PLAP+ve EVs are added to plasma from non-pregnant healthy donor, pregnancy samples are known to contain large amounts of free PLAP in addition to EV-bound PLAP.[22] Free PLAP can interfere and/or confound EV PLAP enrichment which is why pre-enrichment is often used prior to PLAP+ve EV enrichment.[33,34,55] As expected, there was a significant increase in PLAP protein in the preeclamptic plasma samples compared to healthy pregnancy control (8162.9 vs 7081.4 pg/mL, respectively, $p < 0.01$, Figure 4-7A).

To confirm STBEV enrichment even in the presence of free PLAP in the maternal plasma, CD63 was quantified before and after STBEV enrichment with the NW-PLAP (Figure 4-7B). CD63 is a canonical marker expressed by most EV subtypes including both microvesicles and exosomes.[36,56] CD63 was below the limit of detection in whole plasma. In contrast, it was detected in all three plasma samples treated with the NW-PLAP, confirming the successful enrichment of EVs. Interestingly, CD63 was present in similar quantities in all three enriched samples. It has previously been demonstrated that in preeclampsia the number of total EVs increases (not just STBEV), which also coincide with an overall increase of CD63.[57] The relationship between PLAP and CD63 is also known to be altered in preeclampsia and varies between late and early onset.[58] In the absence of pre-enrichment and associated removal of free PLAP proteins, PLAP measured in the enriched samples likely represent a combination of PLAP-associated EVs and free PLAP that bound to the NW-PLAP, thereby preventing meaningful assessment of the EV bound PLAP/CD63.

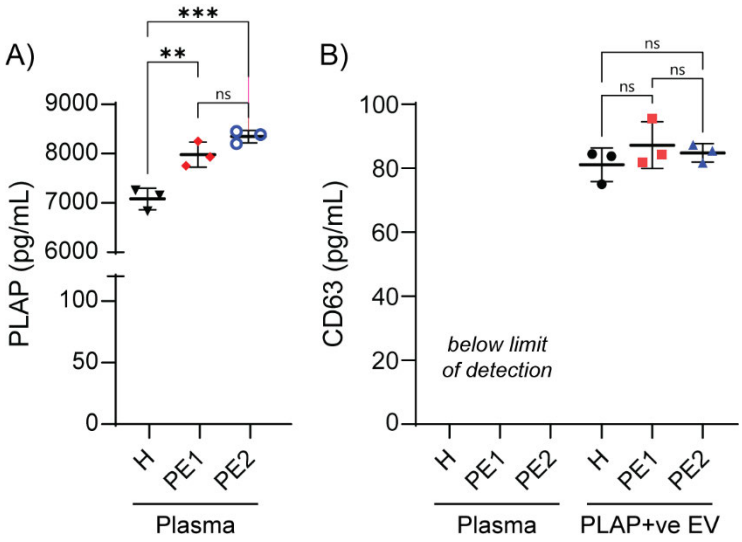

Figure 4-7 Protein concentrations of PLAP and CD63 proteins.
Protein concentrations of (A) PLAP in plasma and (B) CD63 measured in plasma and enriched PLAP+ve EVs in healthy pregnancy (H) and preeclampsia (PE1 and PE2) by ELISA. Data are presented as means ± SD (n = 3, one-way ANOVA with Tukey's post-test, ns: not significant ($p > 0.5$), *$p < 0.1$, **$p < 0.01$, ***$p < 0.001$ and ****$p < 0.0001$).

Having established the successful enrichment of PLAP+ve STBEVs from unprocessed maternal plasma, we next measured the amount of NEP in the enriched STBEV fractions. NEP is known to be associated with EVs including STBEVs, as well as other organ derived EVs.[17] Measurement of NEP before and after PLAP enrichment of pregnancy samples demonstrated that on average 33.8% of NEP was recovered after enrichment (Figure 4-8). If we consider that the whole NEP population is bound to PLAP+ve EVs, this would indicate that approximately a third of all PLAP+ve EVs is recovered and that these EVs are specifically associated with the placenta given this localisation. This is likely an underestimation as NEP may also be present in other sources. Such a recovery suggests that, even considering the complexity of unprocessed plasma samples and presence of free PLAP, direct capture with NW-PLAP recovers sufficient amounts of placental EVs for downstream assays of the molecular cargo, including with ELISA (Figure 4-9A).

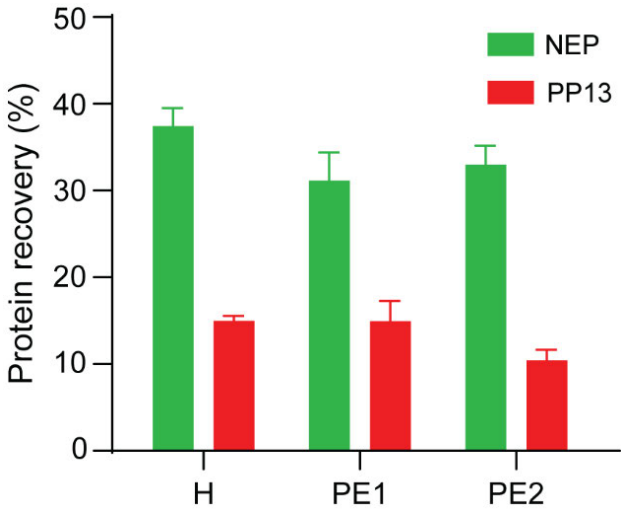

Figure 4-8 Percent protein recovery for NEP and PP13..
Percent protein recovery for NEP and PP13 in enriched PLAP+ve EVs compared to whole plasma measured for the healthy control (H) and two preeclampsia (PE1 and PE2) samples.

Serum NEP has been shown to be higher in both mild and severe preeclampsia and has a positive correlation to systolic and diastolic blood pressure.[31] The placenta is known to release more NEP in preeclampsia and the excessive quantity of active NEP including STBEV-bound NEP likely plays a role in the development of preeclampsia.[17] More work is required to define the clinical utility of NEP as a marker of preeclampsia disease and severity. However, as NEP expression is not specific to the placenta, measurement of STBEV associated NEP may provide a more useful biomarker to establish preeclampsia diagnosis and severity than whole plasma NEP measurements.

PP13 is the earliest known preeclampsia biomarker and has been extensively studied towards establishing diagnosis for preeclampsia. PP13 is specific for the placenta and released in EVs. In addition, degradation of larger vesicles leads to the presence of soluble PP13 in addition to EV-bound PP13, with these two populations thought to have different pathophysiological effects.[29] Enrichment of STBEVs before PP13 analysis may therefore provide improved diagnostic insights in preeclampsia.[30] Throughout gestation PP13 expression is biphasic, and in preeclampsia PP13 levels are lower in the first trimester and higher in the third trimester compared to gestation matched healthy pregnancies.[59] The maternal plasma samples used in the current study were ~32 weeks, and at this gestational timing it is expected that PP13 levels would be ~330 and ~440 pg/mL for healthy and preeclamptic pregnancies, respectively.[60] However, the PP13 levels measured in our small pregnancy cohort were 528.8 and 380.44 pg/mL for the healthy and preeclamptic plasma samples respectively (Figure 4-9B). This result is not entirely

surprising since the 32 weeks timing is close to the inflection point and this expression pattern has also been observed by others.[60] PP13 studies have previously struggled from lack of sample homogeneity, poor detection sensitivity and the requirement for predefined cut-off values.[61] STBEV related PP13 as a biomarker has the potential to address some of these limitations, but further evaluation and method standardisation are required.[61]

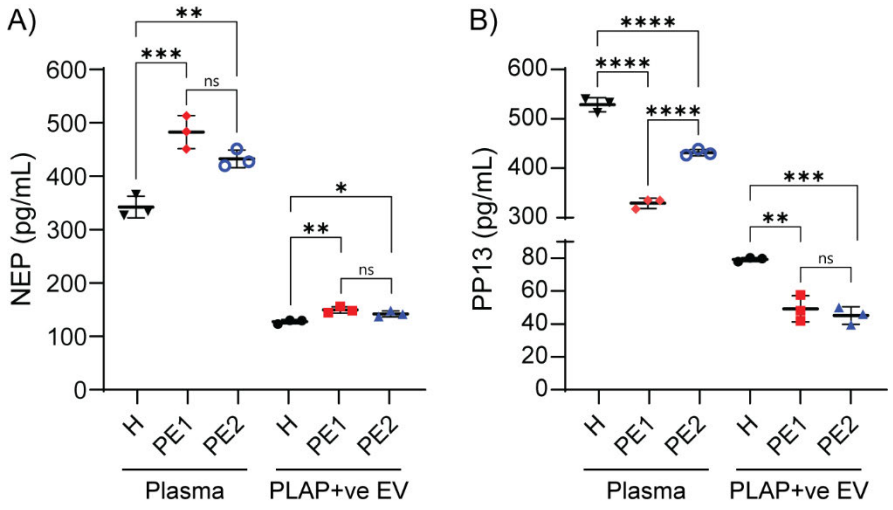

Figure 4-9 Protein concentrations of NEP and PP13 proteins.
Protein concentrations of (A) NEP and (B) PP13 measured in plasma and enriched PLAP+ve EVs in healthy pregnancy (H) and preeclampsia (PE1 and PE2) by ELISA. Data are presented as means ± SD (n = 3, one-way ANOVA with Tukey's post-test, ns: not significant ($p > 0.5$), *$p < 0.1$, **$p < 0.01$, ***$p < 0.001$ and ****$p < 0.0001$).

4.5 Conclusion

Improved diagnostic methods to triage suspected preeclampsia cases by 'ruling in' the condition are required. STBEVs are known to carry molecular markers relevant to placental disease, and their analysis may improve the sensitivity/specificity of predictive assays. However, EV biomarker studies based on EVs have been hampered by a lack of standard methods. This is especially relevant for the analysis of cell-type specific EVs such as STBEVs, with to date only limited data supporting diagnostic utility for preeclampsia.[62] Ideally diagnostic STBEV enrichment needs to be performed rapidly, with minimal sample preparation compatible with routine blood handling.[38] It stand to reason that eliminating the requirement for EV pre-enrichment while still allowing specific analysis of STBEVs protein contents has a huge potential. Not only is pre-enrichment time consuming, it also generally requires specialised equipment. In addition,

ultracentrifugation can lead to significant EV loss and damage.[63,64] Similarly SEC, while rapid, may require a concentration step, which can also decrease EV yield.[65]

Towards addressing these challenges, we demonstrated the feasibility of immuno-enrichment of EVs from unprocessed maternal plasma using magnetic NW biofunctionalized with polyacrylamide polymers that mitigate the issue of the protein corona. Anti-PLAP conjugated NWs successfully enriched STBEVs from plasma within 1.5 hours with minimal sample manipulation and no expensive equipment. We tested the utility of this approach via subsequent downstream measurement of STBEV proteins with known association with preeclampsia, PP13 and NEP. This method is likely compatible with analysis of other molecular EV cargo including miRNA or mRNA[66]. The proposed STBEV enrichment method is particularly advantageous when sample concentration is required for markers which may normally fall below the limit of detection.[67] Given its simplicity, we anticipate this EV enrichment approach to be compatible with Point-of-Care biosensing technologies, with the potential to further accelerate preeclampsia diagnosis.

Further characterisation of coated NWs could involve several aspects, including estimating the number of functional carboxyl groups on the NW surface to understand coating density and coverage, determining the ratio of the two copolymers grafted onto the surface to examine the influence of coating composition on its properties, and assessing the ability of coated NWs to prevent non-specific protein adsorption without using BSA as a passivating agent. Additionally, characterising the corona proteins associated with NWs and performing thermogravimetric analysis to quantify the number of polymers could also provide valuable information about the NW coating. Lastly, the efficiency of antibody conjugation could be improved by utilising a fluorescence approach, wherein a secondary fluorescence-tagged antibody can bind to the primary antibody conjugated onto the NW surface, allowing for quantification of conjugated antibody based on a calibration curve of fluorescence intensity versus antibody amount.

4.6 References

1 Karrar, S. A. & Hong, P. L. in *StatPearls* (2022).

2 Stern, E. M. & Blace, N. in *StatPearls* (2022).

3 Goulopoulou, S. & Davidge, S. T. Molecular mechanisms of maternal vascular dysfunction in preeclampsia. *Trends Mol Med* **21**, 88-97, doi:10.1016/j.molmed.2014.11.009 (2015).

4 Palmer, K. R. & Tong, S. Accurately Predicting the Risk of Serious Maternal Morbidity in Preterm Preeclampsia: Can It Be Done? *Hypertension* **71**, 569-571, doi:10.1161/HYPERTENSIONAHA.117.10442 (2018).

5 Roberts, J. M. *et al.* Subtypes of Preeclampsia: Recognition and Determining Clinical Usefulness. *Hypertension* **77**, 1430-1441, doi:10.1161/HYPERTENSIONAHA.120.14781 (2021).

6 MacDonald, T. M., Walker, S. P., Hannan, N. J., Tong, S. & Kaitu'u-Lino, T. J. Clinical tools and biomarkers to predict preeclampsia. *EBioMedicine* **75**, 103780, doi:10.1016/j.ebiom.2021.103780 (2022).

7 Zeisler, H. *et al.* Predictive Value of the sFlt-1:PlGF Ratio in Women with Suspected Preeclampsia. *N Engl J Med* **374**, 13-22, doi:10.1056/NEJMoa1414838 (2016).

8 Schlembach, D., Hund, M., Schroer, A. & Wolf, C. Economic assessment of the use of the sFlt-1/PlGF ratio test to predict preeclampsia in Germany. *BMC Health Serv Res* **18**, 603, doi:10.1186/s12913-018-3406-1 (2018).

9 Droge, L. A. *et al.* Prediction of Preeclampsia-Related Adverse Outcomes With the sFlt-1 (Soluble fms-Like Tyrosine Kinase 1)/PlGF (Placental Growth Factor)-Ratio in the Clinical Routine: A Real-World Study. *Hypertension* **77**, 461-471, doi:10.1161/HYPERTENSIONAHA.120.15146 (2021).

10 Nakahara, A. *et al.* Circulating Placental Extracellular Vesicles and Their Potential Roles During Pregnancy. *Ochsner J* **20**, 439-445, doi:10.31486/toj.20.0049 (2020).

11 Rice, T. F., Donaldson, B., Bouqueau, M., Kampmann, B. & Holder, B. Macrophage- but not monocyte-derived extracellular vesicles induce placental pro-inflammatory responses. *Placenta* **69**, 92-95, doi:10.1016/j.placenta.2018.07.011 (2018).

12 Ghafourian, M. *et al.* The implications of exosomes in pregnancy: emerging as new diagnostic markers and therapeutics targets. *Cell Commun Signal* **20**, 51, doi:10.1186/s12964-022-00853-z (2022).

13 Abdel-Haq, H. The Potential of Liquid Biopsy of the Brain Using Blood Extracellular Vesicles: The First Step Toward Effective Neuroprotection Against Neurodegenerative Diseases. *Mol Diagn Ther* **24**, 703-713, doi:10.1007/s40291-020-00493-4 (2020).

14 Condrat, C. E. *et al.* Pregnancy-Related Extracellular Vesicles Revisited. *Int J Mol Sci* **22**, doi:10.3390/ijms22083904 (2021).

15 Zhou, B. *et al.* Application of exosomes as liquid biopsy in clinical diagnosis. *Signal Transduct Target Ther* **5**, 144, doi:10.1038/s41392-020-00258-9 (2020).

16 Salomon, C. *et al.* A gestational profile of placental exosomes in maternal plasma and their effects on endothelial cell migration. *PLoS One* **9**, e98667, doi:10.1371/journal.pone.0098667 (2014).

17 Gill, M. *et al.* Placental Syncytiotrophoblast-Derived Extracellular Vesicles Carry Active NEP (Neprilysin) and Are Increased in Preeclampsia. *Hypertension* **73**, 1112-1119, doi:10.1161/HYPERTENSIONAHA.119.12707 (2019).

18 Sarker, S. *et al.* Placenta-derived exosomes continuously increase in maternal circulation over the first trimester of pregnancy. *J Transl Med* **12**, 204, doi:10.1186/1479-5876-12-204 (2014).

19 Salomon, C. *et al.* Placental Exosomes as Early Biomarker of Preeclampsia: Potential Role of Exosomal MicroRNAs Across Gestation. *J Clin Endocrinol Metab* **102**, 3182-3194, doi:10.1210/jc.2017-00672 (2017).

20 Jin, J. & Menon, R. Placental exosomes: A proxy to understand pregnancy complications. *Am J Reprod Immunol* **79**, e12788, doi:10.1111/aji.12788 (2018).

21 Sadovsky, Y. *et al.* Placental small extracellular vesicles: Current questions and investigative opportunities. *Placenta* **102**, 34-38, doi:10.1016/j.placenta.2020.03.002 (2020).

22 Tannetta, D., Collett, G., Vatish, M., Redman, C. & Sargent, I. Syncytiotrophoblast extracellular vesicles - Circulating biopsies reflecting

placental health. *Placenta* **52**, 134-138, doi:10.1016/j.placenta.2016.11.008 (2017).

23 Bohn, H., Kraus, W. & Winckler, W. Purification and characterization of two new soluble placental tissue proteins (PP13 and PP17). *Oncodev Biol Med* **4**, 343-350 (1983).

24 Than, N. G. *et al.* Galectins: guardians of eutherian pregnancy at the maternal-fetal interface. *Trends Endocrinol Metab* **23**, 23-31, doi:10.1016/j.tem.2011.09.003 (2012).

25 Wu, Y., Liu, Y. & Ding, Y. Predictive Performance of Placental Protein 13 for Screening Preeclampsia in the First Trimester: A Systematic Review and Meta-Analysis. *Front Med (Lausanne)* **8**, 756383, doi:10.3389/fmed.2021.756383 (2021).

26 Sammar, M. *et al.* Galectin 13 (PP13) Facilitates Remodeling and Structural Stabilization of Maternal Vessels during Pregnancy. *Int J Mol Sci* **20**, doi:10.3390/ijms20133192 (2019).

27 Than, N. G. *et al.* Placental protein 13 (galectin-13) has decreased placental expression but increased shedding and maternal serum concentrations in patients presenting with preterm pre-eclampsia and HELLP syndrome. *Virchows Arch* **453**, 387-400, doi:10.1007/s00428-008-0658-x (2008).

28 Liu, W., Yao, L., Cao, S., Hou, Q. & Miao, F. Value of combined detection of middle and late gestation serum markers placental growth factor, placental protein 13, β-human choionic gonadotophin and interleukin-18 in diagnosis of preeclampsia. *Int J Clin Exp Pathol* **9**, 146-152 (2016).

29 Sammar, M. *et al.* Reduced placental protein 13 (PP13) in placental derived syncytiotrophoblast extracellular vesicles in preeclampsia - A novel tool to study the impaired cargo transmission of the placenta to the maternal organs. *Placenta* **66**, 17-25, doi:10.1016/j.placenta.2018.04.013 (2018).

30 Balogh, A. *et al.* Placental protein 13 (PP13/galectin-13) undergoes lipid raft-associated subcellular redistribution in the syncytiotrophoblast in preterm preeclampsia and HELLP syndrome. *Am J Obstet Gynecol* **205**, 156 e151-114, doi:10.1016/j.ajog.2011.03.023 (2011).

31 Tuten, N. *et al.* Serum neprilysin levels are elevated in preeclampsia. *Taiwan J Obstet Gynecol* **60**, 869-873, doi:10.1016/j.tjog.2021.07.015 (2021).

32 Reddy, Y. N. V. *et al.* Soluble Neprilysin in the General Population: Clinical Determinants and Its Relationship to Cardiovascular Disease. *J Am Heart Assoc* **8**, e012943, doi:10.1161/JAHA.119.012943 (2019).

33 Nogueras-Ortiz, C. J. *et al.* Astrocyte- and Neuron-Derived Extracellular Vesicles from Alzheimer's Disease Patients Effect Complement-Mediated Neurotoxicity. *Cells* **9**, doi:10.3390/cells9071618 (2020).

34 Sharma, P., Diergaarde, B., Ferrone, S., Kirkwood, J. M. & Whiteside, T. L. Melanoma cell-derived exosomes in plasma of melanoma patients suppress functions of immune effector cells. *Sci Rep* **10**, 92, doi:10.1038/s41598-019-56542-4 (2020).

35 Menon, R. *et al.* Protein Profile Changes in Circulating Placental Extracellular Vesicles in Term and Preterm Births: A Longitudinal Study. *Endocrinology* **161**, doi:10.1210/endocr/bqaa009 (2020).

36 Boriachek, K. *et al.* Avoiding Pre-Isolation Step in Exosome Analysis: Direct Isolation and Sensitive Detection of Exosomes Using Gold-Loaded Nanoporous Ferric Oxide Nanozymes. *Anal Chem* **91**, 3827-3834, doi:10.1021/acs.analchem.8b03619 (2019).

37 Hong, C. S., Muller, L., Boyiadzis, M. & Whiteside, T. L. Isolation and characterization of CD34+ blast-derived exosomes in acute myeloid leukemia. *PLoS One* **9**, e103310, doi:10.1371/journal.pone.0103310 (2014).

38 Tannetta, D., Masliukaite, I., Vatish, M., Redman, C. & Sargent, I. Update of syncytiotrophoblast derived extracellular vesicles in normal pregnancy and preeclampsia. *J Reprod Immunol* **119**, 98-106, doi:10.1016/j.jri.2016.08.008 (2017).

39 Kumeria, T. *et al.* Naturally Derived Iron Oxide Nanowires from Bacteria for Magnetically Triggered Drug Release and Cancer Hyperthermia in 2D and 3D Culture Environments: Bacteria Biofilm to Potent Cancer Therapeutic. *Biomacromolecules* **17**, 2726-2736, doi:10.1021/acs.biomac.6b00786 (2016).

40 Wang, L. *et al.* Iron Oxide Nanowires from Bacteria Biofilm as an Efficient Visible-Light Magnetic Photocatalyst. *ACS Appl Mater Interfaces* **8**, 20110-20119, doi:10.1021/acsami.6b06486 (2016).

41 Thierry, B. & Griesser, H. J. Dense PEG layers for efficient immunotargeting of nanoparticles to cancer cells. *Journal of Materials Chemistry* **22**, 8810-8819, doi:10.1039/C2JM30210A (2012).

42 Pham, Q. N. *et al.* Magnetic enrichment of immuno-specific extracellular vesicles for mass spectrometry using biofilm-derived iron oxide nanowires. *Nanoscale* **15**, 1236-1247, doi:10.1039/d2nr05619d (2023).

43 Krishnan, G. *et al.* Preclinical evaluation of a mannose-labeled magnetic tracer for enhanced sentinel lymph node retention in the head and neck. *Nanomedicine* **42**, 102546, doi:10.1016/j.nano.2022.102546 (2022).

44 Ishii, T. *et al.* Enhanced target recognition of nanoparticles by cocktail PEGylation with chains of varying lengths. *Chem Commun (Camb)* **52**, 1517-1519, doi:10.1039/c5cc06661a (2016).

45 Zhang, H. *et al.* Ligand Size and Conformation Affect the Behavior of Nanoparticles Coated with in Vitro and in Vivo Protein Corona. *ACS Appl Mater Interfaces* **10**, 9094-9103, doi:10.1021/acsami.7b16096 (2018).

46 Jedlovszky-Hajdu, A., Bombelli, F. B., Monopoli, M. P., Tombacz, E. & Dawson, K. A. Surface coatings shape the protein corona of SPIONs with relevance to their application in vivo. *Langmuir* **28**, 14983-14991, doi:10.1021/la302446h (2012).

47 Monopoli, M. P. *et al.* Physical-chemical aspects of protein corona: relevance to in vitro and in vivo biological impacts of nanoparticles. *J Am Chem Soc* **133**, 2525-2534, doi:10.1021/ja107583h (2011).

48 Nguyen, V. H. & Lee, B. J. Protein corona: a new approach for nanomedicine design. *Int J Nanomedicine* **12**, 3137-3151, doi:10.2147/IJN.S129300 (2017).

49 Pustulka, S. M., Ling, K., Pish, S. L. & Champion, J. A. Protein Nanoparticle Charge and Hydrophobicity Govern Protein Corona and Macrophage Uptake. *ACS Appl Mater Interfaces* **12**, 48284-48295, doi:10.1021/acsami.0c12341 (2020).

50 Alberg, I. *et al.* Polymeric Nanoparticles with Neglectable Protein Corona. *Small* **16**, e1907574, doi:10.1002/smll.201907574 (2020).

51 Scientific, T. *Dynabeads® M-270 Carboxylic Acid*, <https://www.thermofisher.com/au/en/home/references/protocols/proteins-

expression-isolation-and-analysis/protein-isolation-protocol/m-270-carboxylic-acid.html> (

52 Bellotti, C., Lang, K., Kuplennik, N., Sosnik, A. & Steinfeld, R. High-grade extracellular vesicles preparation by combined size-exclusion and affinity chromatography. *Sci Rep* **11**, 10550, doi:10.1038/s41598-021-90022-y (2021).

53 Chaparro, A. *et al.* Gingival Crevicular Placental Alkaline Phosphatase Is an Early Pregnancy Biomarker for Pre-Eclampsia. *Diagnostics (Basel)* **11**, 661, doi:10.3390/diagnostics11040661 (2021).

54 Vokalova, L. *et al.* Placental Protein 13 (Galectin-13) Polarizes Neutrophils Toward an Immune Regulatory Phenotype. *Front Immunol* **11**, 145, doi:10.3389/fimmu.2020.00145 (2020).

55 Menon, R. *et al.* Protein Profile Changes in Circulating Placental Extracellular Vesicles in Term and Preterm Births: A Longitudinal Study. *Endocrinology* **161**, 1-19, doi:10.1210/endocr/bqaa009 (2020).

56 Levine, L. *et al.* Syncytiotrophoblast extracellular microvesicle profiles in maternal circulation for noninvasive diagnosis of preeclampsia. *Sci Rep* **10**, 6398, doi:10.1038/s41598-020-62193-7 (2020).

57 Pillay, P., Vatish, M., Duarte, R., Moodley, J. & Mackraj, I. Exosomal microRNA profiling in early and late onset preeclamptic pregnant women reflects pathophysiology. *Int J Nanomedicine* **14**, 5637-5657, doi:10.2147/IJN.S208865 (2019).

58 Pillay, P., Maharaj, N., Moodley, J. & Mackraj, I. Placental exosomes and pre-eclampsia: Maternal circulating levels in normal pregnancies and, early and late onset pre-eclamptic pregnancies. *Placenta* **46**, 18-25, doi:10.1016/j.placenta.2016.08.078 (2016).

59 Gadde, R., Cd, D. & Sheela, S. R. Placental protein 13: An important biological protein in preeclampsia. *J Circ Biomark* **7**, 1849454418786159, doi:10.1177/1849454418786159 (2018).

60 Huppertz, B. *et al.* Longitudinal determination of serum placental protein 13 during development of preeclampsia. *Fetal Diagn Ther* **24**, 230-236, doi:10.1159/000151344 (2008).

61 Pillay, P., Moodley, K., Moodley, J. & Mackraj, I. Placenta-derived exosomes: potential biomarkers of preeclampsia. *Int J Nanomedicine* **12**, 8009-8023, doi:10.2147/IJN.S142732 (2017).

62 Palma, C. *et al.* Extracellular Vesicles and Preeclampsia: Current Knowledge and Future Research Directions. *Subcell Biochem* **97**, 455-482, doi:10.1007/978-3-030-67171-6_18 (2021).

63 Mathivanan, S., Ji, H. & Simpson, R. J. Exosomes: extracellular organelles important in intercellular communication. *J Proteomics* **73**, 1907-1920, doi:10.1016/j.jprot.2010.06.006 (2010).

64 Mol, E. A., Goumans, M. J., Doevendans, P. A., Sluijter, J. P. G. & Vader, P. Higher functionality of extracellular vesicles isolated using size-exclusion chromatography compared to ultracentrifugation. *Nanomedicine* **13**, 2061-2065, doi:10.1016/j.nano.2017.03.011 (2017).

65 Welton, J. L., Webber, J. P., Botos, L. A., Jones, M. & Clayton, A. Ready-made chromatography columns for extracellular vesicle isolation from plasma. *J Extracell Vesicles* **4**, 27269, doi:10.3402/jev.v4.27269 (2015).

66 Hannan, N. J. *et al.* Circulating mRNAs are differentially expressed in pregnancies with severe placental insufficiency and at high risk of stillbirth. *BMC Med* **18**, 145, doi:10.1186/s12916-020-01605-x (2020).

67 Hromadnikova, I., Dvorakova, L., Kotlabova, K. & Krofta, L. The Prediction of Gestational Hypertension, Preeclampsia and Fetal Growth Restriction via the First Trimester Screening of Plasma Exosomal C19MC microRNAs. *Int J Mol Sci* **20**, doi:10.3390/ijms20122972 (2019).

Chapter 5

Proteomic Profiling of Two Placental Extracellular Vesicle Subtypes Sequentially Enriched from Maternal Plasma After Preeclampsia Diagnosis

5 Proteomic profiling of two placental extracellular vesicle subtypes sequentially enriched from maternal plasma after preeclampsia diagnosis

5.1 Abstract

Maternal blood during pregnancy contains valuable transcriptomic and proteomic materials shed from the placenta in extracellular vesicles (EVs). These EVs play an active role in pregnancy health and disease, providing non-invasive information on placenta health. To avoid interference in downstream analysis, it's important to remove irrelevant maternal EVs and proteins found in blood plasma. In addition, immuno-enrichment approach, which is able to specifically interrogate EV subtypes, is needed to harness the full potential of placental EVs. To this end, we developed an immuno-enrichment approach capable of sequentially enriching placental EVs subtypes suitable for small biobanked plasma samples (< 500 µL). Specifically, bacterial biofilm-derived iron oxide magnetic nanowires were modified with two types of block copolymers, a short polymer (RAFT-5-MAPC2-15AAM-3PEO) and a long (RAFT-5MAPC2-70AAM-COOH) polymer. Nanowires were then conjugated with antibodies specific to placental alkaline phosphatase (PLAP) or human leukocyte antigen-G (HLA-G) - placental markers for two key placental cells, syncytiotrophoblasts and extravillous cytotrophoblasts, respectively. The magnetic nanowires efficiently enriched both PLAP+ve and HLA-G+ve EVs from a spiked plasma model which had been pre-enriched with ultracentrifugation (UC). Specifically, sequential enrichment (PLAP+ve then HLA-G+ve EVs) recovered 91.1 ± 5.9% and 71.4 ± 6.2% of PLAP and HLA-G protein, respectively. Subsequent mass spectrometry of the enriched EVs yielded high reproducibility (Pearson correlation 0.785) and recovery of placental related proteins. Placental EVs enriched from maternal blood diagnosed with preeclampsia recovered placental related proteins, including those with known preeclampsia associations. Moreover, given UC is known to be associated with significant EV loss, the sequential enrichment and subsequent proteomics of both PLAP+ve and HLA-G+ve EVs recovered after direct capture has also been described. We anticipate that the analysis of two key placental EV subtypes, facilitated by this method, will provide additional and complementary non-invasive insight regarding the health of the placenta.

5.2 Introduction

Affecting up to 8% of pregnancies and a major contributor to maternal and fetal mortality worldwide, preeclampsia is a multisystem pregnancy-specific disorder primarily characterised by new-onset hypertension and proteinuria after 20 weeks of gestation.[1,2] While clinical symptoms of preeclampsia generally manifest in late gestation, their molecular origins are, in most cases, established in the first trimester.[3] Despite significant research on the pathogenesis of preeclampsia, its underlying molecular triggers are not fully understood[4,5] in part due to the difficulty of collecting invasive biopsies throughout gestation. In addition, the lack of non-invasive insights also makes accurate and timely disease prediction/diagnosis challenging.

Several plasma-derived biomarkers have been identified for preeclampsia, including placental growth factor (PlGF) and soluble fms-like tyrosine kinase-1 (sFlt-1).[6-8] Although these markers are now clinically validated and currently used for "ruling-out" suspected preterm preeclampsia, the positive predictive value of the sFlt-1:PlGF ratio (36.7% within 4 weeks of diagnosis)[9] is not sufficiently high for the monitoring of high-risk pregnancies.[10] This problem is also shared among other reported markers, which is likely due to the heterogeneous nature of preeclampsia.[10] Alternative blood-based approaches are required for better understanding the multifactorial pathogenesis of this placental dysfunction and developing better risk-stratification methods.

Extracellular vesicles (EVs) are involved in intercellular communication during pregnancy, for example mediating feto-maternal crosstalk.[11,12] During pregnancy, the placenta releases a wide range of EVs into maternal blood. These placental EVs can be classified based on their cell of origin as well as based on their size, i.e. as small EVs (exosomes and a small number of microvesicles) and large EVs (the majority of microvesicles and apoptotic bodies).[13,14] These nano- to micron-sized particles carry and transport over distance molecules such as proteins and nucleic acids which are protected within the EVs' bilipid membranes.[15-17] Two key cell types of the placenta, syncytiotrophoblasts (SCTBs) and extravillous trophoblasts (EVTBs) release cell-specific EVs into the maternal circulation. Syncytiotrophoblast EVs (STBEVs), which display Placental alkaline phosphatase (PLAP) on their membrane,[18] are released in response to oxidative stress and likely play a role in immunomodulation.[19,20] Extravillous trophoblasts EVs display human leukocyte antigen G (HLA-G)[21] on their membrane. Their release is also regulated by oxygen tension/stress, and they are likely involved in trophoblast invasion/proliferation,[19] with HLA-G being an immunomodulatory protein,

critical for pregnancy success.[22] In general, placental EVs have immuno-suppressive and pro-inflammatory effects on the maternal immune system in healthy pregnancies, contributing to the establishment of fetal immune tolerance and prevention of fetal rejection in pregnancy.[11,23]

Given their key functional roles in pregnancy and the likelihood of EVs reflecting the state-specific condition of their cell of origin, analyses EVs and their molecular cargo hold promise towards identifying biomarkers of pregnancy conditions including preeclampsia.[24-27] Proteomic profiling of pregnancy-associated EVs comparing preeclamptic to healthy pregnancies has been performed with plasma,[29-31] umbilical cord blood[32] and placental villous explants.[33] Most of these studies analysed the protein profiles of total EVs with an exception for studies with placental explants. Established from villous tissues of the syncytiotrophoblast layer, the majority of EVs enriched from the culture media of explants express PLAP on their membranes.[33]

Importantly, studies investigating and comparing HLA-G+ve and PLAP+ve EVs are limited, with only one previous report of their DNA content.[28] In addition, only two studies focused on plasma-derived EVs use quantitative proteomics in their analyses.[30,31] Although the enrichment of PLAP+ve EVs and HLA-G+ve EVs has been reported before,[24,34-36] quantitative proteomic profiling of these two immuno-specific placental EVs has not been reported before for preeclampsia. This is a significant knowledge gap as better understanding of the roles of placental EV subpopulations and determining which EV proteins result in functional changes can be anticipated to provide important new insights into dysfunction mechanisms.[37]

In this study, we report a method for sequential enrichment and proteomic comparison of HLA-G+ve and PLAP+ve placental EVs. Building on the enrichment protocol for specific EV subtype enrichment established in our previous study,[38] ultracentrifugation (UC) followed by immuno-magnetic enrichment with magnetic iron oxide nanowires (NWs) was used to respectively collect the total plasma EVs and subsequently enrich immuno-specific placental EVs using antibody-conjugated NWs. We first demonstrated the utility of the EV enrichment protocol using EV-spiked plasma and subsequently demonstrated the feasibility of performing sequential isolation of the two different placental EV subtypes. Then as a proof of concept, we sequentially enriched plasma-derived PLAP+ve and HLA-G+ve EVs from a third-trimester pregnancy with clinically

diagnosed preeclampsia. The enriched EVs were directly lysed and subjected to in-gel digestion for label-free liquid chromatography tandem mass spectrometry (LC-MS/MS) quantification. Harnessing the ability of NWs to enrich EVs in a complex plasma environment as shown in Chapter 4, we also demonstrated proteomic analysis of directly enriched placental EV subtypes.

5.3 Methods

5.3.1 Plasma sample collection

Maternal blood samples were collected at the Women's and Children's Hospital (Adelaide). Blood samples from non-pregnant women were collected from healthy volunteers at Clinpath Laboratories. Sample collection was carried out under approval from the Women's and Children's Human Research Ethics committee (WCH Application No: WEC/13/WCHN 45) and The University of South Australia Human Research Ethics Committee (0000036112). Blood (10 mL) was collected into k3EDTA Vacutainers tubes and processed within 6 h after collection. Plasma was separated from blood by centrifugation at 1500 × *g* for 10 min and stored at −80 °C until use. This study used one clinical sample collected from a pregnant woman following a preeclampsia diagnosis, before delivery.

5.3.2 Preparation of iron oxide NWs for the immuno-enrichment of EVs

Iron oxide NWs were purified from bacteria biofilms as previously reported[38] and were first surface functionalised with copolymers synthesised by reversible addition-fragmentation chain transfer and presenting terminal carboxyl groups as described in Chapter 4. Polymer-modified NWs were conjugated with antibodies through carbodiimide coupling reaction, in which the carboxyl groups on the NW surfaces are first activated and then reacted with primary amines of anti-PLAP (Thermo Fisher, 14-9870-82, clone 8B6) and anti-HLA-G (Thermo Fisher, 14-9957-37, clone 87G) antibodies or IgG from human serum (Sigma Aldrich, I4506). After conjugation, non-reacted carboxyl groups on the NW surface were quenched with 50 mM ethanolamine (Sigma Aldrich, 398136). Antibody-conjugated NWs (NW-PLAP, NW-HLA-G and NW-IgG) were further blocked with 0.5% bovine serum albumin (Sigma Aldrich, A8806) prior to resuspension in phosphate buffer saline (1 × PBS pH 7.4, Thermo Fisher, 10010023) for storage at 4 °C and used within one week.

5.3.3 Cell culture for the model EV enrichment study

BeWo (ATCC, CCL-98) and JEG-3 (ATCC, HTB-36) choriocarcinoma cells (trophoblast-like cell lines) were used as SCTB- and EVTB-derived EV models, respectively. BeWo and JEG-3 cells were cultured in Roswell Park Memorial Institute media (RPMI 1640, Gibco) and Minimum Essential Medium α (MEM α, Gibco), respectively, with 10% fetal bovine serum (FBS, Gibco) and penicillin/streptomycin (10,000 U/mL, Gibco) to 90% confluence in a 37 °C humidified incubator supplied with 5% CO_2. After discarding the culture media and washing the cells three times with 1× Dulbecco's phosphate-buffered saline (DPBS, Gibco), the cells were grown in the FBS-free media for another 48 h. Culture media (~90 mL) were collected and pre-cleared by successive centrifugation at 300 × g for 20 min and 2000 × *g* for 20 min at 4 °C (5699-R rotor, Rotanta 460 R, Hettich) to remove cells and cellular components. The resulting supernatants were centrifuged at 12,000 × *g* for 30 min at 4 °C (5699-R rotor) to pellet large EVs and then ultracentrifuged at 120,000 × *g* for 70 min at 4 °C (70 Ti rotor, Optima L-80 XP, Beckman Coulter) to pellet small EVs. Pellets of EVs were washed twice with 1 × DPBS buffer via UC, resuspended again in PBS buffer, combined and kept at −20 °C for use within 2 weeks.

5.3.4 Enrichment of total plasma EVs

Total plasma EVs were collected by UC. Plasma (500 µL) obtained from non-pregnant women was diluted twice with PBS buffer and subsequently centrifuged at 2000 × *g* and 12,000 × *g* for 45 min at 4 °C (5699-R rotor) to remove cells/debris and pellet large EVs, respectively. The obtained supernatant was centrifuged at 12,000 × *g* for 30 min and ultracentrifuged at 120,000 × *g* for 70 min at 4 °C (70 Ti rotor) to pellet large and small EVs, respectively. Pellets of EVs were resuspended in PBS buffer, combined (total 500 µL) and stored at −20 °C for use within 2 weeks.

5.3.5 Nanoparticle tracking analysis

Nanoparticle tracking analysis (NTA, Nanosight NS300, Malvern) was used to determine the concentration and size of EVs. Enriched EVs were diluted in ultrapure water to the appropriate concentration (ideal 20–50 particles/frame as visible by NTA). Each sample was measured in triplicate with 5 videos of 60 s recorded for each measurement. The same camera settings (shutter speed: 30.15 ms, camera level: 15) were used for all measurements.

5.3.6 Preparation of placental EV-spiked plasma for model study

By number PLAP+ve exosomes and PLAP+ve EVs account for 10–20% of the total plasma-derived exosomes in early pregnancy[39] and ~28.8% of the total BeWo EVs, respectively.[40] Therefore, model plasma samples containing PLAP+ve EVs were prepared by determining the number of total EVs enriched from plasma and culture media of BeWo cells by NTA and then spiking BeWo EVs to 500 µL of plasma to obtain a final percentage of 10% of PLAP+ve EVs in the spiked sample. PLAP+ve EVs and HLA-G+ve EVs in a ratio of 1:1 was used to prepare plasma containing both subtypes of placental EVs.

5.3.7 Sequential enrichment of immuno-specific placental EVs from plasma

A combination of UC and immunoaffinity isolation was used to enrich placental EVs (Figure 5-1). Total EVs (pre-enrich EV sample) were collected from 500 µL of plasma obtained from healthy and preeclamptic pregnancies by UC and resuspended in 500 µL of PBS buffer as described in section 2.3. For sequential enrichment of placental EVs, PLAP+ve EVs were first enriched by incubating 400 µL of the pre-enrich sample with NW-PLAP (1 mg). After the removal of the NW-PLAP with a strong magnet, the supernatant was then subjected to another incubation step with NW-HLA-G (1 mg) for the enrichment of HLA-G+ve EVs. As a control, enrichment was performed one more time using NWs conjugated with irrelevant IgG (NW-IgG, 1 mg). After washing three times with PBS buffer, EVs captured by the various NWs were either released for NTA analyses or directly lysed for protein quantification and mass spectrometry.

For NTA measurements, captured EVs were eluted from the NWs by the addition of 0.1 M Glycine-HCl pH 2.8 followed by a 30-min incubation at room temperature. The supernatant containing eluted EVs was neutralised by 1 M Tris pH 8 and diluted to the appropriate concentration with ultrapure water for NTA measurements. For protein quantification, captured EVs were lysed with 1× RIPA buffer (Thermo Fisher, 89900) containing 1 × cOmplete™ Mini EDTA-free Protease Inhibitor Cocktail (Merck, 4693132001) for 30 min on ice. After brief centrifugation at 12,000 × *g* and applying the magnetic field, the lysate containing EV protein was collected and kept at −20 °C for analyses with bicinchoninic acid (BCA) assay, enzyme-linked immunosorbent assay (ELISA) and mass spectrometry. Building on Chapter 4, sequential enrichment of the PLAP+ve and HLA-G+ve EVs was also performed without pre-processing of the plasma.

In this case, 100 µL of plasma (performed in triplicate) was diluted 1:1 with PBS buffer to obtain 50% plasma concentration and then treated with 1 mg of NW-PLAP. All subsequent sequential enrichment steps with NW-HLA-G (1 mg) and NW-IgG (1 mg) were as described for the pre-enrich samples.

5.3.8 Quantification of PLAP and HLA-G proteins

The concentration of PLAP and HLA-G proteins extracted from enriched EVs were quantified by ELISA using a human PLAP ELISA kit (MBS289869, MyBiosource) and a human HLA-G ELISA kit (MBS9716588, MyBiosource). The recovery of PLAP and HLA-G proteins was used to evaluate the enrichment efficiency of EVs calculated by the ratio of measured PLAP or CD63 protein amounts to that of the pre-enrich EV sample.

5.3.9 Liquid chromatography tandem mass spectrometry

In-gel digestion was used to prepare EV proteins for LC-MS/MS as previously described.[38] Equal amounts of EV proteins were mixed with 4× NuPAGE™ LDS sample buffer (Thermo Fisher, NP0007) and heated at 70 °C for 10 min before loading to a NuPAGE 4–12% Bis-Tris Gel (Thermo Fisher). The gel bands were excised according to a PageRuler™ Plus Prestained Protein Ladder (10 to 250 kDa, Thermo Fisher, 26619) and further cut into smaller pieces. Following dehydration using 100% acetonitrile (Sigma, 34851) in 15 min, the gel pieces were air-dried at room temperature, reduced with 10 mM dithiothreitol (Sigma, D0632) in 100 mM NH_4HCO_3 (Sigma, 09830) at 56 °C for 45 min, and alkylated with 55 mM 2-chloroacetamide (Sigma, 22790) in 100 mM NH_4HCO_3 in the dark at room temperature for 30 min. After rehydrating the gel pieces with 5 mM NH_4HCO_3 and dehydrating with 100% acetonitrile, proteins were subsequently digested with 1/50 w/w trypsin (Trypsin/Lys-C mix, Promega, V5071) in 5 mM NH_4HCO_3. The solution of 5 mM NH_4HCO_3 in 20% acetonitrile was then added to obtain a final 10% acetonitrile before digestion was allowed to proceed at 37 °C overnight. The digestion was stopped with 1% formic acid (Fisher Chemical, A117) followed by 15 min of sonication to extract digested peptides. Peptide extraction was performed again with 50% acetonitrile in 1% formic acid and 100% acetonitrile followed by 15 min of sonication. Peptide extracts were vacuum-dried in a SpeedVac and stored at −80 °C for LC-MS/MS analyses. LC–MS/MS analyses were conducted on an EASY-nLC 1200 system (Thermo Scientific) coupled to an Orbitrap Exploris 480 mass spectrometer (Thermo Scientific) as described in Chapter 3.

5.3.10 Label-free quantification of differentially expressed proteins

Raw MS files of FAIMS were split into MzXML formats of corresponding correction voltages using the FAIMS MzXML Generator software (Coon's lab). Converted spectral data files were searched for matching peptide sequences against a human proteome database (UniProt, downloaded on April 2021) using the Andromeda algorithm integrated into Maxquant (v.1.6.2.6) with a false discovery rate (FDR) of 1% for both peptide-spectrum match and protein. Trypsin/P was set as the cleavage site specificity with a maximum of 2 missed cleavages. Fixed modifications include cysteine carbamidomethylation, and variable modifications include protein N-terminal acetylation, methionine oxidation, and asparagine or glutamine deamidation. Label-free quantification was enabled with the minimum ratio count set to 2. MS/MS match tolerances of 20 ppm and 0.1 Da were set for precursor and fragment ions, respectively.

The resulted file proteinGroups.txt generated by Maxquant was analysed by Perseus (v1.6.2.1). The raw mass spectrometry result files were also uploaded to Mass Dynamics for quality control and proteomic analysis. Principal component analysis was performed in R to determine the ability of identified EV proteins to distinguish different NW samples. Venn diagrams were generated by the venn package in R. Protein groups identified by LC-MS/MS were compared with the Vesiclepedia database and Functional Enrichment analysis tool (FunRich v3.1.3). Gene ontology (GO) and tissue expression (UP_TISSUE) of identified proteins were performed using the database for annotation, visualization and integrated discovery (DAVID, v6.8).[41]

5.3.11 Statistics

Data are presented as mean ± standard deviation (SD) with n = 3 technical or biological replicates (unless otherwise stated). Recovery of PLAP and HLA-G protein compared between tested conditioned were assessed using one-way ANOVA with Tukey's post-test (ns = not significant ($p > 0.5$), *$p < 0.1$, **$p < 0.01$, ***$p < 0.001$, and ****$p < 0.0001$) available in Graphpad Prism (v8.3.0).

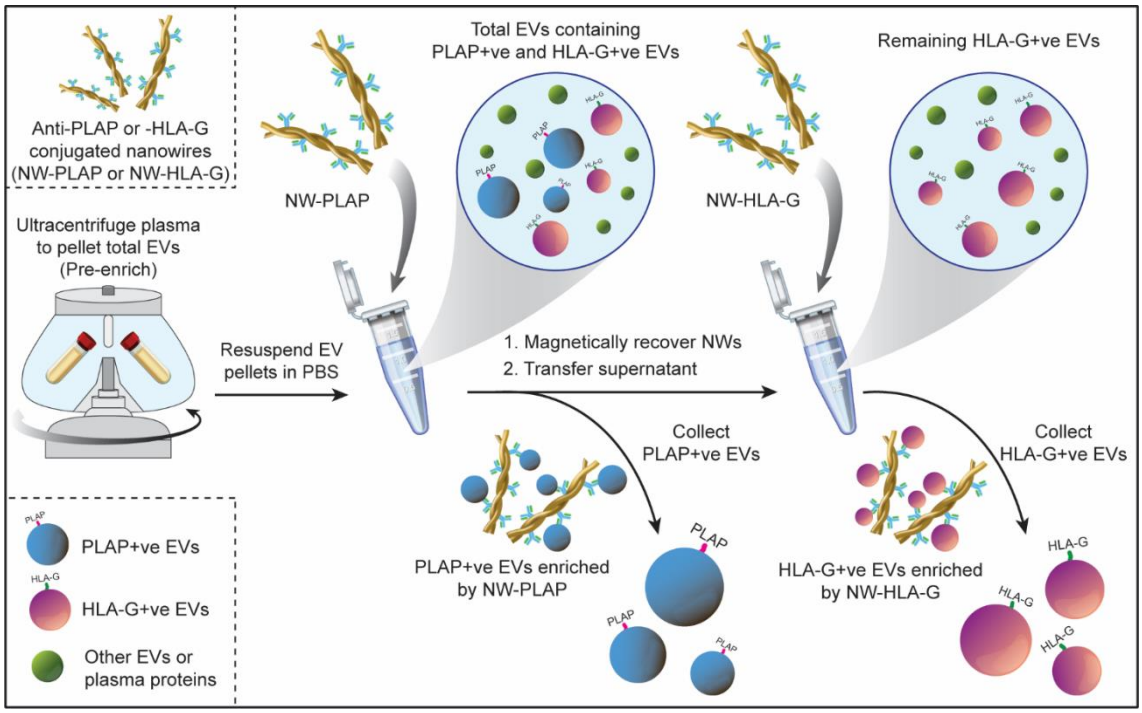

Figure 5-1 Experimental schematic for sequential immuno-enrichment of placental EV subtypes.

5.4 Results and discussion

5.4.1 Enrichment and analysis of spiked plasma-derived placental EVs

Building on the use of iron oxide NWs for immuno-magnetic EV enrichment described in Chapter 3, we first sought to establish the optimum enrichment protocol for PLAP+ve EVs from pre-enriched plasma samples. Specifically, the comparative performance of NW-PLAP to enrich PLAP+ve EVs was tested for ultracentrifuged BeWo culture media (as performed previously in Chapter 3 – referred to as *PBS*) and ultracentrifuged spiked plasma (referred to as *UC spiked plasma*) in order to establish the optimal amount of NWs (mg) for subsequent analysis of the EVs (Figure 5-2A). Despite having undergone pre-enrichment, *UC spiked plasma* is more complex than serum-free cell culture media as it still contains non-neglectable amounts of contaminating soluble proteins, which may interfere with the binding of the PLAP+ve EVs. There were no significant differences in the PLAP recovery between *PBS* and *UC spiked plasma*. Therefore, the previously developed EV enrichment method and utilisation of 1 mg of conjugated NWs was deemed suitable for plasma samples pre-processed using ultracentrifugation. This was further demonstrated by NTA analyses of the captured EVs showing a size distribution from 50 to 300 nm (mean/mode size = 151.2 ± 9.7/113.2 ± 10.4 nm) and high purity[42] (1.83 ± 0.2

$\times 10^{10}$ particles/μg, calculated based on the ratio of EV number and total EV protein measured by NTA and BCA, respectively) (Figure 5-2B).

Next, to confirm the suitability of the enriched samples for proteomic analysis and to further demonstrate the enrichment of the target EVs, mass spectrometry was performed and the protein profiles of enriched EVs were compared. Specifically, 4 sample types were investigated namely (1) *BeWo EVs* (ultracentrifuged culture media) *enriched with NW-PLAP* (positive control), (2) *Non-spiked plasma enriched with NW-PLAP* (negative control), (3) *Spiked plasma enriched with NW-PLAP* and (4) *Spiked plasma enriched with NW-IgG* (negative control). As shown in Figure 5-2C, the largest number of proteins identified in a single sample was found in the positive control *BeWo EVs* with 2518 proteins. In the spiked plasma sample enriched with NW-PLAP, 292 proteins were identified, 82% of which overlapped with the positive control *BeWo EVs*, indicating that the majority of identified proteins are related to the target EVs. In the two negative control samples, 57 and 120 proteins were identified for *Non-spiked plasma + NW-PLAP* and *Spiked plasma + NW-IgG*, respectively, which likely represents the non-specific binding of non-target EVs and plasma proteins. Cellular component ontology analysis of the identified proteins shows that the "Extracellular exosome" category is present in all 4 samples and is a major contributor to the proteins identified in all 3 plasma samples (Figure 5-3**)**. The "blood microparticle" category was identified in all 3 plasma samples, demonstrating the non-specific binding of at least some plasma proteins. Approximately 40% of proteins in the *Spiked plasma + NW-PLAP* sample and the positive control *BeWo EVs* were found to be associated with the placenta as shown by the tissue expression analysis (Figure 5-4), with the "Placenta" category being absent from both negative control samples, demonstrating the capture of "placental" related EVs within the spiked sample.

Principal component analysis was then used to investigate the variance between samples and their replicates (Figure 5-2D). As expected, there was very little variance between the 3 replicates of the positive control *BeWo EVs*, which all clustered into one group (Pearson correlation 0.986). In contrast, both negative control samples were clustered close to each other with the highest variance likely due to the non-specific nature of absorbed proteins. The *Spiked plasma + NW-PLAP* sample (Pearson correlation 0.785) was clustered more closely to the positive control *BeWo EVs*, although demonstrated

greater variance, again likely due to the inevitable presence of contaminating plasma proteins.

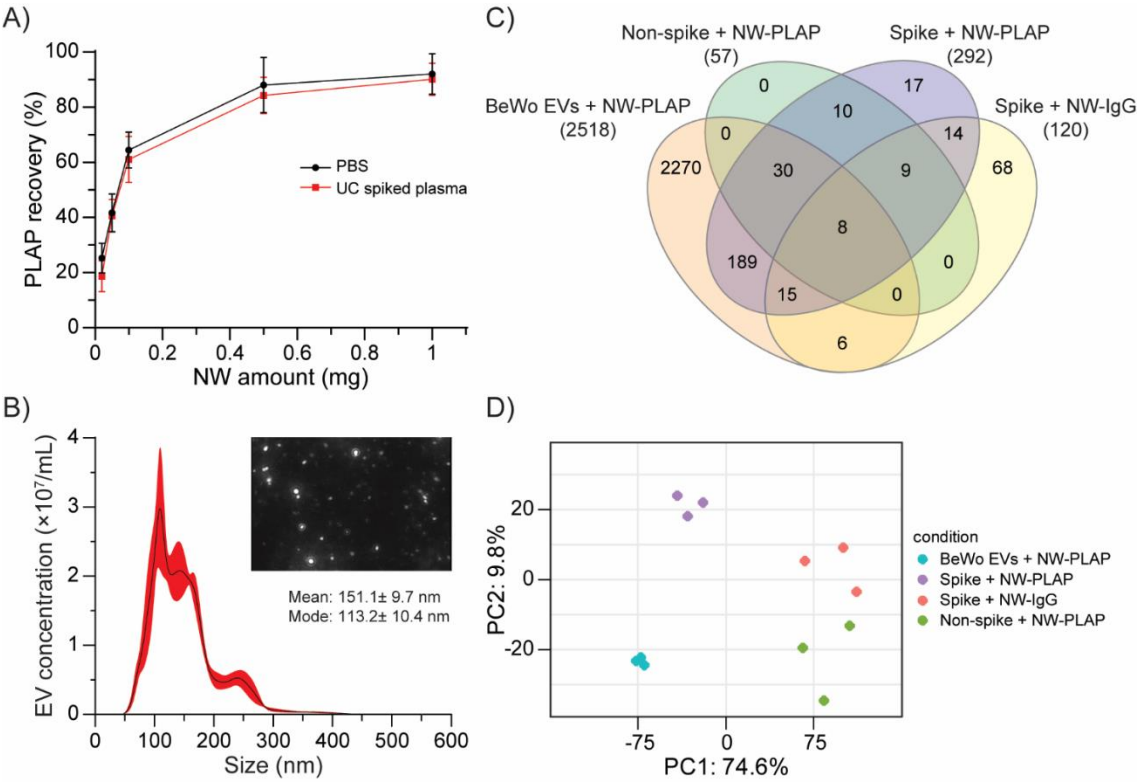

Figure 5-2 Enrichment and analysis of spiked plasma-derived placental EVs.
A) Recovery of PLAP extracted from EVs enriched with different amounts of NW-PLAP (0.02, 0.05, 0.1, 0.5 and 1 mg) from ultracentrifuged BeWo culture media (noted as *PBS*) and ultracentrifuged BeWo EVs-spiked plasma (noted as *UC spiked plasma*). B) NTA measurement of eluted PLAP+ve EVs after immuno-enrichment. C) Overlapping proteins identified in EVs enriched from ultracentrifuged BeWo culture media enriched with NW-PLAP (*BeWo EVs + NW-PLAP*, positive control), non-spiked plasma enriched with NW-PLAP (*Non-spiked plasma + NW-PLAP*, negative control), spiked plasma enriched with NW-PLAP (*Spiked plasma + NW-PLAP*) and spiked plasma enriched with NW-IgG (S*piked plasma + NW-IgG*, negative control). D) Principal component analysis of the proteins enriched from the spiked and non-spiked samples.

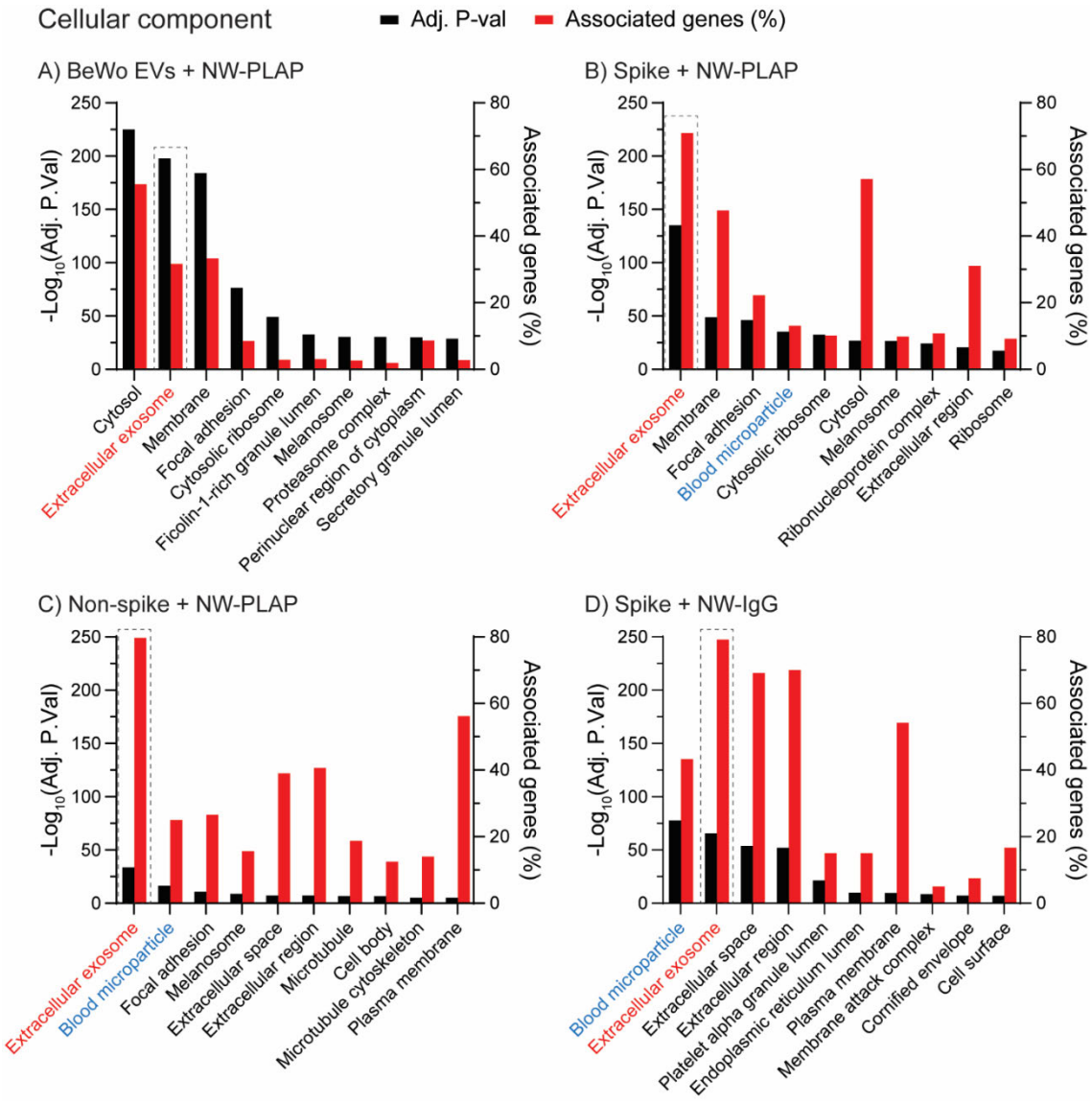

Figure 5-3 Cellular component ontology of identified proteins.
Cellular component ontology of identified proteins analysed by DAVID Bioinformatics Resources. Top 10 categories are reported and ranked by adjusted Benjamini-Hochberg P-value for A) *BeWo EVs + NW-PLAP* (positive control), B) *Spiked plasma + NW-PLAP*, C) *Non-spiked plasma + NW-PLAP* (negative control) and D) *Spiked plasma + NW-IgG* (negative control).

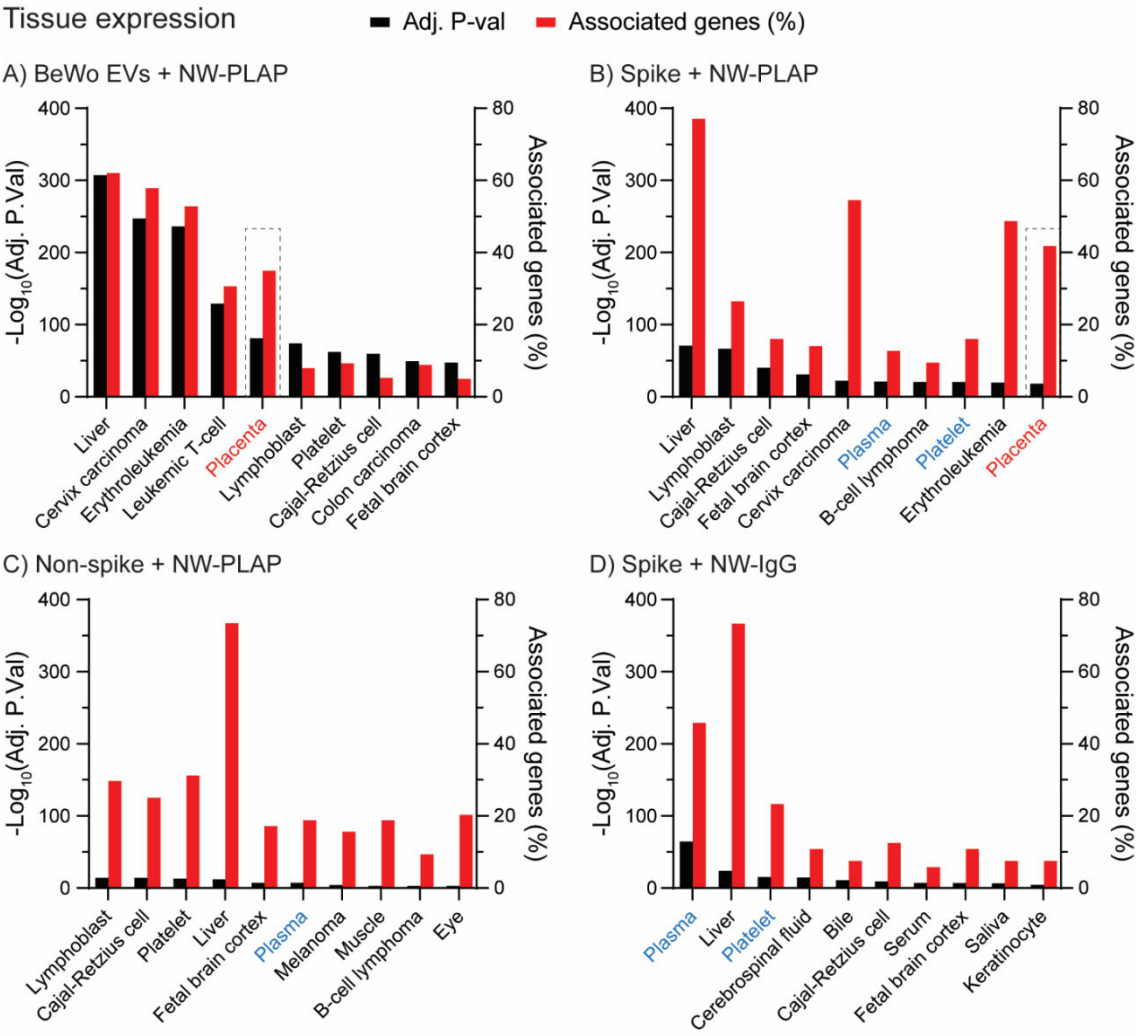

Figure 5-4 Tissue expression of identified proteins.
Tissue expression of identified proteins analysed by DAVID Bioinformatics Resources. Top 10 categories are reported and ranked by adjusted Benjamini-Hochberg P-value for A) *BeWo EVs + NW-PLAP* (positive control), B) *Spiked plasma + NW-PLAP*, C) *Non-spiked plasma + NW-PLAP* (negative control) and D) *Spiked plasma + NW-IgG* (negative control).

5.4.2 Sequential enrichment of placental EVs from spiked plasma (containing PLAP+ve and HLA-G+ve EVs)

Next, we aimed to demonstrate the feasibility of sequentially enriching multiple placental EV subtypes using a single sample (Figure 5-5). To obtain a proof of principle and investigate the difference in protein recovery between sequential and separate enrichment approaches, ultracentrifuged plasma samples were spiked with both BeWo (PLAP+ve) and Jeg3 (HLA-G+ve) EVs. Given PLAP+ve EVs are generally the more abundant subtype, PLAP+ve EVs were chosen to be enriched first within the sequential enrichment protocol. As shown in Figure 5-5A, PLAP protein recovery after enriching with NW-PLAP demonstrated no difference between separate and sequential enrichment (91.8 ± 7.3% and 91.1 ± 5.9% recovery, respectively), which is expected as these samples were processed the same way. HLA-G yielded a similar protein recovery compared to PLAP

when enriched separately (84.1 ± 9.3% compared to 91.8 ± 7.3%). There was also no significant difference in the recovery of HLA-G protein enriched with NW-HLA-G separately or sequentially (84.1 ± 9.3% and 71.4 ± 6.2% recovery, respectively) (Figure 5-5B). Total protein was quantified with BCA, and no significant differences were observed between separate or sequential enrichment for both PLAP+ve and HLA-G+ve EVs (Figure 5-5C), with all samples having significantly higher levels of total protein compared to the NW-IgG negative control. As PLAP and HLA-G ELISAs were performed on all samples, we can determine if PLAP+ve EVs were recovered during the enrichment of HLA-G+ve EVs and vice versa. Figure 5-5A and B demonstrate that there was minimal HLA-G recovered in the PLAP+ve EV enrichment and minimal PLAP recovered in the HLA-G+ve EV enrichment. Specifically, in all control tests approximately 15% of PLAP or HLA-G proteins were detected, likely representing baseline non-specific binding. Both NW-PLAP and NW-HLA-G recovered significantly more PLAP and HLA-G than non-specific HLA-G and PLAP, respectively ($p < 0.0001$).

This data demonstrates that there is no disadvantage to performing sequential enrichment for PLAP+ve and HLA-G+ve EVs. Considering that clinical samples are often available in limited amounts, which is especially the case for biobanked samples, the advantage of being able to perform sequential enrichment becomes evident as this allows for the total volume of plasma to be interrogated rather than having to divide it for separate enrichments. Moreover, we postulate that in clinical samples prior removal of a significant EV population (for example PLAP+ve EVs) may further enhance the recovery specificity for the second enrichment (for example HLA-G+ve EVs).

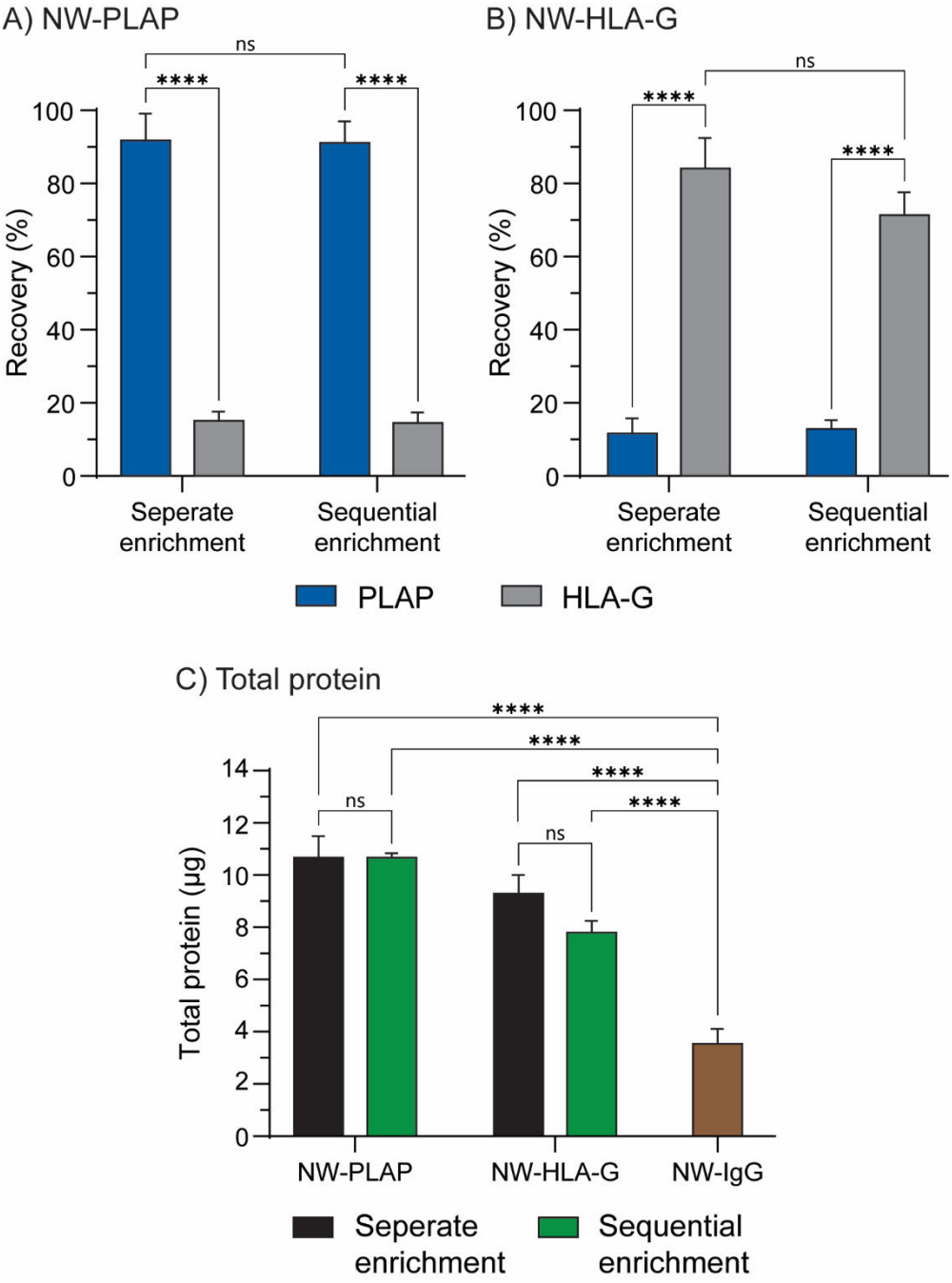

Figure 5-5 Recovery of PLAP and HLA-G measured by ELISA.
Recovery of PLAP and HLA-G measured by ELISA for A) NW-PLAP and B) NW-HLA-G used in separate and sequential enrichment. C) Total protein measured by BCA for NW-PLAP and NW-HLA-G used in separate and sequential enrichment. Data are presented as means ± SD (n = 3, one-way ANOVA with Tukey's post-test, ns: non significant ($p > 0.5$) and ****$p < 0.0001$).

5.4.3 Sequential enrichment of PLAP+ve and HLA-G+ve EVs from a preeclamptic plasma sample

We next sought to establish a proof of principle for performing sequential enrichment of PLAP+ve and HLA-G+ve EVs on a clinical sample. Specifically, we utilised a biobanked plasma sample collected from a pregnancy diagnosed with preeclampsia. To demonstrate

specific EV subtype enrichment, proteomics was performed on plasma samples that had first undergone UC to enrich the total EVs and then treated or not with the magnetic nanowires as follow: 1) *Pre-enrich* (ultracentrifuged plasma alone), 2) *UC + NW-PLAP* (*Pre-enrich* enriched with NW-PLAP), 3) *UC + NW-HLA-G* (*Pre-enrich* enriched with NW-HLA-G following enrichment with NW-PLAP) and 4) *UC + NW-IgG* (*Pre-enrich* enriched with NW-IgG following enrichment with NW-PLAP and NW-HLA-G, negative control). Overall, 288 proteins were identified in the pre-enriched plasma sample, with 149 and 226 identified in PLAP+ve and HLA-G+ve EV enriched fractions, respectively (Figure 5-6A). As expected, the negative control *UC + NW-IgG* detected lower proteins (43 proteins), the lowest of all samples. Identified proteins were then compared with the Vesiclepedia database, with all 4 samples showing > 70% overlap (Figure 5-6B). Given proteins found in the NW-IgG must be non-specific, those which co-occurred in the other samples were removed (specifically, 1 in *UC + NW-HLA-G*, 37 in *UC + NW-PLAP* and 5 in the *Pre-enrich*) (Figure 5-6B) before examining the proteins known to be expressed in the placenta. Specifically, *Pre-enrich* showed 62.5% association with the placenta, indicating the large number of placenta related EVs which must be present within this preeclamptic sample. Both *UC + NW-PLAP* and *UC + NW-HLA-G* show a higher proportion of placenta related proteins, demonstrating successful enrichment of placental EVs (72.5% and 72.2%, respectively).

Gene ontology for the cellular component confirms that as expected, exosomal protein is highly enriched in all 4 samples (Figure 5-7). However, of note the highest ranked adjusted P-value in the *UC + NW-PLAP* and *UC + NW-HLA-G* samples is “Extracellular exosome”, while in *Pre-enrich* and *UC + NW-IgG* samples it is “Blood microparticle”, further demonstrating effective EV enrichment using the magnetic nanowires. Tissue expression demonstrated “Plasma”, “Platelet” and “Serum” categories are present in all samples as expected (Figure 5-8). Again, demonstrating successful placental EV enrichment, the “Placenta” category was present in both *UC + NW-PLAP* and *UC + NW-HLA-G* samples but was absent in the *Pre-enrich* sample and *UC + NW-IgG* negative controls.

Due to limited availability of plasma sample, biological or technical triplicates were not performed for the two-step enrichment, and thus the data in Figure 5-6B was presented without error bars. The results showed that further enrichment of the two placental EV subtypes (HLA-G and PLAP) enriched placenta-associated proteins compared to the pre-

enrichment sample (72.5% vs 62.5%). Although no statistical difference can be drawn due to the lack of replicates, this observation was corroborated by analyzing the data using gene ontology (DAVID). Specifically, tissue expression analysis of the identified proteins (presented in Figure 5-8) revealed that the placenta category was present in both the two placental EVs enrichments, whereas it was absent in the pre-enrichment sample. This figure demonstrates that proteomics can be performed on maternal plasma samples after enrichment of placental specific EVs, and that this also enriches placental related proteins which must be co-localized with the placental EVs.

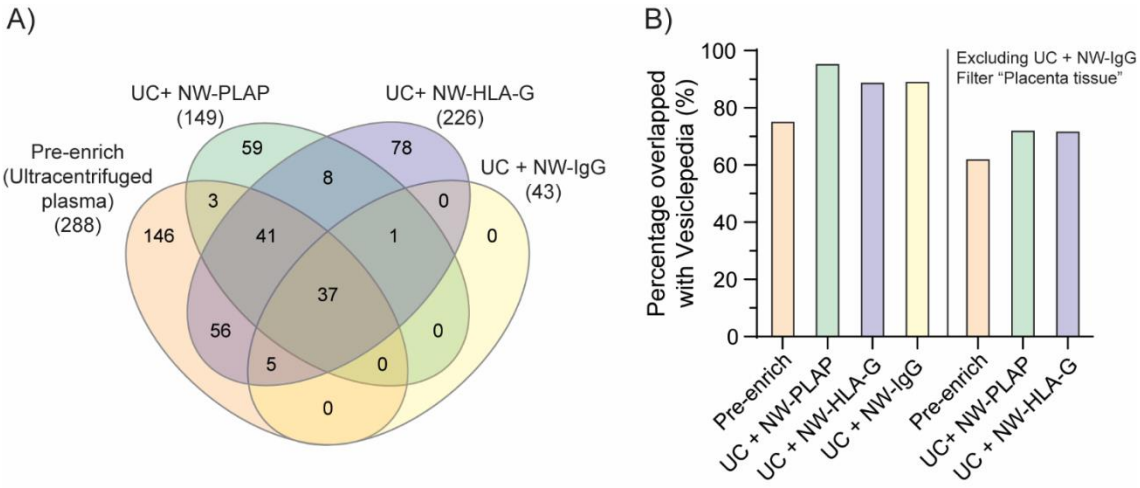

Figure 5-6 Mass spectrometry analysis of EVs sequentially enriched from the preeclamptic plasma sample.
A) Venn diagrams showing overlapping proteins of total plasma EVs (pre-enriched by UC) and immuno-specific placental EVs (PLAP+ve EVs and HLA-G+ve EVs) from a preeclamptic plasma sample. Samples included 1) *Pre-enrich* (ultracentrifuged plasma alone), 2) *UC + NW-PLAP* (*Pre-enrich* enriched with NW-PLAP), 3) *UC + NW-HLA-G* (*Pre-enrich* enriched with NW-HLA-G following enrichment with NW-PLAP) and 4) *UC + NW-IgG* (*Pre-enrich* enriched with NW-IgG following enrichment with NW-PLAP and NW-HLA-G, negative control). B) Proportions of identified proteins overlapped with Vesiclepedia database.

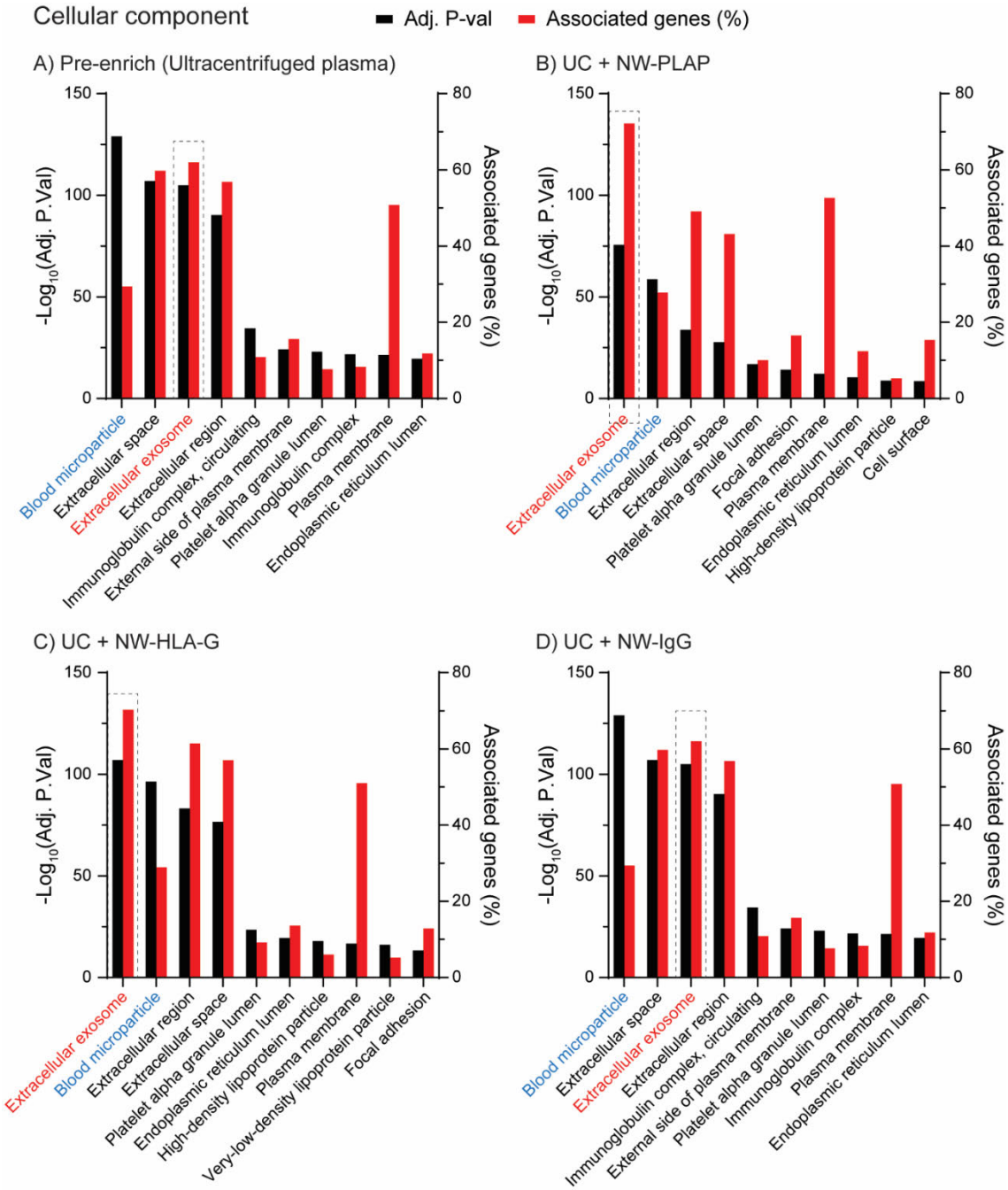

Figure 5-7 Cellular component of identified proteins.
Cellular component of identified proteins analysed by DAVID Bioinformatics Resources. Top 10 categories are reported and ranked by adjusted Benjamini-Hochberg P-value for A) *Pre-enrich* (ultracentrifuged plasma alone), B) *UC + NW-PLAP* (*Pre-enrich* enriched with NW-PLAP), C) *UC + NW-HLA-G* (*Pre-enrich* enriched with NW-HLA-G following enrichment with NW-PLAP) and D) *UC + NW-IgG* (*Pre-enrich* enriched with NW-IgG following enrichment with NW-PLAP and NW-HLA-G, negative control).

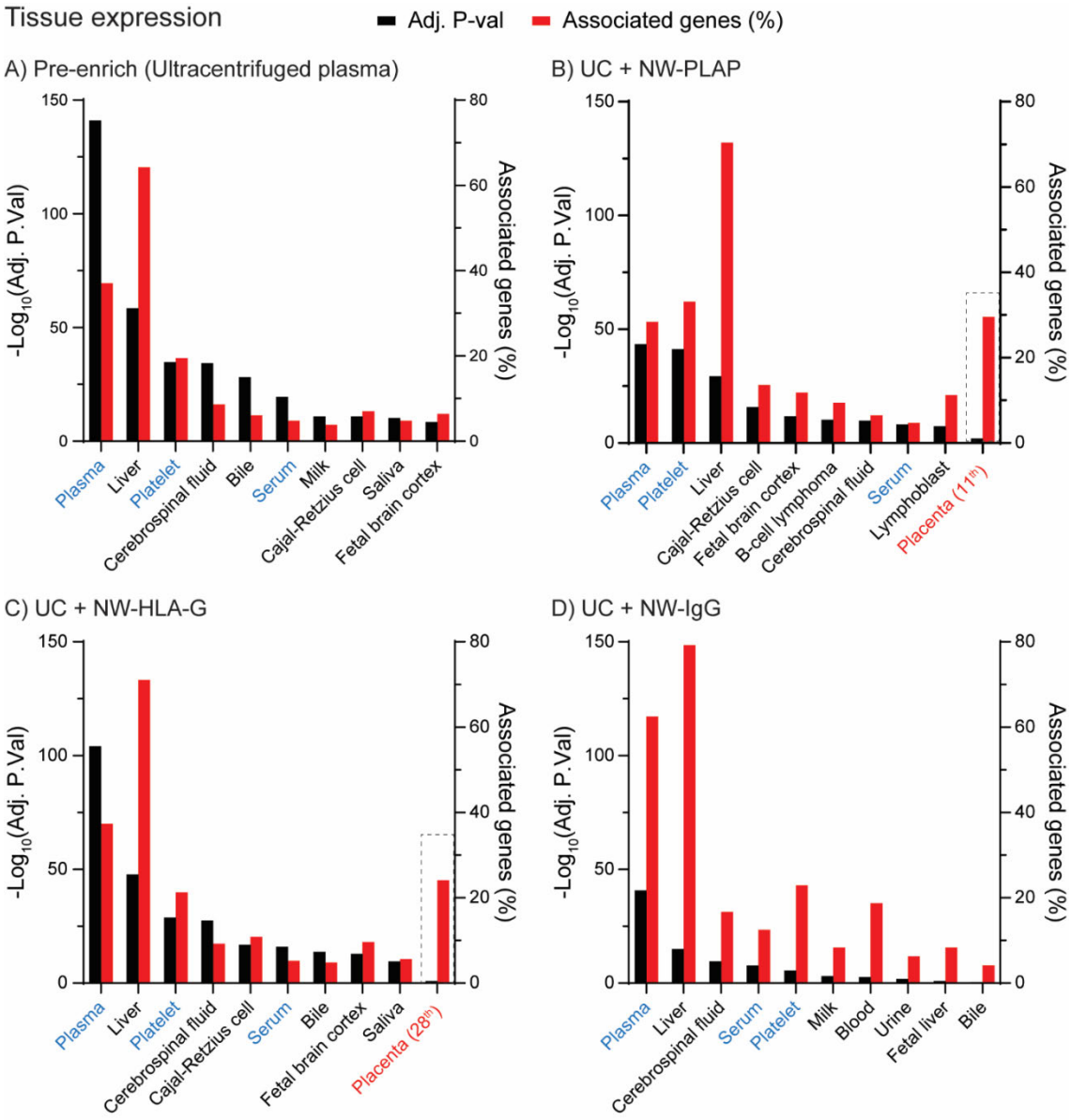

Figure 5-8 Tissue expression of identified proteins.
Tissue expression of identified proteins analysed by DAVID Bioinformatics Resources. Top 10 categories are reported and ranked by adjusted Benjamini-Hochberg P-value for A) *Pre-enrich* (ultracentrifuged plasma alone), B) *UC + NW-PLAP* (*Pre-enrich* enriched with NW-PLAP), C) *UC + NW-HLA-G* (*Pre-enrich* enriched with NW-HLA-G following enrichment with NW-PLAP) and D) *UC + NW-IgG* (*Pre-enrich* enriched with NW-IgG following enrichment with NW-PLAP and NW-HLA-G, negative control).

5.4.4 Placenta associated proteins enriched from NW-PLAP and NW-HLA-G preeclamptic plasma EVs.

Further exploring the proteins identified from EVs enriched with NW-PLAP (Table 5-1) and NW-HLA-G (Table 5-2), we found that 28 proteins from each sample are known to be associated with the placenta based on tissue expression analysis. Of these 28 proteins, 4 proteins (JUP, SELP, QSOX1, HLA-H) were shared across both PLAP+ve and HLA-G+ve EV enriched fractions. Utilising single cell transcriptomics data from Pavlicev et

al. (2017),[43] we further investigated what specific cell types in the placenta were likely to express certain proteins. Specifically, Tables 5-1 and 5-2 outline if either the SCTB or EVTB express RNA related to the proteins we have identified. All proteins identified in both PLAP+ve and HLA-G+ve EV enriched fractions are known to be expressed in SCTBs, while 25 of the proteins in the NW-PLAP fraction also have a known association with EVTBs at least at the RNA level. Moreover, 23 proteins in the NW-HLA-G fraction have a known association with SCTBs. This data warrants further investigations with additional samples aimed at establishing if the two PLAP+ve and HLA-G+ve EV subtypes can provide additional insights into the health of the placenta.

Finally, we wanted to investigate the relevance of the identified proteins to known preeclampsia associated proteins and differentially expressed genes. To do this, we compared the identified proteins to a published manually curated preeclampsia gene database, dpPEC, which was last updated in 2015.[44] We found that 16/28 proteins identified by NW-PLAP and 12/28 proteins identified by NW-HLA-G are listed in dbPEC and therefore, have a known association with preeclampsia. Given dbPEC is recognised to be incomplete, we also compiled a list of known differentially expressed genes in preeclampsia based on previous studies,[45-54] which we then again compared with the identified proteins. Using this approach, we found 14/28 proteins recovered by NW-PLAP and 16/28 proteins recovered by NW-HLA-G have a known association with preeclampsia.

Although we will not discuss all proteins identified with known preeclampsia links, we wanted to highlight several that we think are highly relevant and interesting. For example, Pregnancy specific beta-1-glycoprotein 4 (PSG4) was detected in the NW-HLA-G enriched sample and the *Pre-enrich* sample. This protein is highly enriched in the placenta and has minimal expression elsewhere in the body. PSG4 is associated with placental development and preeclampsia and may regulate angiogenesis, cell proliferation and migration/invasion.[55,56] HLA-C was found specifically in the NW-HLA-G enriched sample. HLA-C is known to be expressed in EVTBs and is tightly transcriptionally regulated to balance tolerance and immunity during pregnancy.[57] Increased HLA-C expression in EVTB is known to occur in preeclamptic pregnancies, demonstrating the likely enrichment of HLA-G+ve EVs and the potential important information that could be obtained from such samples. Quiescin sulfhydryl oxidase 1 (QSOX1) and Serum amyloid A (SAA) were identified uniquely in the NW-PLAP enriched sample. QSOX1

is known to be upregulated due to hypoxia, increasing intracellular H_2O_2 and leading to an increase in apoptosis in preeclamptic placentas.[58] While SSA is a key protein involved in immunoregulation, it is known to be involved in placental microenvironment functions, which regulates metalloprotease activity and trophoblast invasion, as well as to be upregulated in preeclampsia and may contribute to its pathogenesis.[59,60] Pregnancy associated plasma protein A (PAPPA) was found in the PLAP+ve and HLA-G+ve EV enriched fractions and the *Pre-enrich*. PAPPA is known to be dysregulated in preeclampsia in the first and second trimester. Junction Plakoglobin (JUP) was found in both PLAP+ve and HLA-G+ve EV enriched fractions and was not present in the *Pre-enrich* or *UC + NW-IgG* negative control. JUP is a well-known upregulated gene in preeclampsia.[61] The presence of these critical proteins uniquely expressed in the enriched EV fractions indicates that this method can likely provide important insights into the health and disease of the placenta. Further studies with more preeclamptic samples and gestation matched healthy pregnancy controls are required to confirm the relevance of the two enriched subtypes.

Table 5-1 Proteins (28) enriched by UC + NW-PLAP and identified as placenta and preeclampsia associated

Gene symbol	Gene name	SCTB associated	EVTB associated	Preeclampsia associated
F11R	F11 receptor			
LYN	LYN proto-oncogene, Src family tyrosine kinase			
RAB14	RAB14, member RAS oncogene family			
RAB1A	RAB1A, member RAS oncogene family			
RAB6A	RAB6A, member RAS oncogene family			
SACM1L	SAC1 like phosphatidylinositide phosphatase			
ANXA2	Annexin A2			
CNN2	Calponin 2			
ENDOD1	Endonuclease domain containing 1			
ILK	Integrin linked kinase			
JUP(*)	Junction plakoglobin			

LCP1	Lymphocyte cytosolic protein 1			
LAMP1	Lysosomal associated membrane protein 1			
HLA-H(*)	Major histocompatibility complex, class I, H (pseudogene)			
PGK1	Phosphoglycerate kinase			
PLEC	Plectin			
PHB2	Prohibitin 2			
QSOX1(*)	Quiescin sulfhydryl oxidase 1			
RDH11	Retinol dehydrogenase 11			
SELP(*)	Selectin P			
SLC25A5	Solute carrier family 25 member 5			
SNAP23	Synaptosome associated protein 2			
TGM1	Transglutaminase			
TPI1	Triosephosphate isomerase 1			
TPM1	Tropomyosin 1			
TUBA1B	Tubulin alpha 1b			
YWHAE	Tyrosine 3-monooxygenase/tryptophan 5-monooxygenase activation protein epsilon			
YWHAQ	Tyrosine 3-monooxygenase/tryptophan 5-monooxygenase activation protein theta			

Tissue expression analysis to identify placenta-specific proteins performed using UP_TISSUE of DAVID.

(*) denotes proteins shared with UC + NW-HLA-G.

Shaded areas indicate proteins either expressed in SCTB or EVTB tissues based on single-cell transcriptomics data reported by Pavlicev et al. (2017)[43] or associated with preeclampsia.[45-54]

Table 5-2 Proteins (28) enriched by UC + NW-HLA-G and identified as placenta and preeclampsia associated

Gene symbol	Gene name	SCTB associated	EVTB associated	Preeclampsia associated
CLK3	CDC like kinase	■	■	
GNAQ	G protein subunit alpha Q	■	■	■
WDR1	WD repeat domain 1	■	■	
ARPC1B	Actin related protein 2/3 complex subunit 1B	■	■	
ACTN4	Actinin alpha 4	■	■	
CAPN1	Calpain 1	■	■	
CAPZA1	Capping actin protein of muscle z-line subunit alpha 1	■	■	
CDC42	Cell division cycle 42	■	■	
COL6A1	Collagen type vi alpha 1 chain	■		■
COL6A3	Collagen type vi alpha 3 chain	■		■
ENO1	Enolase 1	■	■	
FBN1	Fibrillin 1	■	■	■
FLNB	Filamin B	■	■	■
IGFBP5	Insulin like growth factor binding protein 5	■		■
ITGB1	Integrin subunit beta 1	■	■	■
JUP(*)	Junction plakoglobi	■	■	■
LYZ	Lysozyme	■	■	■
HLA-H(*)	Major histocompatibility complex, class I, H (pseudogene)	■		■
MYADM	Myeloid associated differentiation marker	■	■	
PDE5A	Phosphodiesterase 5A	■	■	■
PLTP	Phospholipid transfer protein	■	■	■
PCYOX1	Prenylcysteine oxidase 1	■	■	■
PTPRA	Protein tyrosine phosphatase receptor type A	■	■	
PTPRC	Protein tyrosine phosphatase receptor type C	■	■	■
QSOX1(*)	Quiescin sulfhydryl oxidase 1	■	■	■

SELP(*)	Selectin P			
TAGLN2	Transgelin 2			
TPM4	Tropomyosin 4			

Tissue expression analysis to identify placenta-specific proteins performed using UP_TISSUE of DAVID.

(*) denotes proteins shared with UC + NW-PLAP.

Shaded areas indicate proteins either expressed in SCTB or EVTB tissues based on single-cell transcriptomics data reported by Pavlicev et al. (2017)[43] or associated with preeclampsia.[45-54]

5.4.5 Comparative proteomic analyses of two-step enrichment and direct enrichment

Chapter 4 outlined a method for the direct enrichment of PLAP+ve and HLA-G+ve EVs without the need for pre-enrichment. Plasma samples with abundant contaminating proteins affect the number of proteins identified and therefore, methods minimising the amount of contaminating proteins should be used. For this reason, in our study and those of others,[24,62-64] EVs are usually first pre-enriched with UC. However, since it is also known that UC leads to significant loss and potential damage of EVs and associated proteins, and other pre-enrichment methods also suffer from significant limitations, we investigated the possibility of using direct EV enrichment for the proteomic analysis of plasma samples with placental EVs. It should be noted that direct EV enrichment presented in this section was also performed sequentially, which started first with NW-PLAP then NW-HLA-G and finally NW-IgG as a control.

As shown in Figure 5-9A, NW-PLAP and NW-HLA-G as well as the negative control NW-IgG identified a similar number of proteins (201, 192 and 175, respectively). The number of proteins identified by the NW-IgG control in the direct enriched sample was much higher than after UC (*UC + NW-IgG*, 43 proteins), which likely originates in the increased presence of protein contamination. The total amount of protein measured by BCA after direct NW-PLAP, NW-HLA-G and NW-IgG enrichment was 16, 18.6 and 13.9 µg respectively, which were much higher than that obtained from their corresponding enrichments preceded by UC (2.9, 3.8 and 3.2 µg respectively) despite the smaller plasma volume used in direct capture. We anticipate this increase in total protein relates to both specific and non-specific protein/EV binding. Principal component analysis of the top 6 differentially expressed proteins from direct enrichment demonstrates there is low variability between sample replicates, and that as expected NW-PLAP and NW-HLA-G are more similar than the negative control NW-IgG (Figure 5-9B). This result can be further explained by the tissue expression analysis of the identified proteins recovered from the direct EV enrichment. While analyses of the total protein of the NW-PLAP, NW-HLA-G or NW-IgG enriched fractions only show "Plasma" and "Serum" as main categories, analyses of 39 proteins exclusive to NW-PLAP or 26 proteins exclusive to NW-HLA-G, which are non-overlapped with

proteins of NW-IgG, shows the presence of "Placenta" category. Of these 39 and 26 proteins, 15 and 9 proteins enriched by NW-PLAP and NW-HLA-G, respectively were identified as placenta-specific as listed in Table 5-3 and 5-4. In addition, many of these placenta-specific proteins were found to associate with preeclampsia when cross-referenced with previous publications[45-54] as shown in Table 5-3 and 5-4. Identified proteins of note from the NW-PLAP enrichment include Talin 1 (TLN1),[65] Pappalysin 2 (PAPPA2)[66] and LIM zinc finger domain containing 1 (LIMS1)[67] which all have known associations with preeclampsia.

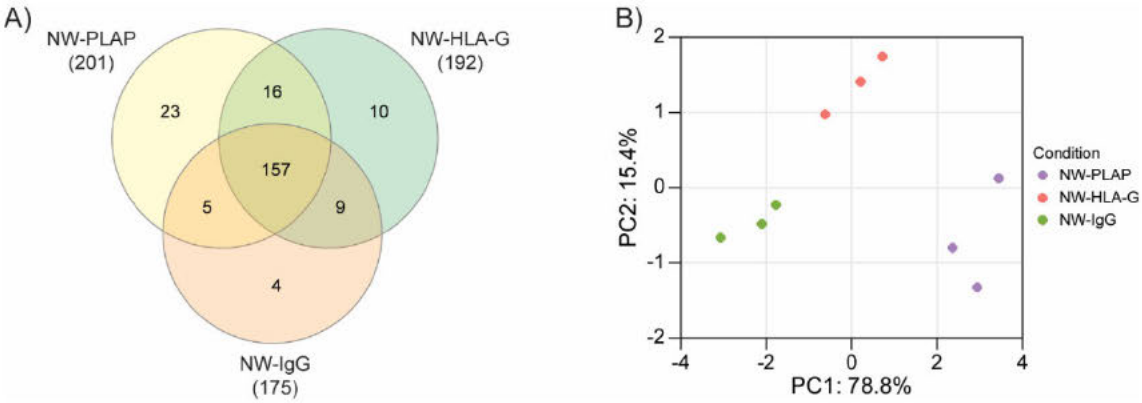

Figure 5-9 Mass spectrometry analysis of EVs directly enriched from the preeclamptic plasma samples.
A) Venn diagrams showing overlapping proteins of direct enrichment of EVs from plasma using NW-PLAP, NW-HLA-G and NW-IgG. B) Principal component analysis of the proteins enriched from the direct enrichment samples.

Table 5-3 Proteins (15) directly enriched by NW-PLAP and identified as placenta and preeclampsia associated

Gene symbol	Gene name	SCTB associated	EVTB associated	Preeclampsia associated
HTRA1	HtrA serine peptidase			
RAP1B	RAP1B, member of RAS oncogene family			
ACTN1	Atinin alpha 1			
CDH1	Cadherin 1			
CFL1	Cofilin 1			
CFD	Complement factor D			
GAPDH(*)	Glyceraldehyde-3-phosphate dehydrogenase			
GP1BA	Glycoprotein Ib platelet subunit alpha			
ITGB3(*)	Integrin subunit beta 3			
PAPPA2	Pappalysin 2			

PCOLCE(*)	Procollagen C-endopeptidase enhancer			
RNASE1	Ribonuclease A family member 1, pancreatic			
TLN1(*)	Talin 1			
TUBA1B	Tubulin alpha 1b			
YWHAZ	Tyrosine 3-monooxygenase/tryptophan 5-monooxygenase activation protein zeta			

Tissue expression analysis to identify placenta-specific proteins performed using UP_TISSUE of DAVID.

(*) denotes proteins shared with UC + NW-HLA-G.

Shaded areas indicate proteins either expressed in SCTB or EVTB tissues based on single-cell transcriptomics data reported by Pavlicev et al. (2017)[43] or associated with preeclampsia.[45-54]

Table 5-4 Proteins (9) directly enriched by NW-HLA-G and identified as placenta and preeclampsia associated

Gene symbol	Gene name	SCTB associated	EVTB associated	Preeclampsia associated
CLK3	CDC like kinase 3			
CSH1	Chorionic somatomammotropin hormone 1			
GAPDH(*)	Glyceraldehyde-3-phosphate dehydrogenase			
GH2	Growth hormone 2			
ITGB3(*)	Integrin subunit beta 3			
LYZ	Lysozyme			
PCOLCE(*)	Procollagen C-endopeptidase enhancer			
SERPINE1	Serpin family E member 1			
TLN1(*)	Talin 1			

Tissue expression analysis to identify placenta-specific proteins performed using UP_TISSUE of DAVID.

(*) denotes proteins shared with UC + NW-PLAP.

Shaded areas indicate proteins either expressed in SCTB or EVTB tissues based on single-cell transcriptomics data reported by Pavlicev et al. (2017)[43] or associated with preeclampsia.[45-54]

When analysing the protein contaminants identified in the direct enrichment method as well as the pre-enrichment (ultracentrifuged plasma) and immune-magnetic enrichments preceded by UC (referred to as two-step enrichment), we can see that overall there is no significant difference between them (Figure 5-10). It is important to note that the amount of plasma used in each sample was 100 µL for the direct enrichment and 400 µL for the two-step enrichment. This difference was imposed due to the limited volume of patient sample available, however, this may have led to the decrease in proteins identified. A direct comparison is needed to demonstrate if, even with an increased amount of protein contaminants, the direct enrichment method performs as well as the two-step enrichment method for the same given plasma volume.

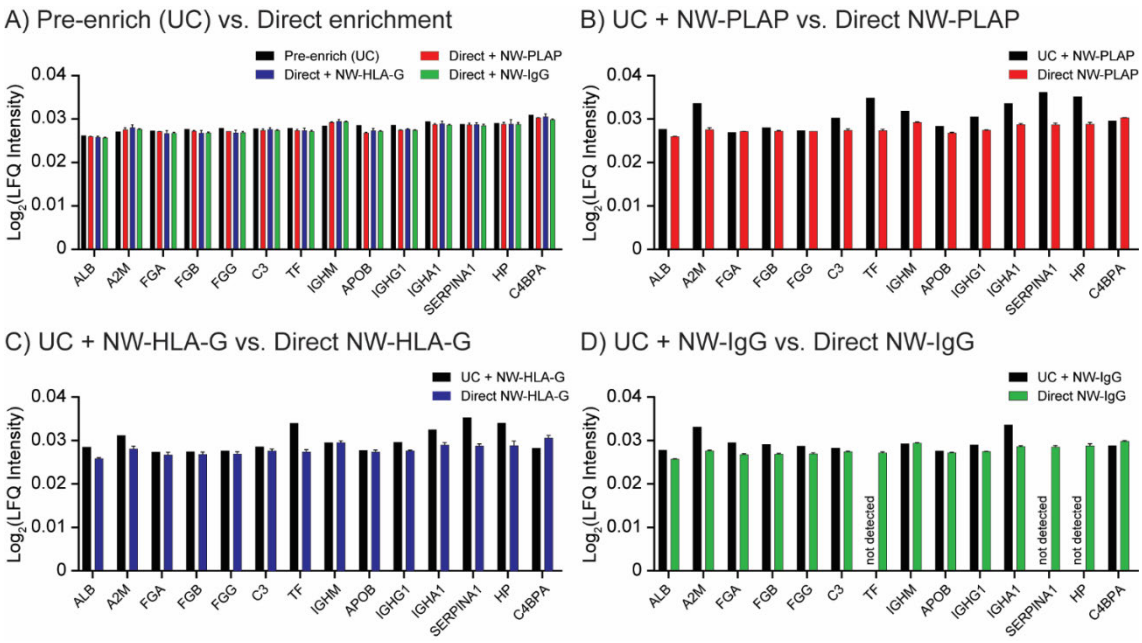

Figure 5-10 Comparison of contaminants between two-step and direct EV enrichment.
Log fold label-free quantification intensity of contaminant proteins compared between direct enrichment with A) *Pre-enrich* (ultracentrifuged plasma), B) enrichment using *UC + NW-PLAP*, C) enrichment using *UC + NW-HLA-G* and D) enrichment using *UC + NW-IgG*.

When comparing data for the direct enrichment approach with that for the two-step enrichment in terms of total proteins identified in each sample, the direct enrichment data clustered with the pre-enrich (ultracentrifuged plasma) data (Figure 5-11A), which is in agreement with previous results and can be explained by the predominant presence of plasma proteins in these samples. Using the top 5 differentially expressed proteins, 3 different clusters were formed including two-step enrichment, direct enrichment using NW-PLAP and NW-HLA-G and finally direct enrichment using NW-IgG (Figure 5-11B). This disparity was possibly due to the contribution of placenta-specific proteins

that separate direct enrichment and two-step enrichment using NW-PLAP and NW-HLA-G from the *Pre-enrich* and NW-IgG.

Focussing on the proteins identified by direct enrichment, there were 34 proteins identified in NW-PLAP and 34 proteins from NW-HLA-G which were not found in the *Pre-enrich* sample (Figure 5-11C). In addition, there were 129 and 68 proteins for the direct enrichment group using NW-PLAP and NW-HLA-G respectively which were not found in the corresponding two-step enrichment (Figure 5-11D). Given proteins identified from the direct capture samples were still able to provide biologically relevant insights into placenta and preeclampsia related biomarkers, direct enrichment approach before proteomics may provide an alternative processing methodology. This approach might be especially useful when only small amounts of samples are available, which is often the case for biobanked samples and motivated these investigations. However, further work is required to establish the definitive validity and utility of this methodology.

The choice between two-step and single step enrichment methods depends on the requirements of the downstream assay. While both methods are compatible with mass spectrometry, two-step enrichment is better suited for biomarker discovery purposes as it typically produces fewer contaminants and identifies a larger number of proteins. On the other hand, single step enrichment is more appropriate when targeting known markers for detection and can be analyzed using techniques such as ELISA or targeted mass spectrometry.

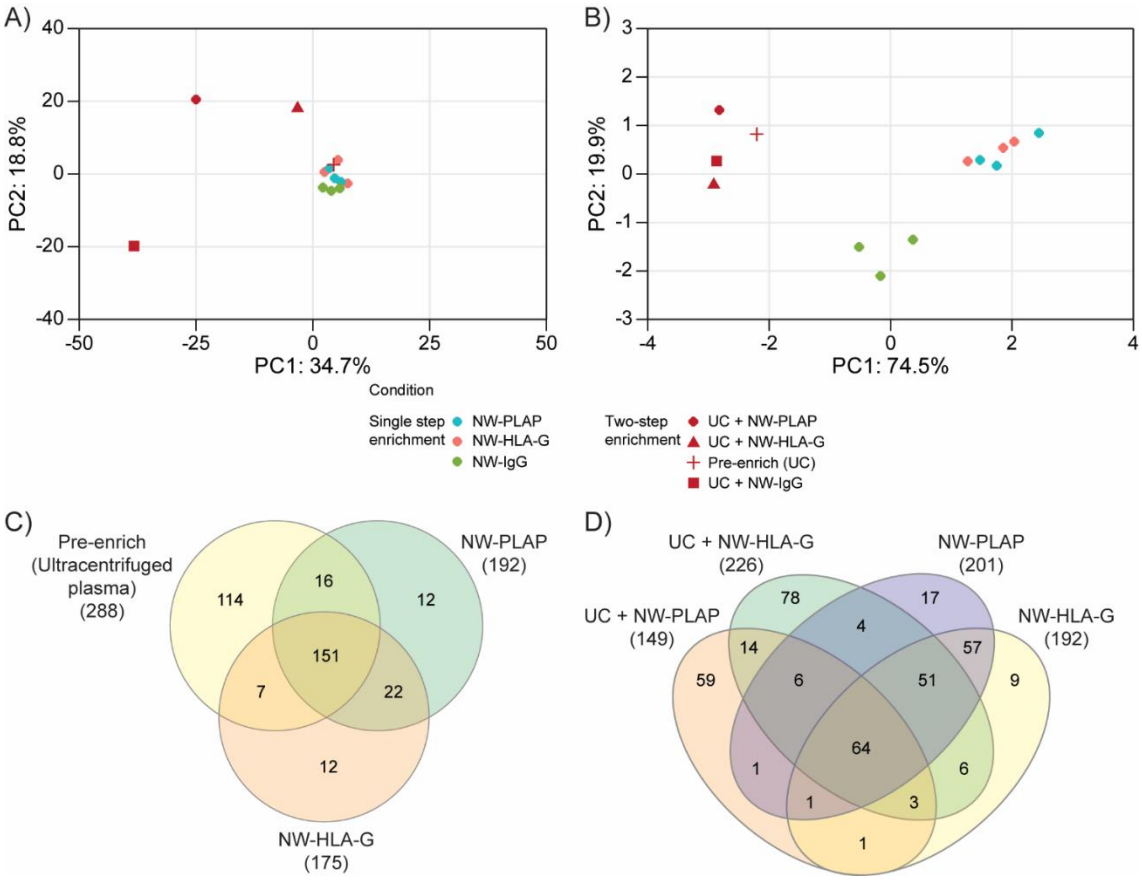

Figure 5-11 Comparative proteomic analyses of two-step and direct EV enrichment. Principal component analysis of the proteins compared between two-step enrichment and direct enrichment using A) total proteins and B) top 5 differentially expressed proteins. Venn diagram showing overlapped proteins of the direct enrichment when compared with C) the pre-enrich (ultracentrifuged plasma) and D) two-step enrichment using NW-PLAP and NW-HLA-G.

5.5 Conclusion

Placental EVs not only reflect the phenotype of placental cells, but also play an active role in pregnancy health and disease. Placental EVs circulating in the maternal blood during pregnancy are valuable materials for proteomic studies of the placenta, especially when carried out at the subtype levels. Here we report first a robust EV-based proteomic approaches and demonstrate relevance in model studies with cell-based EVs and subsequently in a pilot study with a sample obtained from a preeclamptic pregnancy. We also demonstrate the feasibility of performing sequential enrichment of placental EV subtypes (PLAP+ve and HLA-G+ve EVs) using iron oxide NWs coating with dual RAFT copolymers. This approach is especially suitable in the case when limited amount of plasma is available, which is typically the case for biobanked plasma samples (< 500 µL). Subsequent mass spectrometry of the proteins extracted from the enriched placental EV subtypes demonstrated recovery of placenta-specific and preeclampsia-associated

proteins. The proposed comprehensive methodology for proteomic analysis of two key placental EV subtypes is anticipated to provide additional and complementary non-invasive insights into the health of the placenta and warrant further validation in a larger cohort of pregnancies.

5.6 References

1 MacDonald, T. M., Walker, S. P., Hannan, N. J., Tong, S. & Kaitu'u-Lino, T. J. Clinical tools and biomarkers to predict preeclampsia. *EBioMedicine* **75**, 103780, doi:10.1016/j.ebiom.2021.103780 (2022).

2 Staff, A. C. The two-stage placental model of preeclampsia: An update. *J Reprod Immunol* **134-135**, 1-10, doi:10.1016/j.jri.2019.07.004 (2019).

3 Whitehead, C. L., Walker, S. P. & Tong, S. Measuring circulating placental RNAs to non-invasively assess the placental transcriptome and to predict pregnancy complications. *Prenatal diagnosis* **36**, 997-1008 (2016).

4 Roberts, J. M. *et al.* Subtypes of Preeclampsia: Recognition and Determining Clinical Usefulness. *Hypertension* **77**, 1430-1441, doi:10.1161/HYPERTENSIONAHA.120.14781 (2021).

5 Armaly, Z., Jadaon, J. E., Jabbour, A. & Abassi, Z. A. Preeclampsia: Novel Mechanisms and Potential Therapeutic Approaches. *Front Physiol* **9**, 973, doi:10.3389/fphys.2018.00973 (2018).

6 Kar, M. Role of biomarkers in early detection of preeclampsia. *J Clin Diagn Res* **8**, BE01-04, doi:10.7860/JCDR/2014/7969.4261 (2014).

7 Andersen, L. L. T., Helt, A., Sperling, L. & Overgaard, M. Decision Threshold for Kryptor sFlt-1/PlGF Ratio in Women With Suspected Preeclampsia: Retrospective Study in a Routine Clinical Setting. *J Am Heart Assoc* **10**, e021376, doi:10.1161/JAHA.120.021376 (2021).

8 Herraiz, I. *et al.* Clinical implementation of the sFlt-1/PlGF ratio to identify preeclampsia and fetal growth restriction: A prospective cohort study. *Pregnancy Hypertens* **13**, 279-285, doi:10.1016/j.preghy.2018.06.017 (2018).

9 Zeisler, H. *et al.* Predictive Value of the sFlt-1:PlGF Ratio in Women with Suspected Preeclampsia. *N Engl J Med* **374**, 13-22, doi:10.1056/NEJMoa1414838 (2016).

10 Morgan, T. K. Cell- and size-specific analysis of placental extracellular vesicles in maternal plasma and pre-eclampsia. *Transl Res* **201**, 40-48, doi:10.1016/j.trsl.2018.08.004 (2018).

11 Das, M. & Kale, V. Extracellular vesicles: Mediators of embryo-maternal crosstalk during pregnancy and a new weapon to fight against infertility. *Eur J Cell Biol* **99**, 151125, doi:10.1016/j.ejcb.2020.151125 (2020).

12 Czernek, L. & Duchler, M. Exosomes as Messengers Between Mother and Fetus in Pregnancy. *Int J Mol Sci* **21**, doi:10.3390/ijms21124264 (2020).

13 Tong, M. & Chamley, L. W. Placental extracellular vesicles and feto-maternal communication. *Cold Spring Harb Perspect Med* **5**, a023028, doi:10.1101/cshperspect.a023028 (2015).

14 Bai, K. *et al.* Placenta-Derived Exosomes as a Modulator in Maternal Immune Tolerance During Pregnancy. *Front Immunol* **12**, 671093, doi:10.3389/fimmu.2021.671093 (2021).

15 O'Brien, K., Breyne, K., Ughetto, S., Laurent, L. C. & Breakefield, X. O. RNA delivery by extracellular vesicles in mammalian cells and its applications. *Nat Rev Mol Cell Biol* **21**, 585-606, doi:10.1038/s41580-020-0251-y (2020).

16 Joshi, B. S., de Beer, M. A., Giepmans, B. N. G. & Zuhorn, I. S. Endocytosis of Extracellular Vesicles and Release of Their Cargo from Endosomes. *ACS Nano* **14**, 4444-4455, doi:10.1021/acsnano.9b10033 (2020).

17 Skotland, T., Sagini, K., Sandvig, K. & Llorente, A. An emerging focus on lipids in extracellular vesicles. *Adv Drug Deliv Rev* **159**, 308-321, doi:10.1016/j.addr.2020.03.002 (2020).

18 Awoyemi, T. *et al.* Syncytiotrophoblast Extracellular Vesicles From Late-Onset Preeclampsia Placentae Suppress Pro-Inflammatory Immune Response in THP-1 Macrophages. *Front Immunol* **12**, 676056, doi:10.3389/fimmu.2021.676056 (2021).

19 Vatish, M., Redman, C. W. & Davidge, S. T. in *Chesley's Hypertensive Disorders in Pregnancy* 155-163 (Elsevier, 2022).

20 Tersigni, C. *et al.* HLA-DR is aberrantly expressed at feto-maternal interface in pre-eclampsia. *Journal of Reproductive Immunology* **129**, 48-52 (2018).

21 Konecna, B., Tothova, L. & Repiska, G. Exosomes-Associated DNA-New Marker in Pregnancy Complications? *Int J Mol Sci* **20**, doi:10.3390/ijms20122890 (2019).

22 Kshirsagar, S. *et al.* Immunomodulatory molecules are released from the first trimester and term placenta via exosomes. *Placenta* **33**, 982-990 (2012).

23 Nakahara, A. *et al.* Circulating Placental Extracellular Vesicles and Their Potential Roles During Pregnancy. *Ochsner J* **20**, 439-445, doi:10.31486/toj.20.0049 (2020).

24 Menon, R. *et al.* Protein Profile Changes in Circulating Placental Extracellular Vesicles in Term and Preterm Births: A Longitudinal Study. *Endocrinology* **161**, doi:10.1210/endocr/bqaa009 (2020).

25 Sherman, C. D., Lodha, S. & Sahoo, S. EV Cargo Sorting in Therapeutic Development for Cardiovascular Disease. *Cells* **10**, doi:10.3390/cells10061500 (2021).

26 Kolonics, F., Szeifert, V., Timar, C. I., Ligeti, E. & Lorincz, A. M. The Functional Heterogeneity of Neutrophil-Derived Extracellular Vesicles Reflects the Status of the Parent Cell. *Cells* **9**, doi:10.3390/cells9122718 (2020).

27 Palma, C. *et al.* Extracellular Vesicles and Preeclampsia: Current Knowledge and Future Research Directions. *Subcell Biochem* **97**, 455-482, doi:10.1007/978-3-030-67171-6_18 (2021).

28 Orozco, A. F. *et al.* Placental release of distinct DNA-associated micro-particles into maternal circulation: reflective of gestation time and preeclampsia. *Placenta* **30**, 891-897 (2009).

29 Tan, K. H. *et al.* Plasma biomarker discovery in preeclampsia using a novel differential isolation technology for circulating extracellular vesicles. *Am J Obstet Gynecol* **211**, 380 e381-313, doi:10.1016/j.ajog.2014.03.038 (2014).

30 McElrath, T. F. *et al.* Late first trimester circulating microparticle proteins predict the risk of preeclampsia < 35 weeks and suggest phenotypic differences among affected cases. *Sci Rep* **10**, 17353, doi:10.1038/s41598-020-74078-w (2020).

31 Navajas, R. *et al.* Quantitative proteomic analysis of serum-purified exosomes identifies putative pre-eclampsia-associated biomarkers. *Clin Proteomics* **19**, 5, doi:10.1186/s12014-022-09342-4 (2022).

32 Jia, R. *et al.* Comparative Proteomic Profile of the Human Umbilical Cord Blood Exosomes between Normal and Preeclampsia Pregnancies with High-Resolution Mass Spectrometry. *Cell Physiol Biochem* **36**, 2299-2306, doi:10.1159/000430193 (2015).

33 Baig, S. *et al.* Proteomic analysis of human placental syncytiotrophoblast microvesicles in preeclampsia. *Clin Proteomics* **11**, 40, doi:10.1186/1559-0275-11-40 (2014).

34 Sabapatha, A., Gercel-Taylor, C. & Taylor, D. D. Specific isolation of placenta-derived exosomes from the circulation of pregnant women and their

immunoregulatory consequences. *Am J Reprod Immunol* **56**, 345-355, doi:10.1111/j.1600-0897.2006.00435.x (2006).

35 Lai, A., Elfeky, O., Rice, G. E. & Salomon, C. Optimized Specific Isolation of Placenta-Derived Exosomes from Maternal Circulation. *Methods Mol Biol* **1710**, 131-138, doi:10.1007/978-1-4939-7498-6_10 (2018).

36 Fitzgerald, W., Gomez-Lopez, N., Erez, O., Romero, R. & Margolis, L. Extracellular vesicles generated by placental tissues ex vivo: A transport system for immune mediators and growth factors. *Am J Reprod Immunol* **80**, e12860, doi:10.1111/aji.12860 (2018).

37 Favaro, R. R., Murrieta-Coxca, J. M., Gutiérrez-Samudio, R. N., Morales-Prieto, D. M. & Markert, U. R. Immunomodulatory properties of extracellular vesicles in the dialogue between placental and immune cells. *American Journal of Reproductive Immunology* **85**, e13383 (2021).

38 Pham, Q. N. *et al.* Magnetic Enrichment of Immuno-Specific Extracellular Vesicles for Mass Spectrometry Using Biofilm-Derived Iron Oxide Nanowires. *bioRxiv*, 2022.2005.2001.490183, doi:10.1101/2022.05.01.490183 (2022).

39 Sadovsky, Y. *et al.* Placental small extracellular vesicles: Current questions and investigative opportunities. *Placenta* **102**, 34-38, doi:10.1016/j.placenta.2020.03.002 (2020).

40 Levine, L. *et al.* Syncytiotrophoblast extracellular microvesicle profiles in maternal circulation for noninvasive diagnosis of preeclampsia. *Sci Rep* **10**, 6398, doi:10.1038/s41598-020-62193-7 (2020).

41 Huang da, W., Sherman, B. T. & Lempicki, R. A. Systematic and integrative analysis of large gene lists using DAVID bioinformatics resources. *Nat Protoc* **4**, 44-57, doi:10.1038/nprot.2008.211 (2009).

42 Bellotti, C., Lang, K., Kuplennik, N., Sosnik, A. & Steinfeld, R. High-grade extracellular vesicles preparation by combined size-exclusion and affinity chromatography. *Sci Rep* **11**, 10550, doi:10.1038/s41598-021-90022-y (2021).

43 Pavlicev, M. *et al.* Single-cell transcriptomics of the human placenta: inferring the cell communication network of the maternal-fetal interface. *Genome Res* **27**, 349-361, doi:10.1101/gr.207597.116 (2017).

44 Uzun, A., Triche, E. W., Schuster, J., Dewan, A. T. & Padbury, J. F. dbPEC: a comprehensive literature-based database for preeclampsia related genes and phenotypes. *Database (Oxford)* **2016**, doi:10.1093/database/baw006 (2016).

45 Vennou, K. E., Kontou, P. I., Braliou, G. G. & Bagos, P. G. Meta-analysis of gene expression profiles in preeclampsia. *Pregnancy Hypertens* **19**, 52-60, doi:10.1016/j.preghy.2019.12.007 (2020).

46 Ren, Z. *et al.* Distinct placental molecular processes associated with early-onset and late-onset preeclampsia. *Theranostics* **11**, 5028-5044, doi:10.7150/thno.56141 (2021).

47 Tejera, E., Bernardes, J. & Rebelo, I. Preeclampsia: a bioinformatics approach through protein-protein interaction networks analysis. *BMC Syst Biol* **6**, 97, doi:10.1186/1752-0509-6-97 (2012).

48 Biswas, S., Dutta, S. & Acharyya, S. Identification of Disease Critical Genes Using Collective Meta-heuristic Approaches: An Application to Preeclampsia. *Interdiscip Sci* **11**, 444-459, doi:10.1007/s12539-017-0276-x (2019).

49 Hannan, N. J. *et al.* Circulating mRNAs are differentially expressed in pregnancies with severe placental insufficiency and at high risk of stillbirth. *BMC Med* **18**, 145, doi:10.1186/s12916-020-01605-x (2020).

50 Michita, R. T., Kaminski, V. L. & Chies, J. A. B. Genetic Variants in Preeclampsia: Lessons From Studies in Latin-American Populations. *Front Physiol* **9**, 1771, doi:10.3389/fphys.2018.01771 (2018).

51 Tejera, E. *et al.* Consensus strategy in genes prioritization and combined bioinformatics analysis for preeclampsia pathogenesis. *BMC Med Genomics* **10**, 50, doi:10.1186/s12920-017-0286-x (2017).

52 Sahai, K., Saraswathy, S., Yadav, T. P., Arora, D. & Krishnan, M. Pre-eclampsia: Molecular events to biomarkers. *Med J Armed Forces India* **73**, 167-174, doi:10.1016/j.mjafi.2016.09.001 (2017).

53 Medina-Bastidas, D. *et al.* Placental Microarray Profiling Reveals Common mRNA and lncRNA Expression Patterns in Preeclampsia and Intrauterine Growth Restriction. *Int J Mol Sci* **21**, doi:10.3390/ijms21103597 (2020).

54 Leavey, K. *et al.* Unsupervised Placental Gene Expression Profiling Identifies Clinically Relevant Subclasses of Human Preeclampsia. *Hypertension* **68**, 137-147, doi:10.1161/HYPERTENSIONAHA.116.07293 (2016).

55 Horii, M. *et al.* Modeling preeclampsia using human induced pluripotent stem cells. *Sci Rep* **11**, 5877, doi:10.1038/s41598-021-85230-5 (2021).

56 Han, L. *et al.* Downregulation of hsa_circ_0004543 Activates oxLDL-Induced Vascular Endothelial Cell Proliferation and Angiogenesis. *Front Genet* **12**, 632164, doi:10.3389/fgene.2021.632164 (2021).

57 Papuchova, H., Meissner, T. B., Li, Q., Strominger, J. L. & Tilburgs, T. The Dual Role of HLA-C in Tolerance and Immunity at the Maternal-Fetal Interface. *Front Immunol* **10**, 2730, doi:10.3389/fimmu.2019.02730 (2019).

58 Li, J. *et al.* QSOX1 regulates trophoblastic apoptosis in preeclampsia through hydrogen peroxide production. *J Matern Fetal Neonatal Med* **32**, 3708-3715, doi:10.1080/14767058.2018.1471459 (2019).

59 Sandri, S. *et al.* Serum amyloid A in the placenta and its role in trophoblast invasion. *PLoS One* **9**, e90881, doi:10.1371/journal.pone.0090881 (2014).

60 Engin-Ustun, Y. *et al.* Serum amyloid A levels are increased in pre-eclampsia. *Gynecol Obstet Invest* **64**, 117-120, doi:10.1159/000100329 (2007).

61 Alur, V. *et al.* Integrated bioinformatics analysis reveals novel key biomarkers and potential candidate small molecule drugs in gestational diabetes mellitus. *Biosci Rep* **41**, doi:10.1042/BSR20210617 (2021).

62 Nogueras-Ortiz, C. J. *et al.* Astrocyte- and Neuron-Derived Extracellular Vesicles from Alzheimer's Disease Patients Effect Complement-Mediated Neurotoxicity. *Cells* **9**, doi:10.3390/cells9071618 (2020).

63 Sharma, P., Diergaarde, B., Ferrone, S., Kirkwood, J. M. & Whiteside, T. L. Melanoma cell-derived exosomes in plasma of melanoma patients suppress functions of immune effector cells. *Sci Rep* **10**, 92, doi:10.1038/s41598-019-56542-4 (2020).

64 Dasgupta, D. *et al.* IRE1A Stimulates Hepatocyte-Derived Extracellular Vesicles That Promote Inflammation in Mice With Steatohepatitis. *Gastroenterology* **159**, 1487-1503 e1417, doi:10.1053/j.gastro.2020.06.031 (2020).

65 Sado, T. *et al.* Inflammatory pattern recognition receptors and their ligands: factors contributing to the pathogenesis of preeclampsia. *Inflamm Res* **60**, 509-520, doi:10.1007/s00011-011-0319-4 (2011).

66 Kramer, A. W., Lamale-Smith, L. M. & Winn, V. D. Differential expression of human placental PAPP-A2 over gestation and in preeclampsia. *Placenta* **37**, 19-25, doi:10.1016/j.placenta.2015.11.004 (2016).

67 Chang, S. D. *et al.* Analyses of placental gene expression in pregnancy-related hypertensive disorders. *Taiwan J Obstet Gynecol* **50**, 283-291, doi:10.1016/j.tjog.2011.07.005 (2011).

Chapter 6

Discussion of the Research Findings and Future Research Recommendations

6 Discussion of the research findings and future research recommendations

This PhD project aimed to develop a novel placental extracellular vesicle (EV) immuno-enrichment method for maternal plasma. Specifically, it aimed to develop an EV immuno-enrichment approach which was suitable for small plasma volumes including biobanked samples and compatible with various downstream analysis approaches including mass spectrometry. The drive behind the project is the hypothesis that placental EVs enriched from the blood of pregnant women offer critical non-invasive insights into the health of the placenta and hence of the pregnancy. The project had a particular focus on the common and often serious pregnancy complication preeclampsia, driven by two clinical requirements: 1) The molecular mechanisms that underpin preeclampsia development are not well understood, and better non-invasive insights may aid in our understanding of why preeclampsia and related pregnancy complications develop. 2) While the symptoms of preeclampsia typically develop towards the end of the pregnancy, its molecular origins likely occur in the first trimester. More generally, non-invasive preeclampsia biomarkers are presently suboptimal, and better biomarkers are needed to detect the disease early in pregnancy i.e. before clinical onset or at least to identify pregnancies at high risk to develop the condition. In addition, non-invasive biomarkers with high positive predictive values and therefore able to 'rule in' a preeclampsia diagnosis are also needed to improve care and birth outcomes.

Since the discovery of EVs, research on their biological properties and physiological functions in various pathologies has increased greatly, emphasising the significant roles of EVs in many diseases,[1] including preeclampsia.[2] In addition to circulating proteins and RNAs that have long been studied for preeclampsia prediction/diagnosis, EVs particularly placental EVs have emerged as an alternative source of preeclampsia biomarkers, paving a new way to non-invasively investigate the underlying pathophysiologic mechanisms of this placental disorder.[3] More specifically, enriching placental EVs and analysing their molecular content has a unique potential to identify non-invasive preeclampsia biomarkers, therefore aiding in better diagnosis and earlier surveillance strategies for preeclampsia.

Despite the known link between EVs and preeclampsia, i.e. the presence of abnormal amounts of EVs and changes in their molecular content compared to healthy pregnancy,[4]

the specific enrichment of placental EVs from maternal plasma for downstream molecular analyses remains challenging. The complex nature of the plasma as well as the low abundance of placental EVs (present at ~100 times lower amounts compared to maternal plasma proteins and EVs from other cells other than placental cells)[5] is the major reason making their enrichment highly variable. This lack of reproducibility, in addition to the often time-consuming nature of current protocols, limits their diagnostic utility. Therefore, it is necessary to develop enrichment methods that not only efficiently enrich placental EVs but also ensure high purity of the enriched fractions in terms of both non-placental EVs and contaminating maternal plasma proteins. Enrichment of specific placental EVs with high purity is indeed a key parameter towards enabling successful downstream analyses with state-of-the-art omic technology including mass spectrometry of EV proteins.[6] For example, EV enrichment improves the signal to noise ratio caused by contamination with abundant soluble proteins in a pregnant woman's plasma.[7] [8] Efficient enrichment of placental EVs likely provides a powerful means to identify novel preeclampsia biomarkers that are otherwise undetectable. The lack of standardised approaches has hampered EV biomarker discovery with methods demonstrating large inter-laboratory and user dependent differences[9]. Robust and reproducible EV enrichment and analysis are key requirements to improve the biological relevance of EV-based diagnostics in pregnancy.

For that purpose, we investigated throughout this PhD project the use of immuno-affinity enrichment targeted to two subtypes of placental EVs derived from syncytiotrophoblast and extravillous trophoblast. These two prominent placental cells express Placental Alkaline Phosphatase (PLAP) and Human Leukocyte Antigen-G (HLA-G), respectively, providing robust approaches for their specific immune-enrichment.[10,11] We established immuno-affinity magnetic enrichment using iron oxide nanowires (NWs) naturally produced by zetaproteobacteria *Mariprofundus ferrooxydans*. By extracting the NWs from the bacterial biofilms and surface modifying these naturally occurring magnetic nanomaterials with copolymers enabling conjugation of anti-PLAP and anti-HLA-G antibodies to their surface, the developed immuno-enrichment method was shown to enrich placental EVs with reduced non-specific binding of proteins and irrelevant (maternal) EVs.

In the first experimental chapter of this PhD thesis (Chapter 3), we first report the optimised protocol for immuno-magnetic enrichment of specific EV subtypes and

subsequently demonstrated its suitability for liquid chromatography-tandem mass spectrometry (LC-MS/MS) EV analysis. To conduct this study, we modified the surface of the NWs with diblock polymers prepared by reversible addition-fragmentation chain transfer (RAFT)s (RAFT-3MAPC2-20AAm) to conjugate anti-PLAP and proved the feasibility of enriching PLAP+ve EVs using Evs from a trophoblast-like cell line as a model for placental EVs. By collecting the total EVs from the culture media of the cell line via ultracentrifugation and subsequently immuno-enriching PLAP+ve EVs using anti-PLAP conjugated magnetic NWs, we demonstrated good performance comparable to that of the current gold standard magnetic Dynabead in terms of PLAP recovery, high particle-to-protein-ratio (and thus high purity of the EV isolate) and low non-specific binding of irrelevant EVs. More importantly, we demonstrated that the optimised EV enrichment method using NWs was compatible with mass spectrometry analysis of EV proteins, as shown by the high number of identified proteins and excellent reproducibility. The immuno-specific EV enrichment and downstream mass spectrometry approach using naturally occurring iron oxide magnetic NWs or Dynabeads were shown to be an efficient method for placental EV proteomic studies.

Within this project, we utilised bovine serum albumin (BSA) to block the NW surface and reduce non-specific binding which is particularly prevalent in plasma/serum samples. However, the addition of BSA adds an additional complication to mass spectrometry, as the presence of large excess of BSA can significantly reduce the sensitivity of protein detection. In addition to BSA, investigation of other blocking reagents such as amine-modified polyethylene glycol or commercialised chemical-based blockers is of interest for future research. But eliminating the need for blocking/passivation all together through the engineering of the surface coating would be significant. Towards addressing this need, Chapter 4 demonstrates that the use of dual multi-length polymers for NW coating increased the amount of target EV binding compared to coating with only one polymer, demonstrating the importance of the polymeric nanoarchitecture. Importantly, both polymeric coatings better retained the EV binding performance in presence of increasing amount of plasma protein compared to gold standard Dynabeads. Further optimisation of the NW coating would likely lead to further improvement in binding performance and specificity, both in direct and indirect EV capture even without surface passivation.

In the second experimental chapter of the PhD project (Chapter 4), we also applied the optimised immuno-specific EV enrichment method towards enabling single step direct

capture of placental EVs from plasma using the magnetic NWs and subsequent quantification of EV-associated proteins known to be involved in preeclampsia. The introduced direct EV enrichment method was shown to be compatible with the detection of proteins co-located with PLAP+ve EV (e.g Neprilysin and Placental Protein 13) in both preeclamptic pregnancy samples (n = 2) and a gestation matched control using only 100 µL of plasma. The method may provide a clinically useful tool to detect STBEV biomarkers towards developing a rapid diagnostic tool to triage symptomatic pregnancies. Given that many preeclampsia EV biomarker studies have been hampered by a lack of a rapid and reproducible consensus method for EV enrichment, the approach developed in this thesis could provide more reliable placental biomarker quantification. A larger clinical study coupled with the identification of the ideal biomarker/biomarkers is required to further investigate the clinical utility of the dual coating NW enrichment method. Moreover, future research could be potentially expanded to not only preeclampsia associated proteins but also mRNA or miRNA.

In the last experimental chapter of the PhD project (Chapter 5), we enriched and analysed the proteomic profile of two placental EV subtypes namely PLAP+ve EVs and HLA-G+ve EVs from the plasma of a preeclamptic pregnancy. Specifically, we first ultracentrifuged the plasma sample to collect total EVs and sequentially immuno-enriched PLAP+ve EVs and then HLA-G+ve using anti-PLAP and anti-HLA-G conjugated NWs coated with dual RAFT copolymers. Mass spectrometry analyses of the placental EVs enriched from the maternal of a preeclamptic pregnancy recovered placenta related proteins, including several with known preeclampsia associations. A comparison on the proteomic profiles of placental EVs enriched by the two-step enrichment method described in this chapter and single step one described in Chapter 4 was also conducted. Similar to two-step EV enrichment, direct enrichment showed the presence of identified placenta-specific proteins but with increasing amount of background proteins potentially including both specific and non-specific EV proteins. While ultracentrifugation improves the clearance of contaminating maternal plasma proteins, it requires a sufficiently large amount of plasma sample (500 µL used in this study) and potentially results in significant losses of target placental EVs – especially when smaller sample volumes are used. Direct enrichment on the other hand, is applicable for very small plasma volume (only 100 µL was used here), which is advantageous in cases where sample resource is limited such as biobanked samples.

Importantly, building on the achievement of this thesis work, further experimental work is currently underway to investigate the proteomic profiles of the two placental EVs sub-types in a larger cohort of preeclamptic pregnancies and matched gestation controls. The approaches and methodologies described herein have a broader potential to investigate other pregnancy complications, and even to provide improved non-invasive insights into pregnancy development. As EV immuno-enrichment can be easily changed by swapping the conjugated antibodies, this approach also has potential utility in applications beyond pregnancy such as cancer.

In addition to the surface coating discussed throughout this thesis, the selection of magnetic material for immuno-enrichment is a critical consideration in achieving successful results. In this thesis, NWs were selected for the enrichment of placental EVs due to their balanced combination of strong magnetic strength and high surface area. The utilisation of NWs in this research contributes to the selection of magnetic materials for immuno-enrichment applications. Typically, larger sized magnetic materials possess greater magnetic strength. However, this can result in decreased solubility in solution, negatively affecting their effectiveness in immuno-enrichment. Conversely, smaller sized materials such as nanoparticles provide a larger surface area, which is beneficial for immuno-enrichment but may not possess adequate magnetic strength. These findings can aid in the development of an ideal magnetic material for immuno-enrichment with improved performance.

Beyond proteomics, high purity placental EV enrichment with other omics approaches including transcriptomics and lipidomics and the ability to perform multi-omics comparisons would be hugely significant. The analysis of circulating-RNA fragments in maternal blood is a promising field of research for disease detection.[13,14] Placental RNA in maternal blood in early pregnancy reflects changes in gene expression occurring within the placenta, as well as placental dysfunction leading to preeclampsia.[15] However, significant contamination with maternal RNA makes such analysis complex and inaccurate, limiting the diagnostic scope and complicating bioinformatics. For example, miRNAs have been investigated by our collaborators in matched plasma and placental tissue at 6–23 weeks' gestation,[16] unfortunately plasma miRNA did not accurately reflect the placental profile in early-mid gestation. Placental EVs could provide a more accurate reflection of placental status and therefore pregnancy health, compared to free miRNAs, with important implications for biomarker discovery. For example, transcriptomic

analysis of STBEVs from placental explants of preeclamptic and healthy pregnancies revealed 16 differentially expressed miRNAs.[17] Likewise, lipidomic analysis of placental EVs enriched from the placental explants showed a different lipid composition between preeclamptic and healthy pregnancies.[18] Moreover, analysis of placental EV DNA might provide a novel method to improve the sensitivity of non-invasive prenatal testing based on cell-free DNA.

The developed enrichment method for placental EV subtypes has the potential for both biomarker discovery and the diagnosis or prediction of placental disorders such as preeclampsia. However, there is significant work which needs to be done before this could be realised. In particular, the method must be reproducible and although I have shown some aspects to be so, the reproducibility of the whole method must be investigated more thoroughly on a much larger number of samples. Moreover, the method should be tested on a greater number of variables such as fetal gender and different gestational ages with similar medical histories to ensure consistent results. Finally, It may be necessary to adopt a technology that is potentially point-of-need to replace ELISA, as used in this thesis, to enable rapid and precise detection and quantification of target EV proteins.

6.1 References

1 Wang, Z., Zhao, G., Zeng, M., Feng, W. & Liu, J. Overview of extracellular vesicles in the pathogenesis of preeclampsiadagger. *Biol Reprod* **105**, 32-39, doi:10.1093/biolre/ioab060 (2021).

2 Palma, C. *et al.* Extracellular Vesicles and Preeclampsia: Current Knowledge and Future Research Directions. *Subcell Biochem* **97**, 455-482, doi:10.1007/978-3-030-67171-6_18 (2021).

3 Zhang, J., Li, H., Fan, B., Xu, W. & Zhang, X. Extracellular vesicles in normal pregnancy and pregnancy-related diseases. *J Cell Mol Med* **24**, 4377-4388, doi:10.1111/jcmm.15144 (2020).

4 Gilani, S. I., Weissgerber, T. L., Garovic, V. D. & Jayachandran, M. Preeclampsia and Extracellular Vesicles. *Curr Hypertens Rep* **18**, 68, doi:10.1007/s11906-016-0678-x (2016).

5 Cooke, W. R., Jones, G. D., Redman, C. W. G. & Vatish, M. Syncytiotrophoblast Derived Extracellular Vesicles in Relation to Preeclampsia. *Maternal-Fetal Medicine* **3**, 151-160, doi:10.1097/fm9.0000000000000093 (2021).

6 Sodar, B. W. *et al.* Best practice of identification and proteomic analysis of extracellular vesicles in human health and disease. *Expert Rev Proteomics* **14**, 1073-1090, doi:10.1080/14789450.2017.1392244 (2017).

7 Tan, K. H. *et al.* Extracellular vesicles yield predictive pre-eclampsia biomarkers. *Journal of extracellular vesicles* **6**, 1408390 (2017).

8 Vykoukal, J. *et al.* Plasma-derived extracellular vesicle proteins as a source of biomarkers for lung adenocarcinoma. *Oncotarget* **8**, 95466 (2017).

9 Crigna, A. T. *et al.* Inter-laboratory comparison of extracellular vesicle isolation based on ultracentrifugation. *Transfusion Medicine and Hemotherapy* **48**, 48-59 (2021).

10 Awoyemi, T. *et al.* Syncytiotrophoblast Extracellular Vesicles From Late-Onset Preeclampsia Placentae Suppress Pro-Inflammatory Immune Response in THP-1 Macrophages. *Front Immunol* **12**, 676056, doi:10.3389/fimmu.2021.676056 (2021).

11 Goldman-Wohl, D. S., Ariel, I., Greenfield, C., Hanoch, J. & Yagel, S. HLA-G expression in extravillous trophoblasts is an intrinsic property of cell differentiation: a lesson learned from ectopic pregnancies. *Mol Hum Reprod* **6**, 535-540, doi:10.1093/molehr/6.6.535 (2000).

12 Lundqvist, M. *et al.* The nanoparticle protein corona formed in human blood or human blood fractions. *PLoS One* **12**, e0175871, doi:10.1371/journal.pone.0175871 (2017).

13 Whitehead, C. L., Walker, S. P. & Tong, S. Measuring circulating placental RNAs to non-invasively assess the placental transcriptome and to predict pregnancy complications. *Prenatal diagnosis* **36**, 997-1008 (2016).

14 Pavličev, M. *et al.* Single-cell transcriptomics of the human placenta: inferring the cell communication network of the maternal-fetal interface. *Genome research* **27**, 349-361 (2017).

15 Tsang, J. C. *et al.* Integrative single-cell and cell-free plasma RNA transcriptomics elucidates placental cellular dynamics. *Proceedings of the National Academy of Sciences* **114**, E7786-E7795 (2017).

16 Smith, M. D. *et al.* Large-scale transcriptome-wide profiling of microRNAs in human placenta and maternal plasma at early to mid gestation. *RNA biology* **18**, 507-520 (2021).

17 Wei, J. *et al.* Placental trophoblast debris mediated feto-maternal signalling via small RNA delivery: implications for preeclampsia. *Sci Rep* **7**, 14681, doi:10.1038/s41598-017-14180-8 (2017).

18 Baig, S. *et al.* Lipidomic analysis of human placental syncytiotrophoblast microvesicles in adverse pregnancy outcomes. *Placenta* **34**, 436-442, doi:10.1016/j.placenta.2013.02.004 (2013).